

INVESTIGATION OF SUSTAINABLE WASTE- DERIVED ADSORBENTS FOR ARSENIC AND COPPER IN WATER TREATMENT

by

© Roya Sadat Neisan

A Thesis submitted to the

School of Graduate Studies

in partial fulfillment of the requirements for the degree of

Doctor of Philosophy in Civil Engineering

Faculty of Engineering and Applied Science

Memorial University of Newfoundland

May 2025

St. John's

Newfoundland and Labrador

ABSTRACT

Arsenic contamination in drinking water is a global issue, affecting millions and posing serious health risks such as cancer and neurological disorders. This is particularly critical in communities relying on groundwater. This research explores using mussel shells and agricultural waste, including date seeds and orange peels, as sustainable adsorbents for removing arsenic and copper from water.

Nanoparticles were incorporated into calcined mussel shell powder and biochars derived from these biomass wastes to enhance adsorption capacity. The adsorbents were characterized to evaluate their surface properties, and adsorption mechanisms were studied to understand their effectiveness.

Batch experiments were conducted to examine the effects of pH, adsorbent dosage, initial metal concentrations, and contact time. These experiments identified optimal conditions for maximizing removal efficiency. Statistical methods were used to optimize the adsorption processes. The results showed that modified mussel shells have high arsenic adsorption potential, while TiO₂-modified orange peel biochar performed well as a low-cost option for copper removal. Both biochars also demonstrated strong copper adsorption performance.

Kinetic and isotherm models helped describe the rate and equilibrium behavior of arsenic and copper adsorption. Thermodynamic analysis indicated that the adsorption processes were spontaneous and endothermic. The mechanisms of arsenic removal by mussel shells were further studied, considering ionic strength, surface charge, and functional groups using various analytical techniques.

Beyond batch tests, column studies were performed using mussel shells in point-of-use (POU) filtration systems. These tests assessed exhaustion capacity, the influence of co-existing ions, and reusability. Breakthrough curve analysis showed how initial

arsenic concentration, flow rate, and adsorbent mass affected performance. Modified mussel shells demonstrated superior arsenic removal in POU cartridges compared to commercial activated carbon.

This study offers a sustainable and cost-effective approach to arsenic removal, particularly for remote communities with limited access to centralized water treatment, by repurposing mussel shells and agricultural waste as effective adsorbents.

STATEMENT OF CONTRIBUTIONS

I, Roya Sadat Neisan, hereby declare that I am the first author and the main contributor to the work conducted and presented in this doctoral dissertation. I was primarily responsible for the conceptualization, methodology development, investigation, formal analysis, data curation, and preparation of the original manuscript drafts. I also played a key role in interpreting results and generating visualizations.

Dr. Noori M. Cata Saady provided significant guidance throughout this research process. His contributions included funding acquisition, project administration, supervision, providing resources and accommodating the experimental work, validation of methods and results, and extensive involvement in reviewing and editing manuscript drafts.

Dr. Carlos Bazan contributed to funding acquisition, project administration, and manuscript review and editing, offering critical feedback to improve the clarity and quality of the work.

Dr. Sohrab Zendheboudi, Dr. Ponnusami Venkatachalam, and Dr. Talib M. Albayati supported the research through collaborations by providing resources, validating results, and reviewing and editing drafts.

The list of publications arising from this research is provided below:

- 1- Neisan, R. S., Saady, N. M. C., Bazan, C., Zendheboudi, S., and Venkatachalam, P. (2024). Use of Mussel Shells for Removal of Arsenic from Water: Kinetics and Equilibrium Experimental Investigation. *Results in Engineering*, 13, 103587. <https://doi.org/10.1016/j.rineng.2024.103587>.
- 2- Neisan, R. S., Saady, N. M. C., Bazan, C., Zendheboudi, S., and Albayati, T. M. (2023). Adsorption of copper from water using TiO₂-modified activated carbon derived from orange peels and date seeds: Response surface methodology

optimization. *Heliyon*, 9(11), e21420.

<https://doi.org/10.1016/j.heliyon.2023.e21420>.

- 3- Neisan, R. S., Saady, N. M. C., Bazan, C., Zendehboudi, S., Al-nayili, A., Abbassi, B., and Chatterjee, P. (2023). Arsenic removal by adsorbents from water for small communities' decentralized systems: Performance, characterization, and effective parameters. *Clean Technologies*, 5(1), 352-402.
<https://doi.org/10.3390/cleantechnol5010019>.
- 4- Neisan, R. S., Saady, N. M. C., Bazan, C., & Zendehboudi, S. (2025). Investigating arsenic (III and V) continuous flow adsorption by modified calcined mussel shells. *Journal of Water Process Engineering*, 72, 107488.
<https://doi.org/10.1016/j.jwpe.2025.107488>.
- 5- Neisan, R. S., Saady, N. M. C., Bazan, C., & Zendehboudi, S. (2025). Optimization of arsenic removal from water using novel renewable adsorbents derived from orange peels. *Waste Management Bulletin*, 3(2), 21-35.
<https://doi.org/10.1016/j.wmb.2025.02.006>.

The following is a list of conference presentations stemming from this research:

- 1- Neisan, Roya Sadat, Seyed Kamran Niroomand, Carlos Bazan and Noori M. Cata Saady, "Prediction of arsenic removal efficiency from water sources using machine learning methods," International Conference on Persistent, Emerging, and Organic Pollution in the Environment – Challenges and Solutions under Climate Change, UPEI, Charlottetown, Prince Edward Island, Canada, (2022, August 23-26).
- 2- Neisan, R. S., Saady, Noori M. Cata Saady, and Carlos Bazan. “Effective Arsenic Removal from Water by Low-Cost Adsorbents Derived from Mussel Shells.” International Conference – Collaborative Solutions to Environmental

Problems under Climate Change, PEOPLE 2023, Montreal, Canada (2023, August 7-11).

- 3- Neisan, R. S., Saady, Noori M. Cata Saady, and Carlos Bazan. “Efficiency of Waste-Derived Composite Beads for Arsenic Removal.” The 24th Aldrich Multidisciplinary Conference, Memorial University, St. John’s, Canada (2023, November 18-19).

ACKNOWLEDGEMENTS

I would like to express my deepest gratitude to my supervisor, Dr. Noori Saady, for his exceptional guidance, unwavering support, and encouragement throughout my research. I am truly thankful for the opportunity to work under his supervision.

I also extend my sincere thanks to Dr. Calos Bazan and Dr. Helen Zhang for their thoughtful feedback and constructive suggestions, which have greatly enriched my research and helped me improve my work.

I am deeply grateful to the Persistent, Emerging, and Organic Pollution in the Environment (PEOPLE) Network for funding, as well as the Natural Sciences and Engineering Research Council of Canada (NSERC) and Mitacs for their financial support, which made this research possible. I also thank the Government of Newfoundland and Labrador for providing the essential water samples used in my project.

My thanks also go to Memorial University for providing the research space and continuous support throughout my studies. I am especially grateful to the NRPOP Lab, and particularly to Lidao Tao, for fostering a collaborative and productive environment, and to the Memorial University Core Research Equipment & Instrument Training Network (CREAIT) for their assistance with material characterization, which was vital to my research.

Finally, I want to extend my heartfelt appreciation to my family for their constant love and support throughout this journey. A special thanks to my husband, Ghasem, for always being by my side with endless encouragement and care.

This thesis is dedicated to all women in science and engineering, whose dedication, perseverance, and contributions continue to inspire future generations of researchers and innovators.

Table of Contents

ABSTRACT.....	iii
STATEMENT OF CONTRIBUTIONS.....	v
ACKNOWLEDGEMENTS.....	viii
Table of Contents	ix
List of Tables	xvii
List of Figures	xxi
List of Abbreviations and Symbols.....	xxvi
CHAPTER ONE	1
INTRODUCTION	1
1.1. Research Background.....	1
1.2. Statement of Research Problem.....	6
1.3. Objectives of the Study	9
1.4. Organization of Thesis	10
1.5. References	12
ARSENIC REMOVAL BY ADSORBENTS FROM WATER FOR SMALL COMMUNITIES' DECENTRALIZED SYSTEMS: PERFORMANCE, CHARACTERIZATION, AND EFFECTIVE PARAMETERS1	17
2.1. Introduction	18
2.2. Arsenic.....	19
2.2.1. Arsenic occurrence	20
2.2.2. Arsenic structure.....	21
2.2.3. Arsenic oxidation and reduction.....	22
2.2.4. Arsenic treatment.....	24
2.3. Conventional Methods for Arsenic Removal from Aqueous Solutions in	

Decentralized Systems Other than Adsorption.....	25
2.3.1. Ion exchange.....	28
2.3.2. Membrane technologies.....	32
2.3.3. Coagulation-flocculation	36
2.3.4. Oxidation	38
2.3.4.1. Photo-Oxidation	40
2.4. Arsenic Removal by Adsorption	43
2.4.1. Adsorption kinetic	46
2.4.2. Isotherm models	48
2.4.3. Characterization techniques for investigation of adsorbents properties.....	51
2.4.3.1. Surface morphology	54
2.4.3.2. Bulk density and particle size.....	54
2.4.3.3. Dynamic light scattering (DLS)	54
2.4.3.4. Brunauer-Emmett-Teller (BET)-surface area.....	56
2.4.3.5. Crystallinity	56
2.4.3.6. Ultimate (elemental) analysis	56
2.4.3.7. Proximate analysis.....	57
2.4.3.8. Functional groups	58
2.4.3.9. Zeta potential (ZP).....	58
2.4.4. Adsorbent performance	58
2.4.4.1. Removal efficiency and adsorption capacity.....	58
2.4.4.2. Reusability	59
2.4.4.3. Effects of parameters on adsorbent performance	60
2.4.5. Arsenic adsorbents.....	72
2.4.5.1. Industrial waste (fly ash-based adsorbents).....	74

2.4.5.2.	Animal waste (fisheries waste-based adsorbents)	76
2.4.5.3.	Natural materials (zeolites).....	76
2.4.5.4.	Bio-adsorbent (chitin/chitosan)	77
2.4.5.5.	Agricultural waste (fruit peels).....	78
2.5.	Application of Adsorption in Drinking Water Treatment Systems.....	79
2.6.	Conclusion.....	83
2.7.	References	84
CHAPTER THREE		125
USE OF MUSSEL SHELLS FOR REMOVAL OF ARSENIC FROM WATER:		
KINETICS AND EQUILIBRIUM EXPERIMENTAL INVESTIGATION 2		
.....		125
3.1.	Introduction	126
3.2.	Materials and Methods	132
3.2.1.	Preparation of the adsorbent.....	132
3.2.2.	Adsorption experiments.....	133
3.2.3.	Analytical methods.....	136
3.2.4.	Mechanism studies	136
3.2.5.	Kinetic experiments.....	137
3.2.6.	Isotherm studies.....	138
3.2.7.	Thermodynamic studies.....	140
3.3.	Results and Discussion	141
3.3.1.	Adsorbent characterization.....	141
3.3.1.1.	X-ray diffraction crystallography (XRD).....	141
3.3.1.2.	Scanning electron microscopy (SEM).....	142
3.3.1.3.	Fourier-transform infrared spectroscopy (FTIR).....	142

3.3.1.4.	Brunauer-Emmett-Teller (BET) surface area analysis	143
3.3.1.5.	X-ray photoelectron spectroscopy (XPS)	147
3.3.2.	Mechanism of adsorption	153
3.3.3.	Optimization of arsenic removal	156
3.3.3.1.	Effect of pH	160
3.3.3.2.	Effect of adsorbent dose (Ad).....	161
3.3.3.3.	Effect of initial concentration (Ci)	162
3.3.3.4.	Effect of contact time (tc).....	162
3.3.4.	Kinetics studies.....	165
3.3.5.	Isotherm studies.....	167
3.3.6.	Thermodynamic studies.....	170
3.3.7.	The potential and practicalities of calcined mussel shells.....	171
3.4.	Conclusion.....	172
3.5.	References	173
CHAPTER FOUR.....		187
INVESTIGATING ARSENIC (III AND V) ADSORPTION WITH MODIFIED		
CALCINED MUSSEL SHELLS IN CONTINUOUS FLOW		
EXPERIMENTS3.....		187
4.1.	Introduction	188
4.2.	Materials and Methods	194
4.2.1.	Materials	194
4.2.2.	Part I: flow-through experiments in glass columns.....	194
4.2.2.1.	Breakthrough curve Studies	195
4.2.2.2.	Arsenic uptake in the presence of co-ions	196
4.2.2.3.	Adsorbent reusability.....	197

4.2.3.	Part II: comparative arsenic removal in point of use cartridges.....	197
4.2.3.1.	Preparation of cartridges.....	197
4.2.3.2.	Adsorption-desorption.....	198
4.3.	Results and Discussion.....	199
4.3.1.	Part I: flow-through experiments in glass columns.....	199
4.3.1.1.	Breakthrough curve studies	199
4.3.1.2.	Thomas model	204
4.3.1.3.	Yoon-Nelson model.....	206
4.3.1.4.	Arsenic uptake in the presence of co-ions	210
4.3.1.5.	Adsorbent reusability.....	216
4.3.2.	Part II: comparative arsenic removal in point of use cartridges.....	222
4.3.2.1.	Adsorption-desorption experiments	222
4.4.	Conclusion.....	227
4.5.	Reference	228
CHAPTER FIVE		243
REMOVAL OF ARSENIC FROM WATER USING RENEWABLE ADSORBENTS		
DERIVED FROM ORANGE PEELS 4.....		243
5.1.	Introduction	244
5.2.	Materials and Methods	248
5.2.1.	Preparation and characterization of the adsorbent.....	248
5.2.2.	Adsorption experiments.....	250
5.2.3.	Kinetic and isotherm experiments	252
5.2.4.	Thermodynamic studies.....	255
5.3.	Results and Discussion.....	256
5.3.1.	Adsorbent characterization	256

5.3.1.1.	Elemental analysis	256
5.3.1.2.	X-ray diffraction crystallography (XRD)	256
5.3.1.3.	Brunauer-Emmett-Teller (BET) surface area analysis	257
5.3.1.4.	Scanning electron microscopy (SEM)	258
5.3.1.5.	Fourier-transform infrared spectroscopy (FTIR)	259
5.3.2.	Optimization of arsenic removal	261
5.3.2.1.	Effect of pH	266
5.3.2.2.	Effect of adsorbent dose	267
5.3.2.3.	Effect of initial concentration	268
5.3.2.4.	Effect of contact time	268
5.3.3.	Comparison with other studies	269
5.3.4.	Kinetics studies	274
5.3.5.	Isotherm studies	276
5.3.6.	Thermodynamic studies	278
5.4.	Conclusion	279
5.5.	References	280
CHAPTER SIX		299
ADSORPTION OF COPPER FROM WATER USING TiO ₂ -MODIFIED		
ACTIVATED CARBON DERIVED FROM ORANGE PEELS AND		
DATE SEEDS: RESPONSE SURFACE METHODOLOGY		
OPTIMIZATION 5		299
6.1.	Introduction	300
6.2.	Materials and Methods	304
6.2.1.	Preparation and procedures	304
6.2.2.	Preparation of adsorbents	305

6.2.3.	Experimental design	306
6.2.4.	Adsorption experiments.....	307
6.2.5.	Kinetic studies	308
6.3.	Results and Discussion	310
6.3.1.	Adsorbent characterization	310
6.3.1.1.	Scanning electron microscopy (SEM).....	310
6.3.1.2.	X-ray diffraction crystallography (XRD) analysis	311
6.3.1.3.	Fourier transformed infrared radiation (FTIR).....	312
6.3.1.4.	Brunauer-Emmett-Teller (BET) Theory.....	313
6.3.2.	Optimization of copper removal.....	314
6.3.2.1.	Effect of pH	323
6.3.2.2.	Effect of adsorbent dose	323
6.3.2.3.	Effect of initial concentration.....	324
6.3.2.4.	Effect of contact time	324
6.3.3.	Adsorption kinetic study.....	324
6.4.	Strengths, Limitations, and Recommendations	328
6.5.	Conclusion.....	329
6.6.	References	330
CHAPTER SEVEN		341
CONCLUSION AND RECOMMENDATION.....		341
7.1.	Summary.....	341
7.2.	Conclusion.....	346
7.3.	Research Contributions	348
7.4.	Recommendations	350
APPENDIX 1		353

Supplementary Information for Chapter 3	353
Surface modification of calcined mussel shells with iron oxide nanoparticles	353
APPENDIX 2	355
Supplementary Information for Chapter 4	355
APPENDIX 3	356
Supplementary Information for Chapter 5	356
Surface Modification of activated carbon with titanium dioxide nanoparticles	356

List of Tables

Table 2-1 The most common arsenic species in the environment environment (adapted from Chungang & Le (2009)).	21
Table 2-2 Operating conditions and efficiencies of different resins used to remove arsenic.	30
Table 2-3 Overview of pressure-driven membrane processes and their characteristics.	35
Table 2-4 Coagulants/flocculants used in arsenic ion exchange, their operating conditions, and efficiencies.	37
Table 2-5 The standard potential of different oxidants and their efficiencies in arsenite oxidation (Kim & Nriagu, 2000; R. Liu & Qu, 2021; Sorlini & Gialdini, 2010).	39
Table 2-6 Oxidants used in the photo-oxidation of arsenite to arsenate, their operating conditions, and efficiencies.	42
Table 2-7 Advantages and disadvantages of common treatment technologies for arsenic removal.	45
Table 2-8 Kinetic parameters for the adsorption of arsenic on different adsorbents.	48
Table 2-9 Isotherm parameters for arsenic adsorption.	50
Table 2-10 Proximate and ultimate analysis, specific surface area and bulk density of different adsorbents.	52
Table 2-11 Fourier transform infrared spectroscopy (FTIR) and X-ray powder diffraction (XRD) results of different adsorbents.	53
Table 2-12 Scanning electron microscopy (SEM) and particle size distribution results of different adsorbents.	55
Table 2-13 Results of previous studies for several consecutive sorption/regeneration	

cycles.	60
Table 2-14 Summary of previous studies on the mathematical models of arsenic removal by different adsorbents.	62
Table 2-15 Summary of studies on the effect of process parameters on arsenic removal by different adsorbents.	63
Table 2-16 Different adsorbents used in arsenic removal, their operating conditions, and efficiencies for arsenic removal.	73
Table 2-17 The results of using some low-cost adsorbents in arsenic removal.	73
Table 2-18 Chemical composition of coal and biomass fly ash ash (G. Liang et al., 2020; Sarkkinen et al., 2018; Teixeira et al., 2019).	75
Table 2-19 Arsenic removal efficiency by different methods (pilot scale).	81
Table 2-19. Continued.	82
Table 3-1 Experimental factors for optimization of arsenic adsorption using IO-CMS.	134
Table 3-2 Four-factor CCD design for arsenic removal by IO-calcined mussels shell.	135
Table 3-3 Results of the BET analysis of mussel shells.	146
Table 3-4 Binding energies and relative content of As, C, Ca and O in adsorbents..	149
Table 3-5 Optimal solutions for highest arsenic adsorption.	157
Table 3-6 ANOVA for reduced quadratic modeling of arsenic removal.	159
Table 3-7 Summary of arsenic adsorption performance of different adsorbents.	164
Table 3-8 Adsorption parameters from isotherm, kinetic, and thermodynamic models.	166
Table 4-1 Results of mussel shell-based adsorbents for contaminant removal	191
Table 4-2 Well water characteristics (in mg L ⁻¹ unless indicated otherwise).	199

Table 4-3 Thomas parameters for various configurations: Flowrates, adsorbent masses, and initial concentrations.	206
Table 4-4 Yoon-Nelson parameters for various configurations: Flowrates, adsorbent masses, and initial concentrations.	208
Table 4-5 Summary of Thomas and Yoon-Nelson model parameters from various flow-through studies on arsenic removal using different adsorbents.	209
Table 4-6 Thomas and Yoon-Nelson parameters for arsenic adsorption with or without co-ions (Cl^- , SO_4^{2-} , NO_3^- , HCO_3^- , and PO_4^{3-}).	213
Table 4-7 Thomas and Yoon-Nelson parameters for arsenic adsorption over five consecutive cycles.	220
Table 4-8 Thomas and Yoon-Nelson parameters for arsenic adsorption using three cartridges.	225
Table 5-1 Experimental factors for optimization of arsenic adsorption using OP-TiO ₂	252
Table 5-2 Properties of powdered orange peels before and after carbonization (wt.% by dry basis).	256
Table 5-3 Results of the Brunauer-Emmett-Teller (BET) analysis for activated carbon before and after modification.	258
Table 5-4 ANOVA for reduced quadratic modeling of arsenic removal.	262
Table 5-5 Coefficients in terms of coded factors.	262
Table 5-6 Optimal solutions for highest arsenic adsorption.	263
Table 5-7 Summary of adsorptive removal of arsenic by various adsorbents.	271
Table 5-8 Overview of biochar adsorbents derived from different waste sources (agricultural, food, animal, forestry, and aquacultural) and their highest reported adsorption capacities for arsenic removal from similar studies. .	272

Table 5-8 continued.	273
Table 5-9 Kinetic parameters for the pseudo-first-order, pseudo-second-order, Elovich, and intra-particle diffusion models.	276
Table 5-10 Isotherm parameters of Langmuir, Freundlich, Temkin, and D-R models.	278
Table 5-11 Thermodynamic parameters for removal of arsenic at different temperatures.	278
Table 6-1 Summary of adsorptive removal of heavy metals by relevant adsorbents.	302
Table 6-2 The ranges and levels of independent parameters.	306
Table 6-3 The four-factors CCD matrix for Cu removal.	307
Table 6-4 FTIR spectra of OP-TiO ₂ and DS-TiO ₂	313
Table 6-5 Adsorbents results from BET analysis.	314
Table 6-6 Fit statistics of response surface methodology model.	315
Table 6-7 ANOVA for reduced quadratic modelling of Cu removal.	317
Table 6-8 Coefficients in terms of coded factors.	318
Table 6-9 Optimal solutions for highest Cu removal efficiency.....	318
Table 6-10 Summary of adsorptive removal of copper by various adsorbents.	322
Table 6-11 Kinetic parameters of pseudo-first-order and pseudo-second-order models.	328

List of Figures

Figure 1-1 Areas of potential arsenic concentration in well water (Change, 2010).	3
Figure 2-1 Toxicity mechanisms of heavy metals (adopted from (Karcioglu & Arslan, 2019)).	19
Figure 2-2 The global extent of arsenic contamination (adopted from (Shaji et al., 2021)).	20
Figure 2-3 Eh–H diagram for aqueous arsenic species at 25 °C. (reprinted from (Smedley & Kinniburgh, 2002) with Elsevier permission).	23
Figure 2-4 Detailed segmentation of decentralized treatment systems (<i>Decentralized Water Treatment Market Size, Growth 2021-26</i> , n.d.). TDS: totals dissolved solids.	27
Figure 2-5 (a) Small-scale (community) water treatment system, (b) Point-of-use (POU) system, and (c) Point-of-entry (POE) system. HE: heavy metals; OM: organic matter.	28
Figure 2-6 (a) Schematic of the ion-exchange process and (b) resin regeneration.	28
Figure 2-7 Applicability ranges of different membranes based on pore sizes.	33
Figure 2-8 Mechanism of coagulation by cationic and anionic polymers.	38
Figure 2-9 Classification of adsorbents for water treatment (adapted from (Elwakeel et al., 2020)).	44
Figure 2-10 Different configurations for adsorption of impurities: (a) Packed-bed adsorber, (b) Fluidized-bed adsorber, and (c) Batch.	44
Figure 2-11 Overview of main characterization techniques.	51
Figure 2-12 Effects of multiple regeneration cycles on the performance of adsorbents.	60
Figure 3-1 Mussel shell utilization system based on the mussels life cycle diagram (de	

Alvarenga et al., 2012; Iribarren et al., 2010; H. Yang & Yan, 2018)....	128
Figure 3-2 Preparation of method of calcined mussel shells.	133
Figure 3-3 Characterization of adsorbent: (a) XRD patterns for natural (uncalcined) and calcined mussel shells; SEM images of the (b) natural mussel shells, (c) calcined mussel shells, and (d) IO-CMS; FTIR spectra of (e) calcined mussel shells, and (f) IO-CMS.....	144
Figure 3-4 (a) BET adsorption-desorption isotherm, and (b) BJH pore size distribution and cumulative pore volume characterization of natural (uncalcined), calcined mussel shells, and IO-CMS.	145
Figure 3-5 XPS survey spectra of the adsorbent surface (a) before adsorption, (b) after adsorption of As(III), and (c) after adsorption of As(V).....	148
Figure 3-6 XPS spectra of iron oxide-modified calcined mussel shells (IO-CMS) before and after arsenic adsorption: O1s (a) before adsorption, (b) As(III)-loaded, and (c) As(V)-loaded; C1s (d) before adsorption, (e)) As(III)-loaded, and (f) As(V)-loaded.	151
Figure 3-7 XPS spectra of iron oxide-modified calcined mussel shells (IO-CMS) before and after arsenic adsorption: Ca2p (a) before adsorption, (b) As(III)-loaded, and (c) As(V)-loaded; and As3d (d) As(III)-loaded, and (e) As(V)-loaded.....	152
Figure 3-8 (a) Zeta potential and removal efficiency of IO-CMS for As(III) and As(V) as a function of pH. (b) Effect of ionic strength on the removal efficiency of IO-CMS for As(III) and As(V).	155
Figure 3-9 Predicted vs. actual experimental values of removal efficiency for (a) As(III), (b) As(V); residuals vs. runs for (c) As(III), and(d) As(V).....	160
Figure 3-10 Effects of pH-initial concentration on (a) As(III), (b) As(V) removal	

efficiency; and initial concentrations- adsorbent dose on (c) As(III), and	
(d) As(V) removal efficiency. (Room temperature, rpm = 200).....	161
Figure 3-11 Regeneration of the adsorbent over multiple cycles for As(III) and As(V)	
removal.....	165
Figure 3-12 Arsenic adsorption kinetic models (a) PFO, (b) PSO, intra-particle	
diffusion (c), and Elovich models for the arsenic adsorption using IO-	
CMS.	168
Figure 3-13 Arsenic adsorption isotherm models (a) Freundlich, (b) Langmuir, (c)	
Temkin, and (d) D-R models for the arsenic adsorption using IO-CMS.	169
Figure 3-14 (a) Van't Hoff plot; and (b) Gibbs free energy for the arsenic adsorption	
using IO-CMS.	171
Figure 4-1 Schematic of the column apparatus.....	195
Figure 4-2 Preparation of three different cartridges (AC=Activated Carbon, MP=	
Mussel shell Powder, and MD= Mussel shell-coated Disc) for Part II of	
the study.	198
Figure 4-3 Breakthrough curves of a) As(III), d) As(V), and g) total As; Thomas	
linear plots of b) As(III), e) As(V), and h) total As; Yoon-Nelson plots of	
c) As(III), f) As(V), and i) total As (10 mg L ⁻¹).....	202
Figure 4-4 Breakthrough curves of a) As(III), d) As(V), and g) total As; Thomas	
linear plots of b) As(III), e) As(V), and h) total As; Yoon-Nelson plots of	
c) As(III), f) As(V), and i) total As (50 mg L ⁻¹).....	203
Figure 4-5 Arsenic adsorption with or without co-ions (Cl ⁻ , SO ₄ ²⁻ , NO ₃ ⁻ , HCO ₃ ⁻ , and	
PO ₄ ³⁻). a) Breakthrough curves; b) Thomas linear plots; and c) Yoon-	
Nelson plots.....	214
Figure 4-6 Breakthrough curves in five adsorption-desorption cycles of a) As(III), d)	

As(V), and g) total As; with Thomas linear plots for b) As(III), e) As(V), and h) total As; and Yoon-Nelson plots for c) As(III), f) As(V), and i) total As.	218
Figure 4-7 a) Breakthrough curves of; b) Thomas linear plots; c) Yoon-Nelson plots of three cartridges (activated carbon, powdered mussel shells, mussel shell-coated disc).....	224
Figure 4-8 Desorption profiles for mussel shell-based adsorbents using 0.1 M NaOH.	226
Figure 5-1 Preparation of activated carbon from orange peels modified by titanium dioxide (OP-TiO ₂).	249
Figure 5-2 X-ray diffraction crystallography (XRD) patterns for activated carbon before and after modification by TiO ₂	257
Figure 5-3 Scanning electron microscopy (SEM) of the activated carbon (a) before and (b) after modification by TiO ₂ ; energy dispersive X-ray spectroscopy (EDX) of the activated carbon (c) before and (d) after modification by TiO ₂	260
Figure 5-4 Fourier-transform infrared spectroscopy (FTIR) spectra of modified orange peel activated carbon (OP-TiO ₂).	261
Figure 5-5 Combined influence of (a) pH and initial concentration; (b) pH and adsorbent dose; (c) pH and contact time; (d) initial concentration and adsorbent dose; (e) initial concentration and contact time; and (f) adsorbent dose and contact time on adsorbent capacity.....	264
Figure 5-7 Comparison of arsenic adsorption capacities of the biochar adsorbent developed in this research and similar biochars from various sources. ..	270
Figure 5-8 Arsenic adsorption kinetic studies: (a) pseudo-first-order, (b) pseudo-	

second-order, (c) intra-particle diffusion, and (d) Elovich models. All at pH = 4.2, $C_i = 50 \text{ mg L}^{-1}$, and room temperature.....	275
Figure 5-9 Adsorption isotherm models fitted to the experimental data for arsenic adsorption onto OP-TiO ₂ : (a) Freundlich (b) Langmuir (c) Temkin, and (d) D-R models.	277
Figure 5-10 Thermodynamic studies for arsenic adsorption onto OP-TiO ₂	279
Figure 6-1 SEM image of (a) AC-OP, (b) OP-TiO ₂ , (c) AC-DS and d) DS-TiO ₂	310
Figure 6-2 (a) EDX graph of AC-OP, (b) EDX graph of OP-TiO ₂ , (c) EDX graph of AC-DS, and (d) EDX graph of DS-TiO ₂	311
Figure 6-3 XRD patterns of (A) OP-TiO ₂ and (B) DS-TiO ₂	312
Figure 6-4 FTIR spectra of OP-TiO ₂ and DS-TiO ₂	313
Figure 6-5 predicted vs actual values of removal efficiency for (a) orange peel (OP- TiO ₂); (b) date seeds (DS-TiO ₂); and residuals vs runs for (c) OP-TiO ₂ ; and (d) DS-TiO ₂	320
Figure 6-6 Response surface maps of the effects of (a) initial concentration-adsorbent dose on the removal efficiency using OP-TiO ₂ and (b) pH-Cu initial concentrations, (c) pH-adsorbent dose and (d) pH-contact time on the removal efficiency using DS-TiO ₂ . (All at room temperature).....	321
Figure 6-7 Copper adsorption kinetic studies by OP-TiO ₂ (a) pseudo-first-order, (b) pseudo-second-order, (c) intra-particle diffusion model (d) Elovich model. (Room temperature, rpm = 200)	326
Figure 6-8 Copper adsorption kinetic studies by DS-TiO ₂ (a) pseudo-first-order, (b) pseudo-second-order, (c) intra-particle diffusion model (d) Elovich model. (Room temperature, rpm = 200)	327

List of Abbreviations and Symbols

Acronyms:

1JW	N-methyl-D-glucamine functionalized resin: revealing gel
2JW	N-methyl-D-glucamine functionalized resin: expanded gel
2PTN	N-methyl-D-glucamine functionalized resin: epidermal-like structure
AOP	Advanced oxidation processes
AC	Activated carbon cartridge
AC-DPF	Date palm fiber activated carbon
AC-DS	Activated carbon from date seeds
AC-NLP	Activated charcoal from Neem leaf powder
AC-OP	Activated carbon from orange peels
AFM	Atomic force microscopy
ANOVA	Analysis of variance
ATR	Attenuated total reflectance
BBD	Box-Behnken design
BE	Binding energy
BC	Benzalkonium chloride
BET	Brunauer-Emmett-Teller
BWA	Boiling water advisories
CAGR	Compound annual growth rate
CCA	Cellulose-Ca/Al layered double hydroxide nanocomposites
CBC	Canadian broadcasting corporation
CCD	Central composite design

CMGO	Chitosan magnetic graphene oxide nanocomposite
COP	Charred orange peels
CPC	Hexadecylpyridinium chloride
CTAB	Hexadecyltrimethyl ammonium bromide
CZA	Cellulose-Zn/Al layered double hydroxide nanocomposites
D-R	Dubinin-Radushkevich isotherm
DNA	Deoxyribonucleic acid
DLS	Dynamic light scattering
DMA	Dimethylarsinic acid
DS-TiO ₂	Activated carbon from date seeds modified by titanium dioxide
DW	Demineralized water
EDTA	Ethylenediaminetetraacetic acid
EDX	Energy-dispersive X-ray spectroscopy
EPA	Environmental protection agency
EU	European Union
FMCB	Fe-Mn binary oxide impregnated chitosan bead
FWHM	Full width at half maximum
FTIR	Fourier transform infrared spectroscopy
GFH	Granular ferric hydroxide
GW	Groundwater
HE	Heavy metal
HDTMA-Br	Hexadecyltrimethylammonium bromide
HDTMA-Cl	Hexadecyltrimethylammonium chloride
ID	Inner diameter
IO	Iron oxide nanoparticles

IO-CMS	Iron oxide-modified calcined mussel shells
ICP-MS	Inductively coupled plasma mass spectrometry
ICP-OES	Inductively coupled plasma optical emission spectroscopy
ICZ	Iron-coated zeolite
IARC	International agency for research on cancer
LDH	Layered double hydroxide
MF	Microfiltration
MIL	Metal–organic framework
MP	Powdered mussel shells cartridge
MD	Mussel shell-coated disc cartridge
MCL	Maximum contaminant level
MMA	Monomethylarsonic acid
NLP	Neem leaf powder
NOP	Natural orange peels
NZVI/AC	Nanoscale zero-valent iron supported by activated carbon
OD	Outer diameter
ODA	Octadecylamine acetate
OMICS	Magnetic ordered mesoporous Fe/Ce bimetal oxides
OP	Orange peels
OP-TiO ₂	Activated carbon from orange peels modified by titanium dioxide
PAC-500	Activated carbon from citrus limmeta fruit peel
PPAC-500	Activated carbon from citrus limmeta fruit pulp
pH _{pzc}	pH of the Point of zero charge
POE	Point of entry
PFO	Pseudo-first order

PSO	Pseudo-second order
RSM	Response surface methodology
RO	Reverse osmosis
SEM	Scanning electron microscopy
SHWS	Strong heart water study
SDG	Sustainable development goal
TDS	Total dissolved solids
TICB	TiO ₂ -impregnated chitosan bead
TLSB	Thiol-lignocellulose sodium bentonite nanocomposites
USEPA	United states environmental protection agency
UF	Ultrafiltration
UV	Ultraviolet
WHO	World health organization
XPS	X-ray photoelectron spectroscopy
XRD	X-ray diffraction
XRF	X-ray fluorescence
ZP	Zeta potential
ZIF-67-NB	Zeolitic imidazolate framework-67 (3D)
ZIF-67-NS	Zeolitic imidazolate framework-67 (2D)
ZVI	Zero-valent iron

List of variables:

AC	Adsorbent capacity
A _d	Adsorbent dose
<i>B</i>	Constant related to the heat of adsorption (Temkin isotherm)
<i>b</i>	Langmuir constant related to the energy of adsorption

C_i	Initial concentration
C_e	Equilibrium concentration of adsorbate in solution
C_t	Concentration of adsorbate in solution at time t
CV	Coefficient of variation
E	Adsorption energy derived from the Dubinin–Radushkevich isotherm
F	Flowrate
H	Bed height
k_1	Rate constant for pseudo-first-order kinetic model
k_2	Rate constant for pseudo-second-order kinetic model
k_c	Thermodynamic equilibrium constant.
k_f	Freundlich adsorption constant
k_{id}	Intraparticle diffusion rate constant
k_t	Kinetic constant in Temkin model
k_{Th}	Thomas rate constant
k_{YN}	Yoon-Nelson rate constant
M	Adsorbent mass
n	Freundlich intensity parameter
OY	Oxidation yield
q_0	Maximum adsorption capacity of the column
q_e	Amount of adsorbate adsorbed per unit mass of adsorbent at equilibrium
q_m	Maximum adsorption capacity of the adsorbent
q_t	Amount of adsorbate adsorbed per unit mass of adsorbent at time t
R	Universal gas constant
R^2	Coefficient of Determination

RE	Removal efficiency
RT	Room Temperature
t_c	Contact time
W	Mass
V	Volume
α	Initial adsorption rate in Elovich model
β	Desorption constant in Elovich model
β_0	Intercept term in quadratic regression model
β_i	Linear coefficients in quadratic regression model
β_{ij}	Quadratic coefficients in quadratic regression model
β_{ii}	Interaction coefficients in quadratic regression model
x_i, x_j	Independent variables (coded factors)
ϵ	Polanyi potential in the Dubinin–Radushkevich isotherm
ΔS^0	Standard entropy change
ΔH^0	Standard enthalpy change
ΔG^0	Standard Gibbs free energy change
τ	The time at which the concentration of the adsorbate in the effluent reaches 50% of its initial concentration

CHAPTER ONE

INTRODUCTION

1.1. Research Background

With a growing population, the need for clean drinking water has intensified. To address this, the United Nations' Sustainable Development Goal 6 aims to ensure sustainable water and sanitation for all by 2030 (Water, 2021). Over 2.5 billion individuals worldwide depend on groundwater for their drinking water needs. Delivering high-quality drinking water has emerged as a significant challenge for human society (Shaji et al., 2021). Access to safe drinking water is a fundamental human right (Winkler, 2017), yet groundwater contamination, arising from various sources, is a global issue, often resulting in water exceeding the prescribed limits set by the World Health Organization (WHO) and becoming non-potable (Shaji et al., 2021).

Groundwater contamination by arsenic, at concentrations surpassing 10 ppb, impacts approximately 108 nations (32 in Asia, 31 in Europe, 20 in Africa, and 20 in North and South America). The threat of arsenic poisoning affects more than 230 million individuals globally (Shaji et al., 2021).

About 3 million people in Canada rely on a private well for their drinking water (Health Canada, 2019). Limited information is available regarding the extent of the Canadian population exposed to groundwater arsenic concentrations surpassing the national drinking water guidelines of 10 $\mu\text{g L}^{-1}$. However, documented evidence indicates that naturally occurring arsenic concentrations exceeding these guidelines prevail in all provinces and one territory (Chappells et al., 2014). The analysis involved measuring arsenic levels in 10,498 private wells in Nova Scotia, sampled between 1991 and 1999. The highest recorded arsenic concentration in these private wells was 3900

$\mu\text{g L}^{-1}$, with 17% of the wells exceeding the Health Canada Maximum Allowable Concentration (MAC) of $10 \mu\text{g L}^{-1}$ for arsenic (Chappells et al., 2014). In the Southern Oil Sand Regions of Alberta, elevated concentrations of arsenic (As) up to $179 \mu\text{g L}^{-1}$ have been detected in shallow groundwater. A survey conducted on more than 800 water wells in the region revealed that 50% of these wells had arsenic concentrations surpassing the recommended drinking water guidelines of $10 \mu\text{g L}^{-1}$ (Chappells et al., 2014). In the western part of Quebec, Canada, water samples from 59 private wells were collected and the findings indicate that over 50% of the bedrock wells in the area surpass the Canadian guideline value of $10 \mu\text{g L}^{-1}$ for arsenic (Chappells et al., 2014).

About 85% of Newfoundland and Labrador (NL) residents rely on public drinking water systems, managed by various entities. The remaining 15% use private systems, with around 30,000 drilled wells and an equal number of dug wells. There are over 1,000 water supplies for semi-public systems, including 600 year-round facilities and the rest are seasonal (Environment and Climate Change, 2023). Recent studies indicate alarming levels of arsenic in drinking water in various regions of NL, particularly in remote and underserved communities. The Department of Environment recently shared the first set of results from its free well testing program for private wells, which was announced last year. Out of just over 1,000 test results, they found that 112 wells had arsenic levels above 10 parts per billion, the limit set by Health Canada and WHO (Mullin, 2023b). Figure 1-1 displays the regions in Newfoundland and Labrador where arsenic is present, further highlighting the localized crisis and the immediate need for intervention. Chronic exposure to arsenic poses significant health risks, including various cancers and disorders of the cardiovascular and nervous systems (Minatel et al., 2018).

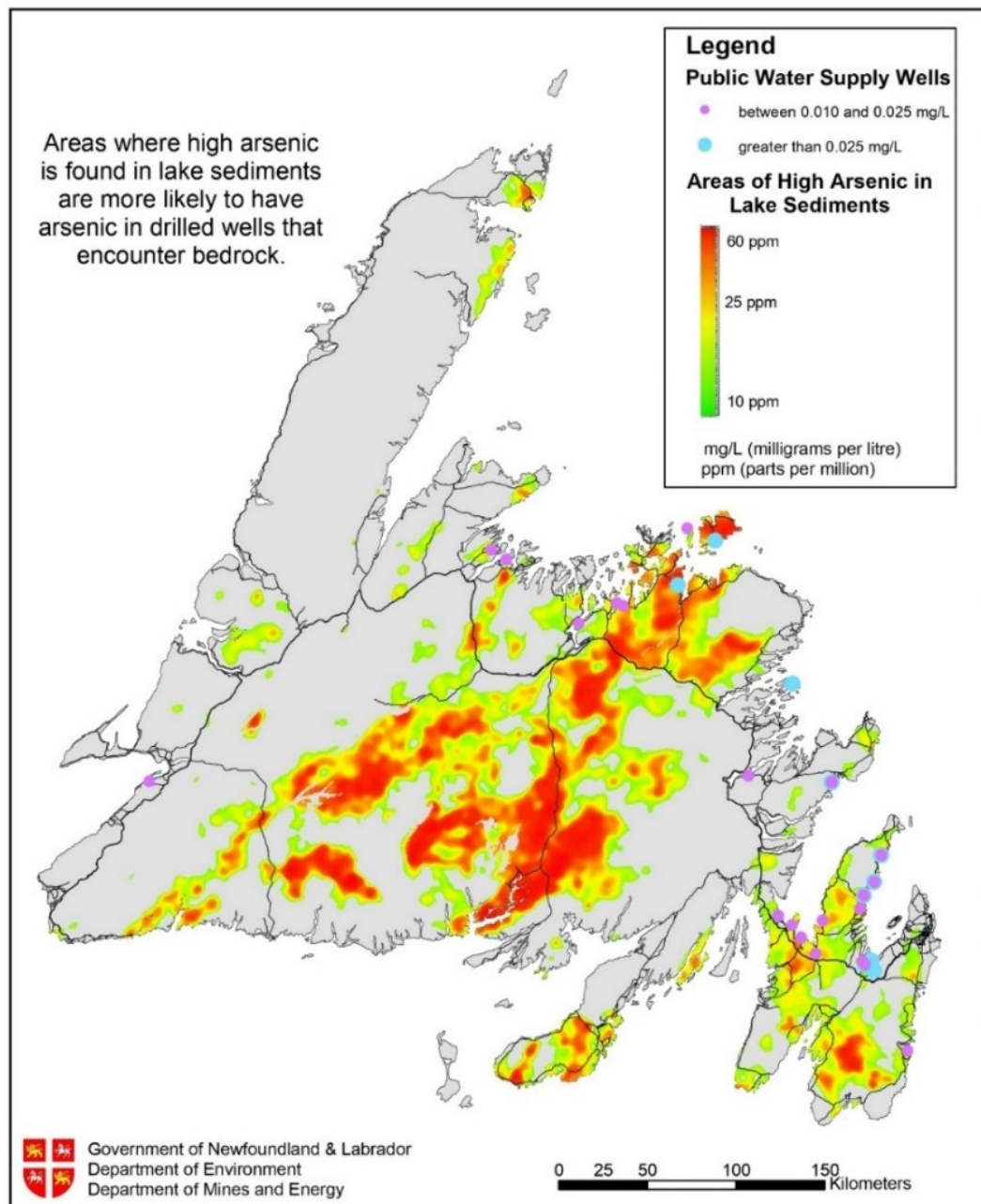


Figure 1-1 Areas of potential arsenic concentration in well water (Change, 2010).

To address this growing concern, our proposed solution centers around point-of-use (POU) systems and decentralized water treatment, which enable communities to treat arsenic-contaminated water at the household level. This approach bypasses the need for costly and complex centralized infrastructure, providing an affordable and practical solution, especially for small or underserved communities. By incorporating

these systems, the water can be treated directly at the point of consumption, ensuring immediate access to safe drinking water. In addressing the arsenic contamination crisis in some NL communities, this thesis focuses on the innovative use of mussel shells, an abundant waste product in the region. NL's aquaculture industry produces a substantial amount of mussel shells annually, and repurposing this waste material not only addresses environmental concerns but also creates a cost-effective solution tailored to the region's specific challenges.

Global fisheries and aquaculture production grew 41% from 2000 to 2019, reaching 178 million tons in 2019 (Topić Popović et al., 2023). More than 10 million tons of mollusk (any of a large phylum of invertebrate animals such as snails, clams, and octopuses with a soft body lacking segments and usually enclosed in a shell containing calcium) shells are produced yearly, with over 70% coming from oyster, clam, scallop, and mussel shells (Topić Popović et al., 2023). Mussels, in particular, have experienced the greatest increase in production and shell contribution compared to other shellfish species (Topić Popović et al., 2023). Mussel shells comprise 56% to 61% of their total weight, and calcium carbonate makes up about 94% of that shell weight (Hamester et al., 2012; Ituen, 2015).

In addition to shellfish waste, agricultural byproducts such as orange peels offer considerable potential for environmental remediation. Orange peels, comprising 50–60% of the fruit's mass, are a major byproduct of the citrus industry and present a significant waste management challenge. Rich in pectin, cellulose, and hemicellulose, they are well-suited for conversion into biochar for environmental applications (Ayala et al., 2021). In 2022-2023, global orange production reached 46.88 million metric tons, generating about 23–28 million metric tons of peel waste. Improper disposal methods like incineration and dumping lead to pollution and health risks (Koiri & Das, 2024).

Utilizing orange peels for biochar production offers a sustainable path for waste valorization and water remediation. Like orange peels, date seeds represent an abundant yet underutilized fruit processing waste with a strong potential for conversion into effective adsorbents.

Various adsorbents, including activated carbon, metal oxides, and biochar, have been extensively studied to remove arsenic and other heavy metals from water. However, many of these materials are expensive to produce or require complex processing, limiting their applicability in low-resource or rural settings. This highlights the necessity of developing low-cost, sustainable adsorbents that can be sourced from abundant waste materials and applied in decentralized water treatment systems. Although mussel shells and other agricultural wastes have shown promise as alternative adsorbents, several research gaps remain. Existing studies on mussel shells have largely been limited to batch experiments with synthetic solutions, offering limited insight into their performance under realistic conditions, such as continuous flow systems and real water matrices. Furthermore, the regeneration potential and long-term stability of mussel shell-based adsorbents remain underexplored, particularly in point-of-use (POU) applications tailored for decentralized treatment in rural or remote communities. Additionally, few studies have directly compared the effectiveness of such adsorbents against commercially available alternatives within practical filtration systems.

This research addresses critical gaps in the existing literature by developing and optimizing low-cost adsorbents derived from mussel shells and agricultural wastes, such as orange peels and date seeds. These materials were modified with nanoparticles to enhance adsorption efficiency and evaluated through batch and column experiments using real groundwater. Unlike many studies that focused solely on synthetic solutions and laboratory-scale tests, this work incorporates continuous flow experiments. It

further examines the adsorbents' performance in practical point-of-use (POU) filtration systems specifically designed for rural and remote Newfoundland and Labrador (NL) communities.

The novelty of this research lies in its unique use of aquaculture waste, mussel shells from NL's fisheries sector, combined with nanopowder modification to enhance surface reactivity. Furthermore, the study goes beyond laboratory evaluation by integrating the modified adsorbent into a cartridge-based POU system, demonstrating its real-world applicability. POU systems offer localized, decentralized treatment options that eliminate the need for costly centralized infrastructure. Compact, user-friendly, and affordable, they are particularly well-suited for small communities with limited resources. By utilizing local waste materials and targeting real water quality challenges, this research provides a sustainable and accessible solution for arsenic contamination in drinking water.

This thesis addresses the urgent need for sustainable and accessible solutions to arsenic contamination in drinking water for vulnerable communities worldwide.

1.2. Statement of Research Problem

(1) Limited research on waste-derived adsorbents for arsenic and copper removal

Although some prior studies have been conducted on this mussel shell's application, they were insufficient overall. Only a few recent publications have examined the use of mussel shells for the removal of heavy metals from solution (Bremner et al., 2020; Q. Wang et al., 2021); other studies have examined the use of mussel shells for the removal of phosphates (Salim et al., 2020) and dyes (El Haddad, 2016). To determine the efficiency of this material, more research is needed on the

properties of mussel shells, as well as their capacity and methods for adsorbing metals from solution. Modifying the calcined mussel shell might increase the efficiency of arsenic removal, which has rarely been investigated.

Furthermore, there is limited research on using agricultural waste-based adsorbents, such as orange peels and date seeds, particularly when modified with metal oxide nanoparticles for enhanced performance. Their potential to remove arsenic and other priority contaminants like copper remains underexplored.

(2) Water contamination in rural communities in Newfoundland

According to the World Health Organization (2015), approximately 663 million people globally lack access to sufficient drinking water resources (Supply & Programme, 2015). The inaccessibility to clean water has been a major challenge in Newfoundland for most remote areas. In NL, around 200 drinking water advisories (DWAs) are imposed each year, with long-term boil water advisories (BWAs) lasting for five years or more being quite prevalent (Jones-Bitton et al., 2015). Samples collected on August 25, 2022, from the new housing area in Chance Cove indicated an arsenic concentration of $30 \mu\text{g L}^{-1}$. In comparison, samples from freshwater on January 24, 2015, revealed an arsenic level of $42 \mu\text{g L}^{-1}$ (Newfoundland and Labrador Water Resources Portal, n.d.). Groundwater samples were collected from the towns of Wabanahad, which had an arsenic concentration of $62.7 \mu\text{g L}^{-1}$ (Coles & Rohail, 2020). Drinking arsenic-contaminated water has resulted in increased occurrence of diseases such as bladder, liver, skin, and lung cancers, cardiovascular disease, and hypertension, posing a major obstacle to a better standard of living (Sarkar et al., 2015). Addressing water quality challenges is not just a necessity but a fundamental step toward improving public health and ensuring a better standard of living for affected communities.

(3) Abundant of fisheries waste and agro-waste

The fishing sector stands as a primary industry in NL (James, 2022). In 2022, the aquaculture production volume reached approximately 12,978 tonnes, with a corresponding market value of \$127 million. The shellfish aquaculture sector in NL consists mainly of blue mussels and American oysters, totaling 4,746 tonnes in 2022 and having a market value of \$23 million. Among these, blue mussels contribute significantly to shellfish production (Resources), 2022). However, the fish processing sector generates a substantial quantity of by-products, ranging from 25% to 70%, constituting a significant form of waste (Caruso et al., 2020). For every tonne of fish consumed, an equivalent amount of fish waste is discarded through either ocean dumping or land disposal (Ahuja et al., 2020). Recognizing the environmental impact, it is imperative to emphasize the necessity of implementing effective waste recycling practices in the fishing and aquaculture industry.

Similarly, large volumes of agricultural waste—such as fruit peels and seeds—are generated globally, yet remain underutilized and often contribute to environmental pollution through improper disposal. In particular, orange peels and date seeds represent promising renewable resources for value-added applications in environmental remediation.

(4) Cost constraints: The challenges of traditional adsorbents in water treatment

Traditional water treatment methods often rely on expensive adsorbents, limiting accessibility, especially in developing countries or underserved communities. However, waste materials such as agricultural residues, industrial by-products, and municipal solid waste, which are abundantly available, could serve as low-cost adsorbents for water treatment. Repurposing waste materials into adsorbents can reduce the cost of

water treatment and environmental pollution resulting from the accumulation of these wastes. Furthermore, utilizing waste materials as adsorbents promotes circular economy principles, as it adds value to waste materials that would otherwise be discarded.

1.3. Objectives of the Study

This research aims to develop, characterize, and evaluate an efficient, cost-effective, flexible, sustainable, and environmentally friendly adsorbent for removing heavy metals from water. Specifically, the research will evaluate the efficacy of modified mussel shells and agricultural waste for arsenic removal in water-based solutions, such as orange peels and date seeds. More specifically, this thesis aims to:

1. Investigate and evaluate the potential of modified mussel shells as an effective adsorbent for removing arsenic from water and compare their removal efficiency under different conditions.
2. Investigate the performance of the developed adsorbent in packed bed columns to determine its exhaustion capacity, a key parameter for practical application in water treatment.
3. Assess the potential of agricultural waste as an adsorbent for removing other heavy metals, such as copper and arsenic.
4. Evaluate the use of mussel shells in a point-of-use (POU) water filtration system to determine its arsenic removal effectiveness and assess its performance in the presence of co-ions, which may affect its adsorption capacity.
5. Investigate the factors influencing the adsorption of arsenic onto mussel shells, focusing on the role of functional groups, the impact of ionic strength, and the correlation between surface charges and arsenic adsorption efficiency. By conducting experiments with modified shells, varying ionic strength, and

measuring surface charge density, we seek to understand the underlying mechanisms and optimize the efficiency of arsenic adsorption onto mussel shells for potential application in water treatment.

1.4. Organization of Thesis

This thesis investigates the use of waste-derived adsorbents for sustainable water treatment. Chapter one introduces the research, outlining the thesis's background, motivation, problem, objectives, and structure. Chapter two reviews the literature on arsenic contamination, conventional treatments, adsorption, and renewable adsorbents. Chapter three focuses on developing and characterizing mussel shell adsorbents, including batch arsenic adsorption studies. Chapter four examines their continuous flow performance, co-ion effects, and reusability, discussing factors like flow rate, adsorbent mass, and initial concentration. Chapter five explores orange peel adsorbents for arsenic removal, including characterization and batch results. Chapter six investigates copper adsorption using orange peel- and date seed-derived adsorbents, focusing on optimization and kinetics. Chapter seven summarizes key findings, contributions, and future work recommendations. Figure 1-2 outlines the thesis structure.

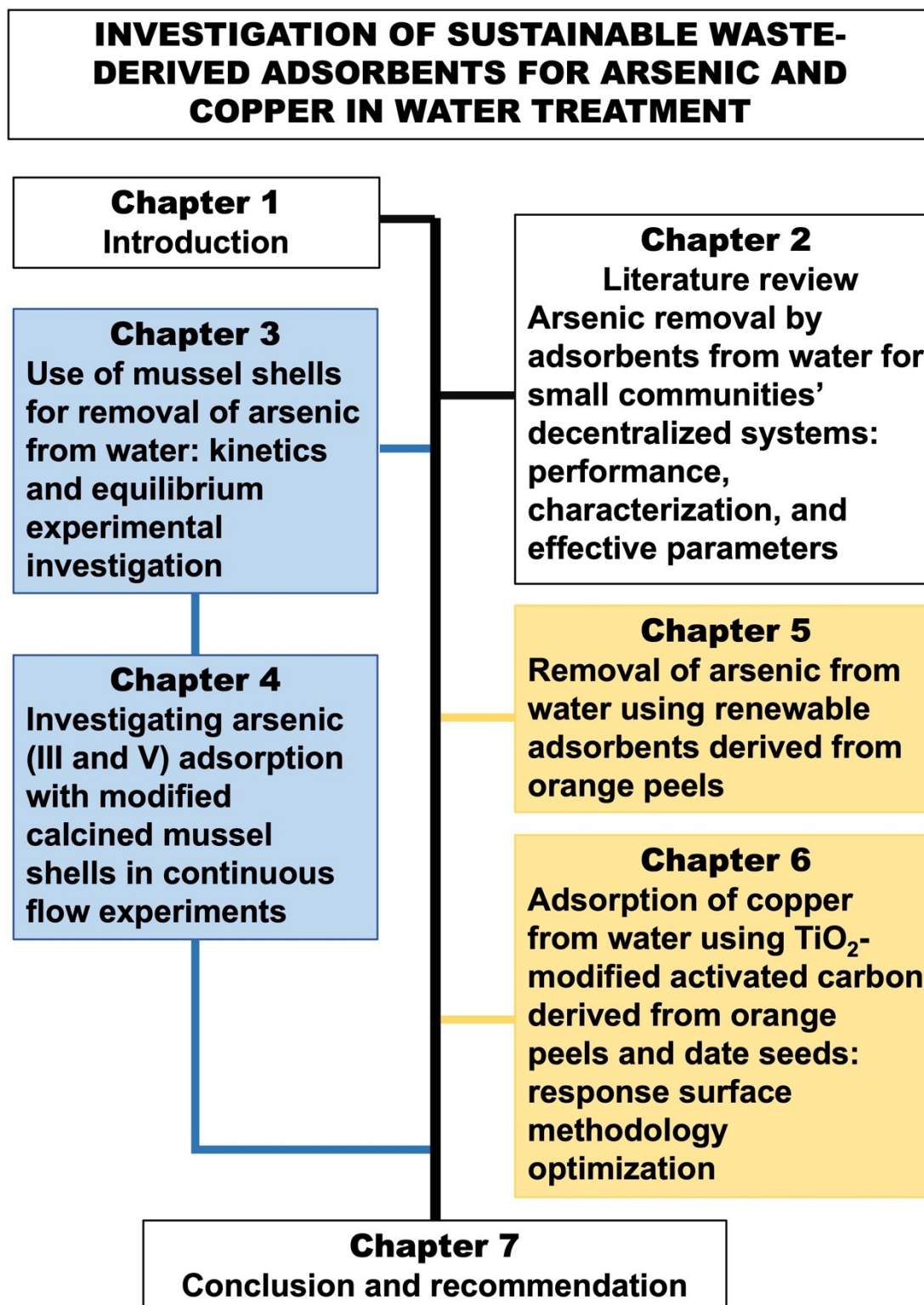


Figure 1-2 Organization of the thesis.

1.5. References

- Ahuja, I., Dauksas, E., Remme, J. F., Richardsen, R., & Løes, A.-K. (2020). Fish and fish waste-based fertilizers in organic farming—With status in Norway: A review. *Waste Management*, *115*, 95–112.
- Ayala, J. R., Montero, G., Coronado, M. A., García, C., Curiel-Alvarez, M. A., León, J. A., Sagaste, C. A., & Montes, D. G. (2021). Characterization of orange peel waste and valorization to obtain reducing sugars. *Molecules*, *26*(5), 5.
<https://doi.org/10.3390/molecules26051348>
- Bremner, C., Cochrane, T. A., McGuigan, P., & Bello-Mendoza, R. (2020). Removal of dissolved heavy metals from stormwater by filtration with granular recycled glass and mussel shell with and without microalgae biofilm. *Environmental Technology & Innovation*, *18*, 100662.
- Caruso, G., Floris, R., Serangeli, C., & Di Paola, L. (2020). Fishery wastes as a yet undiscovered treasure from the sea: Biomolecules sources, extraction methods and valorization. *Marine Drugs*, *18*(12), 622.
- Department of Environment and Climate Change, Government of Newfoundland and Labrador. (2010). *Arsenic in Well Water*.
- Chappells, H., Parker, L., Fernandez, C. V, Conrad, C., Drage, J., O'Toole, G., Campbell, N., & Dummer, T. J. B. (2014). Arsenic in private drinking water wells: an assessment of jurisdictional regulations and guidelines for risk remediation in North America. *Journal of Water and Health*, *12*(3), 372–392.
- Coles, C. A., & Rohail, D. (2020). Effect of aeration, iron and arsenic concentrations, and groundwater matrix on arsenic removal using laboratory sand filtration. *Environmental Geochemistry and Health*, *42*(11), 4051–4064.
- El Haddad, M. (2016). Removal of Basic Fuchsin dye from water using mussel shell

- biomass waste as an adsorbent: Equilibrium, kinetics, and thermodynamics. *Journal of Taibah University for Science*, 10(5), 664–674.
- Government of Newfoundland and Labrador. (n.d.). Water resources portal. <https://www.gov.nl.ca/ecc/waterres/portal/>. [Accessed: Dec. 11, 2024]
- Hamester, M. R. R., Balzer, P. S., & Becker, D. (2012). Characterization of calcium carbonate obtained from oyster and mussel shells and incorporation in polypropylene. *Materials Research*, 15, 204–208.
- Health Canada. (2019). *Be Well Aware: Information for private well owners - Canada.ca*. Government of Canada. <https://www.canada.ca/en/health-canada/services/publications/healthy-living/water-talk-information-private-well-owners.html>
- Iuen, E. U. U. (2015). Mechanical and chemical properties of selected mullusc shells in Nigeria. *International Journal of Agricultural Policy and Research*, 3(1), 53–59.
- James, L. (2022). *Recycling Solutions for End-of-Life Fishing Rope in Newfoundland*.
- Jones-Bitton, A., Gustafson, D. L., Butt, K., & Majowicz, S. E. (2015). Does the public receive and adhere to boil water advisory recommendations? A cross-sectional study in Newfoundland and Labrador, Canada. *BMC Public Health*, 16, 1–7.
- Koiri, P., & Das, S. (2024). Agri-Food Waste Management and Treatment Approaches for Environmental Sustainability. In *Environmental Engineering and Waste Management: Recent Trends and Perspectives* (pp. 343–373). Springer.
- Minatel, B. C., Sage, A. P., Anderson, C., Hubaux, R., Marshall, E. A., Lam, W. L., & Martinez, V. D. (2018). Environmental arsenic exposure: From genetic susceptibility to pathogenesis. *Environment International*, 112, 183–197.

- Mullin, M. (2023). *No Title*. CBC News.
- <https://www.cbc.ca/news/canada/newfoundland-labrador/arsenic-test-results-1.6920066>
- Government of newfoundland and labrador (Fisheries and L. (2022). *Seafood industry review*. <https://www.gov.nl.ca/ffa/files/publications-pdf-syir-2017.pdf>
- Salim, N. A. A., Puteh, M. H., Yusoff, A. R. M., Abdullah, N. H., Fulazzaky, M. A., Rudie Arman, M. A. Z., & Zainuddin, N. A. (2020). Adsorption isotherms and kinetics of phosphate on waste mussel shell. *Malaysian Journal of Fundamental and Applied Sciences*, 16(3), 393–399.
- Sarkar, A., Hanrahan, M., & Hudson, A. (2015). Water insecurity in Canadian Indigenous communities: some inconvenient truths. *Rural and Remote Health*, 15(4), 181–193.
- Shaji, E., Santosh, M., Sarath, K. V., Prakash, P., Deepchand, V., & Divya, B. V. (2021). Arsenic contamination of groundwater: A global synopsis with focus on the Indian Peninsula. *Geoscience Frontiers*, 12(3), 101079.
- Supply, W. J. W., & Programme, S. M. (2015). *Progress on sanitation and drinking water: 2015 update and MDG assessment*. World Health Organization.
- Topić Popović, N., Lorencin, V., Strunjak-Perović, I., & Čož-Rakovac, R. (2023). Shell waste management and utilization: Mitigating organic pollution and enhancing sustainability. *Applied Sciences*, 13(1), 623.
- Wang, Q., Jiang, F., Ouyang, X.-K., Yang, L.-Y., & Wang, Y. (2021). Adsorption of Pb (II) from aqueous solution by mussel shell-based adsorbent: Preparation, characterization, and adsorption performance. *Materials*, 14(4), 741.
- Water, U. N. (2021). *Progress on change in water-use efficiency: Global status and acceleration needs for SDG indicator 6.4. 1, 2021*. Food & Agriculture Org.

Winkler, I. T. (2017). The human right to water. In *Routledge handbook of water law and policy* (pp. 109–119). Routledge.

CHAPTER TWO

ARSENIC REMOVAL BY ADSORBENTS FROM WATER FOR SMALL COMMUNITIES' DECENTRALIZED SYSTEMS: PERFORMANCE, CHARACTERIZATION, AND EFFECTIVE PARAMETERS¹

Roya Sadat Neisan¹, Noori M. Cata Saady¹, Carlos Bazan², Sohrab Zendehboudi³, Abbas Al-nayili⁴, Bassim Abbassi⁵ and Pritha Chatterjee⁶

¹ Department of Civil Engineering, Memorial University, St. John's, NL A1B 3X5, Canada

² Faculty of Business Administration, Memorial University, St. John's, NL A1B 3X5, Canada

³ Department of Process Engineering, Memorial University, St. John's, NL A1B 3X5, Canada

⁴ Chemistry Department, College of Education, University of Al-Qadisiyah, Al Diwaniyah 58001, Iraq

⁵ College of Engineering and Physical Sciences, School of Engineering, University of Guelph, Guelph, ON N1G 2W1, Canada

⁶ Department of Civil Engineering, Indian Institute of Technology Hyderabad, Kandi 502285, India

Abstract

Arsenic (As), a toxic and carcinogenic heavy metal, poses risks to human health and the environment. While various technologies can remove As from drinking water, adsorption stands out as a reliable, affordable, and eco-friendly solution for decentralized water treatment systems (DWTS) in small communities and households. Sustainable low-cost adsorbents further enhance its appeal. This review covers As species classification, toxicity, and treatment methods, including ion exchange, membrane technologies, coagulation-flocculation, oxidation, and adsorption. It compares kinetic and isotherm models for As adsorption, explores characterization techniques, and evaluates key parameters such as pH, temperature, initial concentration, dosage, and contact time. The findings highlight adsorption as a cost-effective and promising solution, with locally developed adsorbents offering sustainable options for DWTS.

¹ This chapter has been published as a peer-reviewed journal article:

Neisan, R. S., Saady, N. M. C., Bazan, C., Zendehboudi, S., Al-nayili, A., Abbassi, B., & Chatterjee, P. (2023). Arsenic removal by adsorbents from water for small communities' decentralized systems: Performance, characterization, and effective parameters. *Clean Technologies*, 5(1), 352-402. <https://doi.org/10.3390/cleantechnol5010019>

2.1. Introduction

Heavy metals such as arsenic, copper, cadmium, nickel, mercury, cobalt, lead, and chromium are a group of metals with specific densities over 5 g cm^{-3} (Z. Li et al., 2014). They are widely used in industrial, agricultural, and technological applications. The most significant environmental pollution of heavy metals is from metal-based industries such as mining and metal casting (Tchounwou et al., 2012).

Heavy metals, which are extremely soluble in water and non-degradable, occur as free ions or are bound in chemical compounds in surface and groundwater. Dissolved heavy metals can interfere with microbial processes and impair aquatic life (Karcioglu & Arslan, 2019). Organisms consume heavy metals and incorporate them into the food chain, where they accumulate and impose detrimental effects on health. Short overexposure. chronic exposure to heavy metals can impair vital organs and neurological systems and kill the organism (H. K. An et al., 2001). Arsenic (As), cadmium (Cd), chromium (Cr), and nickel (Ni) are carcinogenic. They cause the mutation, deletion, or oxidative damage of deoxyribonucleic acid (DNA) (Tchounwou et al., 2012). Figure 2-1 is a schematic of the consequences of exposure to heavy metals.

Heavy metals in drinking water come from either natural geological sources or industrial activities (H. K. An et al., 2001). The application of various standard methods, including chemical precipitation, evaporation, ion exchange, electrolysis, and reverse osmosis, has been investigated to remove heavy metals from drinking water. However, the search continues for cheaper, more efficient, and environmentally friendly methods (Chakraborty et al., 2022).

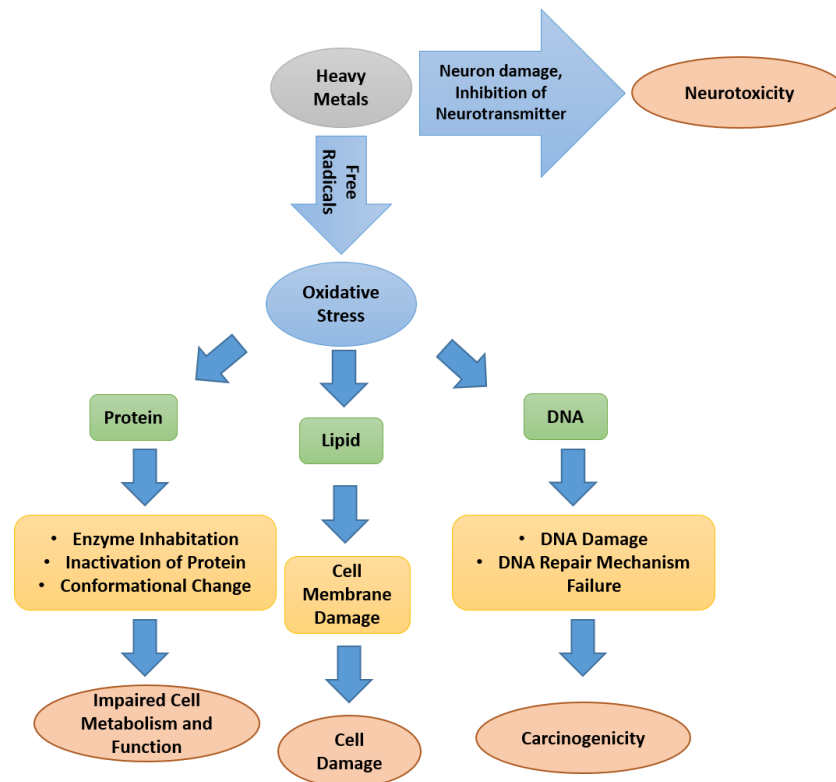


Figure 2-1 Toxicity mechanisms of heavy metals (adopted from Karcioğlu & Arslan (2019)).

2.2. Arsenic

Among the heavy metals, As is toxic and carcinogenic; thus, its inhalation and ingestion pose a cancer risk. Arsenic poses maximum adverse effects on human health through As-contaminated drinking water and the environment since As is a significant groundwater pollutant (Lata & Samadder, 2016). The World Health Organization (WHO) set the maximum allowable level of arsenic in drinking water at 10 ppb. Arsenic contamination in groundwater affects roughly 108 countries, with concentrations exceeding 10 ppb. About 32 countries in Asia, 31 in Europe, 20 in Africa, and 20 in North and South America suffer from As pollution. Arsenic poisoning threatens more than 230 million people worldwide (Shaji et al., 2021). Figure 2-2 shows the global extent of As contamination. Due to the poor water quality in rural areas, people living in small, rural, and remote communities suffer from health problems and diseases caused by dangerous pollutants such as As (Otgon et al., 2016). Even at low

concentrations, exposure to As increases the risk of cardiovascular disease and stroke (Al-Ali et al., 2011; K. Moon et al., 2012; K. A. Moon et al., 2013). In addition, As exposure can cause hypertension (Al-Ali et al., 2011), and As in drinking water can also cause liver damage and skin cancer (D. N. Guha Mazumder, 2005; Kunrath et al., 2013).

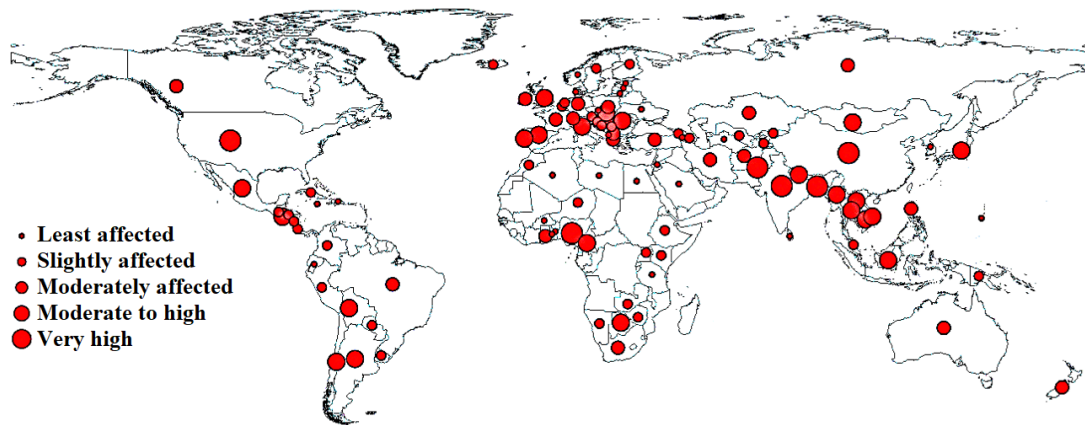


Figure 2-2 The global extent of arsenic contamination (adopted from Shaji et al. (2021)).

2.2.1. Arsenic occurrence

Arsenic concentrations increase in surface and groundwater because of mine and refinery wastes, wastewater sludge, agrochemicals, ceramic industries, and coal fly ash (Viraraghavan et al., 1999). Weathering, erosion of rocks/soils, and volcanic emissions are all natural sources of As in aqueous systems. Naturally, arsenic exists in about 200 different mineral forms. The percentages of these forms are 60% as arsenates, 20% as sulfides and sulfosalts, and 20% as arsenide, arsenite, oxides, silicates and elemental arsenic (Lata & Samadder, 2016). Arsenic is found in water in inorganic (arsenite, arsenate) and organic (methyl and dimethyl arsenic compounds) forms (Smedley & Kinniburgh, 2002). Table 2-1 provides the most common As species in the environment.

Dissolved As usually has an oxidation state of +III (arsenite) and +V (arsenate).

Removing As(V) is easier than removing As(III) because As(III) has to be oxidized to As(V) in the early stage of the removal process (Bissen & Frimmel, 2003b).

Table 2-1 The most common arsenic species in the environment environment (adapted from Chungang & Le (2009)).

Name	Chemical Formula
Arsenous acid (arsenite)	H_3AsO_3
Arsenic acid (arsenate)	H_3AsO_4
Monomethylarsenic acid	$CH_3AsO(OH)_2$
Dimethylarsinic acid	$(CH_3)_2AsO(OH)$
Trimethylarsine oxide	$(CH_3)_2AsO$
Trimethylarsoniopropionate	$(CH_3)_3As^+CH_2CH_2COO^-$
Arsenobetaine	$(CH_3)_3As^+CH_2COOH^-$
Arsenocholine	$(CH_3)_3As^+CH_2CH_2OH^-$
Dimethylarsinyolacetic acid	$(CH_3)_2AsOCH_2COOH$
Phenylarsine oxide	C_6H_5AsO
Phenylarsonic acid	$C_6H_5AsO(OH)_2$

2.2.2. Arsenic structure

As is listed as the 33rd element on the periodic table and belongs to Group 15 (the nitrogen family). It has an atomic mass of 74.92 and an atomic number of 33. Arsenic-75 (^{75}As) has 33 protons and 42 neutrons inside its nucleus; 33 electrons in various energy shells surround the nucleus. Arsenic-75 is the most stable and non-radioactive isotope of As. With an empty p orbital available for electron occupation and five valence electrons allowing As to engage in chemical bonding, the electronic configuration of the stable As form can be represented as $1s^2 2s^2 2p^6 3s^2 3p^6 3d^{10} 4s^2 4p^3$ (Flora, 2015).

The electrons contained in the first, second and third shells of arsenic atom are 2, 8, and 18, respectively, and only five electrons occupy the fourth shell. Arsenic has four common redox states: 3, 0, +3, and +5. Placing three more electrons in the p orbital brings the total number of electrons in this orbital up to six and creates an oxidation state of 3. The elemental arsenic forms a trigonal pyramidal structure by sharing three

electrons in the 4p orbital equally with the three arsenic atoms around it (Flora, 2015; O'Day, 2006).

Arsenic has a higher electronegativity than nitrogen and is similar to phosphorus. Compared to nitrogen and phosphorus, As has a greater oxidation potential, allowing it to easily show the +3 and +5 oxidation states. These variable oxidation states allow As to form covalent compounds with various elements, but in nature, it most frequently bonds to oxygen and sulfur. By sharing its valence electrons, As can display ligands characteristics and occupy electrons in bonding and antibonding orbitals. Thus, arsenic can change from an electropositive to an electronegative state (metal arsenides). It can react with methyl groups to create organic molecules in both oxidation states. Monomethylarsonic acid and dimethylarsinic acid are two typical organic forms of As. However, compared to inorganic forms, they are less common in nature (Flora, 2015; Mohanty, 2017).

2.2.3. Arsenic oxidation and reduction

Redox potential and pH levels significantly impact the oxidation and reduction of As. When naturally occurring in water sources, As is primarily present as the oxyanions of trivalent arsenite or pentavalent arsenate (Flora, 2015). An Eh-pH diagram can explain the effects of complexes, temperature, pressure, potential, and pH. The system is assumed to be in equilibrium with water, or the three components of water (H^+ (+1), O^{2-} (-2), and e^- (-1)), in all Eh-pH diagrams. Each of the areas in the diagrams shows a species that predominates there. While pH indicates the activity of the hydrogen ion (H^+), Eh shows the electrical potential relative to the standard hydrogen potential (SHE). The thermodynamically stable water region is usually represented by two diagonal dashed lines (H.-H. Huang, 2016).

In the system of As-O-H at 25 °C and 1 bar, Figure 2-3 shows the dominance of As

species. As(III), As(V), arsenious acids (H_3AsO_3 , $H_2AsO_3^-$, and $HAsO_3^{2-}$), and As acids (H_3AsO_4 , $H_2AsO_4^-$, $HAsO_4^{2-}$) are the main forms of As discovered in environmental samples. As behaves anionically in aquatic systems. Arsenate predominates under oxidizing conditions, either as the $H_2AsO_4^-$ at low pH (less than about 6.9) or as the $HAsO_4^{2-}$ at higher pH levels. At pH levels lower than about 9.2, the uncharged arsenite species H_3AsO_3 dominates in reducing conditions. As can exist as pentavalent oxyanions (arsenate) at moderate or high redox potentials (E_0 (V)= 0.56 V at 25 °C). These include H_3AsO_4 , $H_2AsO_4^-$, $HAsO_4^{2-}$, and AsO_4^{3-} (Aghaei et al., 2021; Rakhunde et al., 2012). Eqs. (2-1)–(2-6) are the dissociation reactions of H_3AsO_4 and H_3AsO_3 , as well as the associated equilibrium constants (Flora, 2015).

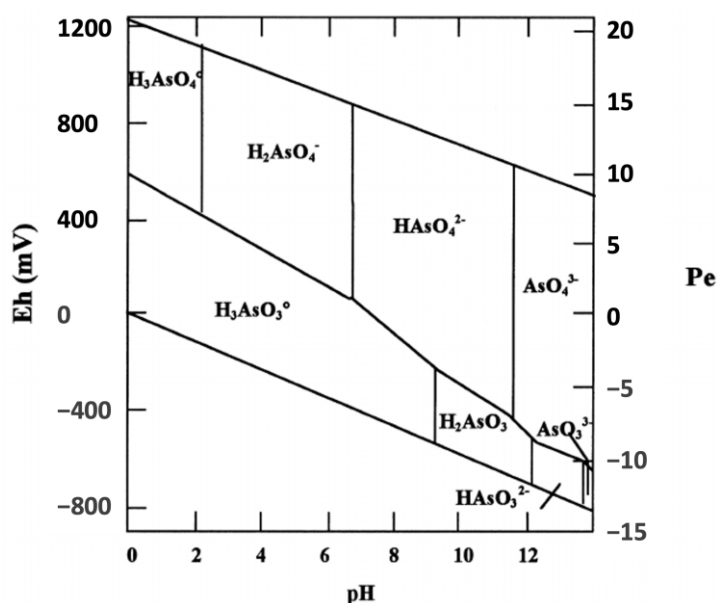
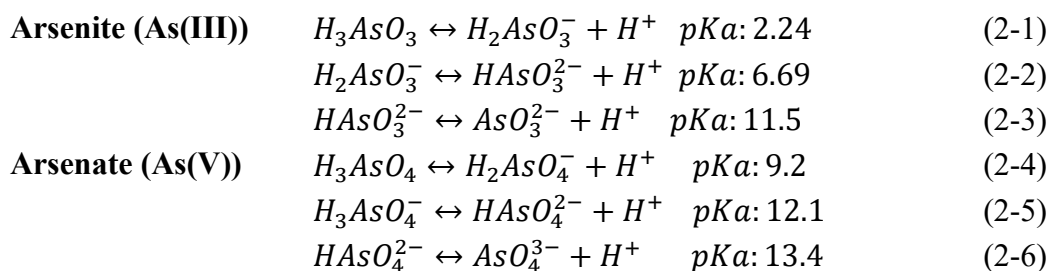


Figure 2-3 Eh–H diagram for aqueous arsenic species at 25 °C. (Reprinted from Smedley & Kinniburgh (2002) with Elsevier permission).

2.2.4. Arsenic treatment

Adsorption, coagulation-flocculation, ion exchange, electrochemical reduction, and membrane filtration technologies are currently available to remove As. Adsorption is frequently employed because, in comparison to the alternatives, it is more affordable and easier to implement in small, rural, and remote communities, and has higher efficiency. Adsorption is defined as the adhesion of ions or molecules to the surface of solid substances (the adsorbents) (Asere et al., 2019).

Many of the conventional adsorbents such as activated carbon, activated alumina, and iron oxide-based adsorbents are economically infeasible for small communities, particularly in developing countries. Hence, locally available natural adsorptive materials provide sustainable and affordable options for removing As pollution in developing countries and rural areas (Asere et al., 2019).

Adsorption is one of the most efficient and economical methods to eliminate As from a water-based solution (D. Guha Mazumder & Dasgupta, 2011; M. K. Mondal & Garg, 2017). The price of the adsorbent affects how much the procedure costs. (D. Guha Mazumder & Dasgupta, 2011). Some common As adsorbents are hydrous titanium dioxide (TiO_2) (Guan et al., 2012), iron oxides/hydroxides (Hao et al., 2018), synthetic zeolites (Shevade, 2003), activated carbon, and activated alumina (Camacho et al., 2015). Biomass, wastes, and industrial by-products are also used for As removal. Due to the toxicity of As, researchers are working to develop more rapid and cost-effective adsorbents compared to the current adsorbents. The development of nanoparticle-based adsorbents is attracting great attention because they offer a large surface area and a high tendency to adsorb As from water (Habuda-Stanić & Nujić, 2015). Metals and metal oxides, e.g., gold (Hua, 2021), titanium oxide (Guan et al., 2012), cupric oxide (Reddy et al., 2013), iron oxide (Hao et al., 2018), impregnated granulated activated carbon

(Kalaruban et al., 2019), and synthetic nanostructured Fe(III)– Cr(III) mixed oxides (Basu & Ghosh, 2011) have been used in As removal in different studies.

Recently, scientists have concentrated on converting waste materials into adsorbents for heavy metal removal from water because such adsorbents are low-cost and effective. However, there is still a need to develop low-cost, high-efficiency, and eco-friendly adsorbents targeting As removal based on material availability in different locations (Jageerani, 2017).

The primary goal of this work is to discuss the widely used options for removing As from drinking water and provide an appropriate starting point for new researchers who want to compare traditional heavy metal removal techniques. Despite its significance as a toxic water contaminant, few comprehensive reviews concentrate on removing As. Particularly, the number of review papers focusing on As removal in decentralized systems is very limited. This review paper aims to provide an overview of the recent development of decentralized drinking water treatment technologies and evaluate the feasibility of various methods, especially adsorption for small treatment systems. In the following sections, As removal methods (with a focus on adsorption) in decentralized water treatment systems and the most common adsorbents are explained and discussed, and their removal efficiencies are evaluated. Finally, several low-cost adsorbents are introduced as cost-effective substitutes for expensive ones.

2.3. Conventional Methods for Arsenic Removal from Aqueous Solutions in

Decentralized Systems Other than Adsorption

One of the problems facing community water treatment systems worldwide is the removal of pollutants, particularly pathogens and heavy metals, to provide clean drinking water; these pollutants put the local residents' health in danger (Bhowmik et

al., 2022). The contamination of groundwater has been reported in both developed (Canada, Japan, and USA) and underdeveloped (Bangladesh, China, and India) nations (Adelolu et al., 2021). Centralized water treatment plants have been essential to managing water supplies in highly populated areas. In centralized water treatment, reasonably high-quality water from various natural sources is treated before water is distributed and used. In contrast, in decentralized water management systems, water from local sources is collected and treated on a small scale (community level) or using a household filtration system (Gikas & Tchobanoglous, 2009; Zaharia, 2017).

The current centralized water treatment facilities cannot provide safe drinking water to millions worldwide (T. H. Nguyen et al., 2020). Some areas of developing countries do not have water infrastructure or reliable water sources. In developed countries, centralized systems face several difficulties, such as reaching their capacities due to population growth, excessive energy and water use due to the aging infrastructure, and downstream re-contamination (Qu et al., 2013). Decentralized water treatment is a suitable solution for households in rural and remote areas where the central water treatment system is unavailable, or in times of emergency, such as epidemic disease. A decentralized water system may also be more affordable due to the lower maintenance and transmission costs (Le et al., 2018). Various treatment methods, such as ion exchange, membrane technologies, and coagulation, are available in decentralized systems. Still, these methods' applications in small communities are limited because they usually require skilled operators, complicated maintenance, high-cost chemicals, and timely procedures (Nanseu-Njiki et al., 2019).

The market for decentralized water treatment was USD 21.45 billion in 2020 and was projected to increase at a compound annual growth rate (CAGR) of 10.70% from 2020 to 2026, reaching USD 39.48 billion (*Decentralized Water Treatment Market | Size,*

Growth | 2021-26, n.d.). Figure 2-4 demonstrates a detailed segmentation of the decentralized system industry. Household filtration units (including point-of-entry (POE) and point-of-use (POU) systems) and community filtration units are two main approaches to providing clean water for communities and rural areas (Figure 2-5) (Kabir & Chowdhury, 2017). Point-of-entry (POE) systems are installed at the location where the water enters the building and is constantly treated for the entire house. In contrast, the point-of-use (POU) systems are installed before a single outlet, such as a kitchen sink tap, to eliminate impurities in drinking water (Nalbandian et al., 2022). Small-scale systems or community filtration units are smaller in size than centralized systems but larger than POU or POE systems. Typically, small-scale systems treat the water used by several households or a community (A. S. C. Chen et al., 2020).

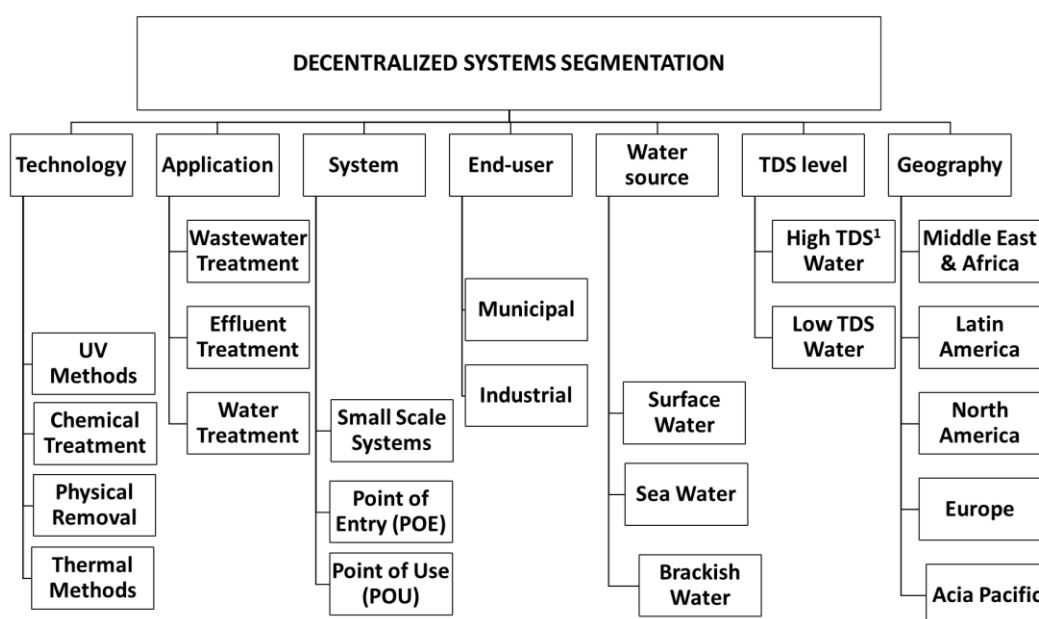


Figure 2-4 Detailed segmentation of decentralized treatment systems (*Decentralized Water Treatment Market | Size, Growth | 2021-26, n.d.*). TDS: totals dissolved solids.

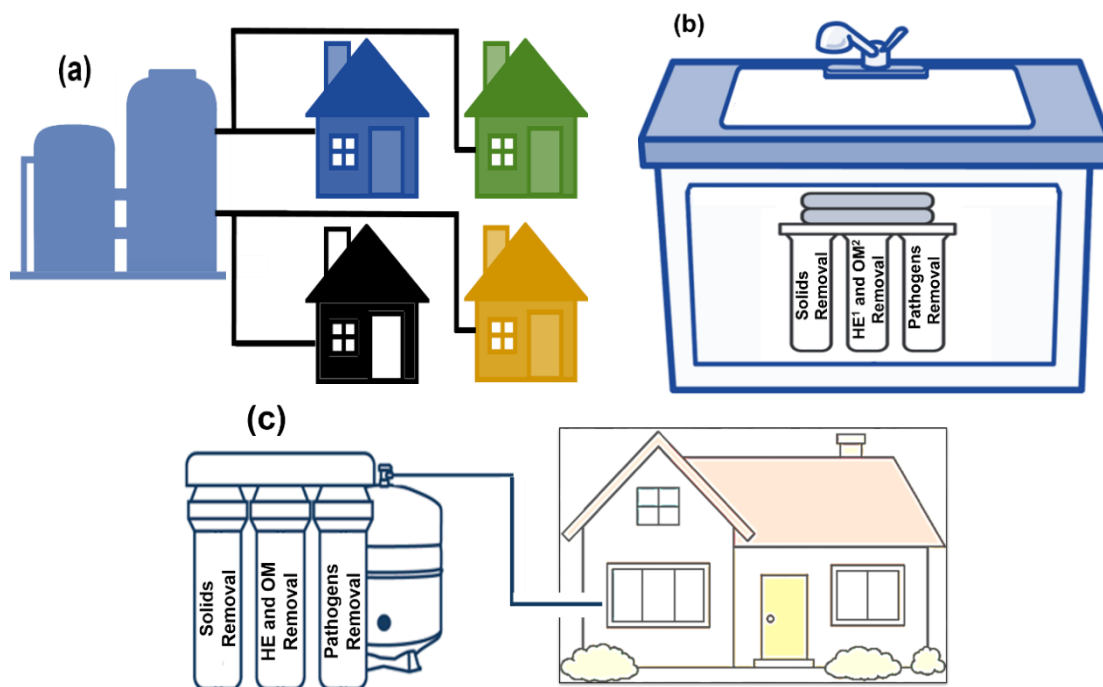


Figure 2-5 (a) Small-scale (community) water treatment system, (b) Point-of-use (POU) system, and (c) Point-of-entry (POE) system. HE: heavy metals; OM: organic matter.

2.3.1. Ion exchange

Ion exchange is a chemical reaction that removes dissolved metal ions from the solution and replaces them with other similarly charged ions (Sarode et al., 2019). It has been used for a long time to soften and demineralize water and eliminate nitrate and other water treatments (Al-Asheh & Aidan, 2020). Figure 2-6 shows the schematic of calcium ion exchange (water softening) and resin regeneration.

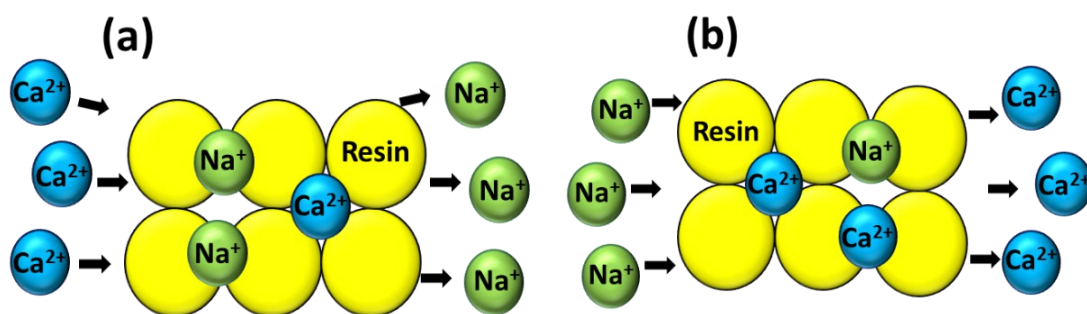
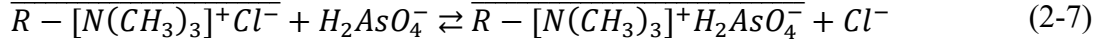


Figure 2-6 (a) Schematic of the ion-exchange process and (b) resin regeneration.

For As species removal, strongly basic ion exchangers are commonly used (Zakhar et al., 2018). The arsenic-chloride ion-exchange reaction is as follows (Eq. (2-7)) (EPA 2000).



where R = matrix, over-barred symbols refer to the exchanger phase. At the exchange sites, As ions replace the chloride ions (Cl⁻); thus, the exiting water contains a higher concentration of Cl and a lower concentration of As than the input water.

When As occupies all or a significant portion of the exchange sites, resin exhaustion occurs and should be regenerated (Kartinen Jr & Martin, 1995). The ion-exchange resin is regenerated using methanol or other organic solvents, an inorganic salt such as sodium chloride, a base such as sodium hydroxide, or a mix of different regenerants (Dixit et al., 2021). Ion exchange removes As species though sulfate, and to some extent nitrate anions impose significant interference. To remove arsenate species efficiently, sulfate concentrations cannot exceed 50 mg L⁻¹ if filter throughputs of 750 bed-volumes between successive regenerations can be obtained; otherwise, the treatment cost-effectiveness is jeopardized because the service cycles become too short (Höll, 2010).

Ion exchange is not efficient for As(III) removal because it exists mostly as an uncharged ion (H₃AsO₃) in water at a pH below 9.0 (Petrusevski et al., 2007). Thus, As(III) must first be oxidized to As(V) prior to being removed by resin (Fox, 1989). Water passes through one or more ion-exchange resin beds to remove As. Arsenate ions and a few other anions, such as sulfate, and follows the preference order for exchange; therefore, competing ions, such as total dissolved solids (TDS) and sulfate, strongly affect the efficiency of the ion-exchange process for As removal. Table 2-2 represents the effectiveness of various resins for As exchange under different conditions.

Table 2-2 Operating conditions and efficiencies of different resins used to remove arsenic.

Resin material	C _i (mg L ⁻¹)	Regeneration	RE (%) and RC (mg g ⁻¹)	Process conditions	Reference
Hybridized ion-exchange fibers containing dispersed hydrated ferric oxide nanoparticles	0.1	2% NaOH + 2% NaCl As recovery > 98%	AC: 5	pH:4–8.5 Competing ions: Na ⁺ =100 ppm SO ₄ ²⁻ =5 ppm HCO ₃ ⁻ =100 ppm	(Greenleaf et al., 2006)
Polymer–clay nanocomposite ion-exchange resin based on N-methyl-D-glucamine ligand groups	60		AC: 55 (Max retention at pH 3.5–6.0, 25 °C, 24 h)	30 mg resin+ 5 mL As solution pH: 2–12	(Urbano et al., 2012)
N-methyl-D-glucamine resins Revealing gel (1JW) Expanded gel (2JW) Epidermal-like structure (2PTN)	0.176		RE: 35.8 RE: 28.8 RE: 22.4	Flow rate: 5 mL min ⁻¹ R _d : 1JW, 2PTN: 4 g L ⁻¹ , 2 JW: 2 g L ⁻¹	(Çermikli et al., 2020)
Ion-exchange fiber with amino groups	5	0.1 M NaOH + 200 mg fiber +100 mL As solution	RE: As(III): 70 RE: As(V): 93	pH: 4–12 T:25 °C	(X. Zhang et al., 2008)
Amine-doped acrylic ion-exchange fiber	10	0.1 N HCl, 0.1 N NaOH, and ultra-pure water sequentially	RE: 83 AC: 205	pH: 3.04 T:25 °C	(C.-G. Lee et al., 2017)
Amberlite IR-400	5–15		RE: 91–99.28	pH: 3–10 R _d : 100–800 mg L ⁻¹ Voltage:5–20 V	(Rathi et al., 2021)

C_i = initial arsenic concentration; T = temperature; R_d = resin dose; RE = removal efficiency; RC = resin capacity.

The performance of the ion exchange depends on other process parameters, such as empty bed contact time and spent brine. Various ions compete for available ion-exchange sites and can significantly impact and reduce the efficiency and economic viability of ion-exchange systems (L. Wang et al., 2000). Typically, the background ion concentration dictates the applicability of the ion exchange procedure at a specific condition. For strong base anion (SBA) resins, the selectivity order is $\text{SO}_4 > \text{NO}_3 > \text{HAsO}_4 > \text{NO}_2, \text{Cl} > \text{H}_2\text{AsO}_4, \text{HCO}_3 \gg \text{Si}(\text{OH})_4, \text{H}_3\text{AsO}_4$ (Ghurye et al., 1999). Therefore, high sulfate and TDS levels can significantly reduce As removal efficiency (Ghurye et al., 1999). When the water contains Fe(III), it forms Fe(III)-As complexes, which affect the As removal because ion-exchange resins cannot remove Fe(III)-As complexes (L. Wang et al., 2000). At high sulfate concentrations, a resin bed may release previously adsorbed As(V), increasing the As concentrations in the effluent compared to the feed water. This phenomenon, which can be dangerous when toxic ions are involved, is called chromatographic peaking (dumping). To avoid this phenomenon, the resin bed should be monitored and regenerated before the onset of the peaking (L. Wang et al., 2000).

Ion exchange is a scalable technique used in centralized and decentralized water treatment systems, such as household treatment units (Amini et al., 2015). However, its applicability in decentralized systems is significantly constrained due to the frequent regeneration needed (Edgar & Boyer, 2022). Since cost is the main factor in waste management, choosing brine treatment methods depends on their technical ability and the implementation strategy, including whether they use centralized or decentralized systems (Korak et al., 2022). Finding cheap, available, and harmless materials to use as ion exchangers is crucial to improve this technology because the high cost of operation and disposal of the toxic regeneration sludge are among the problems facing this

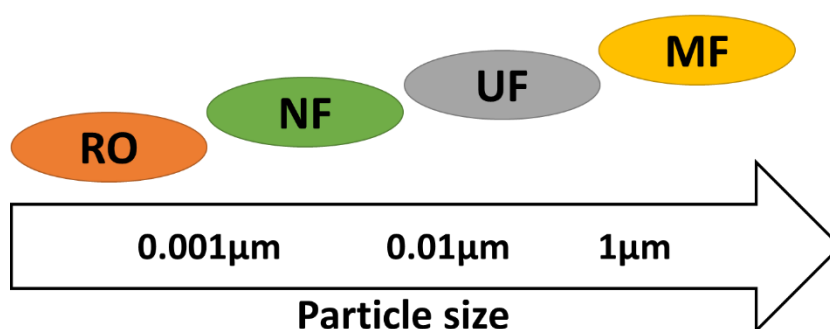
method. Although a resin can be reused after regeneration, it must be replaced after several years (Gaikwad et al., 2010; D. Mohan & Pittman Jr, 2007). Installing an ion-exchange system is often determined by the price of regeneration salt and waste brine disposal. For instance, regenerant salt accounted for 77% of operating costs in an As system. Capital costs could become more affordable by centralizing brine treatment even in decentralized systems (Korak et al., 2022). In other words, a decentralized system's household cartridges can be regularly sent to a centralized regeneration facility and replaced (Tarpeh et al., 2017). A hazardous waste brine produced by the ion-exchange process is too saline to be released into surface water, even if the heavy metal concentration is very low in the inlet. The waste brine heavy metals levels exceed the allowable limits. As a result, waste management improvements are required to make the ion exchange an affordable and environmentally friendly method for small communities (Korak et al., 2022).

A research study showed that cations and anions in the solutions slow down heavy metals removal (Inglezakis et al., 2005). Due to their electrical structure, transition metals can form stable complexes with charged substances such as NH_4^+ , inorganic anions, and water molecules, which typically give their solutions colors. The high stability of the complexes made of SO_4^{2-} and HPO_4^{2-} in the solution caused the poor removal of Cr^{3+} , Cu^{2+} , and Fe^{3+} . These complexes may also precipitate on resin pores and surfaces and clog them, reducing the resin's capacity for ion exchange (Inglezakis et al., 2003, 2005).

2.3.2. Membrane technologies

Membrane technologies are pressure-driven processes where membranes selectively allow the particles (atoms and ions) to cross them. In this case, the membrane allows

water to pass through the filter and retains heavy metals. These technologies are categorized into four main groups (Figure 2-7): microfiltration, ultrafiltration, nanofiltration, and reverse osmosis based on particle size. Table 2-3 reports the results of different membranes for As removal under specific conditions. As in Table 2-3, the removal effectiveness depends on the type of membrane, the solute, and how those two interact. The temperature, pH, pressure, and concentration influence the rejection. The advantage of this method is that the membrane eliminates As and some dissolved minerals or even pathogenic microorganisms (Shih, 2005). Another benefit of membrane technologies is that since membranes do not accumulate impurities, chemical usage is limited to cleaning them (Askenaizer, 2003).



RO = Reverse osmosis; NF = Nanofiltration; UF = Ultrafiltration; MF = Microfiltration

Figure 2-7 Applicability ranges of different membranes based on pore sizes.

Reverse osmosis (RO), ultrafiltration (UF), or microfiltration (MF) are possible options for decentralized membrane systems (X. Liu et al., 2021). The most common membrane types in decentralized systems are the RO systems, mostly used to desalinate water, while MF and UF membranes are designed for disinfection. However, most membrane-based small-scale systems fail to meet all the evaluation criteria, such as performance, ease of use, and low cost (Peter-Varbanets et al., 2009).

Membrane-based water treatment plants are among the most efficient and clean

technologies; however, they have high construction and operation costs and need high-tech maintenance and operation procedures (D. Mohan & Pittman Jr, 2007). Membrane fouling and scaling are still obstacles preventing the widespread industrial utilization of membranes. Effective pre-treatment and cleaning techniques are crucial for managing this issue (Abdel-Karim et al., 2021). There are two types of membrane cleaning: physical cleaning and chemical cleaning. The physical cleaning of membrane surfaces eliminates loosely attached substances and is typically referred to as reversible fouling. In contrast, chemical cleaning removes resistant compounds and is frequently referred to as irreversible fouling (Z. Wang et al., 2014). Although chemical methods are more effective, they may harm membranes (Peters et al., 2021).

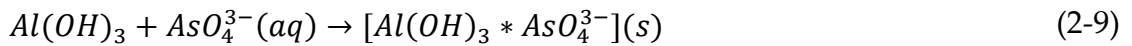
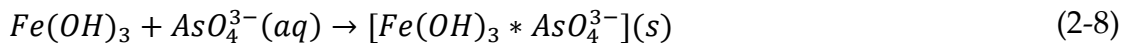
Table 2-3 Overview of pressure-driven membrane processes and their characteristics.

Type	Membrane Model	C _i (µg L ⁻¹)	Process Conditions	Result	Reference
RO	SWHR and BW-30 (FILMTEC)	As(V) = 50 As(III) = 12	pH: 2.1–10.4 P: 10–35 bar	rejection %:SWHR > BW-30 final concentration: 2.86 µg L ⁻¹	(Akin et al., 2011)
	Desal AK, General Electric Co., USA NF-45, a fully aromatic, polyamide, thin-film composite NF membrane from FilmTec (Minnetonka, MN)	As(III) = 50–400 As(V) = 10–316	pH: 2–9, P: 0.41–0.82 MPa pH: 4–8, P: 550 and 690 kPa	Max: 90% 60–90%	(F. Chang et al., 2014) (Vrijenhoek & Waypa, 2000)
NF	NE 90 membrane (Woongjin Chemical, SouthKorea), a TFC negatively charged polyamidemembrane.	As(V) = 20–100	pH: 4–10	As(V): 89–96% As(III): 44–41%	(C. M. Nguyen et al., 2009)
	Negatively charged UF membrane, Osmonics (DESAL) GM	As(V)= 50–5000	pH: 2–11 T: 20–40 °C	88%	(Brandhuber & Amy, 2001)
UF	Micellar-enhanced ultrafiltration (MEUF) (Amicon 8400, USA)	As(V) = 243, 486	Cationic surfactants: hexadecylpyridinium chloride (CPC), hexadecyltrimethyl ammonium bromide (CTAB), octadecylamine acetate (ODA) and benzalkonium chloride (BC)	CPC: 96%, CTAB: 94% BC: 57% ODA: 80%	(Iqbal et al., 2007)
MF	Coagulation/microfiltration: a 0.2 lm membrane disc	As(V) = 100	pH: 4.57–9.53 Coagulant: Ferric (1–7 mg L ⁻¹)	92.8–98.2%	(G. Zhang et al., 2012)
	Micro-/nanostructured MnO ₂ spheres and microfiltration (ADVANTEC MFS Inc., pore size: 0.2 lm, diameter: 47 mm)	As(V) = 4,984	pH: 2–10	>90%	(T. Zhang & Sun, 2013)

C_i = initial concentration; RO = reverse osmosis; NF = nanofiltration; UF = ultrafiltration; MF = microfiltration.

2.3.3. Coagulation-flocculation

Coagulation-flocculation is another standard method for As removal from water. Although these processes are sometimes used interchangeably, they are two different processes (Choong et al., 2007). In the coagulation process, a coagulant is added to destabilize the colloid particles to start aggregation by neutralizing their charges (Figure 2-8) and thus the electrostatic repulsive forces (Sonal & Mishra, 2021). Cationic coagulants lessen the negative electric charge of the colloids by providing positive charges to destabilize the non-settleable particles. Then, gentle (slow) mixing is maintained to promote the agglomeration of the new neutral colloids into larger flocs; the slow mixing process is called flocculation (Choong et al., 2007). The pH can be adjusted in these units to increase removal efficiency. The floc size, strength, and structure may be affected by pH adjustment (Naceradska et al., 2019). Aluminum sulfate ($Al_2(SO_4)_3$) and ferric chloride ($FeCl_3$) are among the common coagulants for water treatment (Ranjbar et al., 2021). Eqs. (2-8) and (2-9), respectively, show the As removal reactions when iron and aluminum are used as the coagulant (Mendoza-Chávez et al., 2021).



The efficiency of several coagulants/flocculants under specific operating conditions is listed in Table 2-4. It was proven that pH has a significant effect on the performance of coagulants/flocculants. Initial concentration and coagulant dose are two other major parameters affecting coagulation performance. Flocculation is the activity of polymers to bridge flocs and form large agglomerates. Bridging happens when

portions of the polymeric chains are adsorbed on some particles, causing the particles to aggregate. An anionic flocculant will be used for a suspension with a positive charge to destabilize the colloid by bridging the particles or neutralizing the charge (Choong et al., 2007).

Table 2-4 Coagulants/flocculants used in arsenic ion exchange, their operating conditions, and efficiencies.

Coagulant/ Flocculant	C _i ($\mu\text{g L}^{-1}$)	pH	Coagulant Dose (mg L^{-1})/Intensity (A)	RE (%)	Reference
Ferric chloride	As(V) = 50–60	7, 8	0.84–3.00	>80	(Laky & Licskó, 2011)
Aluminum sulfate	As(V) = 10 As(V) = 500		66, 42	91	(Baskan & Pala, 2010)
Ferric ions and coarse calcite	As(V) = 5000	5–11	100	> 99	(Song et al., 2006)
Titanium xerogel coagulant	As(III) = 1000	5–10	10	> 90	(Song et al., 2006)
Electrocoagulation (Al and Fe anode)	As(V) = 100	8.4	0.2 A	99%	(Mendoza-Chávez et al., 2021)

C_i = initial concentration; RE = removal efficiency.

Although the substances usually used in coagulation and flocculation processes are efficient and available, they produce toxic sludge in most cases. Therefore, sedimentation and filtration are needed as downstream processes after flocculation. There are still arguments on the effects of some metal coagulants and flocculants, such as aluminum and iron, on people's health and the environment (Lichtfouse et al., 2019; Sieliechi et al., 2010). Another problem with these plants is that they are not feasible in remote areas due to the lack of skilled workers and laboratory facilities to monitor, analyze, and control the process parameters (Muruganandam et al., 2017).

Conventional chemical coagulation-flocculation is unsuitable for small communities because of the lack of capital to support their high operating costs, expensive installation and transportation cost of chemicals, and challenging

management of the chemical sludge generated (Jeon et al., 2016; McBeath et al., 2021). Electrochemical technologies offer a potentially appealing alternative for decentralized applications since they cut out the chemical distribution chain and solve the challenges of working with chemicals involved in traditional coagulation-flocculation methods (McBeath et al., 2021). In electrocoagulation, the anode is sacrificed into the water in ionic form, which occurs when a direct electric current passes through electrodes. The metal ions can create a variety of coagulated species that can either adsorb dissolved pollutants or destabilize suspended particles (Holt et al., 2005).

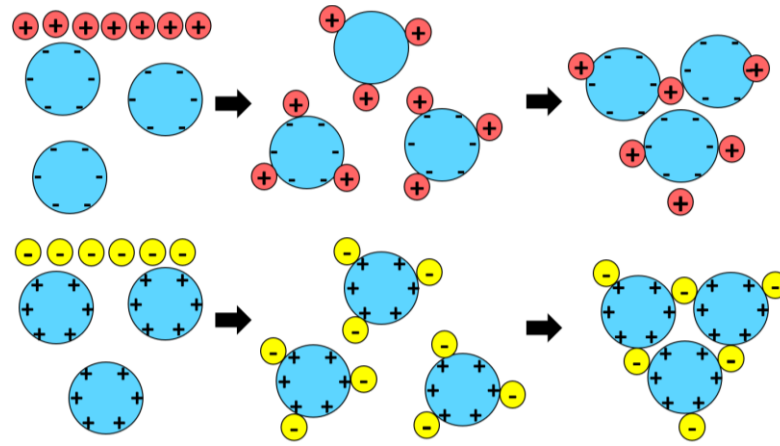
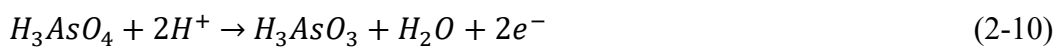


Figure 2-8 Mechanism of coagulation by cationic and anionic polymers.

2.3.4. Oxidation

Oxidation processes are not considered independent As removal methods; they are the primary stages of other technologies. In other words, since the removal of As(III) is less effective than As(V), As removal procedures start with the oxidation of As(III) to As(V), followed by other processes such as adsorption, co-precipitation and coagulation (Y. Lee et al., 2003). The oxidation of As(III) to As(V) can be expressed by Eq. (2-10)

(V. K. Sharma et al., 2007):



Air or oxygen, ozone, chlorine, hypochlorite, chlorine dioxide, manganese compounds, and hydrogen peroxide can be the oxidizing agent in this process. Table 2-5 presents the oxidation yields of different oxidants for arsenite oxidation. Table 2-5 shows that oxidation happens slowly when pure oxygen or air is used. On the other hand, ozone, chlorine, hypochlorite, chlorine dioxide, or H_2O_2 can speed up oxidation (Bissen & Frimmel, 2003a). Other possible means of As oxidation utilize advanced oxidation processes (AOP) such as UV or microbiological oxidation when bacteria are present (Bissen & Frimmel, 2003b).

Table 2-5 The standard potential of different oxidants and their efficiencies in arsenite

oxidation (Kim & Nriagu, 2000; R. Liu & Qu, 2021; Sorlini & Gialdini, 2010)

Oxidant	Standard Potential (V, 25 °C)	Sample ($\mu\text{g L}^{-1}$)	Oxidation yield (%) after (Time)
Air	N/A	GW: 46–62	54 (5 days)
Pure oxygen	1.23	GW: 46–62	57 (5 days)
Ozone	2.07	GW: 46–62	>96 (10 min)
Hypochlorite	1.7	DW: 50	>80 (5 min)
Chlorine dioxide	1.27	DW: 50	>50 (2 days)
Potassium permanganate	1.23	DW: 50	>90 (5 min)
		300	>90 (5 min)
Hydrogen peroxide	1.78		

Note: GW = groundwater; DW = demineralized water.

Conventional oxidation in some treatment plants is one of the first steps because it makes the As removal process easier; however, one of the limitations of air or oxygen oxidation processes is their slow rate and moderate yield (Table 2-5) (Bissen & Frimmel, 2003b). As a result, advanced oxidation processes (AOPs) were developed for treating As-contaminated water. The AOPs use highly reactive radical species to treat environmental waste and pollutants. The main AOPs include hydroxyl-radical-based processes, UV-photolysis-driven processes, ozonation, Fenton oxidation, electrochemical oxidation and heterogeneous photocatalysis (J. Du et al., 2020; Ike et

al., 2018). The combination of various oxidation techniques such as UV, ozone, hydrogen peroxide, and TiO_2 , improves the production of OH radicals. As a result, compared to using one type of oxidant, this combination typically speeds up oxidation reactions (Mohammed et al., 2020). For instance, $\text{O}_3/\text{H}_2\text{O}_2$, O_3/UV , $\text{UV}/\text{H}_2\text{O}_2$, TiO_2/UV , $\text{H}_2\text{O}_2/\text{catalyst}$, and photo-Fenton processes are commonly used combinations in drinking water treatment (Matilainen & Sillanpää, 2010). AOPs are typically employed in full-scale systems or laboratories, mostly for conditions where conventional methods are not highly effective since they often need complex chemicals and light or electricity energy (Hodges et al., 2018). The major challenges of evaluating AOPs are the operational costs (energy and chemical input), sustainability (resource use and carbon footprint), and production of oxidation by-products (Miklos et al., 2018). Centralized water systems mostly rely on conventional oxidation and AOPs such as $\text{O}_3/\text{H}_2\text{O}_2$ and $\text{UV}/\text{H}_2\text{O}_2$ techniques. However, electricity-based techniques like the electrochemical production of oxidants such as chlorine and hydrogen peroxide have great potential in decentralized systems because they do not require chemical transportation (von Gunten, 2018; Y. Zhang, Wang, Li, et al., 2020). In electrochemical oxidation, water contaminants are mostly oxidized by the anodic oxidation surface, by charge transfer on the anodic surface or interaction with the hydroxyl radical produced as a result of water oxidation (Gurung et al., 2018).

2.3.4.1. Photo-Oxidation

Photocatalytic oxidation is a promising among AOPs (Oturán & Aaron, 2014). Generally, As(V) is less harmful than As(III) and easier to remove; thus, oxidizing As(V) to As(III) is an effective step in the removal process (X.-Y. Yu et al., 2011).

Table 2-6 presents the results of the photo-oxidation of arsenite under different

operating conditions. These studies show that in the presence of a heterogeneous catalyst such as titanium dioxide, the As(III) oxidation rate can be significantly improved. Among the catalysts used in the photo-oxidation process, TiO_2 is the most important one. The TiO_2 is important because it has high efficiency in oxidizing As(V) to As(III) due to its large surface-to-volume ratio, stable chemical properties, affordability, non-toxicity, great oxidizing power, and excellent electronic and optical properties (Iervolino et al., 2016a; Rosales et al., 2020). The TiO_2 nanopowder can be used as suspended particles or immobilized on a surface. However, the literature revealed that the immobilization of TiO_2 leads to better results from an engineering and economic point of view. The major limitation of immobilization is that particle aggregation may cause a reduction in surface area. The main parameters that affect the TiO_2 photocatalytic performance include energy gap, particle size, specific surface area, porosity, crystallinity, and exposed surface facets (Ray & Lalman, 2016).

Table 2-6 Oxidants used in the photo-oxidation of arsenite to arsenate, their operating conditions, and efficiencies.

Oxidant	C _i (mg L ⁻¹)	Process Conditions	Results	Reference
Hydrogen peroxide under UVC	0.2	T: 20 °C C _i (H ₂ O ₂): 0–30 mg L ⁻¹ pH: 5.6–6.7	OY = 10% (30 min) As(III) oxidation t _{1/2} = 3.5 s	(Lescano et al., 2012)
TiO ₂ -chitosan bead (TICB) under UV	100, 1000 and 10,000	T = 25 °C TICB: 17.5 mg chitosan + 7.5 mg TiO ₂ in 40 mL solution	2198 mg As(III)/g TICB and 2050 mg As(V)/g TICB	(Miller & Zimmerman, 2010)
MoOx/TiO ₂ under UVA	5	pH: 7.2	OY = 100% (120 min)	(Iervolino et al., 2016b)
ZnO-Au nanocomposite	2	ZnO: 20 mg + 40 mL solution	ZnO: OY = 9.1% (2 h) ZnO-Au (0.5%): OY = 17% (2 h) ZnO-Au (1%): OY = 45% (2 h) ZnO-Au (2%): OY = 23% (2 h)	(M. Huang et al., 2016)
Few and multi-layer Ti ₃ C ₂ T _x nanosheets under UVA	0.7	pH: 7	Multi-layer Ti ₃ C ₂ T _x : 20% (90 min) Few-layer Ti ₃ C ₂ T _x : 44% (45 min)	(Rosales et al., 2020)
Dissolved Fe(III) under UV	10	Fe(II): 180 mg L ⁻¹ pH: 7	Complete oxidation process time: 1–6 h	(Zaw & Emett, 2002)

C_i = initial concentration; OY = oxidation yield for As(III).

2.4. Arsenic Removal by Adsorption

Adsorption is the use of solids to eliminate substances from gaseous and liquid solutions. Activated carbon, metal hydrides, and synthetic resins are common adsorbents used in water and wastewater treatment plants (Choong et al., 2007). The most common adsorbent categories for water treatments are presented in Figure 2-9. Comparing several water treatment methods for heavy metals removal (Table 2-7) shows that adsorption is more affordable than membrane technologies, simpler, and more secure to deal with than contaminated sludge produced by precipitation, and it is multipurpose in contrast to ion exchange (Gallegos-Garcia et al., 2012). The main limitation of the adsorption method is that its effectiveness is affected by the presence of other ions. Various ions compete for the adsorbent's active site, affecting the adsorption capacity (S. I. Siddiqui & Chaudhry, 2017). For example, phosphate ions can compete with As ions due to their similar chemical structure; thus, they can significantly lower the As removal efficiency (Gallegos-Garcia et al., 2012). The presence of $10 \text{ mmol L}^{-1} \text{ H}_2\text{PO}_4^{2-}$ decreased the adsorption efficiency of As(III) on zero-valent iron nanoparticles from 99.9% to 66.3% (Babae et al., 2018). Figure 2-10 shows the different configurations previously suggested for As adsorption. Batch experiments, fixed configurations, and fluidized-bed reactors are the primary categories that are widely used. Adsorbent particles are in motion in the fluidized reactor configurations, while they are stationary in a fixed-bed reactor (Dhoke et al., 2021). In batch experiments, a liquid solution containing a known amount of adsorbate is brought in contact with a given mass of adsorbent, and the adsorbate's concentration is monitored over time. (Brandani, 2021).

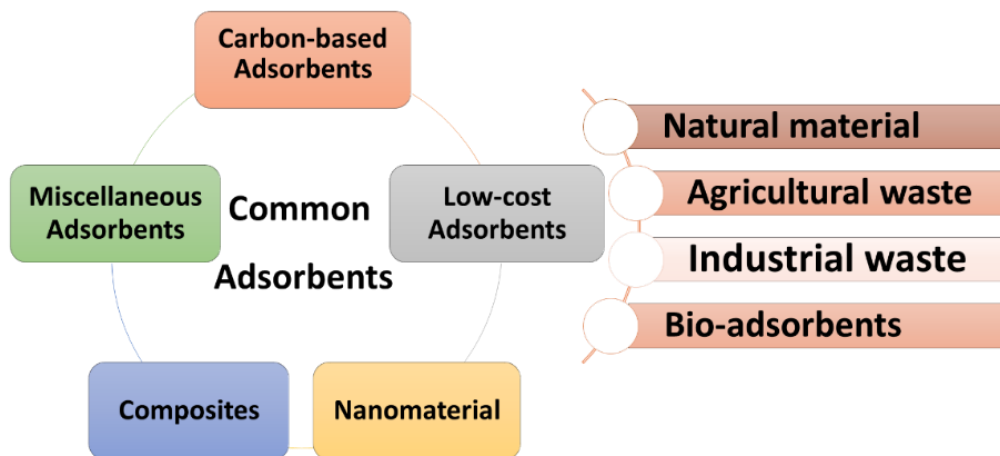


Figure 2-9 Classification of adsorbents for water treatment (adapted from Elwakeel et al. (2020)).

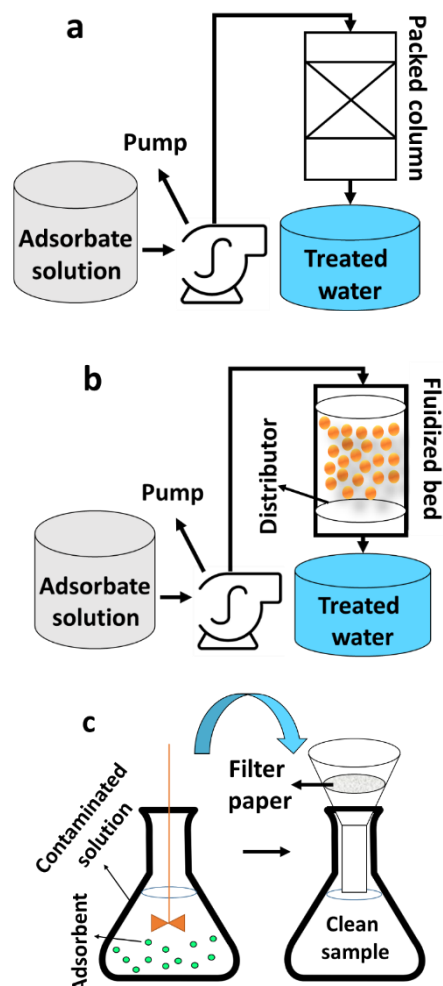


Figure 2-10 Different configurations for adsorption of impurities: (a) Packed-bed adsorber, (b) Fluidized-bed adsorber, and (c) Batch.

Table 2-7 Advantages and disadvantages of common treatment technologies for arsenic removal.

Methods	Advantages	Disadvantages	Reference
Ion exchange	Removes other dissolved pollutants like sulfate Less impacted by water pH Specific resins for specific ions Well-established process with widely available resins	Competing ions affect arsenic removal Low efficiency in concentrated effluents Requires replacement and regeneration, causing sludge issues Unsuitable for high-TDS water High cost and advanced operation/maintenance needed	(Alka et al., 2021; Inglezakis et al., 2005)
Membranes	High removal efficiency No toxic solid waste Removes some microorganisms and pollutants Requires fewer resources (labor and area) Removes dissolved contaminants and partially disinfects water	High capital and operating costs, less effective for arsenite High-tech operation and maintenance Requires pre-treatment and membrane replacement Membrane fouling/biofouling leads to lower flux, higher energy use, reduced performance, and more frequent cleaning	
Coagulation /flocculation	Ideal for Fe- and Mg-rich waters Removes suspended solids from surface water Low capital cost Simple operation Uses common chemicals	Limited removal of As(III) May not meet arsenic removal limits It may require pre-oxidation, forming toxic by-products Effectiveness depends on coagulant type, dose, pH, and competing ions like phosphates or silicates	(M. F. Ahmed, 2001; Alka et al., 2021; Karcioğlu & Arslan, 2019)
Oxidation /AOP	Simple, low-cost process Oxidizes impurities and kills microbes Effective for total As removal	Often very slow Removes only some arsenic Requires pre-treatment followed by another method Generates toxic by-products (e.g., organo-chlorides)	(M. F. Ahmed, 2001; Karcioğlu & Arslan, 2019)
Adsorption	High As removal efficiency with low costs Simple operation, handling, and maintenance Well-established method with available adsorbents Cost-efficient and sludge-free, no harmful by-products	Efficiency impacted by competing ions like phosphate Frequent regeneration or replacement of exhausted adsorbent Recycling small-sized conventional adsorbents is challenging	(M. F. Ahmed, 2001; Alka et al., 2021; Elwakeel et al., 2020)

2.4.1. Adsorption kinetic

The concentration data and adsorption rates obtained from experiments should be interpreted using kinetic models such as pseudo-first-order (PFO), pseudo-second-order (PSO) intra-particle diffusion, and Elovich models.

According to the pseudo first-order (PFO) model (Eq. (2-11)), the adsorption process follows a first-order kinetic mechanism. In this model, the adsorption rate is determined by the difference between the adsorption capacity at a given time and the equilibrium adsorption capacity. Conversely, the PSO model (Eq. (2-12)) proposes that during the chemisorption phase of the adsorption process, the adsorbate and the adsorbent surface interact. The coefficient of determination (R^2), which gauges how well a model matches experimental data, was used to assess the kinetic models' goodness of fit. It shows the percentage of the overall data variation that the model explains. Higher R^2 values indicate a better match between the experimental and projected values (De Almeida Ohana et al., 2022).

$$\log(q_e - q_t) = \log q_e - \left(\frac{k_1}{2.303} \right) t \quad (2-11)$$

where q_e represents the adsorption capacity (mg g^{-1}) at equilibrium, and k_1 is the adsorption rate constant ($\text{g (mg} \cdot \text{min)}^{-1}$).

$$t/q_t = 1/q_e^2 k_2 + t/q_e \quad (2-12)$$

Eq. (2-12) incorporates the following parameters: k_2 , the reaction rate constant ($\text{g (mg} \cdot \text{min)}^{-1}$); q_e , the equilibrium adsorption capacity representing the mass of solute adsorbed per gram of adsorbent (mg g^{-1}); and q_t , the mass of solute adsorbed at a specific time t (mg g^{-1}). The determination of k_2 and q_e involves generating a linear plot of t/q_t versus t (J. Wang & Guo, 2023). This plot allows calculating k_2 using the

slope and intercept according to the equation $k_2 = (\text{slope})^2 / \text{intercept}$. The equilibrium adsorption capacity, q_e , is then obtained by inverting the slope ($q_e = 1/\text{slope}$).

The intra-particle diffusion model (Eq. (2-13)) helps determine if adsorption is primarily controlled by diffusion within the pores of the adsorbent. In this model, a straight line in the plot of qt versus $t^{1/2}$ suggests that intra-particle diffusion is the main mechanism. If multiple linear segments appear, it indicates that adsorption occurs in two or more stages. The initial stage involves the diffusion of molecules from the bulk solution to the adsorbent's outer surface, the second stage represents diffusion within the adsorbent pores, and the third stage shows the system reaching equilibrium.

$$q_t = k_{id}t^{1/2} + C \quad (2-13)$$

where q_t is the amount of adsorbate at time t , k_{id} is the intra-particle diffusion rate constant, and C is the intercept, indicating the boundary layer thickness (J. Wang & Guo, 2023).

The Elovich model, commonly used for chemisorption on heterogeneous surfaces (Inyang et al., 2016), was also applied to further analyze adsorption kinetics. It is especially useful for systems where the adsorption rate decreases over time due to varying activation energies across adsorption sites. The model assumes that the adsorption rate declines exponentially as surface coverage increases (Debord et al., 2022). The Elovich equation is given by Eq. (2-14):

$$q_t = \frac{1}{\beta} \ln(\alpha\beta) + \frac{1}{\beta} \ln(t) \quad (2-14)$$

where qt is the adsorbed amount at time t , α is the initial adsorption rate, and β is related to surface coverage and activation energy (J. Wang & Guo, 2023).

Table 2-8 presents the kinetic parameters for the two most commonly used kinetic models (PFO and PSO) for As adsorption.

Table 2-8 Kinetic parameters for the adsorption of arsenic on different adsorbents.

Adsorbent	Model	C_i (mg L ⁻¹)	k	q_e (μg g ⁻¹)	R ²	Reference
Untreated powdered eggshell	1st	0.5	0.717 h ⁻¹	30	0.944	(Oke et al., 2008)
	2nd		18.47 g mg ⁻¹ ·h ⁻¹	724	0.999	
Dolomitic	1st	2	6.8×10 ⁻³ μg g ⁻¹ min ⁻¹	652.04	0.970	(Salameh et al., 2011)
	2nd		1.75×10 ⁻⁵ μg g ⁻¹ min ⁻¹	652.04	0.975	
A MIL-53(Fe)	1st	5	0.016 min ⁻¹	11,060	0.833	(Vu et al., 2015)
	2nd		0.0120 g mg ⁻¹ min ⁻¹	5180	0.994	
Hematite nanoparticles	2nd	10	6.45 ± 3.11 g mg ⁻¹ h ⁻¹	2899	0.997	(Dickson et al., 2017)
Hematite agglomerate	2nd		6.45 ± 1.39 g mg ⁻¹ h ⁻¹	1689	0.996	
Copper(II) oxide nanoparticles	1st	1	0.02 min ⁻¹	742.48	0.94	(Goswami et al., 2012)
	2nd		0.03 g mg ⁻¹ min ⁻¹	1014.41	0.99	

2.4.2. Isotherm models

Adsorption isotherm is the relation that describes the equilibrium between the quantity adsorbed to the unit mass of adsorbent and the concentration of the remaining adsorbate (pollutant) in a solution at a fixed temperature. A heterogeneous surface with multilayer adsorption is taken into consideration by the Freundlich model, whereas the Langmuir is a model that describes the adsorption of molecules onto a homogeneous surface, forming a monolayer. The Langmuir model is represented by Eq. (2-15).

$$\frac{C_e}{q_e} = \frac{1}{bq_m} + \frac{C_e}{q_m} \quad (2-15)$$

where C_e represents the adsorbate equilibrium concentration (mg L⁻¹), q_e is the mass of adsorbate adsorbed at equilibrium (mg g⁻¹), q_m is the maximum adsorption capacity (mg g⁻¹), and b is the Langmuir constant (J. Wang & Guo, 2023).

The Freundlich model is described by Eq. (2-16).

$$\ln q_e = \ln K_f + \frac{1}{n} \ln C_e \quad (2-16)$$

where K_f is the Freundlich constant giving adsorption capacity, and n is the Freundlich exponent, which is associated with adsorption intensity (J. Wang & Guo, 2023).

The Temkin isotherm model suggests that, as the adsorbate coverage increases, the heat of adsorption decreases linearly rather than logarithmically, as assumed by the Langmuir model. This linear reduction results from adsorbent-adsorbate interactions, which imply a uniform distribution of binding energies (BE) up to a maximum value. The model is represented by Eq. (2-17) (J. Wang & Guo, 2023).

$$q_e = B \ln (k_t C_e) \quad (2-17)$$

where q_e is the adsorbate amount at equilibrium, C_e is the adsorbate concentration at equilibrium, k_t is the Temkin isotherm constant related to maximum binding energy, and B is associated with the adsorption heat (Adebayo et al., 2015).

The Dubinin-Radushkevich (D-R) isotherm, on the other hand, models adsorption on heterogeneous surfaces and assumes adsorption occurs in micropores through a pore-filling mechanism. It does not assume a uniform distribution of adsorption energies and is described by Eq. (2-18) (J. Wang & Guo, 2023)

$$q_e = q_m e^{-\beta \epsilon^2} \quad (2-18)$$

where q_e is the adsorbed amount at equilibrium, q_m is the theoretical saturation capacity, β is a constant related to adsorption energy, and ϵ is the Polanyi potential, calculated as (Eq. (2-19)):

$$\epsilon = RT \ln \left(1 + \frac{1}{C_e}\right) \quad (2-19)$$

where R is the gas constant, T is absolute temperature, and C_e is the equilibrium concentration. In the D-R model, E represents the mean free energy of adsorption per

molecule, indicating the energy required to move one mole of adsorbate from solution to the adsorbent's surface. E is calculated using the D-R constant β with Eq. (2-20) (J. Wang & Guo, 2023):

$$E = \frac{1}{\sqrt{2\beta}} \quad (2-20)$$

Generally, a low activation energy (E), less than 8 kJ mol⁻¹, indicates physical adsorption, while higher Values suggest chemical adsorption (J. Wang & Guo, 2023). Table 2-9 present the adsorption isotherm parameters for the two most commonly applied models (Freundlich and Langmuir) for As adsorption, respectively.

Table 2-9 Isotherm parameters for arsenic adsorption.

Adsorbent	Langmuir			Freundlich			Reference
	q_m (g g ⁻¹)	b (L mg ⁻¹)	R^2	k_f (mg g ⁻¹)	n	R^2	
Zeolite (H-MFI-24)	0.0358	0.009	0.96	3.52	1.11	0.99	(Chutia et al., 2009)
Zeolite (H-MFI-90)	0.0348	0.0109	0.96	4.21	1.12	0.99	(Chutia et al., 2009)
Chitosan magnetic graphene oxide nanocomposite	0.0023	0.021	0.96	86.64	0.514	0.98	(Sherlala et al., 2019)
Watermelon rind	0.0031	1.39	0.96	1.99	0.40	0.88	(Shakoor et al., 2018)
Hydroxyl-eggshell	0.529	0.005	0.81	104.11	5.05	0.92	(Ribeiro et al., 2021)
Maghemite nano-adsorbents	0.0072	17.5	0.98	13.8	1.95	0.93	(S. I. Siddiqui et al., 2020)
Starch functionalized maghemite	0.0086	9.1	0.98	16.5	1.60	0.98	(S. I. Siddiqui et al., 2020)

2.4.3. Characterization techniques for investigation of adsorbents properties

Understanding and identifying the various retention phenomena (adsorbent-adsorbate) and interpreting the kinetic results depend on the characterization results. Moreover, developing technical adsorption methods and conducting adsorption studies require a basic understanding of adsorbents' physical and chemical characteristics. Furthermore, the adsorbent surface characteristics are crucial in determining its sorption capacity because adsorption is a surface phenomenon (Bläker et al., 2019; Kumar & Jiang, 2015; Sihem et al., 2012). Figure 2-11 presents the most common characterization techniques. Table 2-10 presents an overview of the characterization results of different adsorbents (proximate and ultimate analysis, specific surface area, and bulk density). Table 2-11 details typical examples of Fourier transform infrared spectroscopy (FTIR) and X-ray powder diffraction (XRD). Table 2-12 shows typical examples of scanning electron microscopy (SEM) and particle size.

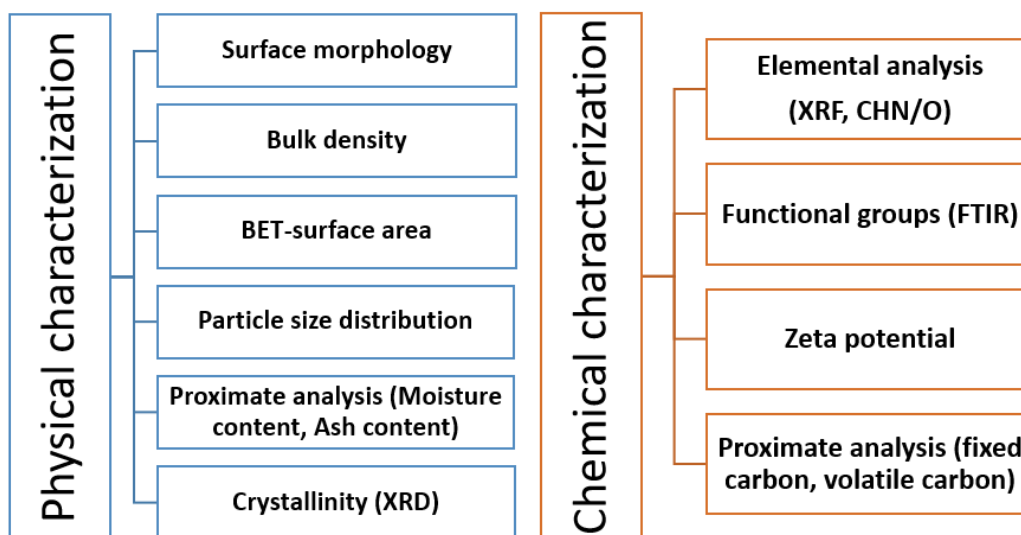
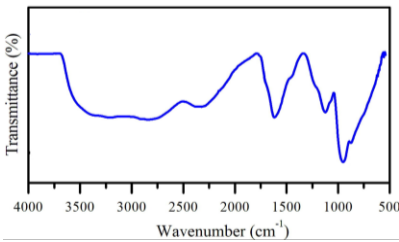
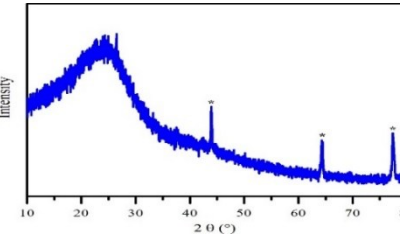
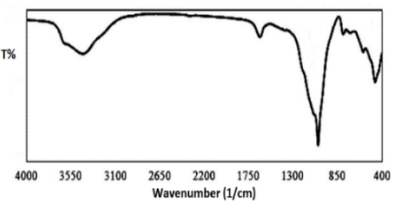
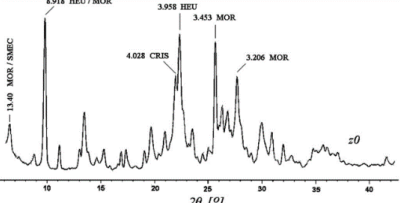
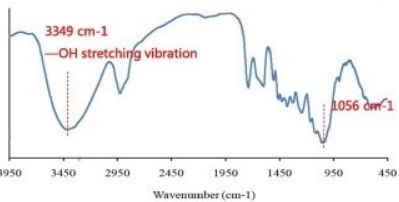
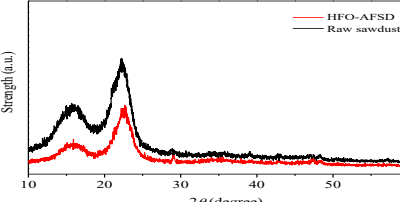
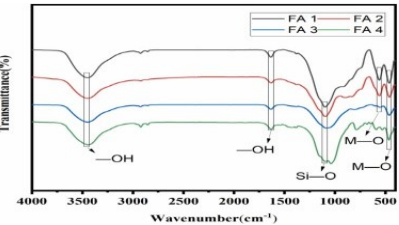
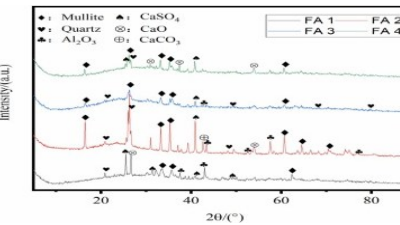
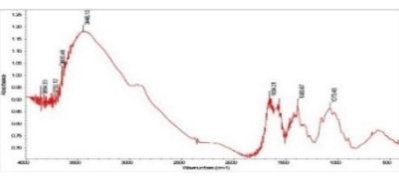
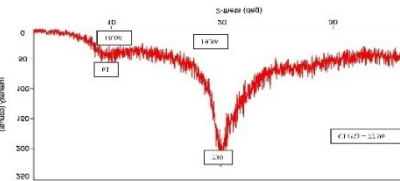


Figure 2-11 Overview of main characterization techniques.

Table 2-10 Proximate and ultimate analysis, specific surface area and bulk density of different adsorbents.

Type (adsorbent)	Proximate analysis		Ultimate analysis (%)		Specific surface area (m ² g ⁻¹)	Bulk density (g cm ⁻³)	Reference
Carbon-based (activated carbon)	Moisture	7.53%	C	68.32	720	0.43	(Hidayu et al., 2013; Wirasnita et al., 2015)
	Volatile	15.23%	H	3.12			
	Fixed carbon	67.66%	N	2.12			
	Ash	9.58%	O	26.44			
Natural (zeolite)	Volatile	9.24%	SiO ₂	86.1	211.97	0.068	(Hung et al., 2009; Quan et al., 2022)
	Fixed carbon	3.94%	Al ₂ O ₃	5.79			
	Ash	86.57%	K ₂ O	0.65			
			Na ₂ O	5.08			
			Fe ₂ O ₃	0.039			
			CuO	0.009			
			MnO	0.064			
			Br	0.04			
			TiO ₂	0.012			
			Cl	2.22			
			ZnO	0.005			
Agricultural waste (sawdust)	Moisture	5.83%	C	46.1	303	0.152	(Chatterjee et al., 2020; Mierzwa-Hersztek et al., 2019)
	Volatile	76.44%	H	6.39			
	Fixed carbon	12.02%	N	0.37			
	Ash	5.73%	O	41			
Industrial waste (fly ash)			S	0.55	450	1.01	(I. Ali et al., 2014; Balsamo et al., 2010)
	Volatile content	3.68%	SiO ₂	60.5			
	Fixed carbon	22.30%	Al ₂ O ₃	15.4			
	Ash content	74.00%	CaO	2.9			
			Fe ₂ O ₃	4.9			
Biosorbent (chitin/chitosan)			MgO	0.81	300	1.008	(Olafadehan et al., 2019)
	Moisture	15.40%	C	49.7			
	Protein	14.88%	H	1.72			
	Fiber	76.40%	N	0.2			
	Ash	9.40%	O	48.3			
			S	0.1			

Table 2-11 Fourier transform infrared spectroscopy (FTIR) and X-ray powder diffraction (XRD) results of different adsorbents. (Reprinted with permissions).

FTIR	XRD	Reference
Carbon-based (Activated carbons)		
		(C. C. de Souza et al., 2022)
Natural (Zeolites)		
		(Elaiopoulos et al., 2010)
Agricultural waste (Sawdust)		
		(Hao et al., 2016)
Industrial waste (Fly ash)		
		(C. Wang et al., 2022)
Biosorbent (Chitosan)		
		(Iber et al., 2022)

2.4.3.1. Surface morphology

Microscopic methods such as optical microscopy (OM), scanning electron microscopy (SEM), transmission electron microscopy (TEM), and atomic force microscopy (AFM) can be employed to directly observe the adsorbent morphology or topography (Al-Maadeed et al., 2020). SEM characterization, a common technique for investigating surface morphology, produces high-resolution images of a sample by applying a focused electron beam on the sample's surface and measuring the secondary or backscattered electrons. An Energy Dispersive X-Ray Analyzer (SEM-EDX) is employed to determine certain elements' atomic percentages (Bakdach et al., 2022).

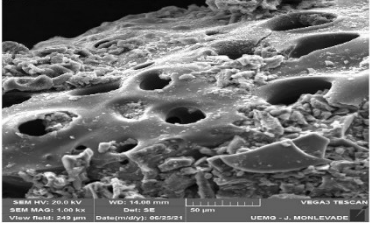
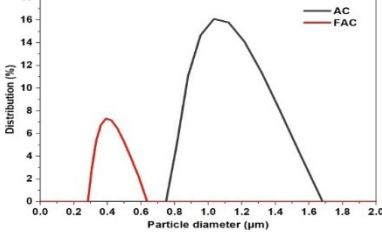
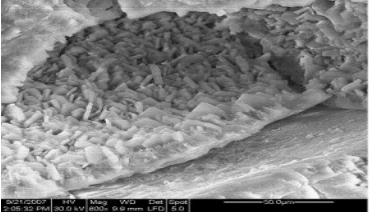
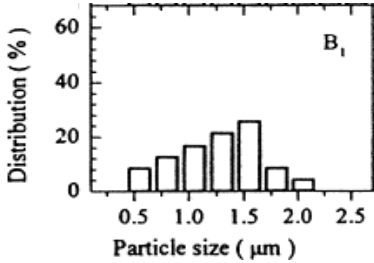
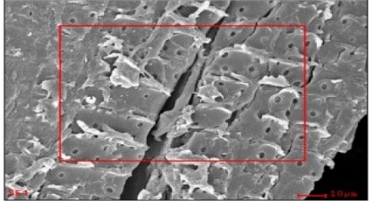
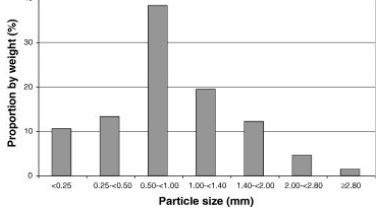
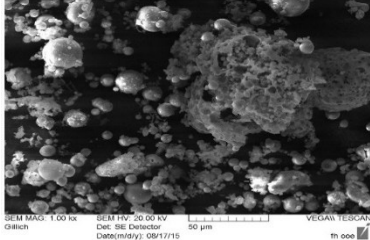
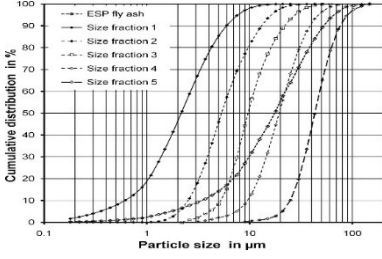
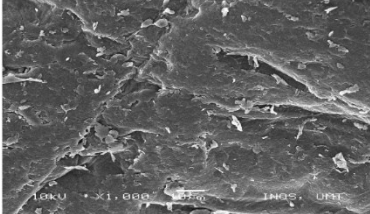
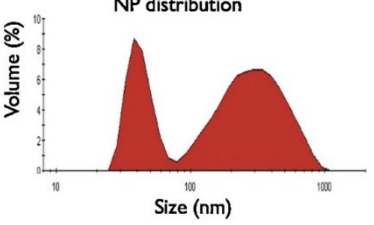
2.4.3.2. Bulk density and particle size

An untapped powder sample's mass-to-volume (including void volume) ratio determines its bulk density. As a result, the powder particles' density and spatial arrangement within the powder bed affect the bulk density. After weighing the contents of a container (m) with a known volume, V, the bulk density can be determined (Al-Maadeed et al., 2020).

2.4.3.3. Dynamic light scattering (DLS)

DLS is a non-destructive, low-cost, relatively easy, and fast technique for measuring particle size distributions in colloidal suspensions and emulsions and detecting the presence of agglomerates and aggregates. The light scattered by small particles irradiated by a laser is recorded with high time resolution under a particular angle; the fluctuation of the scattering signal represents the dynamics of microstructural processes such as the Brownian motion of the particles. Particle size can be measured by analyzing the change in the scattered light intensity in a colloidal suspension. A numerical transformation of spectral measurement signals is required for this purpose (Babick, 2020; T. G. F. Souza et al., 2016).

Table 2-12 Scanning electron microscopy (SEM) and particle size distribution results of different adsorbents. (Reprinted with permissions).

SEM	Particle Size Distribution	Reference
Carbon-based (Activated carbons)		
		(C. C. de Souza et al., 2022; Tauk et al., 2022)
Natural (Zeolites)		
		(Elaiopoulos et al., 2010; Zaiku et al., 2001)
Agricultural waste (Sawdust)		
		(Bergström et al., 2008; Hao et al., 2016)
Industrial waste (Fly ash)		
		(Lanzerstorfer, 2018)
Biosorbent (Chitosan)		
		(Iber et al., 2022; Rampino et al., 2013)

2.4.3.4. Brunauer-Emmett-Teller (BET)-surface area

The BET method for determining surface area is a popular characterization method for different adsorbents. The BET theory states that surface areas can be determined from gas (typically N₂) adsorption isotherms at the boiling point of the gas. In other words, a formation of layers that consists of atoms, ions, or molecules on the surface of a substance that adsorbs gas produces van der Waals forces, which are responsible for this phenomenon. Based on this theory, the surface area and the amount of gas adsorbed on the adsorbent material are correlated (Ambroz et al., 2018).

2.4.3.5. Crystallinity

XRD techniques are frequently employed to identify present phases (qualitative analysis) and to calculate their corresponding quantities (quantitative analysis). X-ray scattering from atoms leads to a diffraction pattern that carries information about the atomic structure in the crystal. Amorphous materials do not show any noticeable peaks in the diffraction pattern because of the lack of periodic arrays with long-range order. The intensity (amount of X-rays recorded in a certain peak) is shown against the detector angle, 2θ , in a diffraction pattern known as a diffractogram (Table 2-11). The wavelength influences the peak position in a diffraction pattern. Bragg's Law, which is the principle of XRD, explains that the incident X-rays' wavelength, the incident angle, and the distance between atoms in crystals are related (Epp, 2016).

2.4.3.6. Ultimate (elemental) analysis

The ultimate analysis provides information about the elemental composition of the adsorbent (Ambroz et al., 2018). X-ray fluorescence (XRF) spectroscopy is an accurate, reliable, and non-destructive analysis that is often used to determine the elemental compositions of various materials. According to the wavelength-dispersive principle, each atom emits an estimated relative quantity of X-ray photons of a certain energy or

wavelength. The electron of an atom is forced out of its inner orbital by the incoming X-rays from an XRF instrument. As a result, the atom is excited, and high-energy radiation is produced (photons, protons, and electrons). The final step involves identifying emission lines and converting the line intensities to elemental concentrations (Oyedotun, 2018). The elemental analysis of some adsorbents can be derived from a CHN analyzer. Dried samples are burned in the combustion box of an elemental analyzer when conducting a CHN test. The complete oxidation of the organic substance, in the presence of ultrapure O₂ and the carrier gas (ultrapure helium), converts carbon, hydrogen, and nitrogen content into CO₂, H₂O, and N₂, respectively. The quantities of the gases are measured by changes in the products' thermal conductivity after the gases are homogenized, depressurized, and separated by analytical columns (Ghosh & Chakraborty, 2013).

2.4.3.7. Proximate analysis

The proximate analysis determines the solid, gaseous, and non-combustible components of an adsorbent, respectively, as fixed carbon (solid), volatile matter (gaseous), ash content (ASH), and moisture content (Ambroz et al., 2018). After being heated to 110 °C in an N₂ environment, a sample loses mass, and this mass loss is used to calculate the moisture content. Except for mineral hydrates that break down beyond 110 °C, the moisture content includes any water that may be chemically or physically bonded. The volatile matter content is equivalent to the products produced by a thermal breakdown at temperatures between 110 and 900 °C in the presence of N₂. What remains after moisture and volatile materials have been removed, minus the combustion ash, is called fixed carbon. For the combustion, the sample is maintained at 900 °C, and the environment is changed from N₂ to air, and what is left over, after burning fixed carbon at 900 °C in air, is ash (Donahue & Rais, 2009).

2.4.3.8. Functional groups

Fourier transform infrared spectroscopy (FTIR) can identify the functional groups in materials by producing infrared beams. The spectrum produced by infrared spectroscopy, which measures the amount of IR radiation absorbed by each bond in a molecule, is often expressed as a percentage of transmittance vs wavenumber (cm^{-1}). The covalent bond of materials with an electric dipole absorbs energy when IR radiation interacts with it, and the bond begins to oscillate back and forth. When a molecule's dipole moment changes due to the oscillation of its bonds, IR light is absorbed by those bonds (S. A. Khan et al., 2018).

2.4.3.9. Zeta potential (ZP)

This is an analytical method to indirectly report the surface net charge and reflect the stability of the particles. It is the electric potential at the shear/slipping plane of a moving colloid particle in an electric field, and it describes the electrochemical equilibrium between particles and liquids in solutions. The electric potential of a surface is defined as the amount of work required to move a unit of positive charge from infinity to the surface without acceleration. Extremely positive or negative ZP values represent strong repulsive forces that restrain similarly charged particles from aggregating, and as a result, the re-dispersion of the solution is guaranteed (Bhattacharjee, 2016; Lunardi et al., 2021).

2.4.4. Adsorbent performance

2.4.4.1. Removal efficiency and adsorption capacity

The success of adsorption is evaluated by calculating the removal efficiency, removal capacity, and removal rate. The adsorption rate can be measured by determining the residual heavy metal after different contact times. Eq. (2-20) calculates

the adsorption efficiency (Lim et al., 2012).

$$\text{Adsorption efficiency (\%)} = \left(\frac{C_i - C_e}{C_i} \right) \times 100 \quad (2-20)$$

where C_i is the initial concentration, and C_e denotes the metal ion concentration in the equilibrium state. Eq. (2-21) is employed to calculate adsorption capacity, as given below (Lim et al., 2012):

$$\text{Adsorption capacity (mg g}^{-1}\text{)} = ((C_i - C_e) \times V)/W \quad (2-21)$$

where V stands for the volume of the metal solution, and W represents the mass of the adsorbent (Lim et al., 2012).

2.4.4.2. Reusability

Effective reusability refers to the ability of an adsorbent to be regenerated and utilized multiple times without considerably losing its adsorption capacity (Suresh Kumar et al., 2018). Many factors can decrease the performance of an adsorbent over time (Figure 2-12). These factors include incomplete adsorbate desorption, surface precipitation, active sites loss as a consequence of adsorbent wear and tear, and changes in adsorbent characteristics such as surface area, porosity and crystalline structure (Cabrera et al., 1981; Chitrakar et al., 2006; Kunaschk et al., 2015). Table 2-13 provides examples of changes in removal efficiency or capacity after several adsorption-desorption cycles.

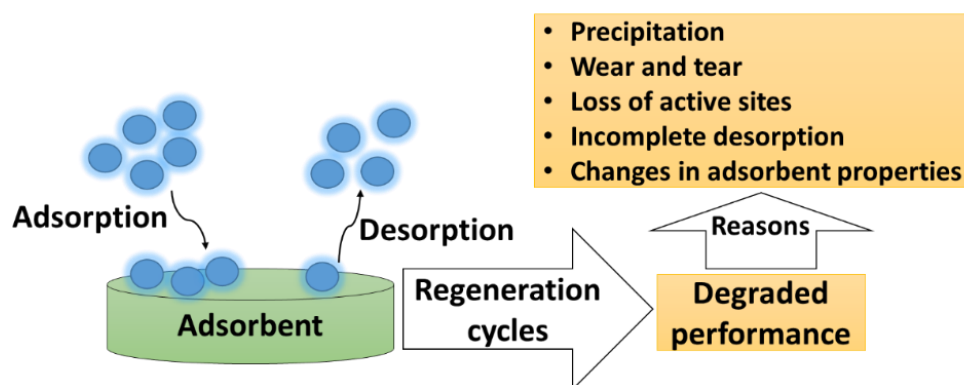


Figure 2-12 Effects of multiple regeneration cycles on the performance of adsorbents.

Table 2-13 Results of previous studies for several consecutive sorption/regeneration cycles.

Ion	Adsorbent	Number of Cycles	AC/RE Change	Reference
As(III)	Fe–Mn binary oxide	5	RC: –14%	(J. Qi et al., 2015)
As(V)	impregnated chitosan bead		RC: –17%	
As(V)	Metal-organic framework MOF-808	5	RE: 17%	(Z.-Q. Li et al., 2015)
As(III)	Magnetite/non-oxidative	5	RC: –14%,	(Yoon et al., 2017)
As(V)	graphene composites		RE: –22%	
			RC: –6%,	
			RE: –0.26	
As(III)	Chitosan magnetic graphene oxide nanocomposite	5	RE: –13%	(Sherlala et al., 2019)
As(V)	MIL-101(Fe)	3	RE: –40%	(Z. Li et al., 2019)

AC=adsorbent capacity; RE=removal efficiency.

2.4.4.3. Effects of parameters on adsorbent performance

It is essential to optimize removal conditions to improve adsorbent performance. Optimization studies have traditionally been conducted by tracking the impact of one factor at a time on an experimental response, while the other variables remained constant (one variable at a time). This method does not consider the interactions between the variables being researched; this approach increases the number of experiments required to find the optimum values (Bezerra et al., 2008). As a result, it is preferred to use a different approach that will be more successful and flexible for the parameter optimization of adsorption studies. One of the most used statistical tools for

optimizing adsorption conditions is response surface methodology (RSM) (Bashir et al., 2015). Recent predictive polynomial equations developed in adsorption research studies to optimize operational conditions are summarized in Table 2-14. The effects of process variables (pH, temperature, contact time, initial concentration, and adsorbent dose) on heavy metal removal efficiency and the adsorption capacity of adsorbents are described in the following sections. Table 2-15 shows the effect of different parameters on the adsorption of As from aqueous solutions.

Table 2-14 Summary of previous studies on the mathematical models of arsenic removal by different adsorbents.

Method	Ion	Adsorbent	Models	Max AC/RE(%)	Reference
CCD	As(V) and As(III)	Iron-impregnated sugarcane carbon	Breakthrough time (min) $= 473.0 - 317.6A + 316.5C - 174.2F - 111.4AC$ $- 87.0AF - 57.8CF$ $+ 3.7A^2 + 486.9C^2 + 38.0F^2$	AC: 147.7 $\mu\text{g g}^{-1}$	(Roy et al., 2014)
	As(V)	Mill scale-derived magnetite particles	AC = $4.4 + 2.10A - 0.9941B + 0.3521D - 0.4235P - 0.7756AB + 0.1931AD - 0.1272BD + 0.1477BP - 0.33063AP - 0.0212DP - 1.2551A^2 - 0.6767B^2 + 0.3406D^2 - 0.1976P^2$	AC: 8.13 mg g^{-1}	(Phearom et al., 2021)
	As(V)	Iron oxide immobilized graphene oxide gadolinium nanocomposite	RE (%) = $-1.760 + 0.548A + 5.014B + 184.496C + 0.291D + 0.017AB - 0.590AC + 0.001AD - 1.362BC - 0.002BD - 0.010CD - 0.015A^2 - 1.129B^2 - 111.685C^2 - 0.001D^2$	RE: 94.8%	(Lingamdinne et al., 2020)
BBD		Metal oxide-precipitated clinoptilolite	AC = $2.583769 + 0.885829A - 0.184399B - 0.074153T - 0.135264AB + 0.005606AT + 0.002475BT + 0.000546T^2 - 0.008533A^2$	AC: 6.1 mg g^{-1}	(Simsek et al., 2013)
	As(III) and As(V)	CeO ₂ /Fe ₂ O ₃ /graphene nanocomposite	RE (%) (AS(III)) = $89.71 - 80.20A - 9.45B + 2.91C - 3.25AB + 1.24AC + 0.39BC - 1.73A^2 - 25.21B^2 - 0.078C^2$ RE (%) (AS(V)) = $66.98 - 7.63A - 27.20B + 2.77C + 0.53AB + 1.68AC - 0.028BC + 3.48A^2 - 8.27B^2 + 4.38C^2$	As(III): 98.53% As(V): 97.26%	(Sahu et al., 2018)

A = initial concentration, B = pH, C = adsorbent dose, CCD = central composite design; BBD=Box- Behnken method; D = contact time, F = flow rate, P = particle size and T = temperature; AC=adsorbent capacity; RE=removal efficiency.

Table 2-15 Summary of studies on the effect of process parameters on arsenic removal by different adsorbents.

Adsorbent	Adsorbate	pH	T(K)	t _c (min)	C _i (mg L ⁻¹)	A _d (g L ⁻¹)	RE (%) (Max)	AC (mg g ⁻¹)	Reference
Magnetic graphene oxide	Pb(II)	3–9	298	10–65	60	0.002– 0.016	Pb(II): 99.97	Pb(II): 200	(Farooq & Jalees, 2020)
	Cr(III)	(Pb(II): 5		(Pb(II), Cu(II),			Cr(III): 97.78	Cr(III):24	
	Cu(II)	Cr(III): 6		Ni II): 25			Cu(II): 96.65	Cu(II):62	
	Zn(II)	Cu(II):7		Cr(III),			Zn(II): 91.88	Zn(II):63	
	Ni(II)	Ni(II):8)		Zn(II):35)			Ni(II): 95.28	Ni(II):51	
Carboxyl modified lignocellulose-biomass jute fiber	Pb(II)	2–6 (6)	298	0–180 (20)	200	1.0		157.21,	(Z. Du et al., 2016)
	Cd(II)							88.98,	
	Cu(II)							43.98	
Magnetic carboxymethyl chitosan nanoparticles	Pb(II),	5.2	298	2–60	100	1.0		Pb(II): 243,	(Charpentier et al., 2016)
	Cu(II)			(60)				Cu(II): 232,	
	Zn(II)							Zn(II): 13	
Esterified hydroxyapatite	Pb(II)	3–7 (3)	298	10–720 (60)	30–300 (100)	0.1	Pb(II): 99% < 60 ppm	2397	(M. Wang, Zhang, et al., 2019)
Peanut hull	Cu(II)	1.5–4 (4)	298 to 338 (298)	5–180 (60)	150- 500 (150)	0.1–1(1)	> 80%	14	(R. M. Ali et al., 2016)
Microcrystalline cellulose-based nanogel	Cd(II)	6	300	10–90 (30)	20	0.05–1 (0.5)	97%	595	(El-Naggar et al., 2018)
Magnetic Zr-MOF	Pb(II)	Pb(II) 1–7	298	10–250	Pb(II): 10–500	1		Pb(II): 273	(C. Wang et al., 2021)
	Cr(VI)	(4) Cr(VI) 1–10 (3)		(Pb(II): 60 and Cr(VI): 30)	(500) Cr(VI):10– 1000 (1000)			Cr(VI): 429	

T = temperature; C_i = initial concentration; t_c = contact time A_d = adsorbent dose AC = adsorbent capacity; RE = removal efficiency.

1- pH

The solution pH significantly impacts the distributions of the metals, their mobilization, and the surface charge of the adsorbents during the adsorption (Tahmasebpour et al., 2022). In a lead removal study, the adsorption capacity of the mussel shell increased from 43.62 mg g^{-1} to 63.49 mg g^{-1} upon an increase in pH (4–6). Low pH decreased the Ca(II) dissociation in the solution, and Pb(II) exchanges with a limited quantity of Ca(II) ; when the pH is high, there is more dissociation of Ca(II) , and Pb(II) exchanges with more Ca(II) , implying that the adsorption capacity increases. (Q. Wang et al., 2021).

As(V) adsorption on the granitic material decreased as the pH increased from 4 onward, according to a previous study (Seco-Reigosa et al., 2015). The granitic material compounds with variable charges pose a positive charge at an acidic pH, which helps them retain H_2AsO and HAsO_2 . As the pH rises, they suffer from progressive deprotonation and an increase in negative charge, which can reduce As(V) adsorption (Seco-Reigosa et al., 2015).

The effects of pH on the removal of As(III) and As(V) were studied to find the ideal pH for the highest adsorption of As on biochar-stabilized iron and copper oxide nanoparticles. In the pH range of 6–8, the highest adsorption of As occurs at pH 7, with $> 95\%$ removal. The surface charge of the composite adsorbents and the ionization potential of the As species are both influenced by the pH of the solution. A pH between 6.5 and 7, which is mildly acidic to neutral, encourages the ionization of H_3AsO_4 to produce $\text{H}_3\text{AsO}_4^{2-}$, which has a negative charge, while the composite mixture acquires a mildly positive charge as a result of the conversion of Fe-OH and Cu-OH to Fe-OH^{2+} and Cu-OH^{2+} . Due to the opposite charges of the composite mixture and As(V) species, the electrostatic attraction between adsorbate and adsorbent increases, leading to higher

adsorption (Priyadarshni et al., 2020).

In a pH range of 1.0–13.5, the behavior of As adsorption on octahedral TiO₂ nanocrystals was studied. As(III) and As(V) exhibited their highest adsorptions at pH values of 8 and 4, respectively. The smallest As(III) and As(V) adsorptions occurred at pH 12, and at higher pH levels, such as 13.0 and 13.5, their adsorptions increased once again. The primary cause of the significant adsorption of As should be the electrostatic interactions between the As species and the TiO₂ surface (Wei et al., 2016). Another work assessed the effects of solution pH and ionic strength on As(III) uptake by a nanostructured iron-copper-manganese tri-metal oxide. As the pH of the solution increases, As(III) sorption decreases. Strong repulsive forces between the produced anions of As(V) and the surface of trimetal oxide with a negative charge may be the reason for the low adsorption of As(III) at high pH levels (G. Zhang et al., 2020).

The impact of pH has been investigated in As(III) removal by a chitosan magnetic graphene oxide nanocomposite (CMGO). The removal efficiency improved by increasing the pH from an acidic to a neutral pH; at an alkaline pH, it dropped. The maximum removal and adsorption capacities were attained at pH 7.3. The pH of the point zero charge (pH_{pzc}) of the nanocomposite was about 6.8. As a result, the surface of the adsorbent will be negatively charged at pH levels greater than pH_{pzc} and positively charged at pH levels lower than pH_{pzc}. Thus, the surface of the CMGO is negatively charged, where the maximum As(III) was found. Since As(III) usually exists in the nonionic state (H₃AsO₃) at pH levels below 9.2, surface complexation rather than electrostatic interactions govern the adsorption of As(III) (Sherlala et al., 2019).

2- Temperature

The endothermic process experiences an increase in sorption capacity with increasing temperature, and the exothermic process exhibits a reduction in sorption

capacity with increasing temperature (Afroze & Sen, 2018). As temperature has little effect on the adsorbent's ability to adsorb heavy metal, room temperature is frequently used in this kind of study (Fernández-López et al., 2019).

Mussel shell powder was added to a Pb(II) solution, and the sample was stirred until equilibrium was achieved in the range of 293–308 K, in order to investigate the impact of temperature on the adsorption performance of the adsorbent. According to the results, as the temperature rose from 293 to 308 K, the q_e increased from 53.86 to 65.41 mg g⁻¹. This may be due to increased molecular mobility at higher temperatures, which increases the likelihood that Pb(II) will come into contact with the adsorption sites (Q. Wang et al., 2021). As(V) removal effectiveness and modified saxaul ash removal effectiveness increased with temperature from 293 to 323 K. By increasing the temperature, the viscosity of the solution was reduced. The increased removal efficiency was also caused by increasing the release of adsorbent molecules in the pores of adsorbent particles and through the external boundary layer (Rahdar et al., 2019).

In the adsorption of lead and As ions by activated carbon from Tamarix leaves, the adsorption efficiency decreased upon an increase in the temperature between 25 and 55 °C, because heavy metal ions have a strong tendency to leave the adsorbent surface and return to the solution as the temperature goes up (Koohzad et al., 2019). According to the findings of a different investigation, as the temperature increased from 25 to 45 °C, the percentage of As removed by co-modified bentonite with manganese oxides and poly (dimethyl diallyl ammonium chloride) increased gradually from 87% to 91%. This might be caused by an increase in the mobility of As species or by the adsorbate faster diffusion rate through the pores due to a reduction in the viscosity of the solution (Hua, 2018).

3- Contact Time

Since it influences the operation's economics and adsorption kinetics, it is crucial to determine the ideal contact time for the adsorption process (Iftekhhar et al., 2018). A Pb(II) solution (100 mg L^{-1}) was mixed with shell powder (0.02 g), the pH was adjusted to 6, and the adsorption process was carried out at 25°C for 10–540 min. The results demonstrated the existence of more active sites that caused the calcined sample's adsorption capacity to grow quickly, 360 min after the process began. Due to the gradual saturation of the powdered calcined mussel shell, a further extension of the adsorption duration led to a marginal increase in the adsorption capacity (Q. Wang et al., 2021).

In another study, with increasing contact time, the effectiveness of removing cadmium increased from 56 to 78%, chromium from 90 to 94%, and lead from 93 to 96% (Flora, 2015). The green mussel shell adsorbed more metal ions as the agitation time increased. After a certain amount of time, the adsorbent surface area slowly exhausts, reducing the adsorption capacity. According to the results, the equilibrium adsorption capacities for these metals were 2.1 , 2.6 , and 2.7 mg g^{-1} , obtained after 8 h. The uptake trend increased and then became constant after 8 h (Rahman et al., 2017).

An experiment was conducted for 48 h with initial concentrations of 100, 500, and 1000 g L^{-1} of As(III) and 50 mg L^{-1} of nanoparticles to examine the influence of the contact time evaporation of As(III) and As(V) by Fe/Cu nanoparticles. The findings showed that most of the reaction occurs within the first hour (Babaei et al., 2018). According to the findings of an investigation on As(III) sorption (As(III) removal by a nanostructured iron-copper-manganese tri-metal oxide), the removal rate was rapid within the first 2 h, and over 85% of the equilibrium uptake capacity was achieved. Afterward, As(III) sorption began to slow down, and sorption equilibrium was attained after about 24 h (G. Zhang et al., 2020). Arsenic was quickly absorbed into the Fe-

modified biochar and Cu-modified biochar adsorbent during the first 5–40 min, increasing significantly after that. The process continued at quite a slow rate until the equilibrium was achieved after 60 min. After 60 min of stirring, there was no noticeable change in the amount of As that was adsorbing; hence, 60 min was regarded as an effective equilibrium contact period for 95.3% As removal efficiency (Priyadarshni et al., 2020).

Furthermore, the impact of contact time on lead and As ion adsorption by activated carbon prepared from Tamarix leaves was examined for 5–120 min. After 60 and 40 min for lead and As, respectively, the adsorption efficiency stabilized, revealing that the adsorbent's active sites had been saturated (Koohzad et al., 2019). Modified saxaul ash was used to remove As(V) from water-based solutions, and the As removal increased with longer contact times. The absorption rate was high in the first 30 min and equilibrium time was 60 min; changing As initial concentration did not affect the amount of time to reach equilibrium (Rahdar et al., 2019).

In general, the quantity of adsorption sites in the adsorbent structure is what causes the rapid adsorption process in the initial stages of the process. As a result of the ions occupying these sites, the efficiency starts to decline, but after a period, no changes in the adsorption efficiencies are noticed. The occupation of the remaining unoccupied sites becomes more challenging as the contact time increases because of the gradual occupancy of the vacant sites and the ions-liquid phase repulsive interactions (Koohzad et al., 2019).

4- Initial Concentration

Increasing the initial metal ion concentration in a solution usually enhances the adsorption uptake (Hilal et al., 2012). A research study showed that as a function of equilibrium As and initial concentration, As adsorption on mussel shell ash increases

linearly (Seco-Reigosa et al., 2013). Another study showed that the adsorption capacity of Pb(II) on the calcined shell powder increased from 14.72 to 57.79 mg g⁻¹ as the starting lead concentration increased from 20 to 100 mg L⁻¹. Lower Pb(II) concentrations prevented the adsorbent from reaching saturation, whereas larger concentrations caused the accessible adsorption sites on the surface of the calcined shell powder to gradually fill up and attain saturation (Q. Wang et al., 2021).

Batch mode investigations on the adsorption of heavy metals on the green mussel shell-derived adsorbent revealed that with an increase in the initial concentration from 1 to 20 mg L⁻¹, the removal efficiency of cadmium, chromium, and lead was changed from 80 to 59%, 28 to 92% and 79 to 95%, respectively. The pattern may be justified because a higher initial concentration of ions increases the adsorption capacity temporarily, but as the process progresses, an increasing amount of ions come into contact with fewer active sites on the adsorbent surface. (Rahman et al., 2017). Investigations were conducted on the removal efficiency of As by co-modified bentonite with manganese oxides and poly (dimethyl diallyl ammonium chloride) as a function of initial As concentrations between 0.25 and 2.00 mg L⁻¹. The removal efficiency of As was initially high, reaching 90% (initial concentration = 0.25 mg L⁻¹), then constant for values between 0.25 and 0.5 mg L⁻¹, then gradually declined with increasing concentration, and finally, the decrease was rapid for the initial concentration higher than 1.5 mg L⁻¹ (Hua, 2018). In another study, 2 mg of nanofibers was fixed at a neutral pH by conducting the adsorption at various concentrations from 10 ppb to 10 ppm. The highest absorption of the porous carbon nanofibers was at 1 ppm concentration (Mahar et al., 2019).

In the adsorption of lead and As by zeolite modified with copper oxide and iron oxide, initial concentrations of 20 to 100 mg L⁻¹ did not significantly change the

removal efficiency (Alswat et al., 2016). Changes in lead concentration between 1 mg L⁻¹ and 180 mg L⁻¹ were used to maximize removal efficiency by Bentonite clay. It was observed that lead removal efficiency increases initially upon an increase in the initial concentration. From 35 mg L⁻¹, the lead removal efficiency slightly declines. Adsorption reduces once the saturation level is reached since no more ions can be absorbed (M. R. Khan et al., 2017). The reduction in the removal percentage at higher concentrations is likely because of the adsorbent's limited available active sites and the additional heavy metal ions that compete for these sites, which become more saturated as metal ion concentration increases. (Alswat et al., 2016).

5- Adsorbent Dose

Adsorbent dose affects adsorption surface area and the number of active sites on the adsorbent's surface. If interference from active sites interacts after a specific dose limit, adsorption may stay the same or even decrease (Othmani et al., 2022). The effect of the mussel shell adsorbent dose (0.01–0.05 g) on the adsorption of Pb(II) was studied. The results showed that the removal rate increased from 41.21% to 65.08% as the adsorbent dose increased, while the q_e of the adsorbent reduced from 82.42 to 26.03 mg g⁻¹ (Q. Wang et al., 2021). This might be explained by taking into account the greater number of adsorption sites provided by increasing the shell powder concentration (Rahman et al., 2017).

The larger concentrations of green mussel shell increased cadmium, chromium and lead removal efficiency from 50% to 67%, 70% to 93%, and 51% to 97%, respectively. (Rahman et al., 2017). The As(III) adsorption rose with the increase in adsorbent dose, as the results of As removal by iron oxide/nano-porous carbon magnetic composite showed that 1.8 g L⁻¹ of adsorbent removed the maximum percentage of As (about 75%). After that, an equilibrium was reached, and subsequent additions did not affect

the adsorption (Joshi et al., 2019). The impact of the adsorbent dose on the As(III) adsorption was examined by adjusting the concentration of chitosan magnetic graphene oxide nanocomposite (CMGO) in the solution between 1 and 5 g L⁻¹. As the adsorbent dosage increased from 1 to 5 g L⁻¹, the removal efficiency improved, but the adsorption capacity dropped (Sherlala et al., 2019).

According to the investigation of the effect of Fe/Cu nanoparticle dose (10–100 mg L⁻¹) on the removal of As(III) and As(V), the removal percentage increased with increasing adsorbent dose. However, the rate of increase in As removal was less noticeable when the dose of nanoparticles increased from 50 to 100 mg L⁻¹ (Babae et al., 2018). The highest removal of As was determined to be nearly 98% at the adsorbent (co-modified bentonite with manganese oxides and poly (dimethyl diallyl ammonium chloride)) dosage of 15 mg per 70 mL, according to the results of another experiment. The removal of As rose slowly with increasing adsorbent dosage. After a dosage of 15 mg per 70 mL, the As removal percentage did not change noticeably (Hua, 2018). The optimum quantity of clay for lead removal was identified for an initial metal concentration of 50 mg L⁻¹ at a pH of 6 by adjusting the clay amount from 0.1 g to 0.9 g. It was found that as the clay dose increases, the adsorption efficiency increases. This is because the adsorbent's surface area increases. The optimum clay concentration for removing lead (Pb) was 0.3 g per 50 mL (M. R. Khan et al., 2017).

Increasing the adsorbent dose generates bigger surface areas and more active sites, which increase the adsorption capacity. In contrast, the decrease in the percentage of adsorption with a higher adsorbent dosage after a certain amount may be caused by the loss in adsorbent surface area due to the accumulation of adsorbent particles or the low quantity of ions in the solution in comparison to the accessible vacant sites, or interference between the high adsorbent dosage and active sites (Alswat et al., 2016).

2.4.5. Arsenic adsorbents

Some known adsorbents used to remove As are hydrous titanium dioxide (TiO₂) (Guan et al., 2012), iron oxides/hydroxides (Hao et al., 2018), zeolites (Shevade, 2003), activated carbon (Koohzad et al., 2019), and alumina (Camacho et al., 2015). Nanoparticles such as gold (Hua, 2021), cupric oxide (Reddy et al., 2013), metal oxide nanomaterials (Hristovski et al., 2007), impregnated granulated activated carbon (Q. Chang et al., 2010), and nanostructured Fe(III)–Cr(III) mixed oxides (Basu & Ghosh, 2011) have also been used in As removal. The literature showed that nanomaterials can be efficient adsorbents for heavy metal removal.

Due to the toxic nature of As, scientists are seriously working on developing new cost-effective adsorbents. Table 2-16 provides examples of the efficiency of different adsorbents under different process conditions. Although commercial adsorbents such as activated carbon (Karnib et al., 2014), activated alumina (Camacho et al., 2015), and iron oxide-based (Hao et al., 2018) sorbents have shown high efficiency in removing As, finding economically feasible adsorbents and locally available solutions is still strongly desired. Nowadays, researchers investigate the application of natural materials, including soils (R. Mondal et al., 2019), rocks (Maji et al., 2015), hydroxylapatite and struvite (Rouff et al., 2016), zeolites (Shevade, 2003), industrial wastes (Sosa et al., 2020), polymer resins (Önnby et al., 2012), and biosorbents (Shakoor et al., 2019). Recent studies used low-cost adsorbents such as iron oxide-coated fungal biomass (Pokhrel & Viraraghavan, 2006), methylated yeast biomass (Seki et al., 2005), residue rice polish (Ranjan et al., 2009), crab shells (Sumaila et al., 2020), modified coconut coir pith (Bahar et al., 2018), cotton-based adsorbents (Akpomie & Conradie, 2020), bone char (Alkurdi et al., 2020), shrimp wastes (Dehghani et al., 2018), and modified sawdust (J. Yang et al., 2022).

Table 2-16 Different adsorbents used in arsenic removal, their operating conditions, and efficiencies for arsenic removal.

Adsorbent	Conditions	RE (%) and/or AC (mg g ⁻¹)	Reference
Activated alumina	pH: 7.6, C _i (As(III)) = 1 mg L ⁻¹ Contact time: 0–6 h	RE: 96.2	(T. S. Singh & Pant, 2004)
Manganese oxide	pH: 7.9 C _i : <1 mg L ⁻¹	AC: 0.172	(As(V)): (Ouvrard et al., 2002)
Porous resin loaded with crystalline hydrous zirconium oxide	C _i : 0–5 mmol L ⁻¹ pH 4.5 for As(V) pH: 8.0 for As(III)	AC 79.42, AC 53.94	(As(V)): (Suzuki et al., 2000) (As(III)):
Iron-oxide-impregnated activated carbon	Adsorbent dose: 0–0.2 g L ⁻¹ pH: 7 C _i (As(V)): 1 mg L ⁻¹	AC: 4.5	(Vaughan Jr & Reed, 2005)
Titanium dioxide-loaded Amberlite XAD-7 resin	pH (As(v)): 1–5 pH (As(III)): 5–10 Contact time (As(v)): 6 h Contact time (As(III)): 2 h	AC (As(V)): 9.74 AC 4.72	(Balaji & (As(III)): Matsunaga, 2002)

RE = removal efficiency; AC = adsorption capacity (mg (As) g⁻¹ (Adsorbent)); C_i = initial concentration.

The low-cost adsorbents used in recent studies can be classified as industrial waste, animal waste, natural materials, bio-adsorbent, and agricultural waste (Chakraborty et al., 2022). Table 2-17 provides an example of each category in specific conditions.

Table 2-17 The results of using some low-cost adsorbents in arsenic removal.

Ion	Adsorbent	pH	T (°C)	t _c (h)	C _i (mg L ⁻¹)	A _d (g L ⁻¹)	RE (%)	AC (mg g ⁻¹)	Reference
As(III) As(V)	Fly ash	7.3	20	24	1	0.5	87.6 99.6		(Shadbahr & Husain, 2019)
As(V)	Mussel shells	~10		24	0.5–100	100	96		(Seco-Reigosa et al., 2013)
As(V)	Natural orange peel Charred orange peel	6.5	20	24	200	4	68 98	32.7 60.9	(Abid et al., 2016)
As(III) As(V)	Fe–Mn binary oxides-loaded zeolite	7.0	25	3	2	5		296.23 201.10	(Kong et al., 2014)
As(III) As(V)	Modified chitosan beads	7.0	25	36	5–60	1		54.2 39.1	(J. Qi et al., 2015)

RE = removal efficiency; AC = adsorption capacity; C_i = initial concentration; A_d = adsorbent dose, T = temperature, t_c = contact time.

2.4.5.1. Industrial waste (fly ash-based adsorbents)

The presence of toxic elements in fly ash makes this powdery material toxic; therefore, fly ash disposal is a challenging process (Gadore & Ahmaruzzaman, 2021). Researchers have studied the application of waste material such as fly ash in different processes since the utilization of fly ash, rather than its disposal, has environmental and economic benefits. Fly ash can be efficiently used as a low-cost adsorbent of heavy metal and organic pollutants from water solutions and flue gas. Bagasse fly ash (3 g L⁻¹) at pH 7 and 20.0 °C removed 95.0 and 89.5% of As(V) and As(III) from water, respectively, after 50 min, with an initial concentration of 50 g L⁻¹ (I. Ali et al., 2014). Another adsorbent for As(V) removal was synthesized using special iron-abundant fly ash. The adsorption capacity of the adsorbent was 19.46 mg g⁻¹, and removal efficiency was above 99% (Y. Li et al., 2009). In another study, a low-cost adsorbent was developed to remove As from Bell Island's (Government of Newfoundland and Labrador, Canada) well water using modified fly ash from the Corner Brook Pulp and Paper mill. For local well water, the highest adsorption capacity was 35.6 µg g⁻¹ and 1428.6 µg g⁻¹ for local well water and synthetic water, respectively (Shadbahr & Husain, 2019).

Coal, as a source of energy in electric power generation, produces tons of fly ash worldwide. Coal fly ash (CFA) is 65–95% of the total ash generated by burning coal. Some coals contain high ash content (30–50%), while others have a low ash content, of the order of 10–15% (Dwivedi & Jain, 2014; Mushtaq et al., 2019; Tiwari et al., 2016). The type of coal that is burned (anthracite, bituminous, sub-bituminous, and lignite) and the way it is handled and stored affect the coal fly ash chemical properties. The main components of fly ash are generally carbon, silica, alumina, iron oxide, and calcium. Using fly ash in heavy metal adsorbents not only prevents environmental problems

caused by this contaminant but also is a convincing way to remove heavy metal pollutants from water and wastewater streams (Ayanda et al., 2012).

Burning biomass is another source of fly ash that causes environmental problems; however, in contrast to coal ash, there are no toxic metals in fly ash produced after burning biomass. The composition of this type of fly ash depends on the type of the original biomass. The combustion method determines the crystallinity and mineralogy of this fly ash.

In general, Ca, Na, Si, P, and silicon and alkali metals, in some cases, are the inorganic elements that form biomass fly ash. Biomass fuels have higher concentrations and amounts of inorganic material variation than coal. Therefore, depending on the origin of the biomass and production factors such as weather and storage conditions, there are various compositions of biomass fly ash (Bridgeman et al., 2007; Masiá et al., 2007; Wiseloge et al., 1996). Due to this variation, there are not sufficient records of the utilization of biomass fly ash in contrast to coal fly ash. However, several studies have demonstrated the applications of biomass fly ash as an adsorbent (Ahmaruzzaman, 2010), raw material for ceramics (Kizinievic & Kizinievic, 2016), cement (L. Wang et al., 2020), and concrete additive (Popławski & Lelusz, 2017). Table 2-18 provides the chemical composition of several types of fly ash.

Table 2-18 Chemical composition of coal and biomass fly ash ash (G. Liang et al., 2020; Sarkkinen et al., 2018; Teixeira et al., 2019).

Fly Ash Type	SiO ₂	CaO	Al ₂ O ₃	Fe ₂ O ₃	K ₂ O	MgO	Na ₂ O	P ₂ O ₅	TiO ₂
Coal	54.08	3.27	26.38	6.12	1.64	1.55	0.51	0.80	1.44
Biomass	36.03	27.41	8.33	4.12	4.92	3.56	0.87	3.21	0.94
Biomass	44.41	23.84	10.80	3.63	3.99	3.76	1.27	2.02	1.05
Biomass	20.38	40.13	8.20	17.40	2.41	3.26	0.43	3.20	0.42
Biomass	37.43	10.96	12.97	9.74	3.21	2.30	1.50	1.61	0.91

2.4.5.2. Animal waste (fisheries waste-based adsorbents)

Crab shell has been used to prepare an adsorbent to remove heavy metal ions (Pb, Cd, Cu, Cr) from solutions. The preparation procedure included separating the shell and meat by boiling or steaming, washing, and drying the shell, and finally pulverizing the dried shell. Compared to conventional methods, crab shells showed a higher removal rate than cation exchange resin (CER), zeolite, powdered activated carbon, and granular activated carbon for Pb, Cd, and Cr. In contrast, the capacity of the crab shell was less than CER for Cu (H. K. An et al., 2001). In another study, calcined mussel shell showed an adsorption capacity of 102.04 mg g⁻¹ for lead removal, proving that calcined mussel shell is a promising adsorbent for heavy metals (Q. Wang et al., 2021).

Fish scales are another available waste that is abundant and easy to prepare as an adsorbent. Fish scales were used to investigate their efficiency in removing Pb(II) and Zn(II) ions (Onwordi et al., 2019; Othman et al., 2016). In a study, fish scales were used in batch adsorption experiments. The results proved the potential of fish scales for Pb(II) and Zn(II) removal with a maximum removal efficiency of 81.97% and 80.37%, respectively (Stevens & Batlokwa, 2017).

Fish bones have been used to remove copper and cobalt from wastewater. The results revealed that the contact time for equilibrium is 270 min for Cu(II) and 300 min for Co(II). By increasing the initial metal concentration from 50 ppm to 300 ppm, the removal efficiency dropped from almost 40% to nearly 25% (Rezk et al., 2018).

2.4.5.3. Natural materials (zeolites)

HDTMA-Br and HDTMA-Cl as surfactants were employed to modify two natural zeolites (clinoptilolite and phillipsite). These developed adsorbents were synthesized and evaluated as adsorbents for As(V) removal from wastewater. Results revealed that As(V) removal has a fast adsorption rate and follows a pseudo-second-order kinetic

model, with 100% removal occurring in all samples in 2 h (de Gennaro et al., 2020).

In another study, the adsorption capacity of zeolite, nanomagnetite, and a nanomagnetite-zeolite composite were found to be 0.3, 4.7 and 6.2 mg g⁻¹ for the adsorption of arsenate in hydroponic tomato cultures, respectively (Pizarro et al., 2021). The application of 2D zeolitic imidazolate framework-67 porous nanosheets (ZIF-67-NS) was evaluated as a potential adsorbent for As(III) removal from water. In contrast to its 3D bulk-type counterpart (ZIF-67-NB), ZIF-67-NS showed much better adsorption capacity (516 mg g⁻¹) and faster absorption kinetics (2 h). After three cycles, ZIF-67-NS was effectively regenerable, with minimal adsorption capacity loss (Zhao et al., 2020).

2.4.5.4. Bio-adsorbent (chitin/chitosan)

Silica-stabilized hybrid chitosan microspheres were used to remove As from water. When compared to chitosan beads alone, hybrid beads have a higher As(V) adsorption efficiency because the addition of magnetite (Fe₃O₄) nanoparticles increases the beads' surface area. Furthermore, the hybrid and chitosan beads' adsorption capacities were 1.699 and 0.082 mg g⁻¹, respectively (Malwal & Gopinath, 2017).

Fe-Mn binary oxide was impregnated into chitosan beads to produce a sorbent known as Fe-Mn binary oxide impregnated chitosan bead (FMCB). The highest adsorption capacities for As(V) and As(III) were 39.1 and 54.2 mg g⁻¹, respectively. NaOH solution could be employed to effectively regenerate and reuse the As-loaded FMCB (J. Qi et al., 2015).

In another study, chitin was pyrolyzed and treated with nitric acid to increase surface area. Then, Ca(OH)₂ was loaded onto the char to develop a new type of biomaterial to eliminate As. According to the kinetic experiments, an adsorbent dosage of 0.4 g L⁻¹ and a concentration of 10 mg L⁻¹ produced an optimal equilibrium time of

2 h. The highest removal efficiency was around 99.8% with 0.4 g L⁻¹ of adsorbent (Z. Yang et al., 2021).

2.4.5.5. Agricultural waste (fruit peels)

Column-scale laboratory experiments were conducted using synthetic solutions and groundwater to determine the As removal efficiency by orange peel and banana peel. In As-contaminated groundwater of 5, 10, and 50 µg L⁻¹ after 1 h, the removal efficiency of both adsorbents was 100%, 100%, and 90%, respectively. In synthetic As-spiked water of 10, 50, and 100 µg L⁻¹, the removal efficiency was 50%, 90%, and 90%, respectively (Tabassum et al., 2019).

Batch sorption studies were used to compare the biosorption capacities of natural orange peel (NOP) and charred orange peel (COP) for As(V) removal in aqueous environments. The largest amount of As(V) adsorption occurred at pH 6.5, and COP removed As(V) by 98%, which was higher than that obtained by NOP (68%) at the optimal adsorbent dose of 4 g L⁻¹ (Abid et al., 2016).

Column-scale laboratory experiments were conducted using synthetic solutions and groundwater to determine the As removal efficiency by orange peel and banana peel. In As-contaminated groundwater of 5, 10, and 50 µg L⁻¹ after 1 h, the removal efficiency of both adsorbents was 100%, 100%, and 90%, respectively. In synthetic As-spiked water of 10, 50, and 100 µg L⁻¹, the removal efficiency was 50%, 90%, and 90%, respectively (Tabassum et al., 2019).

Batch sorption studies were used to compare the biosorption capacities of natural orange peel (NOP) and charred orange peel (COP) for As(V) removal in aqueous environments. The largest amount of As(V) adsorption occurred at pH 6.5, and COP removed As(V) by 98%, which was higher than that obtained by NOP (68%) at the optimal adsorbent dose of 4 g L⁻¹ (Abid et al., 2016). The peel (PAC-500) and pulp

(PPAC-500) of the *Citrus limmeta* fruit were used to develop activated carbon with magnetic characteristics at 500 °C. The PAC-500 has a higher As(III) adsorption capacity (714.3 g g^{-1}) than the PPAC-500 (526.316 g g^{-1}). For As(V) removal, PAC-500 and PPAC-500 showed an adsorption capability of 2000 g g^{-1} . Concentrations $< 300 \text{ g L}^{-1}$ were completely removed by PAC-500 and PPAC-500 (Verma et al., 2019).

2.5. Application of Adsorption in Drinking Water Treatment Systems

Cost considerations play a critical role in selecting appropriate arsenic removal technologies for low-resource settings, where financial constraints often outweigh technical performance. Ion exchange involves high material costs due to expensive resins and recurring expenses from chemical regenerants, making it financially burdensome for decentralized applications. Membrane filtration methods, such as reverse osmosis and nanofiltration, require substantial capital investment for equipment and ongoing costs for energy, maintenance, and membrane replacement. Coagulation–flocculation, while relatively inexpensive in terms of coagulant chemicals, incurs additional operational costs associated with sludge handling, including sludge dewatering, transportation, and safe disposal—expenses that are often overlooked but critical in cost evaluations. Oxidation processes, particularly advanced oxidation methods, involve high costs related to chemical reagents and energy input, which limit their economic feasibility in low-income or off-grid communities. In contrast, adsorption offers the lowest overall cost among these methods, especially when using waste-derived materials like modified mussel shells or agricultural biochars. Adsorption is regarded as the most economically advantageous method for removing As for small communities because of its high removal and energy efficiency, ease of design and operation, and minimum disposal cost and toxicity. As can be removed from

water using commercial adsorbents such as activated carbon. However, its relatively high cost might exclude its use in rural areas (T. H. Nguyen et al., 2020).

Numerous adsorbents have been developed over recent years; however, few options are efficient, affordable, or easy to install, particularly in developing nations (R. Liu & Qu, 2021). Another challenge is that removing fine powder adsorbents from the water after adsorption is not easy. Additionally, fine powders may block the filters and cause hydraulic issues in columns, increasing the energy and maintenance costs (T. H. Nguyen et al., 2020). Granulating the adsorbents and using them in fixed-bed filters represents a common solution to this issue; however, these treatments significantly reduce the active sites available for As and raise the price of adsorbents' production (R. Liu & Qu, 2021; Usman et al., 2021). When fine particles or micro-sized fractions ($< 250\ \mu\text{m}$) are used in a fluidized-bed reactor for As removal, a downstream membrane reactor is required to separate the adsorbent (Usman et al., 2021). The necessity to regenerate and reuse adsorbents to lower costs adds another difficulty. The regenerating process requires strong basic solutions, which challenge the maintenance of the reactors and the treatment of basic waste (R. Liu & Qu, 2021).

As a result, these important issues must be solved to promote adsorption in decentralized systems. More research and engineering investigations are required to successfully employ adsorption in the treatment of community drinking water supplies, since most adsorption studies are limited to laboratory-scale experiments. Table 2-19 includes several pilot-size (small-scale) investigations of As removal by different treatment methods.

Table 2-19 Arsenic removal efficiency by different methods (pilot scale).

	Removal Agent	Flowrate (m ³ d ⁻¹)/Volume	C _i (µg L ⁻¹)	Removal (%)/ Final Concentration (µg L ⁻¹)	Other Available Data	Reference
Adsorption	ZVI adsorption–aeration	0.14–1.4	130	90–95	Operation life: 30 days	(Litter et al., 2019)
	Laterite	5	220–300	86.0	Initial ZVI loading = 500 g Mn: 96.9%, Cd: 79.6%, Zn: 52.9%, and Pb: 38.7%.	(H. T. H. Nguyen et al., 2019)
	GFH-based adsorbent	96–3840	12–28	>80	Hydraulic EBCT: 3–10 min pH = 7–8	(Driehaus, 2002)
	ZVI two-steps system	1.44	100–130	77–96	Adsorption capacity: 20.5 mg g ⁻¹ Neutral pH	(Casentini et al., 2016)
	TiO ₂ -based adsorption	52	32	91	Initial fluorides: 2.8 mg L ⁻¹	(Sorlini et al., 2014)
	Berea red sand and ZVIs	0.006–0.290	13,000–17,000	100	Porosity: 38–60% Void ratio (e): 0.6–1.5 Specific gravity: 4.3–7 g cm ⁻³	(Trois & Cibati, 2015)
Ion Exchange	Arsenex II (SBA type II)	2943	16.7	<10 µg L ⁻¹	Empty-bed contact time: (2.6 min) Regeneration frequency: 1.7 day	(A. S. C. Chen et al., 2020)
	A300E (SBA type II)	1362	49.7	<10 µg L ⁻¹	Empty-bed contact time: (4.8 min) Regeneration frequency: 1.7 day	(A. S. C. Chen et al., 2020)
	npXtra system (Arsenex)	1.47	15–68	0 µg L ⁻¹	pH = 6.8	(Möller et al., 2009)
	npXtra system (Arsenex)	0.71	27–47	4.5 µg L ⁻¹	pH = 7.8	(Möller et al., 2009)
	npXtra system (Arsenex)	1.18	173	6 µg L ⁻¹	pH = 7.1	(Möller et al., 2009)
Membrane	POE RO	4.5	18.1	>99	Sediment filter pore size: 5 µm	(A. S. C. Chen et al., 2020)
	POU RO	0.13	57.8	>99	Sediment filter pore size: 20 µm	(A. S. C. Chen et al., 2020)
	POU RO	variable	14.34	85.5	261 samples (100 mL)	(Slotnick et al., 2006)
	Softener + RO	variable	9.76	19	261 samples (100 mL)	(Slotnick et al., 2006)

Table 2-19. Continued.

	Removal Agent	Flowrate (m ³ d ⁻¹) /Volume	C _i (µg L ⁻¹)	Removal (%) / Final Concentration (µg L ⁻¹)	Other Available Data	Reference
Coagulation	Naturally occurring Fe +oxidizing agent (KMnO ₄)	1L	1000 500	50 µg L ⁻¹ : (Fe/As < 13) 10 µg L ⁻¹ : (Fe/As > 13)	pH= 6.0–7.5	(A. K. Sharma et al., 2016)
	Iron electrocoagulation	100 L	153.2	<10 µg L ⁻¹	Current: 5.8 A, Charge dose: 100 C L ⁻¹	(Glade et al., 2021)
	SuMeWa SYSTEM + chlorine as oxidant	1.44	300	96	Alum: 7.5 mg L ⁻¹ pH= 5.56–7.05	(Feistel et al., 2016)
	Iron electrocoagulation	1.87	118	30 µg L ⁻¹ (< 5 min) 20 µg L ⁻¹ (> 5 min)	Retention time: 19 s, Charge dose: 233 C L ⁻¹ , Alum: 5 mg L ⁻¹	(Bandaru et al., 2020)
Oxidation	Solar-driven inline-electrolytic oxidation followed by co- precipitation and filtration	1.2–1.44	187 202 195 165	80 88 76 94	In situ chlorine production using water chloride, Fe > 99%, MN: 96%, PO4: 72%, NH4: 84%	(Otter et al., 2017)
	Sodium hypochlorite (0.33 mg L ⁻¹) followed by filtration	840	12	95	Removing As from 18 to 2 µg L ⁻¹	(Duarte et al., 2009)
	Immobilized acid othiobacillus ferrooxidans bacteria) followed by adsorptive filtration (granulated activated carbon)	0.004	1000 to 30,000	>50 (after oxidation)	Final concentration: 0.2 mg L ⁻¹ (after adsorptive filtration)	(Kamde et al., 2019)

2.6. Conclusion

Water contamination with toxic heavy metals, such as arsenic, is one of the most significant environmental issues worldwide. Arsenic must be removed from drinking water because it has many negative impacts, including neurotoxicity and carcinogenicity. Many methods can be used to remove arsenic from water. In the present review paper, various As removal methods with a particular focus on adsorption have been reviewed. The reviewed literature confirms the application of oxidation, ion exchange, coagulation-flocculation, adsorption, etc., in heavy metal removal from drinking water. However, technical and financial challenges affect the feasibility of these techniques for small communities' decentralized systems. In other words, the simplicity, affordability, and availability of the material, equipment, and skilled operators are the major factors that should be considered to find an ideal solution for small communities. With these considerations, adsorption is a very appealing option for decentralized systems of arsenic removal because of the ease of installation and use and also the low-cost and straightforward operational process.

Common adsorbents such as commercial activated carbon, nanomaterials, composites and miscellaneous adsorbents have been used in heavy metal removal from water sources. However, cost-effective adsorbents such as agricultural, industrial or animal waste, natural materials, and bio-adsorbent should be employed to keep costs low and increase the effectiveness of heavy metal removal. In most adsorption studies, physical characteristics of conventional or cost-effective adsorbents have been analyzed through techniques such as SEM, DLS, XRD, BET-surface area, etc., while the common methods such as XRF, CHN/O, FTIR, zeta potential, etc., were widely used for chemical characterization. It should be noted that there are some considerations that should be taken because adsorption effectiveness depends on various factors, including

the initial concentration of arsenic ions, pH levels, adsorbent dose, contact time, and temperature. In terms of kinetic and isotherm modelling, it seems that the pseudo-second-order model and Freundlich isotherm provide a more accurate fit to the arsenic adsorption data.

The research knowledge gaps should be filled through further investigations on arsenic removal in water by adsorption. First, more studies should focus on the bench-scale and large-scale application of arsenic adsorption from drinking water supplies, including surface and groundwater. Moreover, since financial resources are usually limited in small communities, cost-effectiveness and cost-benefit studies need to be conducted in greater detail. Furthermore, the adsorbent removal effectiveness and capacity should be improved to be able to use low-cost adsorbents for industrial purposes and at a large scale, as alternatives for commercial adsorbents. For this purpose, it is necessary to carry out more research on the impact of surface modification on removal efficiency. Additionally, the applicability of the integrated systems, such as photocatalytic-adsorption or adsorption-membrane, and other possible combinations of different methods in decentralized water treatment systems should be examined, to improve efficiency and overcome the drawbacks of each particular technique. Finally, to save time and cost, more modelling studies, particularly multi-scale modelling, are required to predict removal performance before running numerous experiments.

2.7. References

- Abdel-Karim, A., Leaper, S., Skuse, C., Zaragoza, G., Gryta, M., & Gorgojo, P. (2021). Membrane cleaning and pretreatments in membrane distillation—a review. *Chemical Engineering Journal*, 422, 129696.
- Abid, M., Niazi, N. K., Bibi, I., Farooqi, A., Ok, Y. S., Kunhikrishnan, A., Ali, F., Ali,

- S., Igalavithana, A. D., & Arshad, M. (2016). Arsenic (V) biosorption by charred orange peel in aqueous environments. *International Journal of Phytoremediation*, 18(5), 442–449.
- Adebayo, G. B., Adegoke, H. I., Jamiu, W., Balogun, B. B., & Jimoh, A. A. (2015). Adsorption of Mn (II) and Co (II) ions from aqueous solution using Maize cob activated carbon: kinetics and Thermodynamics Studies. *Journal of Applied Sciences and Environmental Management*, 19(4), 737–748.
- Adelaju, S. B., Khan, S., & Patti, A. F. (2021). Arsenic contamination of groundwater and its implications for drinking water quality and human health in under-developed countries and remote communities—a review. *Applied Sciences*, 11(4), 1926.
- Afroze, S., & Sen, T. K. (2018). A Review on Heavy Metal Ions and Dye Adsorption from Water by Agricultural Solid Waste Adsorbents. *Water, Air, and Soil Pollution*, 229(7), 1–50. <https://doi.org/10.1007/s11270-018-3869-z>
- Aghaei, E., Wang, Z., Tadesse, B., Tabelin, C. B., Quadir, Z., & Alorro, R. D. (2021). Performance evaluation of Fe-Al bimetallic particles for the removal of potentially toxic elements from combined acid mine drainage-effluents from refractory gold ore processing. *Minerals*, 11(6), 590.
- Ahmaruzzaman, M. (2010). A review on the utilization of fly ash. *Progress in Energy and Combustion Science*, 36(3), 327–363.
- Ahmed, M. F. (2001). An overview of arsenic removal technologies in Bangladesh and India. *Proceedings of BUET-UNU International Workshop on Technologies for Arsenic Removal from Drinking Water, Dhaka*, 5–7.
- Akin, I., Arslan, G., Tor, A., Cengeloglu, Y., & Ersoz, M. (2011). Removal of arsenate [As(V)] and arsenite [As(III)] from water by SWHR and BW-30

reverse osmosis. *Desalination*, 281(1), 88–92.

<https://doi.org/10.1016/j.desal.2011.07.062>

Akpomie, K. G., & Conradie, J. (2020). Advances in application of cotton-based adsorbents for heavy metals trapping, surface modifications and future perspectives. *Ecotoxicology and Environmental Safety*, 201, 110825.

Al-Ali, F., Barrow, T., Duan, L., Jefferson, A., Louis, S., Luke, K., Major, K., Smoker, S., Walker, S., & Yacobozzi, M. (2011). Vertebral artery ostium atherosclerotic plaque as a potential source of posterior circulation ischemic stroke: result from borgess medical center vertebral artery ostium stenting registry. *Stroke*, 42(9), 2544–2549.

Al-Asheh, S., & Aidan, A. (2020). A comprehensive method of ion exchange resins regeneration and its optimization for water treatment. In *Promising Techniques for Wastewater Treatment and Water Quality Assessment*. IntechOpen.

Al-Maadeed, M. A. A., Ponnammam, D., & Carignano, M. A. (2020). *Polymer science and innovative applications: materials, techniques, and future developments*. Elsevier.

Ali, I., Al-Othman, Z. A., Alwarthan, A., Asim, M., & Khan, T. A. (2014). Removal of arsenic species from water by batch and column operations on bagasse fly ash. *Environmental Science and Pollution Research*, 21(5), 3218–3229.

Ali, R. M., Hamad, H. A., Hussein, M. M., & Malash, G. F. (2016). Potential of using green adsorbent of heavy metal removal from aqueous solutions: adsorption kinetics, isotherm, thermodynamic, mechanism and economic analysis. *Ecological Engineering*, 91, 317–332.

Alka, S., Shahir, S., Ibrahim, N., Ndejiko, M. J., Vo, D.-V. N., & Abd Manan, F. (2021). Arsenic removal technologies and future trends: a mini review.

- Journal of Cleaner Production*, 278, 123805.
- Alkurdi, S. S. A., Al-Juboori, R. A., Bundschuh, J., Bowtell, L., & McKnight, S. (2020). Effect of pyrolysis conditions on bone char characterization and its ability for arsenic and fluoride removal. *Environmental Pollution*, 262, 114221. <https://doi.org/10.1016/j.envpol.2020.114221>
- Alswat, A. A., Ahmad, M. Bin, & Saleh, T. A. (2016). Zeolite modified with copper oxide and iron oxide for lead and arsenic adsorption from aqueous solutions. *Journal of Water Supply: Research and Technology—AQUA*, 65(6), 465–479.
- Ambroz, F., Macdonald, T. J., Martis, V., & Parkin, I. P. (2018). Evaluation of the BET Theory for the Characterization of Meso and Microporous MOFs. *Small Methods*, 2(11), 1800173.
- Amini, A., Kim, Y., Zhang, J., Boyer, T., & Zhang, Q. (2015). Environmental and economic sustainability of ion exchange drinking water treatment for organics removal. *Journal of Cleaner Production*, 104, 413–421.
- An, H. K., Park, B. Y., & Kim, D. S. (2001). Crab shell for the removal of heavy metals from aqueous solution. *Water Research*, 35(15). [https://doi.org/10.1016/S0043-1354\(01\)00099-9](https://doi.org/10.1016/S0043-1354(01)00099-9)
- Asere, T. G., Stevens, C. V., & Du Laing, G. (2019). Use of (modified) natural adsorbents for arsenic remediation: a review. *Science of the Total Environment*, 676, 706–720.
- Askenaizer, D. (2003). Drinking water quality and treatment. *Encyclopedia of Physical Science and Technology*, 3.
- Ayanda, O. S., Fatoki, O. S., Adekola, F. A., & Ximba, B. J. (2012). Characterization of fly ash generated from Matla power station in Mpumalanga, South Africa. *E-Journal of Chemistry*, 9(4), 1788–1795.

- Babae, Y., Mulligan, C. N., & Rahaman, M. S. (2018). Removal of arsenic (III) and arsenic (V) from aqueous solutions through adsorption by Fe/Cu nanoparticles. *Journal of Chemical Technology & Biotechnology*, 93(1), 63–71.
- Babick, F. (2020). Dynamic light scattering (DLS). In *Characterization of Nanoparticles* (pp. 137–172). Elsevier.
- Bahar, M. M., Mahbub, K. R., Naidu, R., & Megharaj, M. (2018). As(V) removal from aqueous solution using a low-cost adsorbent coir pith ash: Equilibrium and kinetic study. *Environmental Technology and Innovation*, 9, 198–209. <https://doi.org/10.1016/j.eti.2017.12.005>
- Bakdach, W. M. M., Haiba, M., & Hadad, R. (2022). Changes in surface morphology, chemical and mechanical properties of clear aligners during intraoral usage: A systematic review and meta-analysis. *International Orthodontics*, 20(1), 100610.
- Balaji, T., & Matsunaga, H. (2002). Adsorption characteristics of As (III) and As (V) with titanium dioxide loaded Amberlite XAD-7 resin. *Analytical Sciences*, 18(12), 1345–1349.
- Balsamo, M., Di Natale, F., Erto, A., Lancia, A., Montagnaro, F., & Santoro, L. (2010). Arsenate removal from synthetic wastewater by adsorption onto fly ash. *Desalination*, 263(1–3), 58–63.
- Bandaru, S. R. S., van Genuchten, C. M., Kumar, A., Glade, S., Hernandez, D., Nahata, M., & Gadgil, A. (2020). Rapid and efficient arsenic removal by iron electrocoagulation enabled with in situ generation of hydrogen peroxide. *Environmental Science & Technology*, 54(10), 6094–6103.
- Bashir, M. J. K., Amr, S. S. A., Aziz, S. Q., Aun, N. C., & Sethupathi, S. (2015). Wastewater treatment processes optimization using response surface

- methodology (RSM) compared with conventional methods: Review and comparative study. *Middle-East Journal of Scientific Research*, 23(2), 244–252.
- Basan, M. B., & Pala, A. (2010). A statistical experiment design approach for arsenic removal by coagulation process using aluminum sulfate. *Desalination*, 254(1–3), 42–48.
- Basu, T., & Ghosh, U. C. (2011). Influence of groundwater occurring ions on the kinetics of As (III) adsorption reaction with synthetic nanostructured Fe (III)–Cr (III) mixed oxide. *Desalination*, 266(1–3), 25–32.
- Bergström, D., Israelsson, S., Öhman, M., Dahlqvist, S.-A., Gref, R., Boman, C., & Wästerlund, I. (2008). Effects of raw material particle size distribution on the characteristics of Scots pine sawdust fuel pellets. *Fuel Processing Technology*, 89(12), 1324–1329.
- Bezerra, M. A., Santelli, R. E., Oliveira, E. P., Villar, L. S., & Escaleira, L. A. (2008). Response surface methodology (RSM) as a tool for optimization in analytical chemistry. *Talanta*, 76(5), 965–977.
- Bhattacharjee, S. (2016). DLS and zeta potential—what they are and what they are not? *Journal of Controlled Release*, 235, 337–351.
- Bhowmik, T., Sarkar, S., Bhattacharya, A., & Mukherjee, A. (2022). A review of arsenic mitigation strategies in community water supply with insights from South Asia: Options, opportunities and constraints. *Environmental Science: Water Research & Technology*.
- Bissen, M., & Frimmel, F. H. (2003a). Arsenic—a review. Part II: oxidation of arsenic and its removal in water treatment. *Acta Hydrochimica et Hydrobiologica*, 31(2), 97–107.

- Bissen, M., & Frimmel, F. H. (2003b). Arsenic - A review. Part II: Oxidation of arsenic and its removal in water treatment. *Acta Hydrochimica et Hydrobiologica*, 31(2), 97–107. <https://doi.org/10.1002/aheh.200300485>
- Bläker, C., Muthmann, J., Pasel, C., & Bathen, D. (2019). Characterization of activated carbon adsorbents—state of the art and novel approaches. *ChemBioEng Reviews*, 6(4), 119–138.
- Brandani, S. (2021). Kinetics of liquid phase batch adsorption experiments. *Adsorption*, 27(3), 353–368.
- Brandhuber, P., & Amy, G. (2001). Arsenic removal by a charged ultrafiltration membrane- Influences of membrane operating conditions and water quality on arsenic rejection. *Desalination*, 140(1), 1–14. [https://doi.org/10.1016/S0011-9164\(01\)00350-2](https://doi.org/10.1016/S0011-9164(01)00350-2)
- Bridgeman, T. G., Darvell, L. I., Jones, J. M., Williams, P. T., Fahmi, R., Bridgwater, A. V, Barraclough, T., Shield, I., Yates, N., Thain, S. C., & Donnison, I. S. (2007). Influence of particle size on the analytical and chemical properties of two energy crops. *Fuel*, 86(1–2), 60–72. <https://doi.org/10.1016/j.fuel.2006.06.022>
- Cabrera, F., De Arambarri, P., Madrid, L., & Toga, C. G. (1981). Desorption of phosphate from iron oxides in relation to equilibrium pH and porosity. *Geoderma*, 26(3), 203–216.
- Camacho, L. M., Ponnusamy, S., Campos, I., Davis, T. A., & Deng, S. (2015). Evaluation of Novel Modified Activated Alumina as Adsorbent for Arsenic Removal. In *Handbook of Arsenic Toxicology* (pp. 121–136). Elsevier. <https://doi.org/10.1016/B978-0-12-418688-0.00005-8>
- Casentini, B., Falcione, F. T., Amalfitano, S., Fazi, S., & Rossetti, S. (2016). Arsenic

- removal by discontinuous ZVI two steps system for drinking water production at household scale. *Water Research*, 106, 135–145.
- Çermikli, E., Şen, F., Altıok, E., Wolska, J., Cyganowski, P., Kabay, N., Bryjak, M., Arda, M., & Yüksel, M. (2020). Performances of novel chelating ion exchange resins for boron and arsenic removal from saline geothermal water using adsorption-membrane filtration hybrid process. *Desalination*, 491, 114504.
- Chakraborty, R., Asthana, A., Singh, A. K., Jain, B., & Susan, A. B. H. (2022). Adsorption of heavy metal ions by various low-cost adsorbents: a review. *International Journal of Environmental Analytical Chemistry*, 102(2), 342–379.
- Chang, F., Liu, W., & Wang, X. (2014). Comparison of polyamide nanofiltration and low-pressure reverse osmosis membranes on As (III) rejection under various operational conditions. *Desalination*, 334(1), 10–16.
- Chang, Q., Lin, W., & Ying, W. (2010). Preparation of iron-impregnated granular activated carbon for arsenic removal from drinking water. *Journal of Hazardous Materials*, 184(1–3), 515–522.
- Charpentier, T. V. J., Neville, A., Lanigan, J. L., Barker, R., Smith, M. J., & Richardson, T. (2016). Preparation of magnetic carboxymethylchitosan nanoparticles for adsorption of heavy metal ions. *ACS Omega*, 1(1), 77–83.
- Chatterjee, R., Sajjadi, B., Chen, W.-Y., Mattern, D. L., Hammer, N., Raman, V., & Dorris, A. (2020). Effect of pyrolysis temperature on physicochemical properties and acoustic-based amination of biochar for efficient CO₂ adsorption. *Frontiers in Energy Research*, 8, 85.
- Chen, A. S. C., Wang, L., Sorg, T. J., & Lytle, D. A. (2020). Removing arsenic and co-occurring contaminants from drinking water by full-scale ion exchange and

- point-of-use/point-of-entry reverse osmosis systems. *Water Research*, 172, 115455.
- Chitrakar, R., Tezuka, S., Sonoda, A., Sakane, K., Ooi, K., & Hirotsu, T. (2006). Phosphate adsorption on synthetic goethite and akaganeite. *Journal of Colloid and Interface Science*, 298(2), 602–608.
<https://doi.org/10.1016/j.jcis.2005.12.054>
- Choong, T. S. Y., Chuah, T. G., Robiah, Y., Koay, F. L. G., & Azni, I. (2007). Arsenic toxicity, health hazards and removal techniques from water: an overview. *Desalination*, 217(1–3), 139–166.
- Chungang, Y., & Le, X. C. (2009). Arsenic speciation analysis. *Progress in Chemistry*, 21(2–3), 467–473.
- Chutia, P., Kato, S., Kojima, T., & Satokawa, S. (2009). Arsenic adsorption from aqueous solution on synthetic zeolites. *Journal of Hazardous Materials*, 162(1), 440–447.
- De Almeida Ohana, N., HM, L. F., & Luis, N.-G. (2022). Adsorption of arsenic anions in water using modified lignocellulosic adsorbents. *Results in Engineering*, 13, 100340.
- de Gennaro, B., Aprea, P., Liguori, B., Galzerano, B., Peluso, A., & Caputo, D. (2020). Zeolite-rich composite materials for environmental remediation: Arsenic removal from water. *Applied Sciences*, 10(19), 6938.
- de Souza, C. C., de Souza, L. Z. M., Yılmaz, M., de Oliveira, M. A., da Silva Bezerra, A. C., da Silva, E. F., Dumont, M. R., & Machado, A. R. T. (2022). Activated carbon of *Coriandrum sativum* for adsorption of methylene blue: Equilibrium and kinetic modeling. *Cleaner Materials*, 3, 100052.
- Debord, J., Harel, M., Bollinger, J.-C., & Chu, K. H. (2022). The Elovich isotherm

- equation: Back to the roots and new developments. *Chemical Engineering Science*, 262, 118012.
- Decentralized Water Treatment Market | Size, Growth | 2021-26*. (n.d.). Retrieved December 13, 2022, from <https://www.arizton.com/market-reports/decentralized-water-treatment-market>
- Dehghani, M. H., Maroosi, M., & Heidarinejad, Z. (2018). Experimental dataset on adsorption of Arsenic from aqueous solution using Chitosan extracted from shrimp waste; optimization by response surface methodology with central composite design. *Data in Brief*, 20, 1415–1421.
- Dhoke, C., Zaabout, A., Cloete, S., & Amini, S. (2021). Review on reactor configurations for adsorption-based CO₂ capture. *Industrial & Engineering Chemistry Research*, 60(10), 3779–3798.
- Dickson, D., Liu, G., & Cai, Y. (2017). Adsorption kinetics and isotherms of arsenite and arsenate on hematite nanoparticles and aggregates. *Journal of Environmental Management*, 186, 261–267.
- Dixit, F., Dutta, R., Barbeau, B., Berube, P., & Mohseni, M. (2021). PFAS removal by ion exchange resins: A review. In *Chemosphere* (Vol. 272, p. 129777). Elsevier. <https://doi.org/10.1016/j.chemosphere.2021.129777>
- Donahue, C. J., & Rais, E. A. (2009). Proximate analysis of coal. *Journal of Chemical Education*, 86(2), 222.
- Driehaus, W. (2002). Arsenic removal-experience with the GEH® process in Germany. *Water Science and Technology: Water Supply*, 2(2), 275–280.
- Du, J., Zhang, B., Li, J., & Lai, B. (2020). Decontamination of heavy metal complexes by advanced oxidation processes: A review. *Chinese Chemical Letters*, 31(10), 2575–2582.

- Du, Z., Zheng, T., Wang, P., Hao, L., & Wang, Y. (2016). Fast microwave-assisted preparation of a low-cost and recyclable carboxyl modified lignocellulose-biomass jute fiber for enhanced heavy metal removal from water. *Bioresource Technology*, 201, 41–49.
- Duarte, A. A. L. S., Cardoso, S. J. A., & Alçada, A. J. (2009). Emerging and innovative techniques for arsenic removal applied to a small water supply system. *Sustainability*, 1(4), 1288–1304.
- Dwivedi, A., & Jain, M. K. (2014). Fly ash–waste management and overview: A Review. *Recent Research in Science and Technology*, 6(1).
- Edgar, M., & Boyer, T. H. (2022). Nitrate adsorption and desorption during biological ion exchange. *Separation and Purification Technology*, 285, 120363.
- El-Naggar, M. E., Radwan, E. K., El-Wakeel, S. T., Kafafy, H., Gad-Allah, T. A., El-Kalliny, A. S., & Shaheen, T. I. (2018). Synthesis, characterization and adsorption properties of microcrystalline cellulose based nanogel for dyes and heavy metals removal. *International Journal of Biological Macromolecules*, 113, 248–258.
- Elaipoulos, K., Perraki, T., & Grigoropoulou, E. (2010). Monitoring the effect of hydrothermal treatments on the structure of a natural zeolite through a combined XRD, FTIR, XRF, SEM and N₂-porosimetry analysis. *Microporous and Mesoporous Materials*, 134(1–3), 29–43.
- Elwakeel, K. Z., Elgarahy, A. M., Khan, Z. A., Almughamisi, M. S., & Al-Bogami, A. S. (2020). Perspectives regarding metal/mineral-incorporating materials for water purification: with special focus on Cr (vi) removal. *Materials Advances*, 1(6), 1546–1574.
- Epp, J. (2016). X-ray diffraction (XRD) techniques for materials characterization. In

- Materials characterization using nondestructive evaluation (NDE) methods* (pp. 81–124). Elsevier.
- Farooq, M. U., & Jalees, M. I. (2020). Application of magnetic graphene oxide for water purification: heavy metals removal and disinfection. *Journal of Water Process Engineering*, 33, 101044.
- Feistel, U., Otter, P., Kunz, S., Grischek, T., & Feller, J. (2016). Field tests of a small pilot plant for the removal of arsenic in groundwater using coagulation and filtering. *Journal of Water Process Engineering*, 14, 77–85.
- Fernández-López, J. A., Angosto, J. M., Roca, M. J., & Doval Miñarro, M. (2019). Taguchi design-based enhancement of heavy metals bioremoval by agroindustrial waste biomass from artichoke. *Science of the Total Environment*, 653, 55–63. <https://doi.org/10.1016/j.scitotenv.2018.10.343>
- Flora, S. J. S. (2015). Arsenic: chemistry, occurrence, and exposure. In *Handbook of arsenic toxicology* (pp. 1–49). Elsevier.
- Fox, K. R. (1989). Field Experience With Point-of-Use Treatment Systems for Arsenic Removal. *Journal-American Water Works Association*, 81(2), 94–101.
- Gadore, V., & Ahmaruzzaman, M. (2021). Tailored fly ash materials: A recent progress of their properties and applications for remediation of organic and inorganic contaminants from water. *Journal of Water Process Engineering*, 41, 101910.
- Gaikwad, R. W., Sapkal, V. S., & Sapkal, R. S. (2010). Ion exchange system design for removal of heavy metals from acid mine drainage wastewater. *Acta Montanistica Slovaca*, 15(4), 298.
- Gallegos-Garcia, M., Ramírez-Muñiz, K., & Song, S. (2012). Arsenic removal from water by adsorption using iron oxide minerals as adsorbents: a review. *Mineral*

Processing and Extractive Metallurgy Review, 33(5), 301–315.

Ghosh, U., & Chakraborty, S. (2013). Pharmaceutical and phytochemical evaluation of a novel anti–white spot syndrome virus drug derived from terrestrial plants.

Int J Nat Prod Res, 3(4), 92–101.

Ghurye, G. L., Clifford, D. A., & Tripp, A. R. (1999). Combined arsenic and nitrate removal by ion exchange. *Journal-American Water Works Association*, 91(10), 85–96.

Gikas, P., & Tchobanoglous, G. (2009). The role of satellite and decentralized strategies in water resources management. *Journal of Environmental Management*, 90(1), 144–152.

Glade, S., Bandaru, S. R. S., Nahata, M., Majmudar, J., & Gadgil, A. (2021).

Adapting a drinking water treatment technology for arsenic removal to the context of a small, low-income California community. *Water Research*, 204, 117595.

Goswami, A., Raul, P. K., & Purkait, M. K. (2012). Arsenic adsorption using copper (II) oxide nanoparticles. *Chemical Engineering Research and Design*, 90(9), 1387–1396. <https://doi.org/10.1016/j.cherd.2011.12.006>

Greenleaf, J. E., Lin, J. C., & Sengupta, A. K. (2006). Two novel applications of ion exchange fibers: Arsenic removal and chemical-free softening of hard water. *Environmental Progress*, 25(4). <https://doi.org/10.1002/ep.10163>

Guan, X., Du, J., Meng, X., Sun, Y., Sun, B., & Hu, Q. (2012). Application of titanium dioxide in arsenic removal from water: a review. *Journal of Hazardous Materials*, 215, 1–16.

Guha Mazumder, D., & Dasgupta, U. B. (2011). Chronic arsenic toxicity: Studies in West Bengal, India. In *Kaohsiung Journal of Medical Sciences* (Vol. 27, Issue

- 9, pp. 360–370). Elsevier. <https://doi.org/10.1016/j.kjms.2011.05.003>
- Guha Mazumder, D. N. (2005). Effect of chronic intake of arsenic-contaminated water on liver. *Toxicology and Applied Pharmacology*, 206(2), 169–175.
<https://doi.org/10.1016/j.taap.2004.08.025>
- Gurung, K., Ncibi, M. C., Shestakova, M., & Sillanpää, M. (2018). Removal of carbamazepine from MBR effluent by electrochemical oxidation (EO) using a Ti/Ta₂O₅-SnO₂ electrode. *Applied Catalysis B: Environmental*, 221, 329–338.
- Habuda-Stanić, M., & Nujić, M. (2015). Arsenic removal by nanoparticles: a review. *Environmental Science and Pollution Research*, 22(11), 8094–8123.
<https://doi.org/10.1007/s11356-015-4307-z>
- Hao, L., Liu, M., Wang, N., & Li, G. (2018). A critical review on arsenic removal from water using iron-based adsorbents. *RSC Advances*, 8(69), 39545–39560.
- Hao, L., Zheng, T., Jiang, J., Zhang, G., & Wang, P. (2016). Removal of As (III) and As (V) from water using iron doped amino functionalized sawdust: characterization, adsorptive performance and UF membrane separation. *Chemical Engineering Journal*, 292, 163–173.
- Hidayu, A. R., Mohamad, N. F., Matali, S., & Sharifah, A. (2013). Characterization of activated carbon prepared from oil palm empty fruit bunch using BET and FT-IR techniques. *Procedia Engineering*, 68, 379–384.
- Hilal, N. M., Ahmed, I. A., & El-Sayed, R. E. (2012). Activated and Nonactivated Date Pits Adsorbents for the Removal of Copper(II) and Cadmium(II) from Aqueous Solutions. *ISRN Physical Chemistry*, 2012, 1–11.
<https://doi.org/10.5402/2012/985853>
- Hodges, B. C., Cates, E. L., & Kim, J.-H. (2018). Challenges and prospects of advanced oxidation water treatment processes using catalytic nanomaterials.

- Nature Nanotechnology*, 13(8), 642–650.
- Höll, W. H. (2010). Mechanisms of arsenic removal from water. *Environmental Geochemistry and Health*, 32(4), 287–290.
- Holt, P. K., Barton, G. W., & Mitchell, C. A. (2005). The future for electrocoagulation as a localised water treatment technology. *Chemosphere*, 59(3), 355–367.
- Hristovski, K., Baumgardner, A., & Westerhoff, P. (2007). Selecting metal oxide nanomaterials for arsenic removal in fixed bed columns: from nanopowders to aggregated nanoparticle media. *Journal of Hazardous Materials*, 147(1–2), 265–274.
- Hua, J. (2018). Adsorption of low-concentration arsenic from water by co-modified bentonite with manganese oxides and poly (dimethyldiallylammonium chloride). *Journal of Environmental Chemical Engineering*, 6(1), 156–168.
- Hua, J. (2021). Synthesis and characterization of gold nanoparticles (AuNPs) and ZnO decorated zirconia as a potential adsorbent for enhanced arsenic removal from aqueous solution. *Journal of Molecular Structure*, 1228, 129482.
<https://doi.org/10.1016/j.molstruc.2020.129482>
- Huang, H.-H. (2016). The Eh-pH diagram and its advances. *Metals*, 6(1), 23.
- Huang, M., Feng, W., Xu, W., & Liu, P. (2016). An in situ gold-decorated 3D branched ZnO nanocomposite and its enhanced absorption and photo-oxidation performance for removing arsenic from water. *RSC Advances*, 6(114), 112877–112884. <https://doi.org/10.1039/c6ra22243a>
- Hung, C., Bai, H., & Karthik, M. (2009). Ordered mesoporous silica particles and Si-MCM-41 for the adsorption of acetone: A comparative study. *Separation and Purification Technology*, 64(3), 265–272.
- Iber, B. T., Torsabo, D., Chik, C. E. N. C. E., Wahab, F., Abdullah, S. R. S., Hassan,

- H. A., & Kasan, N. A. (2022). The impact of re-ordering the conventional chemical steps on the production and characterization of natural chitosan from biowaste of Black Tiger Shrimp, *Penaeus monodon*. *Journal of Sea Research*, 190, 102306.
- Iervolino, G., Vaiano, V., Rizzo, L., Sarno, G., Farina, A., & Sannino, D. (2016a). Removal of arsenic from drinking water by photo-catalytic oxidation on MoOx/TiO₂ and adsorption on γ -Al₂O₃. *Journal of Chemical Technology and Biotechnology*, 91(1), 88–95. <https://doi.org/10.1002/jctb.4581>
- Iervolino, G., Vaiano, V., Rizzo, L., Sarno, G., Farina, A., & Sannino, D. (2016b). Removal of arsenic from drinking water by photo-catalytic oxidation on MoOx/TiO₂ and adsorption on γ -Al₂O₃. *Journal of Chemical Technology & Biotechnology*, 91(1), 88–95.
- Iftekhhar, S., Ramasamy, D. L., Srivastava, V., Asif, M. B., & Sillanpää, M. (2018). Understanding the factors affecting the adsorption of Lanthanum using different adsorbents: A critical review. *Chemosphere*, 204, 413–430. <https://doi.org/10.1016/j.chemosphere.2018.04.053>
- Ike, I. A., Linden, K. G., Orbell, J. D., & Duke, M. (2018). Critical review of the science and sustainability of persulphate advanced oxidation processes. *Chemical Engineering Journal*, 338, 651–669.
- Inglezakis, V. J., Zorpas, A. A., Loizidou, M. D., & Grigoropoulou, H. P. (2003). Simultaneous removal of metals Cu²⁺, Fe³⁺ and Cr³⁺ with anions SO₄²⁻ and HPO₄²⁻ using clinoptilolite. *Microporous and Mesoporous Materials*, 61(1–3), 167–171.
- Inglezakis, V. J., Zorpas, A. A., Loizidou, M. D., & Grigoropoulou, H. P. (2005). The effect of competitive cations and anions on ion exchange of heavy metals.

Separation and Purification Technology, 46(3), 202–207.

- Inyang, H. I., Onwawoma, A., & Bae, S. (2016). The Elovich equation as a predictor of lead and cadmium sorption rates on contaminant barrier minerals. *Soil and Tillage Research*, 155, 124–132.
- Iqbal, J., Kim, H.-J., Yang, J.-S., Baek, K., & Yang, J.-W. (2007). Removal of arsenic from groundwater by micellar-enhanced ultrafiltration (MEUF). *Chemosphere*, 66(5), 970–976.
- Jageerani, saqaf. (2017). Review: Arsenic Remediation by Synthetic and Natural Adsorbents. *Pakistan Journal of Analytical & Environmental Chemistry*, 18(1), 18–36. <https://doi.org/10.21743/pjaec/2017.06.02>
- Jeon, S.-B., Kim, S., Park, S.-J., Seol, M.-L., Kim, D., Chang, Y. K., & Choi, Y.-K. (2016). Self-powered electro-coagulation system driven by a wind energy harvesting triboelectric nanogenerator for decentralized water treatment. *Nano Energy*, 28, 288–295.
- Joshi, S., Sharma, M., Kumari, A., Shrestha, S., & Shrestha, B. (2019). Arsenic removal from water by adsorption onto iron oxide/nano-porous carbon magnetic composite. *Applied Sciences*, 9(18), 3732.
- Kabir, F., & Chowdhury, S. (2017). Arsenic removal methods for drinking water in the developing countries: technological developments and research needs. *Environmental Science and Pollution Research*, 24(31), 24102–24120.
- Kalaruban, M., Loganathan, P., Nguyen, T. V., Nur, T., Hasan Johir, M. A., Nguyen, T. H., Trinh, M. V., & Vigneswaran, S. (2019). Iron-impregnated granular activated carbon for arsenic removal: Application to practical column filters. *Journal of Environmental Management*, 239, 235–243. <https://doi.org/10.1016/j.jenvman.2019.03.053>

- Kamde, K., Dahake, R., Pandey, R. A., & Bansawal, A. (2019). Integrated bio-oxidation and adsorptive filtration reactor for removal of arsenic from wastewater. *Environmental Technology*, 40(10), 1337–1348.
- Karcioglu, O., & Arslan, B. (2019). *Poisoning in the Modern World: New Tricks for an Old Dog?* BoD–Books on Demand.
- Karnib, M., Kabbani, A., Holail, H., & Olama, Z. (2014). Heavy metals removal using activated carbon, silica and silica activated carbon composite. *Energy Procedia*, 50, 113–120. <https://doi.org/10.1016/j.egypro.2014.06.014>
- Kartinen Jr, E. O., & Martin, C. J. (1995). An overview of arsenic removal processes. *Desalination*, 103(1–2), 79–88.
- Khan, M. R., Hegde, R. A., & Shabiimam, M. A. (2017). Adsorption of lead by bentonite clay. *International Journal of Scientific Research and Management*, 5(7), 5800–5804.
- Khan, S. A., Khan, S. B., Khan, L. U., Farooq, A., Akhtar, K., & Asiri, A. M. (2018). Fourier transform infrared spectroscopy: fundamentals and application in functional groups and nanomaterials characterization. In *Handbook of materials characterization* (pp. 317–344). Springer.
- Kim, M. J., & Nriagu, J. (2000). Oxidation of arsenite in groundwater using ozone and oxygen. *Science of the Total Environment*, 247(1), 71–79. [https://doi.org/10.1016/S0048-9697\(99\)00470-2](https://doi.org/10.1016/S0048-9697(99)00470-2)
- Kizinievic, O., & Kizinievic, V. (2016). Utilisation of wood ash from biomass for the production of ceramic products. *Construction and Building Materials*, 127, 264–273.
- Kong, S., Wang, Y., Zhan, H., Yuan, S., Yu, M., & Liu, M. (2014). Adsorption/oxidation of arsenic in groundwater by nanoscale Fe-Mn binary

- oxides loaded on zeolite. *Water Environment Research*, 86(2), 147–155.
- Koohzad, E., Jafari, D., & Esmacili, H. (2019). Adsorption of lead and arsenic ions from aqueous solution by activated carbon prepared from tamarix leaves. *ChemistrySelect*, 4(42), 12356–12367.
- Korak, J. A., Mungan, A. L., & Watts, L. T. (2022). Critical Review of Waste Brine Management Strategies for Drinking Water Treatment Using Strong Base Ion Exchange. *Journal of Hazardous Materials*, 129473.
- Kumar, A. S. K., & Jiang, S.-J. (2015). Preparation and characterization of exfoliated graphene oxide–L-cystine as an effective adsorbent of Hg (II) adsorption. *RSC Advances*, 5(9), 6294–6304.
- Kunaschk, M., Schmalz, V., Dietrich, N., Dittmar, T., & Worch, E. (2015). Novel regeneration method for phosphate loaded granular ferric (hydr) oxide—a contribution to phosphorus recycling. *Water Research*, 71, 219–226.
- Kunrath, J., Gurzau, E., Gurzau, A., Goessler, W., Gelmann, E. R., Thach, T. T., McCarty, K. M., & Yeckel, C. W. (2013). Blood pressure hyperreactivity: An early cardiovascular risk in normotensive men exposed to low-to-moderate inorganic arsenic in drinking water. *Journal of Hypertension*, 31(2), 361–369. <https://doi.org/10.1097/HJH.0b013e32835c175f>
- Laky, D., & Licskó, I. (2011). Arsenic removal by ferric-chloride coagulation - Effect of phosphate, bicarbonate and silicate. *Water Science and Technology*, 64(5), 1046–1055. <https://doi.org/10.2166/wst.2011.419>
- Lanzerstorfer, C. (2018). Fly ash from coal combustion: Dependence of the concentration of various elements on the particle size. *Fuel*, 228, 263–271.
- Lata, S., & Samadder, S. R. (2016). Removal of arsenic from water using nano adsorbents and challenges: a review. *Journal of Environmental Management*,

166, 387–406.

- Le, D. Q., Pham, T. T., Pham, H. G., & Nguyen, M. K. (2018). Evaluation of iron-rich adsorbent to remove arsenic from groundwater in decentralized water supply treatment. *Vietnam Journal of Science, Technology and Engineering*, 60(4), 78–81.
- Lee, C.-G., Alvarez, P. J. J., Nam, A., Park, S.-J., Do, T., Choi, U.-S., & Lee, S.-H. (2017). Arsenic (V) removal using an amine-doped acrylic ion exchange fiber: kinetic, equilibrium, and regeneration studies. *Journal of Hazardous Materials*, 325, 223–229.
- Lee, Y., Um, I., & Yoon, J. (2003). Arsenic (III) oxidation by iron (VI)(ferrate) and subsequent removal of arsenic (V) by iron (III) coagulation. *Environmental Science & Technology*, 37(24), 5750–5756.
- Lescano, M., Zalazar, C., Cassano, A., & Brandi, R. (2012). Kinetic modeling of arsenic (III) oxidation in water employing the UV/H₂O₂ process. *Chemical Engineering Journal*, 211, 360–368.
- Li, Y., Zhang, F.-S., & Xiu, F.-R. (2009). Arsenic (V) removal from aqueous system using adsorbent developed from a high iron-containing fly ash. *Science of the Total Environment*, 407(21), 5780–5786.
- Li, Z.-Q., Yang, J.-C., Sui, K.-W., & Yin, N. (2015). Facile synthesis of metal-organic framework MOF-808 for arsenic removal. *Materials Letters*, 160, 412–414.
- Li, Z., Liu, X., Jin, W., Hu, Q., & Zhao, Y. (2019). Adsorption behavior of arsenicals on MIL-101 (Fe): the role of arsenic chemical structures. *Journal of Colloid and Interface Science*, 554, 692–704.
- Li, Z., Ma, Z., van der Kuip, T. J., Yuan, Z., & Huang, L. (2014). A review of soil heavy metal pollution from mines in China: Pollution and health risk

- assessment. In *Science of the Total Environment* (Vols. 468–469, pp. 843–853). <https://doi.org/10.1016/j.scitotenv.2013.08.090>
- Liang, G., Li, Y., Yang, C., Zi, C., Zhang, Y., Hu, X., & Zhao, W. (2020). Production of biosilica nanoparticles from biomass power plant fly ash. *Waste Management*, 105, 8–17.
- Lichtfouse, E., Morin-Crini, N., Fourmentin, M., Zemmouri, H., do Carmo Nascimento, I. O., Queiroz, L. M., Tadza, M. Y. M., Picos-Corrales, L. A., Pei, H., & Wilson, L. D. (2019). Chitosan for direct bioflocculation of wastewater. *Environmental Chemistry Letters*, 17(4), 1603–1621.
- Lim, H. K., Teng, T. T., Ibrahim, M. H., Ahmad, A., & Chee, H. T. (2012). Adsorption and Removal of Zinc (II) from Aqueous Solution Using Powdered Fish Bones. *APCBEE Procedia*, 1, 96–102. <https://doi.org/10.1016/j.apcbee.2012.03.017>
- Lingamdinne, L. P., Choi, J.-S., Choi, Y.-L., Chang, Y.-Y., Yang, J.-K., Karri, R. R., & Koduru, J. R. (2020). Process modeling and optimization of an iron oxide immobilized graphene oxide gadolinium nanocomposite for arsenic adsorption. *Journal of Molecular Liquids*, 299, 112261.
- Litter, M. I., Ingallinella, A. M., Olmos, V., Savio, M., Difeo, G., Botto, L., Torres, E. M. F., Taylor, S., Frangie, S., & Herkovits, J. (2019). Arsenic in Argentina: technologies for arsenic removal from groundwater sources, investment costs and waste management practices. *Science of the Total Environment*, 690, 778–789.
- Liu, R., & Qu, J. (2021). Review on heterogeneous oxidation and adsorption for arsenic removal from drinking water. *Journal of Environmental Sciences (China)*, 110, 178–188. <https://doi.org/10.1016/j.jes.2021.04.008>

- Liu, X., Ren, Z., Ngo, H. H., He, X., Desmond, P., & Ding, A. (2021). Membrane technology for rainwater treatment and reuse: A mini review. *Water Cycle*, 2, 51–63.
- Lunardi, C. N., Gomes, A. J., Rocha, F. S., De Tommaso, J., & Patience, G. S. (2021). Experimental methods in chemical engineering: Zeta potential. *The Canadian Journal of Chemical Engineering*, 99(3), 627–639.
- Mahar, F. K., He, L., Wei, K., Mehdi, M., Zhu, M., Gu, J., Zhang, K., Khatri, Z., & Kim, I. (2019). Rapid adsorption of lead ions using porous carbon nanofibers. *Chemosphere*, 225, 360–367.
- Maji, S. K., Kao, Y. H., Wang, Y. Bin, & Liu, C. W. (2015). Dynamic column adsorption of As on iron-oxide-coated natural rock (IOCNR) and sludge management. *Desalination and Water Treatment*, 55(8), 2171–2182.
<https://doi.org/10.1080/19443994.2014.928912>
- Malwal, D., & Gopinath, P. (2017). Silica stabilized magnetic-chitosan beads for removal of arsenic from water. *Colloid and Interface Science Communications*, 19, 14–19.
- Masiá, A. A. T., Buhre, B. J. P., Gupta, R. P., & Wall, T. F. (2007). Use of TMA to predict deposition behaviour of biomass fuels. *Fuel*, 86(15), 2446–2456.
<https://doi.org/10.1016/j.fuel.2007.01.024>
- Matilainen, A., & Sillanpää, M. (2010). Removal of natural organic matter from drinking water by advanced oxidation processes. *Chemosphere*, 80(4), 351–365.
- McBeath, S. T., English, J. T., Wilkinson, D. P., & Graham, N. J. D. (2021). Circumneutral electrosynthesis of ferrate oxidant: An emerging technology for small, remote and decentralised water treatment applications. *Current Opinion*

in Electrochemistry, 27, 100680.

- Mendoza-Chávez, C. E., Carabin, A., Dirany, A., Drogué, P., Buelna, G., Meza-Montenegro, M. M., Ulloa-Mercado, R. G., Diaz-Tenorio, L. M., Leyva-Soto, L. A., & Gortáres-Moroyoqui, P. (2021). Statistical optimization of arsenic removal from synthetic water by electrocoagulation system and its application with real arsenic-polluted groundwater. *Environmental Technology*, 42(22), 3463–3474.
- Mierzwa-Hersztek, M., Gondek, K., Jewiarz, M., & Dziedzic, K. (2019). Assessment of energy parameters of biomass and biochars, leachability of heavy metals and phytotoxicity of their ashes. *Journal of Material Cycles and Waste Management*, 21(4), 786–800.
- Miklos, D. B., Remy, C., Jekel, M., Linden, K. G., Drewes, J. E., & Hübner, U. (2018). Evaluation of advanced oxidation processes for water and wastewater treatment—A critical review. *Water Research*, 139, 118–131.
- Miller, S. M., & Zimmerman, J. B. (2010). Novel, bio-based, photoactive arsenic sorbent: TiO₂-impregnated chitosan bead. *Water Research*, 44(19), 5722–5729. <https://doi.org/10.1016/j.watres.2010.05.045>
- Mohammed, H. A., Ali, S. A. K., & Basheer, M. I. (2020). Heavy metal ions removal using advanced oxidation (UV/H₂O₂) technique. *IOP Conference Series: Materials Science and Engineering*, 870(1), 12026.
- Mohan, D., & Pittman Jr, C. U. (2007). Arsenic removal from water/wastewater using adsorbents—a critical review. *Journal of Hazardous Materials*, 142(1–2), 1–53.
- Mohanty, D. (2017). Conventional as well as emerging arsenic removal technologies—a critical review. *Water, Air, & Soil Pollution*, 228(10), 1–21.

- Möller, T., Sylvester, P., Shepard, D., & Morassi, E. (2009). Arsenic in groundwater in New England—point-of-entry and point-of-use treatment of private wells. *Desalination*, 243(1–3), 293–304.
- Mondal, M. K., & Garg, R. (2017). A comprehensive review on removal of arsenic using activated carbon prepared from easily available waste materials. *Environmental Science and Pollution Research*, 24(15), 13295–13306.
- Mondal, R., Mondal, S., Kurada, K. V., Bhattacharjee, S., Sengupta, S., Mondal, M., Karmakar, S., De, S., & Griffiths, I. M. (2019). Modelling the transport and adsorption dynamics of arsenic in a soil bed filter. *Chemical Engineering Science*, 210, 115205.
- Moon, K. A., Guallar, E., Umans, J. G., Devereux, R. B., Best, L. G., Francesconi, K. A., Goessler, W., Pollak, J., Silbergeld, E. K., & Howard, B. V. (2013). Association between exposure to low to moderate arsenic levels and incident cardiovascular disease: a prospective cohort study. *Annals of Internal Medicine*, 159(10), 649–659.
- Moon, K., Guallar, E., & Navas-Acien, A. (2012). Arsenic exposure and cardiovascular disease: an updated systematic review. *Current Atherosclerosis Reports*, 14(6), 542–555.
- Muruganandam, L., Kumar, M. P. S., Jena, A., Gulla, S., & Godhwani, B. (2017). Treatment of waste water by coagulation and flocculation using biomaterials. *IOP Conference Series: Materials Science and Engineering*, 263(3), 032006.
- Mushtaq, F., Zahid, M., Bhatti, I. A., Nasir, S., & Hussain, T. (2019). Possible applications of coal fly ash in wastewater treatment. *Journal of Environmental Management*, 240, 27–46.
- Naceradska, J., Pivokonska, L., & Pivokonsky, M. (2019). On the importance of pH

- value in coagulation. *Journal of Water Supply: Research and Technology-Aqua*, 68(3), 222–230.
- Nalbandian, M. J., Kim, S., Gonzalez, H., Myung, N. V., & Cwiertny, D. M. (2022). Recent advances and remaining barriers to the development of electrospun nanofiber and nanofiber composites for point-of-use and point-of-entry water treatment systems. *Journal of Hazardous Materials Advances*, 100204.
- Nanseu-Njiki, C. P., Gwenzi, W., Pengou, M., Rahman, M. A., & Noubactep, C. (2019). Fe⁰/H₂O filtration systems for decentralized safe drinking water: Where to from here? *Water*, 11(3), 429.
- Nguyen, C. M., Bang, S., Cho, J., & Kim, K.-W. (2009). Performance and mechanism of arsenic removal from water by a nanofiltration membrane. *Desalination*, 245(1–3), 82–94.
- Nguyen, H. T. H., Nguyen, B. Q., Duong, T. T., Bui, A. T. K., Nguyen, H. T. A., Cao, H. T., Mai, N. T., Nguyen, K. M., Pham, T. T., & Kim, K.-W. (2019). Pilot-scale removal of arsenic and heavy metals from mining wastewater using adsorption combined with constructed wetland. *Minerals*, 9(6), 379.
- Nguyen, T. H., Tran, H. N., Vu, H. A., Trinh, M. V., Nguyen, T. V., Loganathan, P., Vigneswaran, S., Nguyen, T. M., Vu, D. L., & Nguyen, T. H. H. (2020). Laterite as a low-cost adsorbent in a sustainable decentralized filtration system to remove arsenic from groundwater in Vietnam. *Science of The Total Environment*, 699, 134267.
- O'Day, P. A. (2006). Chemistry and mineralogy of arsenic. *Elements*, 2(2), 77–83.
- Oke, I. A., Olarinoye, N. O., & Adewusi, S. R. A. (2008). Adsorption kinetics for arsenic removal from aqueous solutions by untreated powdered eggshell. *Adsorption*, 14(1), 73–83.

- Olafadehan, O. A., Abhulimen, K. E., Adeleke, A. I., Njoku, C. V., & Amoo, K. O. (2019). Production and characterization of derived composite biosorbents from animal bone. *African Journal of Pure and Applied Chemistry*, 13(2), 12–26.
- Önnby, L., Pakade, V., Mattiasson, B., & Kirsebom, H. (2012). Polymer composite adsorbents using particles of molecularly imprinted polymers or aluminium oxide nanoparticles for treatment of arsenic contaminated waters. *Water Research*, 46(13), 4111–4120. <https://doi.org/10.1016/j.watres.2012.05.028>
- Onwordi, C. T., Uche, C. C., Ameh, A. E., & Petrik, L. F. (2019). Comparative study of the adsorption capacity of lead (II) ions onto bean husk and fish scale from aqueous solution. *Journal of Water Reuse and Desalination*, 9(3), 249–262.
- Otgon, N., Zhang, G., & Yang, C. (2016). Arsenic removal from waste water by ozone oxidation combined with ferric precipitation. *Mongolian Journal of Chemistry*, 17(43), 18–22.
- Othman, N., Abd-Kadir, A., & Zayadi, N. (2016). Waste fish scale as cost effective adsorbent in removing zinc and ferum ion in wastewater. *J Eng Appl Sci*, 11(3), 1584–1592.
- Othmani, A., Magdouli, S., Kumar, P. S., Kapoor, A., Chellam, P. V., & Gökkuş, Ö. (2022). Agricultural waste materials for adsorptive removal of phenols, chromium (VI) and cadmium (II) from wastewater: A review. *Environmental Research*, 204, 111916.
- Otter, P., Malakar, P., Jana, B. B., Grischek, T., Benz, F., Goldmaier, A., Feistel, U., Jana, J., Lahiri, S., & Alvarez, J. A. (2017). Arsenic removal from groundwater by solar driven inline-electrolytic induced co-precipitation and filtration—a long term field test conducted in West Bengal. *International Journal of Environmental Research and Public Health*, 14(10), 1167.

- Oturan, M. A., & Aaron, J.-J. (2014). Advanced oxidation processes in water/wastewater treatment: principles and applications. A review. *Critical Reviews in Environmental Science and Technology*, 44(23), 2577–2641.
- Ouvrard, S., Simonnot, M. O., & Sardin, M. (2002). Reactive behavior of natural manganese oxides toward the adsorption of phosphate and arsenate. *Industrial and Engineering Chemistry Research*, 41(11), 2785–2791.
<https://doi.org/10.1021/ie0106534>
- Oyedotun, T. D. T. (2018). X-ray fluorescence (XRF) in the investigation of the composition of earth materials: a review and an overview. *Geology, Ecology, and Landscapes*, 2(2), 148–154.
- Peter-Varbanets, M., Zurbrügg, C., Swartz, C., & Pronk, W. (2009). Decentralized systems for potable water and the potential of membrane technology. *Water Research*, 43(2), 245–265.
- Peters, C. D., Rantissi, T., Gitis, V., & Hankins, N. P. (2021). Retention of natural organic matter by ultrafiltration and the mitigation of membrane fouling through pre-treatment, membrane enhancement, and cleaning-A review. *Journal of Water Process Engineering*, 44, 102374.
- Petrusevski, B., Sharma, S., Schippers, J. C., & Shordt, K. (2007). Arsenic in drinking water. *Delft: IRC International Water and Sanitation Centre*, 17(1), 36–44.
- Phearom, S., Shahid, M. K., & Choi, Y.-G. (2021). Optimization of Arsenic Adsorption by Mill Scale-Derived Magnetite Particles Using Response Surface Methodology. *Journal of Hazardous, Toxic, and Radioactive Waste*, 25(3), 4021022.
- Pizarro, C., Escudey, M., Caroca, E., Pavez, C., & Zúñiga, G. E. (2021). Evaluation of zeolite, nanomagnetite, and nanomagnetite-zeolite composite materials as

- arsenic (V) adsorbents in hydroponic tomato cultures. *Science of the Total Environment*, 751, 141623.
- Pokhrel, D., & Viraraghavan, T. (2006). Arsenic removal from an aqueous solution by a modified fungal biomass. *Water Research*, 40(3), 549–552.
- Popławski, J., & Lelusz, M. (2017). Utility assessment of biomass fly-ash for production of concrete products. *Technical Transactions*, 114(8), 129–142.
- Priyadarshni, N., Nath, P., & Chanda, N. (2020). Sustainable removal of arsenate, arsenite and bacterial contamination from water using biochar stabilized iron and copper oxide nanoparticles and associated mechanism of the remediation process. *Journal of Water Process Engineering*, 37, 101495.
- Qi, J., Zhang, G., & Li, H. (2015). Efficient removal of arsenic from water using a granular adsorbent: Fe–Mn binary oxide impregnated chitosan bead. *Bioresource Technology*, 193, 243–249.
- Qu, X., Brame, J., Li, Q., & Alvarez, P. J. J. (2013). Nanotechnology for a safe and sustainable water supply: enabling integrated water treatment and reuse. *Accounts of Chemical Research*, 46(3), 834–843.
- Quan, C., Chu, H., Zhou, Y., Su, S., Su, R., & Gao, N. (2022). Amine-modified silica zeolite from coal gangue for CO₂ capture. *Fuel*, 322, 124184.
- Rahdar, S., Taghavi, M., Khaksefidi, R., & Ahmadi, S. (2019). Adsorption of arsenic (V) from aqueous solution using modified saxaul ash: isotherm and thermodynamic study. *Applied Water Science*, 9(4), 1–9.
- Rahman, N. A. A., Said, M. I. M., & Azman, S. (2017). Carbonized green mussel shell as heavy metal removal. *Malaysian Journal of Civil Engineering*, 29.
- Rakhunde, R., Jasudkar, D., Deshpande, L., Juneja, H. D., & Labhasetwar, P. (2012). Health effects and significance of arsenic speciation in water. *International*

Journal of Environmental Sciences and Research, 1(4), 92–96.

- Rampino, A., Borgogna, M., Blasi, P., Bellich, B., & Cesàro, A. (2013). Chitosan nanoparticles: Preparation, size evolution and stability. *International Journal of Pharmaceutics*, 455(1–2), 219–228.
- Ranjan, D., Talat, M., & Hasan, S. H. (2009). Biosorption of arsenic from aqueous solution using agricultural residue ‘rice polish.’ *Journal of Hazardous Materials*, 166(2–3), 1050–1059.
- Ranjbar, F., Karrabi, M., Danesh, S., & Gheibi, M. (2021). Improvement of wastewater sludge dewatering using ferric chloride, aluminum sulfate, and calcium oxide (experimental investigation and descriptive statistical analysis). *Water Environment Research*, 93(7), 1138–1149.
- Rathi, B. S., Kumar, P. S., Ponprasath, R., Rohan, K., & Jahnavi, N. (2021). An effective separation of toxic arsenic from aquatic environment using electrochemical ion exchange process. *Journal of Hazardous Materials*, 412, 125240.
- Ray, S., & Lalman, J. A. (2016). Fabrication and characterization of an immobilized titanium dioxide (TiO₂) nanofiber photocatalyst. *Materials Today: Proceedings*, 3(6), 1582–1591.
- Reddy, K. J., McDonald, K. J., & King, H. (2013). A novel arsenic removal process for water using cupric oxide nanoparticles. *Journal of Colloid and Interface Science*, 397, 96–102. <https://doi.org/10.1016/j.jcis.2013.01.041>
- Rezk, R. A., Galmed, A. H., Abdelkreem, M., Abdel Ghany, N. A., & Harith, M. A. (2018). Detachment of Cu (II) and Co (II) ions from synthetic wastewater via adsorption on Lates niloticus fish bones using LIBS and XRF. *Journal of Advanced Research*, 14. <https://doi.org/10.1016/j.jare.2018.05.002>

- Ribeiro, I. C. A., Vasques, I. C. F., Teodoro, J. C., Guerra, M. B. B., da Silva Carneiro, J. S., Melo, L. C. A., & Guilherme, L. R. G. (2021). Fast and effective arsenic removal from aqueous solutions by a novel low-cost eggshell byproduct. *Science of The Total Environment*, 783, 147022.
- Rosales, M., Garcia, A., Fuenzalida, V. M., Espinoza-González, R., Song, G., Wang, B., Yu, J., Gracia, F., & Rosenkranz, A. (2020). Unprecedented arsenic photo-oxidation behavior of few-and multi-layer Ti3C2Tx nano-sheets. *Applied Materials Today*, 20, 100769.
- Rouff, A. A., Ma, N., & Kustka, A. B. (2016). Adsorption of arsenic with struvite and hydroxylapatite in phosphate-bearing solutions. *Chemosphere*, 146, 574–581.
- Roy, P., Mondal, N. K., & Das, K. (2014). Modeling of the adsorptive removal of arsenic: a statistical approach. *Journal of Environmental Chemical Engineering*, 2(1), 585–597.
- Sahu, U. K., Mahapatra, S. S., & Patel, R. K. (2018). Application of Box–Behnken Design in response surface methodology for adsorptive removal of arsenic from aqueous solution using CeO₂/Fe₂O₃/graphene nanocomposite. *Materials Chemistry and Physics*, 207, 233–242.
- Salameh, Y., Ahmad, M. N. M., Allen, S. J., & Walker, G. M. (2011). Investigations on arsenic adsorption onto dolomitic sorbents. In *Water Production and Wastewater Treatment* (Vol. 160, Issue 2, pp. 133–158). Elsevier.
- Sarkkinen, M., Kujala, K., Kemppainen, K., & Gehör, S. (2018). Effect of biomass fly ashes as road stabilisation binder. *Road Materials and Pavement Design*, 19(1), 239–251.
- Sarode, S., Upadhyay, P., Khosa, M. A., Mak, T., Shakir, A., Song, S., & Ullah, A. (2019). Overview of wastewater treatment methods with special focus on

- biopolymer chitin-chitosan. *International Journal of Biological Macromolecules*, 121, 1086–1100.
- Seco-Reigosa, N., Cutillas-Barreiro, L., Nóvoa-Muñoz, J. C., Arias-Estévez, M., Álvarez-Rodríguez, E., Fernández-Sanjurjo, M. J., & Núñez-Delgado, A. (2015). Adsorption, desorption and fractionation of As (V) on untreated and mussel shell-treated granitic material. *Solid Earth*, 6(1), 337–346.
- Seco-Reigosa, N., Peña-Rodríguez, S., Nóvoa-Muñoz, J. C., Arias-Estévez, M., Fernández-Sanjurjo, M. J., Álvarez-Rodríguez, E., & Núñez-Delgado, A. (2013). Arsenic, chromium and mercury removal using mussel shell ash or a sludge/ashes waste mixture. *Environmental Science and Pollution Research*, 20(4), 2670–2678.
- Seki, H., Suzuki, A., & Maruyama, H. (2005). Biosorption of chromium(VI) and arsenic(V) onto methylated yeast biomass. *Journal of Colloid and Interface Science*, 281(2), 261–266. <https://doi.org/10.1016/j.jcis.2004.08.167>
- Shadbahr, J., & Husain, T. (2019). Affordable and efficient adsorbent for arsenic removal from rural water supply systems in Newfoundland. *Science of the Total Environment*, 660, 158–168.
- Shaji, E., Santosh, M., Sarath, K. V., Prakash, P., Deepchand, V., & Divya, B. V. (2021). Arsenic contamination of groundwater: A global synopsis with focus on the Indian Peninsula. *Geoscience Frontiers*, 12(3), 101079.
- Shakoor, M. B., Niazi, N. K., Bibi, I., Shahid, M., Saqib, Z. A., Nawaz, M. F., Shaheen, S. M., Wang, H., Tsang, D. C. W., & Bundschuh, J. (2019). Exploring the arsenic removal potential of various biosorbents from water. *Environment International*, 123, 567–579.
- Shakoor, M. B., Niazi, N. K., Bibi, I., Shahid, M., Sharif, F., Bashir, S., Shaheen, S.

- M., Wang, H., Tsang, D. C. W., & Ok, Y. S. (2018). Arsenic removal by natural and chemically modified water melon rind in aqueous solutions and groundwater. *Science of the Total Environment*, 645, 1444–1455.
- Sharma, A. K., Sorlini, S., Crotti, B. M., Collivignarelli, M. C., Tjell, J. C., & Abbà, A. (2016). Enhancing arsenic removal from groundwater at household level with naturally occurring iron. *Revista Ambiente & Água*, 11, 486–498.
- Sharma, V. K., Dutta, P. K., & Ray, A. K. (2007). Review of kinetics of chemical and photocatalytical oxidation of arsenic (III) as influenced by pH. *Journal of Environmental Science and Health, Part A*, 42(7), 997–1004.
- Sherlala, A. I. A., Raman, A. A. A., Bello, M. M., & Buthiyappan, A. (2019). Adsorption of arsenic using chitosan magnetic graphene oxide nanocomposite. *Journal of Environmental Management*, 246, 547–556.
- Shevade, S. S. (2003). Utility of zeolites in arsenic removal from water. *Abstracts of Papers of the American Chemical Society*, 226, U589–U590.
- Shih, M.-C. (2005). An overview of arsenic removal by pressure-driven membrane processes. *Desalination*, 172(1), 85–97.
- Siddiqui, S. I., & Chaudhry, S. A. (2017). Iron oxide and its modified forms as an adsorbent for arsenic removal: a comprehensive recent advancement. *Process Safety and Environmental Protection*, 111, 592–626.
- Siddiqui, S. I., Singh, P. N., Tara, N., Pal, S., Chaudhry, S. A., & Sinha, I. (2020). Arsenic removal from water by starch functionalized maghemite nano-adsorbents: Thermodynamics and kinetics investigations. *Colloid and Interface Science Communications*, 36, 100263.
- Sieliechi, J. M., Kayem, G. J., & Sandu, I. (2010). Effect of water treatment residuals (aluminum and iron ions) on human health and drinking water distribution

- systems. *International Journal of Conservation Science*, 1(3), 175–182.
- Sihem, A., Lehocine, M. B., & Miniai, H. A. (2012). Preparation and characterisation of an natural adsorbent used for elimination of pollutants in wastewater. *Energy Procedia*, 18, 1145–1151.
- Simsek, E. B., Özdemir, E., & Beker, U. (2013). Process optimization for arsenic adsorption onto natural zeolite incorporating metal oxides by response surface methodology. *Water, Air, & Soil Pollution*, 224(7), 1–14.
- Singh, T. S., & Pant, K. K. (2004). Equilibrium, kinetics and thermodynamic studies for adsorption of As(III) on activated alumina. *Separation and Purification Technology*, 36(2), 139–147. [https://doi.org/10.1016/S1383-5866\(03\)00209-0](https://doi.org/10.1016/S1383-5866(03)00209-0)
- Slotnick, M. J., Meliker, J. R., & Nriagu, J. O. (2006). Effects of time and point-of-use devices on arsenic levels in Southeastern Michigan drinking water, USA. *Science of the Total Environment*, 369(1–3), 42–50.
- Smedley, P. L., & Kinniburgh, D. G. (2002). A review of the source, behaviour and distribution of arsenic in natural waters. *Applied Geochemistry*, 17(5), 517–568.
- Sonal, S., & Mishra, B. K. (2021). Role of coagulation/flocculation technology for the treatment of dye wastewater: trend and future aspects. In *Water pollution and management practices* (pp. 303–331). Springer.
- Song, S., Lopez-Valdivieso, A., Hernandez-Campos, D. J., Peng, C., Monroy-Fernandez, M. G., & Razo-Soto, I. (2006). Arsenic removal from high-arsenic water by enhanced coagulation with ferric ions and coarse calcite. *Water Research*, 40(2), 364–372. <https://doi.org/10.1016/j.watres.2005.09.046>
- Sorlini, S., & Gialdini, F. (2010). Conventional oxidation treatments for the removal of arsenic with chlorine dioxide, hypochlorite, potassium permanganate and

- monochloramine. *Water Research*, 44(19), 5653–5659.
- Sorlini, S., Gialdini, F., & Collivignarelli, M. C. (2014). Survey on full-scale drinking water treatment plants for arsenic removal in Italy. *Water Practice and Technology*, 9(1), 42–51.
- Sosa, A., Armienta, M. A., Aguayo, A., & Cruz, O. (2020). Evaluation of the influence of main groundwater ions on arsenic removal by limestones through column experiments. *Science of the Total Environment*, 727, 138459.
<https://doi.org/10.1016/j.scitotenv.2020.138459>
- Souza, T. G. F., Ciminelli, V. S. T., & Mohallem, N. D. S. (2016). A comparison of TEM and DLS methods to characterize size distribution of ceramic nanoparticles. *Journal of Physics: Conference Series*, 733(1), 12039.
- Stevens, M. G. F., & Batlokwa, B. S. (2017). Environmentally Friendly and Cheap Removal of Lead (II) and Zinc (II) from Wastewater with Fish Scales Waste Remains. *International Journal of Chemistry*, 9(4), 22.
<https://doi.org/10.5539/ijc.v9n4p22>
- Sumaila, A., Ndamitso, M. M., Iyaka, Y. A., Abdulkareem, A. S., Tijani, J. O., & Idris, M. O. (2020). Extraction and Characterization of Chitosan from Crab Shells: Kinetic and Thermodynamic Studies of Arsenic and Copper Adsorption from Electroplating Wastewater. *Iraqi Journal of Science*, 2156–2171.
- Suresh Kumar, P., Ejerssa, W. W., Wegener, C. C., Korving, L., Dugulan, A. I., Temmink, H., van Loosdrecht, M. C. M., & Witkamp, G. J. (2018). Understanding and improving the reusability of phosphate adsorbents for wastewater effluent polishing. *Water Research*, 145, 365–374.
<https://doi.org/10.1016/j.watres.2018.08.040>

- Suzuki, T. M., Bomani, J. O., Matsunaga, H., & Yokoyama, T. (2000). Preparation of porous resin loaded with crystalline hydrous zirconium oxide and its application to the removal of arsenic. *Reactive and Functional Polymers*, 43(1–2), 165–172.
- Tabassum, R. A., Shahid, M., Niazi, N. K., Dumat, C., Zhang, Y., Imran, M., Bakhat, H. F., Hussain, I., & Khalid, S. (2019). Arsenic removal from aqueous solutions and groundwater using agricultural biowastes-derived biosorbents and biochar: a column-scale investigation. *International Journal of Phytoremediation*, 21(6), 509–518.
- Tahmasebpour, M., Hosseini Nami, S., Khatamian, M., & Sanaei, L. (2022). Arsenate removal from contaminated water using Fe₂O₃-clinoptilolite powder and granule. *Environmental Technology*, 43(1), 116–130.
- Tarpeh, W. A., Udert, K. M., & Nelson, K. L. (2017). Comparing ion exchange adsorbents for nitrogen recovery from source-separated urine. *Environmental Science & Technology*, 51(4), 2373–2381.
- Tauk, M., Bechelany, M., Lagerge, S., Sistat, P., Habchi, R., Cretin, M., & Zaviska, F. (2022). Influence of particle size distribution on carbon-based flowable electrode viscosity and desalination efficiency in flow electrode capacitive deionization. *Separation and Purification Technology*, 122666.
- Tchounwou, P. B., Yedjou, C. G., Patlolla, A. K., & Sutton, D. J. (2012). Heavy metal toxicity and the environment. In *EXS* (Vol. 101, pp. 133–164). https://doi.org/10.1007/978-3-7643-8340-4_6
- Teixeira, E. R., Camões, A., Branco, F. G., Aguiar, J. B., & Fangueiro, R. (2019). Recycling of biomass and coal fly ash as cement replacement material and its effect on hydration and carbonation of concrete. *Waste Management*, 94, 39–

- Tiwari, M. K., Bajpai, S., & Dewangan, U. K. (2016). Fly ash utilization: A brief review in Indian context. *International Research Journal of Engineering and Technology*, 3(4), 949–956.
- Trois, C., & Cibati, A. (2015). South African sands as a low cost alternative solution for arsenic removal from industrial effluents in permeable reactive barriers: Column tests. *Chemical Engineering Journal*, 259, 981–989.
- Urbano, B. F., Rivas, B. L., Martinez, F., & Alexandratos, S. D. (2012). Water-insoluble polymer-clay nanocomposite ion exchange resin based on N-methyl-d-glucamine ligand groups for arsenic removal. *Reactive and Functional Polymers*, 72(9). <https://doi.org/10.1016/j.reactfunctpolym.2012.06.008>
- Usman, M., Katsoyiannis, I., Rodrigues, J. H., & Ernst, M. (2021). Arsenate removal from drinking water using by-products from conventional iron oxyhydroxides production as adsorbents coupled with submerged microfiltration unit. *Environmental Science and Pollution Research*, 28(42), 59063–59075.
- Vaughan Jr, R. L., & Reed, B. E. (2005). Modeling As (V) removal by a iron oxide impregnated activated carbon using the surface complexation approach. *Water Research*, 39(6), 1005–1014.
- Verma, L., Siddique, M. A., Singh, J., & Bharagava, R. N. (2019). As (III) and As (V) removal by using iron impregnated biosorbents derived from waste biomass of Citrus limmeta (peel and pulp) from the aqueous solution and ground water. *Journal of Environmental Management*, 250, 109452.
- Viraraghavan, T., Subramanian, K. S., & Aruldoss, J. A. (1999). Arsenic in drinking water—problems and solutions. *Water Science and Technology*, 40(2), 69–76.
- von Gunten, U. (2018). Oxidation processes in water treatment: are we on track?

Environmental Science & Technology, 52(9), 5062–5075.

Vrijenhoek, E. M., & Waypa, J. J. (2000). Arsenic removal from drinking water by a “loose” nanofiltration membrane. *Desalination*, 130(3), 265–277.

[https://doi.org/10.1016/S0011-9164\(00\)00091-6](https://doi.org/10.1016/S0011-9164(00)00091-6)

Vu, T. A., Le, G. H., Dao, C. D., Dang, L. Q., Nguyen, K. T., Nguyen, Q. K., Dang, P. T., Tran, H. T. K., Duong, Q. T., Nguyen, T. V, & Lee, G. D. (2015). Arsenic removal from aqueous solutions by adsorption using novel MIL-53(Fe) as a highly efficient adsorbent. *RSC Advances*, 5(7), 5261–5268.

<https://doi.org/10.1039/c4ra12326c>

Wang, C., Liu, K., Huang, D., Chen, Q., Tu, M., Wu, K., & Shui, Z. (2022).

Utilization of fly ash as building material admixture: Basic properties and heavy metal leaching. *Case Studies in Construction Materials*, 17, e01422.

Wang, C., Xiong, C., He, Y., Yang, C., Li, X., Zheng, J., & Wang, S. (2021). Facile preparation of magnetic Zr-MOF for adsorption of Pb (II) and Cr (VI) from water: Adsorption characteristics and mechanisms. *Chemical Engineering Journal*, 415, 128923.

Wang, J., & Guo, X. (2023). Adsorption kinetics and isotherm models of heavy metals by various adsorbents: An overview. *Critical Reviews in Environmental Science and Technology*, 53(21), 1837–1865.

Wang, L., Chen, A., & Fields, K. (2000). Arsenic Removal from Drinking Water by Ion Exchange and Activated Alumina Plants. *Environmental Protection Agency, USA, October*.

Wang, L., Chen, L., Tsang, D. C. W., Guo, B., Yang, J., Shen, Z., Hou, D., Ok, Y. S., & Poon, C. S. (2020). Biochar as green additives in cement-based composites with carbon dioxide curing. *Journal of Cleaner Production*, 258, 120678.

- Wang, M., Zhang, K., Wu, M., Wu, Q., Liu, J., Yang, J., & Zhang, J. (2019). Unexpectedly high adsorption capacity of esterified hydroxyapatite for heavy metal removal. *Langmuir*, 35(49), 16111–16119.
- Wang, Q., Jiang, F., Ouyang, X.-K., Yang, L.-Y., & Wang, Y. (2021). Adsorption of Pb (II) from aqueous solution by mussel shell-based adsorbent: Preparation, characterization, and adsorption performance. *Materials*, 14(4), 741.
- Wang, Z., Ma, J., Tang, C. Y., Kimura, K., Wang, Q., & Han, X. (2014). Membrane cleaning in membrane bioreactors: A review. *Journal of Membrane Science*, 468, 276–307.
- Wei, Z., Liang, K., Wu, Y., Zou, Y., Zuo, J., Arriagada, D. C., Pan, Z., & Hu, G. (2016). The effect of pH on the adsorption of arsenic (III) and arsenic (V) at the TiO₂ anatase [1 0 1] surface. *Journal of Colloid and Interface Science*, 462, 252–259.
- Wirasnita, R., Hadibarata, T., Yusoff, A. R. M., & Lazim, Z. M. (2015). Preparation and characterization of activated carbon from oil palm empty fruit bunch wastes using zinc chloride. *Jurnal Teknologi*, 74(11).
- Wiselogle, A. E., Agblevor, F. A., Johnson, D. K., Deutch, S., Fennell, J. A., & Sanderson, M. A. (1996). Compositional changes during storage of large round switchgrass bales. *Bioresource Technology*, 56(1), 103–109.
[https://doi.org/10.1016/0960-8524\(95\)00171-9](https://doi.org/10.1016/0960-8524(95)00171-9)
- Yang, J., Liang, X., Jiang, N., Huang, Z., Mou, F., Zu, Y., & Li, Y. (2022). Adsorption Characteristics of Modified Eucalyptus Sawdust for Cadmium and Arsenic and Its Potential for Soil Remediation. *Bulletin of Environmental Contamination and Toxicology*, 1–8.
- Yang, Z., Yan, G., Song, Z., Zhang, J., Wang, C., Yu, Z., Bai, Z., Zhuang, G., &

- Liang, F. (2021). Study on adsorption of As (III) by a new bio-material from chitin pyrolysis. *Water*, 13(21), 2944.
- Yoon, Y., Zheng, M., Ahn, Y.-T., Park, W. K., Yang, W. S., & Kang, J.-W. (2017). Synthesis of magnetite/non-oxidative graphene composites and their application for arsenic removal. *Separation and Purification Technology*, 178, 40–48.
- Yu, X.-Y., Luo, T., Jia, Y., Zhang, Y.-X., Liu, J.-H., & Huang, X.-J. (2011). Porous hierarchically micro-/nanostructured MgO: morphology control and their excellent performance in As (III) and As (V) removal. *The Journal of Physical Chemistry C*, 115(45), 22242–22250.
- Zaharia, C. (2017). Decentralized wastewater treatment systems: Efficiency and its estimated impact against onsite natural water pollution status. A Romanian case study. *Process Safety and Environmental Protection*, 108, 74–88.
- Zaiku, X., Qingling, C., Bo, C., & Chengfang, Z. (2001). Influence of alkalinity on particle size distribution and crystalline structure in synthesis of zeolite beta. *Crystal Engineering*, 4(4), 359–372.
- Zakhar, R., Derco, J., & Cacho, F. (2018). An overview of main arsenic removal technologies. *Acta Chimica Slovaca*, 11(2), 107–113.
- Zaw, M., & Emmett, M. T. (2002). Arsenic removal from water using advanced oxidation processes. *Toxicology Letters*, 133(1), 113–118.
[https://doi.org/10.1016/S0378-4274\(02\)00081-4](https://doi.org/10.1016/S0378-4274(02)00081-4)
- Zhang, G., Li, X., Wu, S., & Gu, P. (2012). Effect of source water quality on arsenic (V) removal from drinking water by coagulation/microfiltration. *Environmental Earth Sciences*, 66(4), 1269–1277.
- Zhang, G., Liu, Y., Wang, J., & Li, H. (2020). Efficient arsenic (III) removal from

- aqueous solution by a novel nanostructured iron-copper-manganese trimetal oxide. *Journal of Molecular Liquids*, 309, 112993.
- Zhang, T., & Sun, D. D. (2013). Removal of arsenic from water using multifunctional micro-/nano-structured MnO₂ spheres and microfiltration. *Chemical Engineering Journal*, 225, 271–279.
- Zhang, X., Jiang, K., Tian, Z., Huang, W., & Zhao, L. (2008). Removal of arsenic in water by an ion-exchange fiber with amino groups. *Journal of Applied Polymer Science*, 110(6), 3934–3940.
- Zhang, Y., Wang, H., Li, Y., Wang, B., Huang, J., Deng, S., Yu, G., & Wang, Y. (2020). Removal of micropollutants by an electrochemically driven UV/chlorine process for decentralized water treatment. *Water Research*, 183, 116115.
- Zhao, P., Jian, M., Xu, R., Zhang, Q., Xiang, C., Liu, R., Zhang, X., & Liu, H. (2020). Removal of arsenic (III) from water by 2D zeolitic imidazolate framework-67 nanosheets. *Environmental Science: Nano*, 7(11), 3616–3626.

CHAPTER THREE

USE OF MUSSEL SHELLS FOR REMOVAL OF ARSENIC FROM WATER: KINETICS AND EQUILIBRIUM EXPERIMENTAL INVESTIGATION ²

Roya Sadat Neisan¹, Noori M. Cata Saady¹, Carlos Bazan², Sohrab Zendehboudi³, Ponnusami Venkatachalam⁴

¹ Department of Civil Engineering, Memorial University, St. John's, NL A1B 3X5, Canada

² Faculty of Business Administration, Memorial University, St. John's, NL A1B 3X5, Canada

³ Department of Process Engineering, Memorial University, St. John's, NL A1B 3X5, Canada

⁴ School of Chemical & Biotechnology, SASTRA Deemed University, , 613401, India

Abstract

This study investigated the potential of calcined mussel shells (CMS) as an adsorbent for arsenic (As(III) and As(V)) removal from water through optimization, kinetics, and equilibrium studies. The effects of pH, initial arsenic concentration (C_i), adsorbent dose (A_d), and contact time (t_c) were evaluated using response surface methodology (RSM) to maximize adsorption efficiency. Optimal conditions for As(III) removal (pH 6.4, C_i 57.9 mg L⁻¹, A_d 3.4 g L⁻¹, and t_c 4.4 h) achieved a 94.9% efficiency, while As(V) removal (pH 5.7, C_i 59.9 mg L⁻¹, A_d 2.7 g L⁻¹, and t_c 4.9 h) reached 98.5%. Kinetic studies showed that the pseudo-second-order model best described the adsorption process. Equilibrium studies indicated that the Langmuir model provided the best fit, suggesting monolayer adsorption on the iron oxide–modified CMS surface (As(III): $q_{\max} = 28.74$, $R^2 = 0.87$; As(V): $q_{\max} = 31.54$, $R^2 = 0.98$). The adsorption process for both arsenic species was spontaneous and endothermic. These findings underscore the potential of CMS as an affordable, environmentally acceptable adsorbent for arsenic removal from water.

² This chapter has been published as a peer-reviewed journal article:

Neisan, R. S., Saady, N. M. C., Bazan, C., Zendehboudi, S., & Venkatachalam, P. (2024). Use of Mussel Shells for Removal of Arsenic from Water: Kinetics and Equilibrium Experimental Investigation. Results in Engineering, 103587. <https://doi.org/10.1016/j.rineng.2024.103587>

3.1. Introduction

Arsenic, an element classified as a metalloid, is found naturally and is very poisonous; thus, it threatens human health (Genchi et al., 2022). Arsenic has many oxidation states, with arsenite (As(III)) and arsenate (As(V)) are the most commonly found oxidation states in water sources (Smedley & Kinniburgh, 2002). Numerous health problems have been connected to chronic exposure to arsenic through contaminated drinking water. (e.g., skin lesions, cardiovascular disorders, and several kinds of cancer) (Neisan et al., 2023). The maximum allowable concentrations of arsenic in drinking water vary worldwide. The WHO (Frisbie & Mitchell, 2022), the United States Environmental Protection Agency (USEPA) (Read et al., 2001), European Union (EU) (Azara et al., 2018), Canada (Frisbie & Mitchell, 2022), Argentina (Frisbie & Mitchell, 2022), Brazil (Frisbie & Mitchell, 2022), and Russia (Medunić et al., 2020) set the maximum arsenic level in drinking water to $10 \mu\text{g L}^{-1}$, India (Métral et al., 2008), China (Frisbie & Mitchell, 2022), and Bangladesh (Frisbie & Mitchell, 2022) set it at $50 \mu\text{g L}^{-1}$. However, millions of people worldwide still drink water with unsafe levels of arsenic, due to naturally occurring arsenic in groundwater or industrial contamination (Shaji et al., 2021).

Arsenic is currently removed from water using several conventional techniques; including coagulation, precipitation, adsorption, and membrane filtration (Neisan et al., 2023). While these techniques have varying degrees of effectiveness, they often come with limitations. Coagulation and precipitation techniques can generate large amounts of sludge requiring disposal, while membrane filtration can be expensive and suffers from membrane fouling (Chong et al., 2019). Adsorption offers a promising alternative owing to its excellent selectivity, efficiency, and ease of use (Neisan et al., 2023).

Developing affordable and eco-friendly adsorbents to remove arsenic from

drinking water is an active area of research. Mussel shells, abundant byproducts of the seafood industry, have garnered attention as potential adsorbents due to their high calcium carbonate content and porous structure (Zhan et al., 2022). Using mussel shells as adsorbents offers several advantages, including low cost, abundance, and biodegradability (Açıkgöz et al., 2017). Repurposing waste materials such as mussel shells for environmental remediation aligns with circular economy principles and sustainable development (Veríssimo et al., 2021). The shell forms between 56% and 61% of the weight of mussels. Approximately 94% of the shells is made up of calcium carbonate, which, by calcination, can be converted into calcium oxide (CaO) (Mititelu et al., 2021). Calcination modifies the layered structure into a porous material with an expanded surface area. This enhanced surface area facilitates greater contact between the adsorbent and both the solution and the targeted heavy metals. Moreover, hydroxyl (OH) groups exhibit a significant electrostatic attraction to calcium oxide (CaO) at its coordination sites. This affinity facilitates hydrolysis and complexation reactions with heavy metal ions (W. An et al., 2024). Figure 3-1 presents an integrated life cycle diagram of mussels, incorporating the subsystem of shell waste management. It begins with mussels harvesting and the subsequent shell waste generation. The subsystem of shell waste management is then detailed, showing the processes of cleaning, calcination, and modification. These treated shells are repurposed for multiple applications, including water treatment, soil amendment, construction materials, and catalyst support.

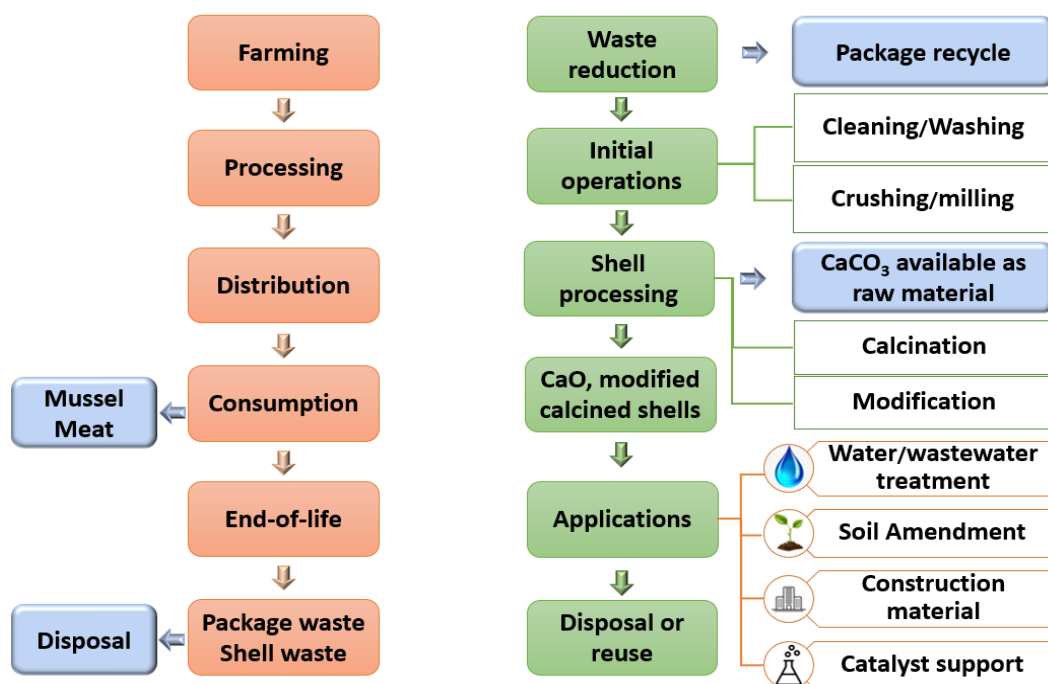


Figure 3-1 Mussel shell utilization system based on the mussels life cycle diagram (de Alvarenga et al., 2012; Iribarren et al., 2010; H. Yang & Yan, 2018).

Response surface methodology (RSM) is a potent statistical technique commonly employed in the design and optimization of experiments. It enables researchers to explore complex response surfaces and identify optimal process conditions by systematically varying multiple factors simultaneously. Central composite design (CCD), a specific type of RSM that excels at fitting second-order models, allows researchers to understand how individual factors influence a response variable and how they interact (K. P. Singh et al., 2010). Due to its efficient use of experimental runs, CCD offers a compelling alternative to other RSM techniques. By incorporating both factorial points and star points, CCD estimates main effects, explores curvature, and minimizes the total number of experiments required. This advantage is particularly significant in studies with a high number of factors, where traditional factorial designs become impractical. Compared to simpler RSM designs, CCD's ability to capture non-linear relationships among factors (variable) and the response proves particularly useful

in real-world scenarios where linearity cannot always be assumed (Azcarate et al., 2023). The CCD facilitates the optimization of adsorption parameters (pH, adsorbent dosage, initial contaminant concentration, and contact time). By systematically varying these factors within predetermined ranges and analyzing the response surface, CCD enables researchers to identify the most favorable conditions that maximize adsorption efficiency and minimize the use of resources.

In removing arsenic from water, commonly studied adsorbents include activated carbon, iron oxides and hydroxides, clay minerals, agricultural waste products such as rice husk, coconut shell, and natural materials like zeolites (Neisan et al., 2023). Because it has an extensive surface area and well-developed porosity, activated carbon has demonstrated notable arsenic removal efficiency (Luo et al., 2019). Cerium oxide-modified activated carbon effectively removed arsenate and arsenite (43.60 and 36.77 mg g⁻¹, respectively) at pH 5. Iron-based materials have also shown promise, with their capacity for arsenic adsorption linked to surface complexation and precipitation reactions (Y. Yu et al., 2017). The use of superparamagnetic Fe₃O₄ nanoparticles with large surface area as adsorbents for removing arsenic from water was investigated, and this iron-based adsorbent exhibited great capacity, reaching a maximum adsorption (mg g⁻¹) of 46.06 for arsenite, and 16.56 for arsenate (Feng et al., 2012). Because they are abundant and have low cost, agricultural waste products have been explored as sustainable adsorbents, exhibiting varying degrees of arsenic adsorption capacity (E. L. Ungureanu et al., 2023). Titanium-modified ultrasonic biochar effectively removed cadmium and arsenic from water, achieving maximum adsorption capacities (mg g⁻¹) of 72.62 for cadmium and 118.06 for arsenic (Luo et al., 2019). While each adsorbent offers unique advantages and challenges, solution chemistry, surface chemistry, and pore structure govern their arsenic removal performance (Mane et al., 2024).

Waste mussel shells effectively removed dyes and heavy metals from water. Nearly all the dye was eliminated, and metals, particularly chromium, and cadmium, were reduced to very low levels ($< 1 \text{ mg L}^{-1}$) from an initial value of 50 mg L^{-1} (Baskan & Pala, 2011). In another study, mussel shells were utilized to prepare an adsorbent, removing a maximum of 57.79 mg Pb(II) per gram of adsorbent at equilibrium (Luo et al., 2019). Previous research on adsorption for environmental remediation has also targeted phosphate (Azcarate et al., 2023), triphenylmethane dye-crystal violet (Dandil et al., 2019), and pyrethroids (Ma et al., 2023).

This study investigates the potential of calcined mussel shells (CMS) to adsorb As(III) and As(V) from water. The adsorbent's structural and surface properties are then characterized using several techniques. The study used RSM-CCD optimization and conducted isotherm, kinetic, and thermodynamic studies to explain the removal mechanism.

No prior research has explored, to our knowledge, the performance of iron oxide modified calcined mussel shells in adsorbing arsenic from water. While numerous studies have investigated various adsorbents and conditions for heavy metal removal, several distinct advantages and contributions are offered by this work. First, the innovative use of mussel shells to adsorb arsenic from water addresses a critical environmental and public health challenge. This research introduces a unique approach by repurposing mussel shells, a readily available by-product of the aquaculture industry, which not only mitigates waste management issues but also provides an eco-friendly, cost-effective solution for arsenic remediation. A relevant example can be found in Newfoundland and Labrador (NL), where the fishing sector is a cornerstone of the local economy. In 2022, the aquaculture production volume in NL reached approximately 12,978 tonnes, with a market value of \$127 million. Within this, the shellfish

aquaculture sector, predominantly involving blue mussels and American oysters, accounted for 4,746 tonnes and a market value of \$23 million (Resources), 2022). Blue mussels, in particular, are a significant contributor to shellfish production. However, the fish processing industry generates a substantial quantity of by-products, ranging from 25% to 70%, representing a significant waste management challenge (Caruso et al., 2020). For every tonne of fish consumed, an equivalent amount of waste is produced, often discarded through ocean dumping or land disposal (Ahuja et al., 2020). Repurposing mussel shells as an adsorbent not only addresses this waste issue but also offers a sustainable solution for environmental concerns, such as arsenic contamination. This dual benefit of waste utilization and water decontamination underlines the applicability and necessity of the research, offering a scalable and regionally tailored solution to a significant global problem. In addition, iron oxide (IO) was incorporated into the mussel shells to enhance their adsorption capacity and surface properties. This modification significantly increased the surface area, leading to improved arsenic removal efficiency. A systematic optimization approach using RSM and CCD was employed to identify the optimal conditions for arsenic removal. This statistical approach allowed for a precise understanding of the interactions between various parameters (pH, adsorbent dosage, initial concentration, and contact time) and their impact on adsorption performance. Furthermore, the kinetics and isotherms of the experiments were extensively explored, providing valuable insights into the underlying mechanisms of arsenic adsorption. These innovations make the work a significant contribution to the development of sustainable and efficient adsorbents for arsenic removal.

3.2. Materials and Methods

3.2.1. Preparation of the adsorbent

The iron (II, III) oxide Nanopowder (97% trace metal basis, particle size 50-100 nm) was procured from Sigma-Aldrich, U.S.A. Sodium hydrogen arsenate (AsHNa_2O_4) and sodium arsenite (NaAsO_2) were obtained from A&C American Chemicals Ltd., Quebec, Canada, and Sigma-Aldrich, U.S.A, respectively. Praxair Canada Inc. supplied high-purity nitrogen gas (99.99%). Mussels were sourced locally in St. John's, N.L. As(V) stock solution (1000 mg L^{-1}) and As(III) solution (1000 mg L^{-1}) were prepared by dissolving $\text{HAsNa}_2\text{O}_4 \cdot 7\text{H}_2\text{O}$ and NaAsO_2 in deionized water, respectively.

Figure 3-2 illustrates the preparation method of the CMS. Once the shells were collected, they were cleaned and all organic matter, including any remaining mussel flesh, was removed. The collected mussel shells underwent a multi-step process to remove impurities and ensure a clean, pure material. Following the manual removal of any large stones or debris, the mussels were subjected to a 6-hour immersion in a 20% bleach solution. After being removed from the solution, the shells were washed and dried for an hour at 80°C in the oven. The cleaned mussel shells were crushed with a mortar and pestle and then further refined in a coffee grinder (Hamilton Beach, model#: 80396C, 150 W). After being ground, the powder was sieved through a mesh with a mesh size of $106 \mu\text{m}$. All particles that passed through were collected and labeled CMS. To eliminate carbon dioxide and volatile impurities, the sieved shells were calcinated at 700°C for 2 h under air and nitrogen gas. 200 mL of deionized water were used to mix the 3 g of calcined mussel shell powder and the 30 mg of iron oxide nanoparticles. The mixture was then stirred for 10 hours at 300 rpm at room temperature. Subsequently, the particles were separated by centrifugation and subjected to lyophilization (IO-CMS).



Figure 3-2 Preparation of method of calcined mussel shells.

3.2.2. Adsorption experiments

To assess the effectiveness of different mussel shell treatments for arsenic removal, preliminary experiments were conducted comparing natural mussel shells, shells calcined under air, shells calcined under nitrogen, and iron oxide-modified calcined shells. Notably higher arsenic adsorption capacities for both As(III) and As(V) were observed with the IO-CMS compared to the other adsorbent. Based on these results, the iron oxide-modified shells were selected for further optimization studies, as detailed in this section. The impact of pH, adsorbent dose (A_d), initial arsenic concentration (C_i), and contact time (t_c), was examined. The low and high levels of these variables are given in Table 3-1. 0.1 M HCl and/or 0.1 M NaOH were added to the solutions to adjust their pH prior to the sorption process. After adsorption tests, the adsorbent was separated by a paper filter (pore size 45 μm , diameter 47 mm), and ICP-MS determined the arsenic (As) concentration. A CCD design with four factors which is a frequently used design in RSM, was applied to identify the ideal conditions for the arsenic removal

process with a minimum number of experimental trials. This design evaluated the impact of pH (A), C_i (B), A_d (C), and t_c (D).

A mathematical model (Eq. (3-1)) is developed to represent the correlation between these process parameters and the adsorption efficiency (response). The model considers the individual effects of each factor (linear terms, denoted by β_i), their combined effects (interaction terms, denoted by β_{ij}), and the squared effects (denoted by β_{ii}) (Neisan et al., 2023):

$$R = \beta_0 + \sum_{i=1}^4 \beta_i x_i + \sum_{i=1}^3 \sum_{j=i+1}^4 \beta_{ij} x_i x_j + \sum_{i=1}^4 \beta_{ii} x_i^2 + \varepsilon \quad (3-1)$$

where R represents the response (removal efficiency (%)), and β_0 and ε denote the offset, and residual term, respectively. Design Expert software (version 12.0.8.0, Stat-Ease Inc., Minneapolis, MN, U.S.A.) was employed to design 30 experiments (Table 3-2) for this study.

Table 3-1 Experimental factors for optimization of arsenic adsorption using IO-CMS.

Parameter	Unit	$-\alpha$	-1	+1	$+\alpha$
A-pH		2	3.5	6.5	8
B-Initial concentration (C_i)	mg L ⁻¹	10	22.5	47.5	60
C-Adsorbent dose (A_d)	g L ⁻¹	1	2	4	5
D-Contact time (t_c)	h	1	2	4	5

Eqs. (3-2) and (3-3) calculated the removal efficiency and adsorbent capacity.

$$\text{Removal efficiency (\%)} = \left(\frac{C_0 - C_t}{C_0} \right) \times 100 \quad (3-2)$$

$$\text{Adsorbent capacity: } q_t = (C_0 - C_t) \times V/m \quad (3-3)$$

where V represents the solution volume (L), m is the adsorbent mass (g), and C_0 and C_t are the concentrations of the arsenic ions in the initial and final solutions, respectively (Neisan et al., 2023).

Table 3-2 Four-factor CCD design for arsenic removal by IO-calcined mussels shell.

run #	pH	C _i (mg L ⁻¹)	A _d (g L ⁻¹)	t _c (h)
1	5	35	1	3
2	6.5	22.5	4	4
3	5	35	3	3
4	5	10	3	3
5	6.5	47.5	4	4
6	5	35	3	3
7	3.5	22.5	4	4
8	6.5	22.5	4	2
9	3.5	22.5	2	4
10	3.5	47.5	2	4
11	6.5	47.5	2	4
12	3.5	22.5	2	2
13	5	35	3	3
14	6.5	22.5	2	2
15	3.5	47.5	2	2
16	8	35	3	3
17	5	35	3	3
18	5	60	3	3
19	3.5	47.5	4	2
20	5	35	3	1
21	2	35	3	3
22	5	35	3	3
23	3.5	22.5	4	2
24	6.5	47.5	2	2
25	6.5	22.5	2	4
26	5	35	3	5
27	5	35	5	3
28	5	35	3	3
29	6.5	47.5	4	2
30	3.5	47.5	4	4

To assess the regeneration potential of the adsorbent, adsorption experiments were repeated for five cycles under the optimal conditions determined by the RSM and CCD optimization. For desorption, a 0.1 M NaOH solution was used, with a stirring speed of 250 rpm for 2 h to remove the adsorbed arsenic from the adsorbent. After each desorption cycle, the arsenic removal efficiency was calculated and compared to the initial removal efficiency. This process allowed for the evaluation of the adsorbent's reusability and its capacity to maintain high removal efficiency over multiple cycles.

3.2.3. Analytical methods

Characterization studies were conducted to explore the physical and chemical characteristics of materials, aiming to gain insights into the effectiveness of the procedure employed in producing adsorbent and the mechanisms of adsorption. The surface structure and composition of adsorbent were analyzed by the use of a Scanning Electron Microscope (SEM) (JSM-7100F, JEOL Ltd, Japan). Additionally, functional groups on the adsorbent surface were identified using a Bruker Tensor 27 FTIR operated in the ZnSe ATR mode within the range of 4000–450 cm^{-1} , with a spectral resolution of 4 cm^{-1} and 32 scans. A surface area analyzer was used to quantify the specific surface area and pore volume of nitrogen adsorption-desorption at 77 K. Material elements and structural composition were analyzed using X-ray diffraction (XRD) with a Copper source (Ultima-IV, 40 kV/44 mA, Rigaku, Japan). X-ray photoelectron spectroscopy (XPS; VG Microtech MultiLab ESCA 2000, UK; Monochrome Al $K\alpha$, $h\nu = 1486.6 \text{ eV}$) was employed to analyze the surface elemental compositions of the IO-CMS before and after As adsorption.

3.2.4. Mechanism studies

In addition to XPS analysis, other tests were conducted to identify the mechanisms of arsenic adsorption onto calcined mussel shells. The role of electrostatic interactions in arsenic adsorption was assessed by measuring the zeta potential of the calcined mussel shell powder at different pH values using a Zetasizer Nano instrument (Malvern Instruments, Malvern, UK). The pH of the suspension was varied across a broad range (3 to 11), and the surface charge at each pH value was measured. These measurements provided insights into the surface charge behavior of the mussel shells and helped determine the pH at which the net surface charge becomes zero (point of zero charge, pH_{pzc}). Moreover, Adsorption experiments were conducted by varying the solution pH

while maintaining optimal adsorbent doses of 3.4 g L⁻¹ for As(III) and 2.7 g L⁻¹ for As(V) and initial concentrations of 57.9 mg L⁻¹ and 59.9 mg L⁻¹, respectively. Insights from zeta potential measurements and these results were used to identify the effect of electrostatic interactions on the adsorption process. All experiments were carried out at room temperature.

To investigate the effect of ionic strength on arsenic adsorption, a series of experiments were designed to vary the ionic strength of the solution. The experimental setup involved preparing arsenic solutions with varying ionic strengths (0, 0.001, 0.01, 0.1, and 1 M), using sodium chloride (NaCl) as the electrolyte. Different concentrations of NaCl were added to the arsenic solutions to create solutions with increasing ionic strengths. The adsorption process was allowed to proceed for a predetermined duration, after which the adsorbent material was separated via filtration. Arsenic concentrations in the filtrates were analyzed using ICP-MS.

3.2.5. Kinetic experiments

Arsenic concentration was monitored between 5-180 min after treatment to assess the arsenic adsorption/removal mechanism. Pseudo-first (PFO), pseudo-second-order (PSO), intra-particle diffusion and Elovich kinetic models were fitted to the data. According to the pseudo-first-order (PFO) model (Eq. (3-4)), the adsorption process follows a first-order kinetic mechanism. Conversely, the PSO model (Eq. (3-5)) proposes that during the chemisorption phase of the adsorption process, the adsorbate and the adsorbent surface interact.

$$\log(q_e - q_t) = \log q_e - \left(\frac{K_1}{2.303} \right) t \quad (3-4)$$

where q_e represents the adsorption capacity (mg g⁻¹) at equilibrium, and k_1 is the adsorption rate constant (g (mg·min)⁻¹).

$$t/q_t = 1/q_e^2 k_2 + t/q_e \quad (3-5)$$

Eq. (3-5) incorporates the following parameters: k_2 , the reaction rate constant ($\text{g} \cdot \text{mg}^{-1} \cdot \text{min}^{-1}$); q_e , the equilibrium adsorption capacity representing the mass of solute adsorbed per gram of adsorbent (mg g^{-1}); and q_t , the mass of solute adsorbed at a specific time t (mg g^{-1}). The determination of k_2 and q_e involves generating a linear plot of t/q_t versus t (J. Wang & Guo, 2023). This plot allows for calculating k_2 using the slope and intercept according to the equation $k_2 = (\text{slope})^2/\text{intercept}$. The equilibrium adsorption capacity, q_e , is then obtained by inverting the slope ($q_e = 1/\text{slope}$).

The intra-particle diffusion model (Eq. (3-6)) helps determine if adsorption is primarily controlled by diffusion within the pores of the adsorbent.

$$q_t = k_{id} t^{1/2} + C \quad (3-6)$$

where q_t is the amount of adsorbate at time t , k_{id} is the intra-particle diffusion rate constant, and C is the intercept, indicating the boundary layer thickness (J. Wang & Guo, 2023).

The Elovich model (Eq. (3-7)), commonly used for chemisorption on heterogeneous surfaces, was also applied to further analyze adsorption kinetics:

$$q_t = \frac{1}{\beta} \ln(\alpha\beta) + \frac{1}{\beta} \ln(t) \quad (3-7)$$

where q_t is the adsorbed amount at time t , α is the initial adsorption rate, and β is related to surface coverage and activation energy (J. Wang & Guo, 2023).

3.2.6. Isotherm studies

The arsenic adsorption on the developed adsorbent in synthetic water samples was examined using samples containing varying concentrations of arsenic (10-60 mg L^{-1})

and 3.4 g L⁻¹ adsorbent for As(III), and 2.7 g L⁻¹ for As(V). A 50 mL from each sample was agitated for 24 hours at 200 rpm to achieve equilibrium, then filtered (0.45 µm membrane) prior to characterization. Four isotherm models, such as Freundlich, Langmuir, Temkin and Dubinin-Radushkevich (D-R) were fitted to the data. The Langmuir model is represented by Eq. (3-8).

$$\frac{C_e}{q_e} = \frac{1}{bq_{max}} + \frac{C_e}{q_{max}} \quad (3-8)$$

where C_e represents the adsorbate equilibrium concentration (mg L⁻¹), q_e is the mass of adsorbate adsorbed at equilibrium (mg g⁻¹), q_{max} is the maximum adsorption capacity (mg g⁻¹), and b is the Langmuir constant (J. Wang & Guo, 2023).

The Freundlich model is described by Eq. (3-9).

$$\ln q_e = \ln K_f + \frac{1}{n} \ln C_e \quad (3-9)$$

where K_f is the Freundlich constant representing adsorption capacity, and n represents the Freundlich exponent, which is associated with adsorption intensity (J. Wang & Guo, 2023).

The Temkin isotherm model is represented by Eq. (3-10) (J. Wang & Guo, 2023).

$$q_e = B \ln (k_t C_e) \quad (3-10)$$

where q_e is the adsorbate amount at equilibrium, C_e is the adsorbate concentration at equilibrium, k_t is the Temkin isotherm constant related to maximum binding energy, and B is associated with the adsorption heat (Adebayo et al., 2015).

The Dubinin-Radushkevich (D-R) isotherm does not assume a uniform distribution of adsorption energies and is described by Eq. (3-11) (J. Wang & Guo, 2023).

$$q_e = q_m e^{-\beta \epsilon^2} \quad (3-11)$$

where q_e is the adsorbed amount at equilibrium, q_m is the theoretical saturation capacity, β is a constant related to adsorption energy, and ϵ is the Polanyi potential, calculated as (Eq. (3-12)):

$$\epsilon = RT \ln \left(1 + \frac{1}{C_e} \right) \quad (3-12)$$

where R is the gas constant, T is absolute temperature, and C_e is the equilibrium concentration. In the D-R model, E represents the mean free energy of adsorption per adsorbate mole, indicating the energy required to move one mole of adsorbate from solution to the adsorbent's surface. E is calculated using the D-R constant β with Eq. (3-13) (J. Wang & Guo, 2023):

$$E = \frac{1}{\sqrt{2\beta}} \quad (3-13)$$

Generally, a low activation energy (E)—typically less than 8 kJ mol⁻¹—indicates physical adsorption, while higher values suggest chemical adsorption (J. Wang & Guo, 2023).

3.2.7. Thermodynamic studies

Thermodynamic tests at 25, 35, and 50 °C were used to examine the effect of temperature on arsenic adsorption by the IO-CMS adsorbent while maintaining other parameters at optimal levels. These studies aimed to understand the thermodynamic parameters associated with the adsorption process and obtain insights into the nature of the adsorption mechanism.

The thermodynamic characteristics ΔS° , ΔH° , and ΔG° can be determined using Eqs. (3-14) and (3-15), which give the relationship between these parameters (Sahmoune, 2019):

$$\Delta G^\circ = \Delta H^\circ - T\Delta S^\circ \quad (3-14)$$

$$\ln K_c = \frac{\Delta S^\circ}{R} - \frac{\Delta H^\circ}{RT} \quad (3-15)$$

where R is the ideal gas constant ($8.314 \text{ J K}^{-1} \text{ mol}^{-1}$), and T represents the temperature in Kelvin (K). The equilibrium constant (K_c) is expressed by the equation $K_c = q_e/C_e$. By plotting $\ln(K_c)$ vs $1/T$, a linear relationship was obtained, allowing the calculation of ΔH° and ΔS° using the slope and intercept of the line, respectively (Sahmoune, 2019).

3.3. Results and Discussion

3.3.1. Adsorbent characterization

3.3.1.1. X-ray diffraction crystallography (XRD)

Figure 3-3a presents the X-ray diffraction (XRD) pattern of natural (un-calcined) and calcined mussel shells. The dominant peaks in the natural shells are calcium carbonate (CaCO_3) in calcite form at 29.5° (JCPDS No. 05-0586) (Cardell et al., 2017; Derkani et al., n.d.) and also aragonite (another calcium carbonate form), identified by peaks at 26.3° and 45.9° (JCPDS No. 41-1475) (Mass et al., 2012; Ogundiran et al., 2022). Calcination at 700°C results in its transformation into calcium oxide (CaO) through the release of carbon dioxide (CO_2). This transformation is evident in the XRD patterns. New peaks emerge around 2θ values of 32.3° , 37.4° , 54.1° , 63.9° , and 67.7° are characteristic of the cubic phase of CaO (JCPDS No. 37-1497) (Hossain et al., 2023; Onyeaka & Hart, 2021; Santoso et al., 2019). Calcined shells still exhibit CaCO_3 peaks since complete conversion occurs above 800°C . A small amount of calcium hydroxide (Ca(OH)_2) might also be present in the calcined product. This could be due to the hydration reaction of CaO upon exposure to moisture in the air (Seo et al., 2019). The diffraction peaks in the XRD spectra, such as 17.9° , 34.0° , and 47.0° (JCPDS No. 04-0733), imply the presence of Ca(OH)_2 (Faria et al., 2020; Z. Liang et al., 2018).

3.3.1.2. Scanning electron microscopy (SEM)

The Scanning electron microscopic images of natural mussel shells, calcined mussel shells, and IO-CMS are visualized in Figure 3-3b, c, and d. The SEM images clearly show a dramatic shift in the mussel shell structure due to calcination. Before calcination, the natural shell exhibits a compact and uniform layered structure with small particles likely from the crushing process. In contrast, calcination creates a non-uniform, porous structure of small, separated CaO particles. This change is attributed to the elimination of CO₂ during calcination, and is consistent with findings in the literature (Hossain et al., 2023; Tekin, 2015). After modification with IO nanoparticles, the calcined shells retain their porous structure. This well-preserved porosity and a good surface area make the IO-CMS suitable for adsorption processes.

3.3.1.3. Fourier-transform infrared spectroscopy (FTIR)

Figure 3-3e, and f present FTIR spectra (400-4000 cm⁻¹) of calcined mussel shells before and after modification with Iron oxide (IO) nanoparticles. The peak observed at 3639.5 cm⁻¹ (before modification) and 3641.5 cm⁻¹ (after modification) are indicative of the stretching vibration of a hydroxyl (Benni et al., 2021). These sharp peaks indicate the presence of water molecules weakly bound (physisorbed) to the surface of the CaO. This observation aligns with the presence of Ca(OH)₂ detected in the XRD analysis (Linggawati, 2016). The FTIR analysis reveals the presence of carbonate groups in the sample. This is evident from the characteristic vibrational peaks (O-C-O out-of-plane bending (v₂)) observed at 871.8 cm⁻¹ and 872.7 cm⁻¹ and also (in-plane bending (v₄)) at 711.7 cm⁻¹ and 712.1 cm⁻¹ (Huh et al., 2016). The IR vibrational bands observed around 1411.8 and 1410.3 cm⁻¹ are attributed to the characteristic stretching mode of the C=O bonds in the carbonate group (Kim et al., 2005). The increased intensity of the peaks observed at 1410.3 indicates a higher carbonate surface concentration or

improved crystallinity of the calcium carbonate phase following iron oxide coating. Additionally, the interaction between iron oxide nanoparticles and the calcite structure may influence the surface chemistry, leading to stronger carbonate-related vibrations. These peaks correspond to stretching vibrations in the Fe-OH (Salim et al., 2021; Ventruti et al., 2016).

3.3.1.4. Brunauer-Emmett-Teller (BET) surface area analysis

The BET surface area of the mussel shell samples was evaluated before calcination, after calcination, and following modification with nanoparticles, using N₂ adsorption/desorption isotherms. The isotherm and BJH cumulative pore volume (determined using the BJH method) are presented in Figure 3-4. As per IUPAC classification, porous materials are categorized based on pore diameter size: microporous (< 2 nm), mesoporous (2–50 nm), and macroporous (> 50 nm) (Mohadi et al., 2016).

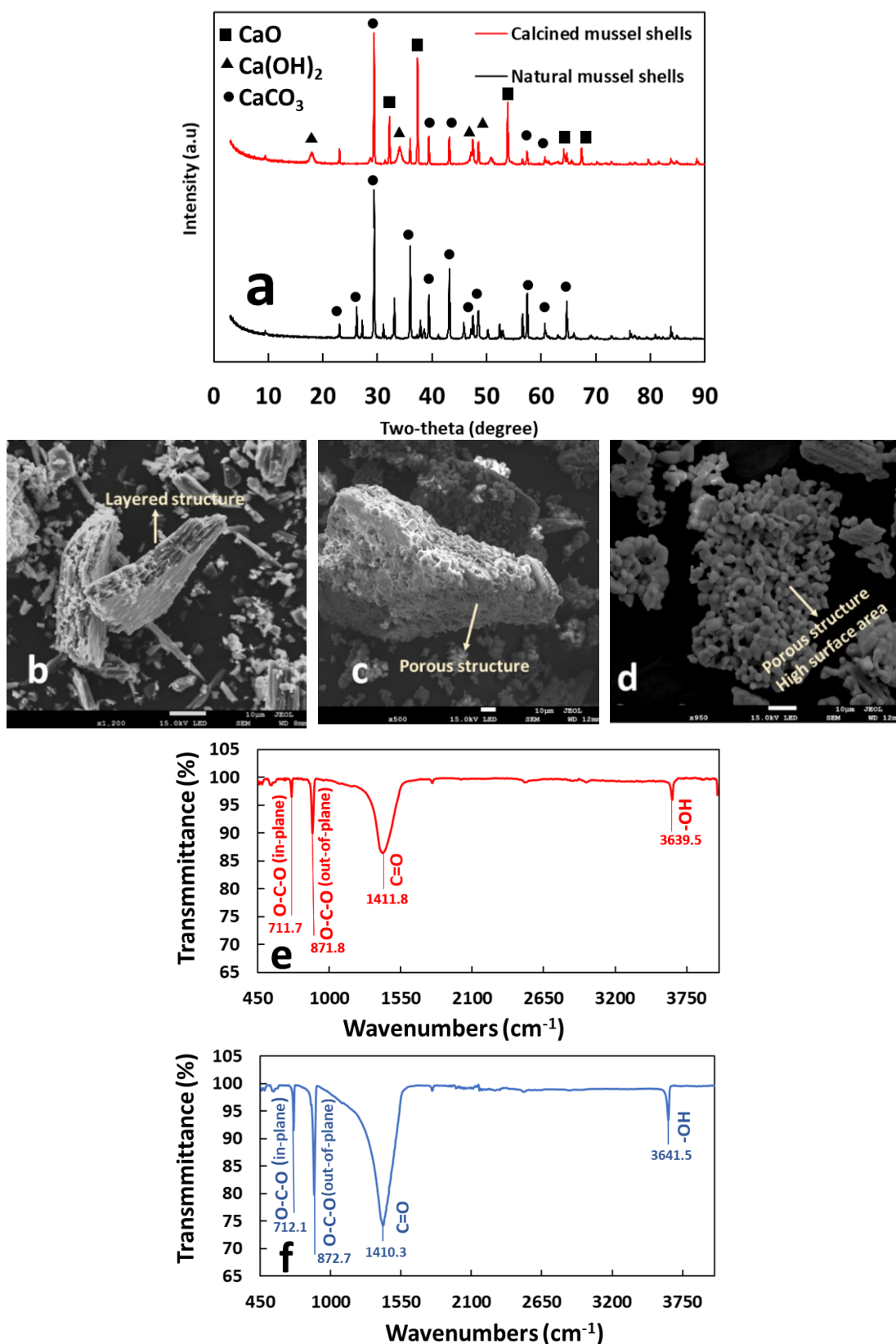


Figure 3-3 Characterization of adsorbent: (a) XRD patterns for natural (uncalcined) and calcined mussel shells; SEM images of the (b) natural mussel shells, (c) calcined mussel shells, and (d) IO-CMS; FTIR spectra of (e) calcined mussel shells, and (f) IO-CMS.

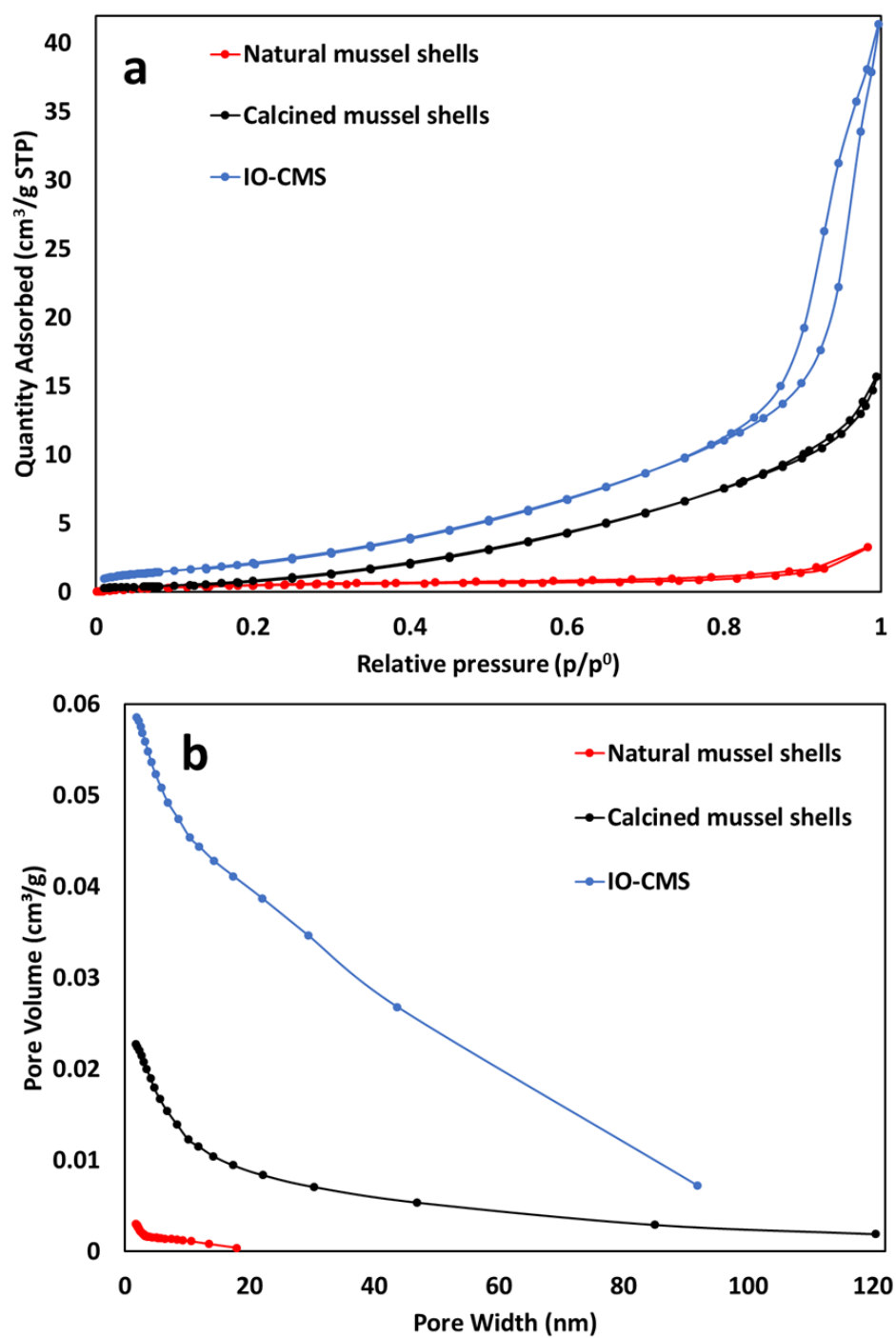


Figure 3-4 (a) BET adsorption-desorption isotherm, and (b) BJH pore size distribution and cumulative pore volume characterization of natural (uncalcined), calcined mussel shells, and IO-CMS.

Figure 3-4, in the raw sample, only micropores are observed, whereas in the calcined and modified samples, mesopores and macropores are also present. This change can be attributed to the calcination process, when the organic components and impurities in the mussel shells are removed, leading to the formation of a more porous structure. Calcination dramatically increases the mussel shells surface area and pore volume. Compared to natural shells, calcined mussel shells exhibit a 152.9% increase in BET surface area (from 2.0125 to 5.0897 m² g⁻¹) and a significant increase in pore volume (from 0.00012 to 0.02278 cm³ g⁻¹). This significant increase can be the result of the release of CO₂ during calcination, which creates pores within the material. In comparison to calcined mussel shells, modification with IO nanoparticles (IO-CMS) further enhances surface area and pore volume. IO-CMS boasts a 78.62% increase in surface area (from 5.0897 to 9.0987 m² g⁻¹) and a 157.52% increase in pore volume (from 0.02278 to 0.05858 cm³ g⁻¹) compared to calcined shells. This additional improvement suggests that the IO nanoparticles create new pores or enlarge existing ones within the CMS structure.

Additionally, Table 3-3 indicates that pore size increased after modification and calcination. The average pore size of calcined mussel shells is 84.84% larger than that of natural shells (from 4.0253 to 7.4403 nm). As compared to calcined shells, IO-CMS exhibits an increase in pore size, rising 74.24% (from 7.4403 to 12.9672 nm). This trend suggests that both calcination and modification processes create not only more pores but also larger pores within the mussel shell structure.

Table 3-3 Results of the BET analysis of mussel shells.

Sample Parameter	Natural mussel shells	Calcined mussel shells	IO-CMS
BET surface area (m ² g ⁻¹)	2.0125	5.0897	9.0987
Pore volume (cm ³ g ⁻¹)	0.00012	0.02278	0.05858
Pore size (nm)	4.0253	7.4403	12.9672

3.3.1.5. *X-ray photoelectron spectroscopy (XPS)*

The elemental composition and chemical oxidation states of the surface and near-surface species were analyzed using XPS. Survey scans (Figure 3-5) revealed that the primary components of the adsorbent were C, O, and Ca. It is possible that trace amounts of other elements are also present, though their concentrations are likely near the detection limit of XPS (approximately 0.01%). In the As-loaded samples, new peaks were observed, indicating the presence of arsenic. All peaks and their corresponding binding energies (BE) are listed in Table 3-4.

As shown in Figure 3-6 and Figure 3-7, the X-ray photoelectron spectra of IO-CMS were compared before and after arsenic adsorption, providing insights into the surface elemental composition and bonding configuration of the material.

High-resolution O 1s scans for IO-CMS before and after (As(III) and As(V)) adsorption are shown in Figure 3-6(a-c). The chemical adsorption between the adsorbent and adsorbate caused a shift in the O 1s spectra peak of surface complexes to lower binding energy, decreasing from 531.15 eV to 530.94 eV for As(III) and to 530.97 eV for As(V), indicating the extent and direction of electron transfer. The O1s spectra of the adsorbent, both before and after adsorption, display a peak associated with oxide ion (O^{2-}). After adsorption, shifts in the peak position were observed due to interactions between surface O^{2-} and arsenic (Babaei et al., 2017).

In Figure 3-6(d-f), The C 1s spectrum was decomposed into three peaks corresponding to C-C, C-H- adventitious, C=O, and O-C=O With Binding energies at 285, 288, and 289.99, respectively. After arsenic adsorption, C 1s peak position remained unchanged but the intensities vary, it typically indicates that the carbon species on the material's surface have not undergone any significant chemical changes, such as oxidation or reduction, but the surface concentration of carbon has altered. This

could be due to the presence of adsorbed arsenic on the surface, which might block or expose different amounts of carbon-containing functional groups without affecting the overall bonding of carbon.

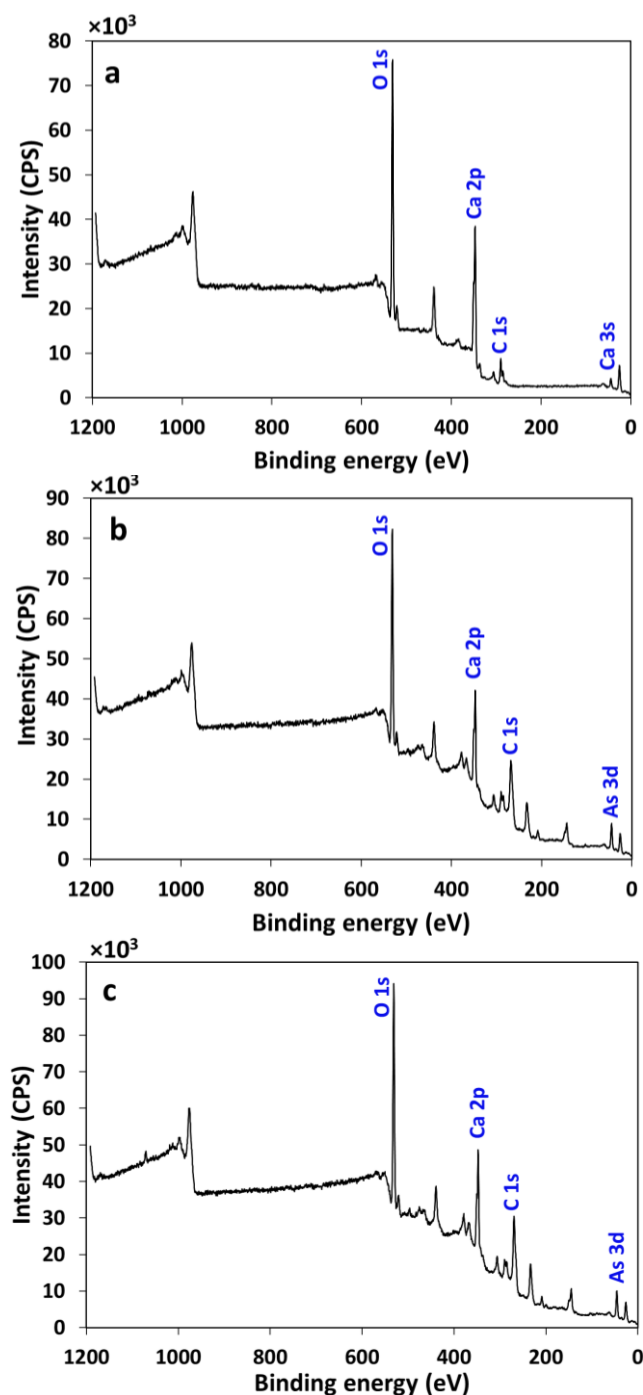


Figure 3-5 XPS survey spectra of the adsorbent surface (a) before adsorption, (b) after adsorption of As(III), and (c) after adsorption of As(V).

Table 3-4 Binding energies and relative content of As, C, Ca and O in adsorbents.

Sample	Valence state	Peak	Binding energy (eV)	Peak area (%)	FWHM
IO-CMS	O 1s	Metal oxide	531.15	100	2.54
	C 1s	C-C, C-H	285.00	39.46	2.38
		Adventitious			
	C 1s	O-C=O	289.99	53.92	1.98
	C 1s	-C=O	288.00	6.62	2.38
	Ca 2p	2p3/2	347.03	66.74	2.44
	Ca 2p	2p1/2	350.06	33.26	2.57
As(III)-loaded IO-CMS	O 1s	Metal oxide	530.94	100	2.69
	C 1s	C-C, C-H	285.00	52.35	2.84
		Adventitious			
	C 1s	O-C=O	289.76	41.78	2.22
	C 1s	-C=O	288.00	5.87	2.84
	Ca 2p	2p3/2	347.15	66.74	2.22
	Ca 2p	2p1/2	350.74	33.26	2.37
	Ca 3s	Ca 3s	44.55	65.74	2.38
	As 3d5/2	As 3d5/2	44.41	20.56	3.50
	As 3d3/2	As 3d3/2	45.10	13.70	2.44
As(V)-loaded IO-CMS	O 1s	Metal oxide	530.97	100	2.61
	C 1s	C-C, C-H	285.00	60.02	3.16
		Adventitious			
	C 1s	O-C=O	289.56	38.56	2.36
	C 1s	-C=O	288.00	1.42	3.16
	Ca 2p	2p3/2	347.19	66.74	2.21
	Ca 2p	2p1/2	350.75	33.26	2.27
	Ca 3s	Ca 3s	44.45	62.56	2.81
	As 3d5/2	As 3d5/2	44.85	22.47	3.11
	As 3d3/2	As 3d3/2	45.54	14.98	2.31

The XPS spectra of Ca 2p (Figure 3-7 (a-c)) display two peak positions at 347.03 eV and 350.60 which could be assigned to 2p3/2 and 2p1/2 for the virgin adsorbent. The binding energies of Ca 2p shifted to higher values after the adsorption of As(V) (BE = 347.19, 350.75) and As(III) (BE=347.15, 350.74), which could be due to the formation of Ca–O–As bonds during the arsenic uptake.

The As 3d spectrum (Figure 3-7d, and Figure 3-7e) of the arsenic-loaded adsorbent can be separated into two distinct component peaks, reflecting the presence of arsenic atoms in different oxidation states. The As 3d5/2 peak for As(III) typically falls within a binding energy range of 44.0 eV to 45.5 eV, while for As(V), it is within 45.2 eV to

46.8 eV. It has also been reported that the binding energies (BEs) for As(V) vary across different species, with $\text{BE}(\text{AsO}_4^{3-})$ at 44.9 eV, $\text{BE}(\text{HAsO}_4^{2-})$ at 45.5 eV, and $\text{BE}(\text{H}_2\text{AsO}_4^-)$ at 46.7 eV, while the BE for As(III) is observed at 44.2 eV (Chowdhury et al., 2011; S. Zhang et al., 2010). In Figure 3-6j, and Figure 3-6k, the peaks at 44.45 eV (3d5/2) and 45.54 eV (3d3/2) after As(V) adsorption, as well as the peaks at 44.41 eV (3d5/2) and 45.10 eV (3d3/2) after As(III) adsorption, suggest the presence of arsenic on the adsorbent surface. This result suggests a possible solid-state redox interaction between arsenate and arsenite on the sorbent surface. As As(III)-O bonded compound is observed at ~44.5 eV in the XPS spectra, the peak at 45.10 indicates that some As(III) was oxidized to As(V) on the As(III)-loaded sorbent, likely due to oxidation occurring during sample preparation. Additionally, some reduction of As(V) to As(III) appears to have taken place on the surface of the As(V)-loaded sorbent. A reduction of As(V) to As(III) has been reported during the adsorption of arsenate on iron-based materials (S. Zhang et al., 2010).

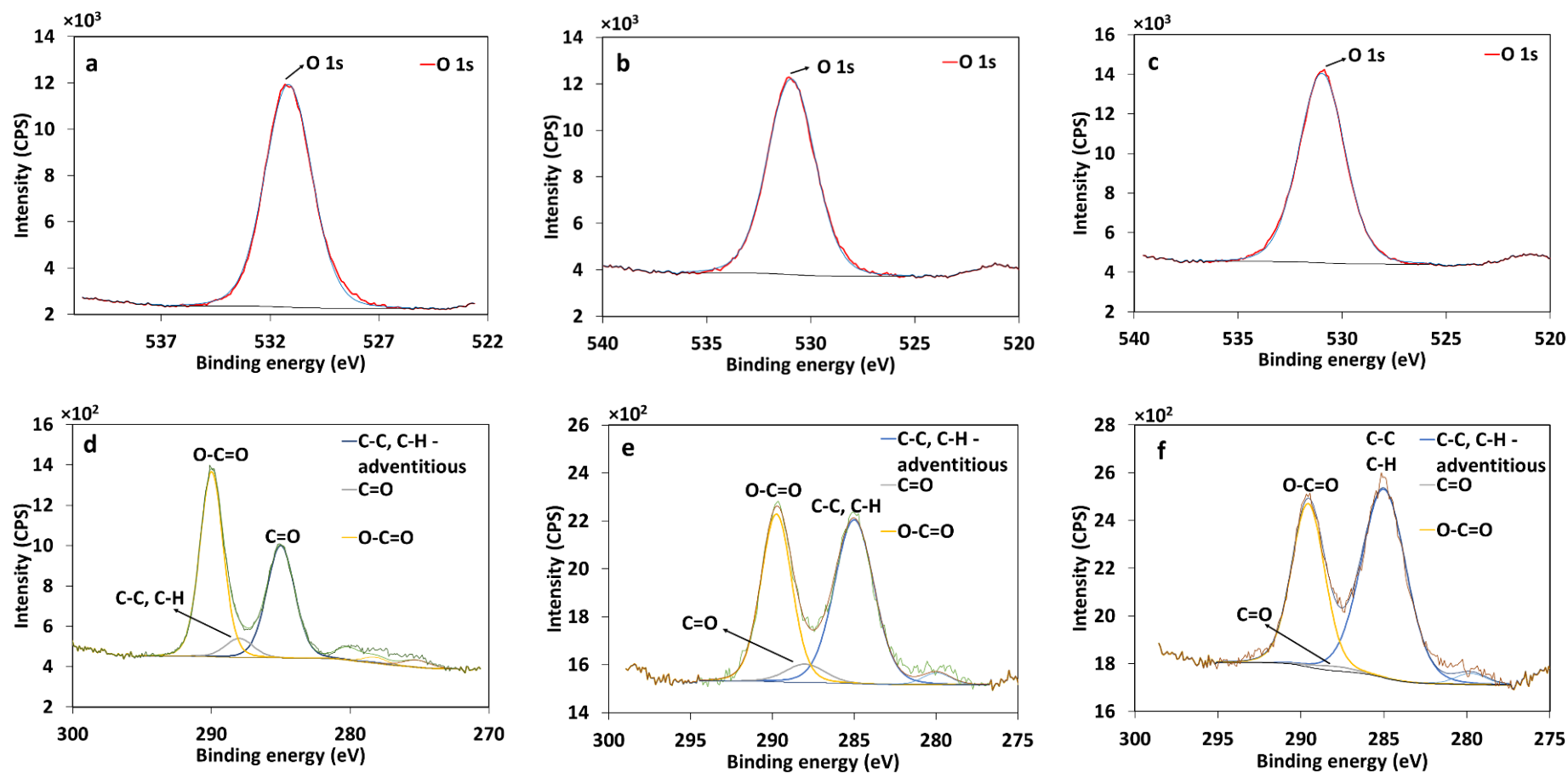


Figure 3-6 XPS spectra of iron oxide-modified calcined mussel shells (IO-CMS) before and after arsenic adsorption: O1s (a) before adsorption, (b) As(III)-loaded, and (c) As(V)-loaded; C1s (d) before adsorption, (e) As(III)-loaded, and (f) As(V)-loaded.

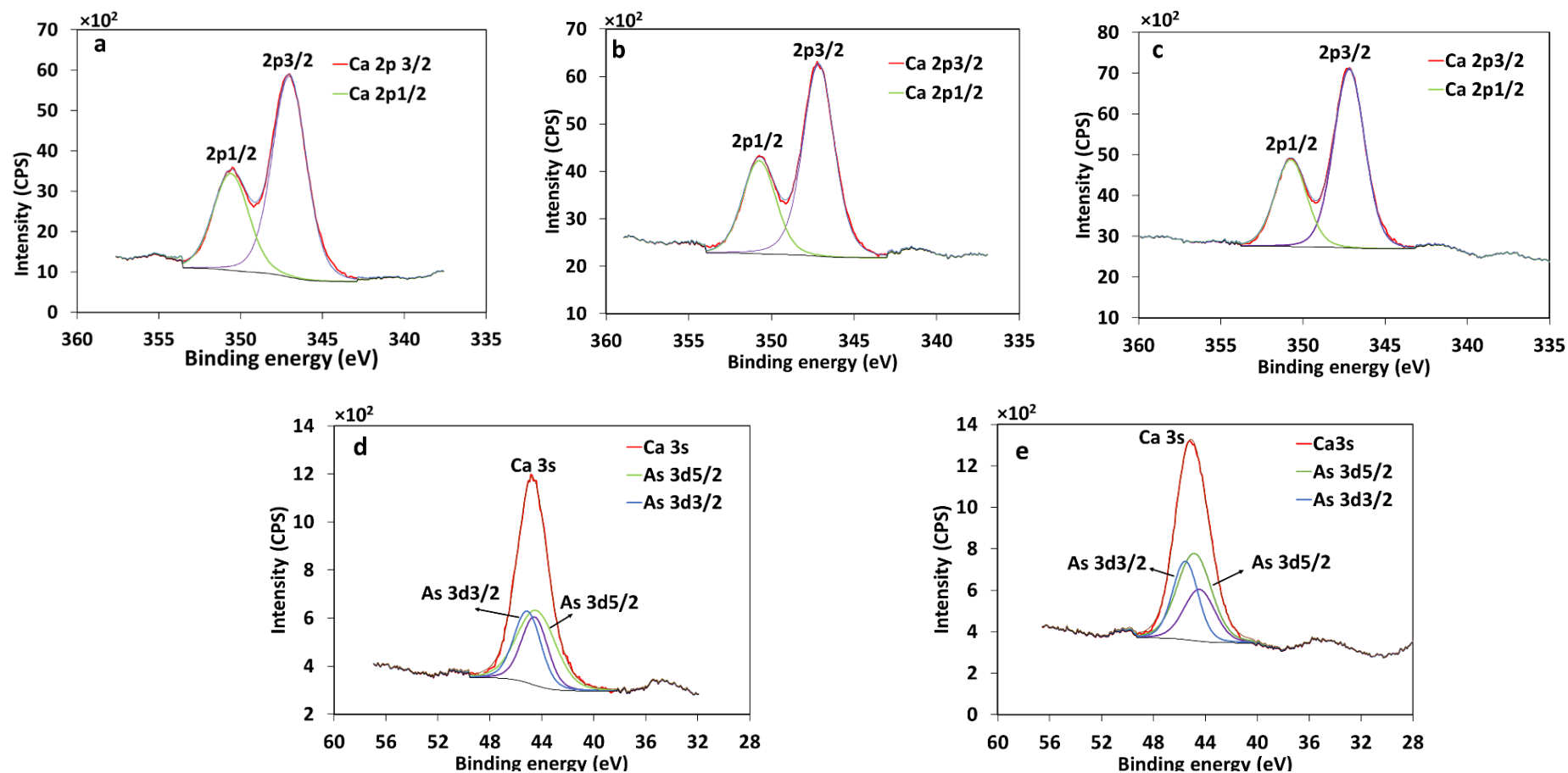


Figure 3-7 XPS spectra of iron oxide-modified calcined mussel shells (IO-CMS) before and after arsenic adsorption: Ca2p (a) before adsorption, (b) As(III)-loaded, and (c) As(V)-loaded; and As3d (d) As(III)-loaded, and (e) As(V)-loaded.

3.3.2. Mechanism of adsorption

The influence of pH on the adsorption of As(III) and As(V) onto the IO-CMS adsorbent was studied across a range of pH values. The results (Figure 3-7) indicate that while pH does affect adsorption efficiency, the overall impact is not highly significant. Zeta potential measurements of the adsorbent across the same pH range revealed values ranging from approximately -20 mV to +20 mV, suggesting that the adsorbent surface is not strongly charged under the tested conditions. However, trends in both pH and zeta potential provide insights into the adsorption mechanisms.

At lower (acidic) pH values, the zeta potential was positive, reaching its maximum positive value near pH 5. This reflects the protonation of surface groups, resulting in a positively charged adsorbent surface. In basic environments, the zeta potential became increasingly negative due to deprotonation, indicating the prevalence of negatively charged surface sites. The adsorption of As(III) and As(V) followed trends similar to the zeta potential curve. For As(III), the highest adsorption occurred at approximately pH 7, which coincides with the pH near the point of zero charge (pHpzc) of the adsorbent. At this pH, the surface of the adsorbent is neutrally charged (Neisan et al., 2023), minimizing electrostatic repulsion and allowing for enhanced interaction with uncharged arsenite species (H_3AsO_3). In the case of As(V), maximum removal occurred at pH 5, where the surface of the adsorbent is positively charged due to protonation. Under these conditions, the dominant form of arsenate is H_2AsO_4^- , and HAsO_4^{2-} , which is negatively charged (Neisan et al., 2023). The positive surface charge at this pH results in strong electrostatic attraction, facilitating the removal of As(V).

Ionic strength plays a key role in heavy metal removal via specific and non-specific adsorption. In specific adsorption, the removal of heavy metals may remain unchanged or increase with higher ionic strength if the metals form inner-sphere complexes with

surface functional groups. Conversely, non-specific adsorption of Pb(II), As(V), and Cd(II) decreases with increasing ionic strength. This is because higher ionic strength promotes the formation of outer-sphere complexes, which weakens adsorption by affecting the ions' hydration shell and electrostatic interactions with the adsorbent (Egbosiuba et al., 2022). Figure 3-8 illustrates the effect of ionic strength on the adsorption of As(III) and As(V) using IO-CMS at various ionic strengths. The results indicate that ionic strength from 0 to 0.1 M has a minimal and statistically insignificant impact on the adsorption of both As(III) and As(V), suggesting that electrostatic interactions remain largely unaffected within this range. This behavior aligns with the characteristic independence of ionic strength typically observed in inner-sphere complex formation (Tang et al., 2010; F. Wu et al., 2021). Previous studies have shown that the removal of arsenic from water using various materials, such as goethite (Tang et al., 2010), different-sized polystyrene microplastic particles (Dong et al., 2020), and magnetic ordered mesoporous Fe/Ce bimetal oxides (OMICs) (Wen et al., 2020), is minimally affected by ionic strength. However, at an ionic strength of 1 M, a significant decrease in adsorption efficiency was observed for both arsenic species. This substantial drop can be attributed to the increased concentration of competing ions in the solution, which can inhibit the adsorption of heavy metals. Additionally, increased ionic strength affects the potential energy of the heavy metal ions, reducing their migration or diffusion toward the adsorbent surface (Y. Zhang, Wang, Zhang, et al., 2020).

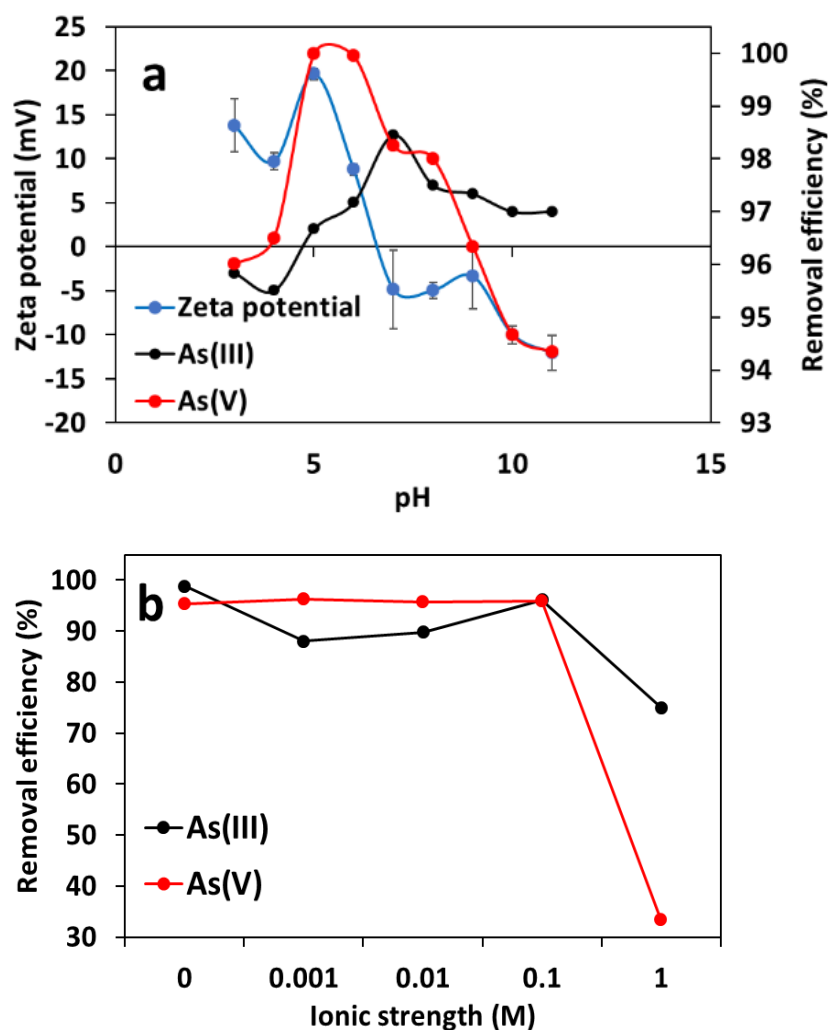
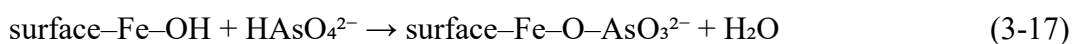
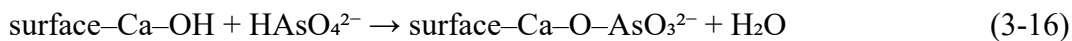


Figure 3-8 (a) Zeta potential and removal efficiency of IO-CMS for As(III) and As(V) as a function of pH. (b) Effect of ionic strength on the removal efficiency of IO-CMS for As(III) and As(V).

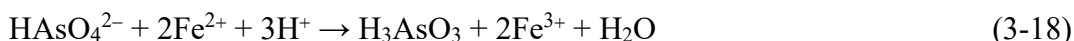
Considering the results from the zeta potential analysis, pH_{Hpzc} determination, ionic strength experiments, and XPS findings, the arsenic adsorption on the sorbent appears to mostly involve surface complexation between arsenic species (both As(III) and As(V)) and functional groups on the adsorbent, such as Ca-O and Fe-O. Additionally, there may be a redox interaction on the surface, with As(V) being reduced to As(III) in the process. The changes in carbon species intensity suggest that the adsorption of arsenic may also involve modifications to surface functional groups, facilitating the binding of arsenic species.

The surface complexation of arsenic species with the adsorbent can be represented by the following reactions (Eqs. (3-16) to (3-20)).

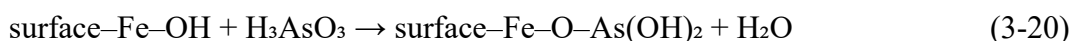
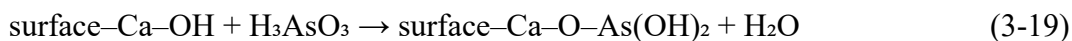
For the interaction of arsenate (As(V)) with calcium or iron oxide sites:



For the reduction of arsenate (As(V)) to arsenite (As(III)):



For the interaction of arsenite (As(III)) with the surface:



In these equations, Ca-O and Fe-O represent surface sites on the adsorbent (calcium or iron oxide), and AsO_4^{3-} and AsO_3^{2-} represent arsenate (As(V)) and arsenite (As(III)) ions, respectively. The electron transfer in the second reaction represents the reduction of As(V) to As(III), which is likely occurring on the adsorbent surface.

In addition to complexation, electrostatic interactions are involved in the adsorption of arsenic onto IO-CMS. However, their role is insignificant, as evidenced by the minimal changes in adsorption efficiency across varying ionic strengths and pH conditions.

3.3.3. Optimization of arsenic removal

Thirty experiments were conducted to investigate the influence of four factors on arsenic removal. Table 3-5 details the statistical analysis (ANOVA) conducted on the chosen quadratic model. The coefficient's statistical significance is assessed by F-values and p-values. Higher F-values and lower p-values suggest a stronger significance

of the corresponding coefficient on the model's outcome. The analysis reveals statistically significant models for As(III) and As(V) adsorption capacity. This signifies a strong correlation between the process parameters and the amount of metal adsorbed. Both the model p-values below 0.05 and the lack of fit p-value exceeding 0.05 indicate that the models accurately describe the experimental data (Al-mahbashi et al., 2023) and effectively capture the key factors influencing arsenic adsorption. The mathematical relationships between the process variables and removal efficiency for As(III) and As(V) are provided by the regression Eqs. (3-21) and (3-22).

Based on the quadratic models, Table 3-5 presents the optimum values for the process parameters. According to the desirability function used in this study, unfavorable process condition According to the desirability function used in this study, unfavorable process conditions are represented by 0, 0.5 for moderately desirable conditions, and 1 to signify the most favorable conditions (Arabkhani et al., 2023); thus, the desirability value of 1.0 is identified as the best circumstance.

$$As(III)removal(\%) = 79.08 - 0.2773A + 13.70B + 17.73C \quad (3-21)$$

$$+ 2.65D - 6.0BC - 2.33A^2 - 3.57B^2 - 8.55C^2$$

$$As(V)removal(\%) = 89.71 - 1.42A + 5.32B + 2.54C \quad (3-22)$$

$$+ 1.74D + 1.73AB - 1.84BC - 1.56B^2 - 4.31C^2$$

In these equations, the coded terms of A, B, C and D are pH, initial concentration (mg L⁻¹), Adsorbent dose (g L⁻¹) and contact time (h), respectively.

Table 3-5 Optimal solutions for highest arsenic adsorption.

Contaminant	pH	C _i (mg L ⁻¹)	A _d (g L ⁻¹)	C _t (h)	Efficiency (%)	Desirability
As(III)	6.4	57.9	3.4	4.4	94.9	1.0
As(V)	5.7	59.9	2.7	4.9	98.5	1.0

C_i = initial concentration; A_d = adsorbent dose; C_t = contact time.

According to Table 3-6, for As(v) removal, all linear terms, including (A-pH, B-Ci, C-Ad, and D-tc) have a significant impact (p-value < 0.05). Squared term for Ci (B^2), interactions between Ci and pH (AB), and interactions between Ci and Ad (BC) are significant. Other interactions are not statistically significant. While for As(III) all linear factors (B-Ci, C-Ad, and D-tc) have a significant impact (p-value < 0.05), except A-pH, which is slightly significant (p-value = 0.7752). Squared terms for pH (A^2), Ci (B^2), and Ad (C^2), as well as the interaction between Ad and Ci (BC), are significant. Other squared terms and interactions are not statistically significant.

Graphical methods are utilized to confirm the accuracy of the CCD model for predicting arsenic adsorption. Figure Figure 3-9c and Figure 3-9d present the plots of standardized residuals versus the order of experiments. Random scattering of data points across the plots, with no specific pattern or unusual clusters, serves as an indicator of the model's suitability (Ghelich et al., 2019). Figure 3-9a and Figure 3-9b depict arsenic adsorption's actual and predicted removal efficiencies. A linear regression analysis of these figures suggests a strong correlation between predicted and experimentally determined values, further supporting the model's validity.

The analysis yields regression coefficients of 0.97 and 0.89 for As(III) and As(V), respectively. A good fit between the model's predictions and the experimental data is shown by these values near 1, indicating that the model meets the established acceptance criteria.

Table 3-6 ANOVA for reduced quadratic modeling of arsenic removal.

As(III)						As(V)				
Source	Sum of Squares	df	Mean Square	F-value	p-value	Sum of Squares	df	Mean Square	F-value	p-value
Model	15043.73	8	1880.47	85.25	< 0.0001	1620.76	8	202.59	21.96	< 0.0001
A- pH	1.85	1	1.85	0.0837	0.7752	48.45	1	48.45	5.25	0.0324
B- Initial concentration	4505.51	1	4505.51	204.25	< 0.0001	679.47	1	679.47	73.66	< 0.0001
C- Adsorbent dose	7540.33	1	7540.33	341.83	< 0.0001	154.53	1	154.53	16.75	0.0005
D- Contact time	168.57	1	168.57	7.64	0.0116	72.45	1	72.45	7.85	0.0107
AB						47.96	1	47.96	5.20	0.0332
BC	575.36	1	575.36	26.08	< 0.0001	54.39	1	54.39	5.90	0.0242
A ²	152.23	1	152.23	6.90	0.0158					
B ²	357.71	1	357.71	16.22	0.0006	69.65	1	69.65	7.55	0.0121
C ²	2045.57	1	2045.57	92.73	< 0.0001	529.58	1	529.58	57.41	< 0.0001
Residual	463.23	21	22.06			193.72	21	9.22		
Lack of Fit	433.65	16	27.10	4.58	0.0505	160.87	16	10.05	1.53	0.3367
Pure Error	29.59	5	5.92			32.85	5	6.57		
Cor Total	15506.96	29				1814.48	29			

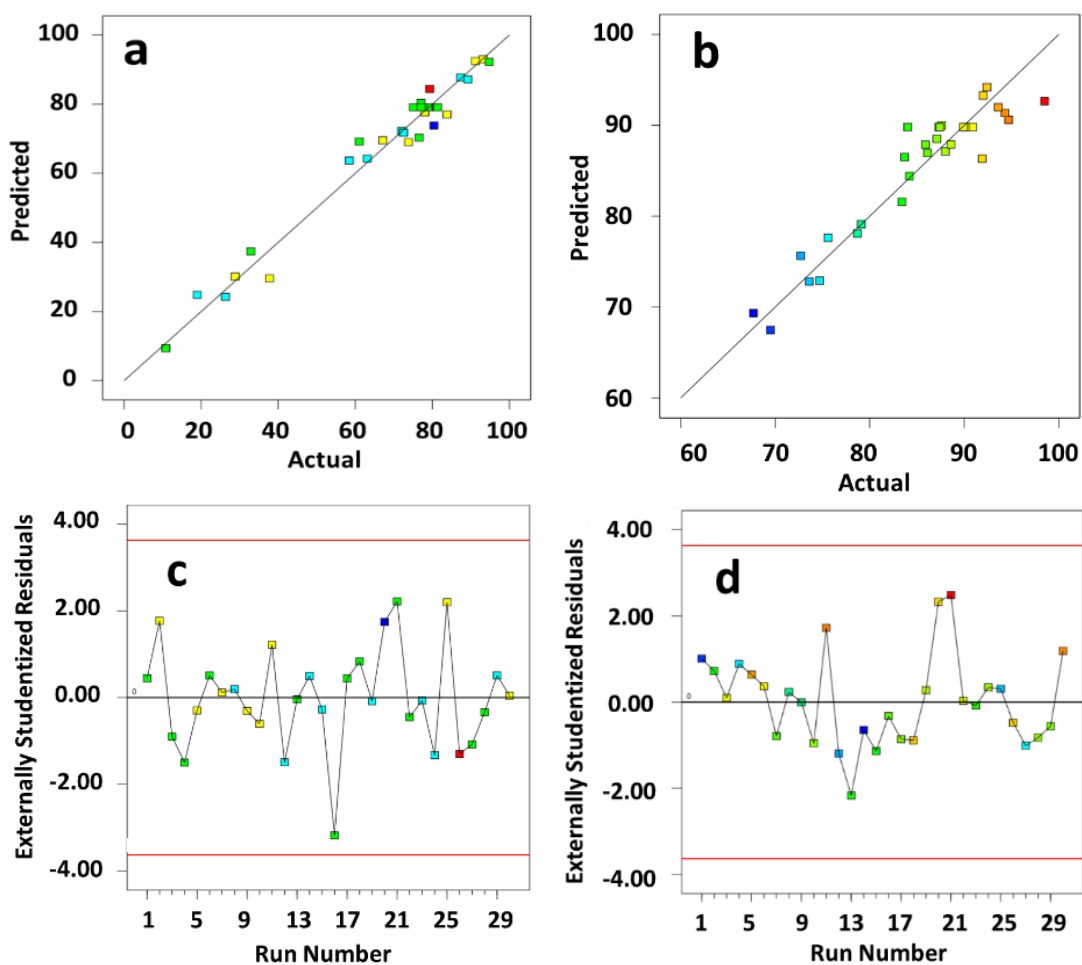


Figure 3-9 Predicted vs. actual experimental values of removal efficiency for (a) As(III), (b) As(V); residuals vs. runs for (c) As(III), and (d) As(V).

3.3.3.1. Effect of pH

The results from removal efficiency modeling using RSM with CCD suggest that pH (Figure 3-10a and Figure 3-10b) has a minimal effect on arsenic adsorption by IO-CMS within the tested range. Similarly, hematite effectively removed 100% arsenate (As(V)) from water across a wide pH range (2 to 11). Other iron-based adsorbents in the study (goethite, magnetite, and zero-valent iron) showed similar strong adsorption (100%) at pH 2 to 8 (Mamindy-Pajany et al., 2011). Similarly, studies on lepidocrocite reported minimal impact on adsorption within a specific pH range (L. Wang & Giammar, 2015). The model in this study predicts the highest adsorption efficiency for As(III) and As(V) at pH of 6.4 and 5.7, respectively. Furthermore, the model's

prediction of higher As(V) removal at slightly acidic conditions (around pH 5.7) is consistent with research on black soil (Fan et al., 2020), where lower pH generally favors As(V) adsorption.

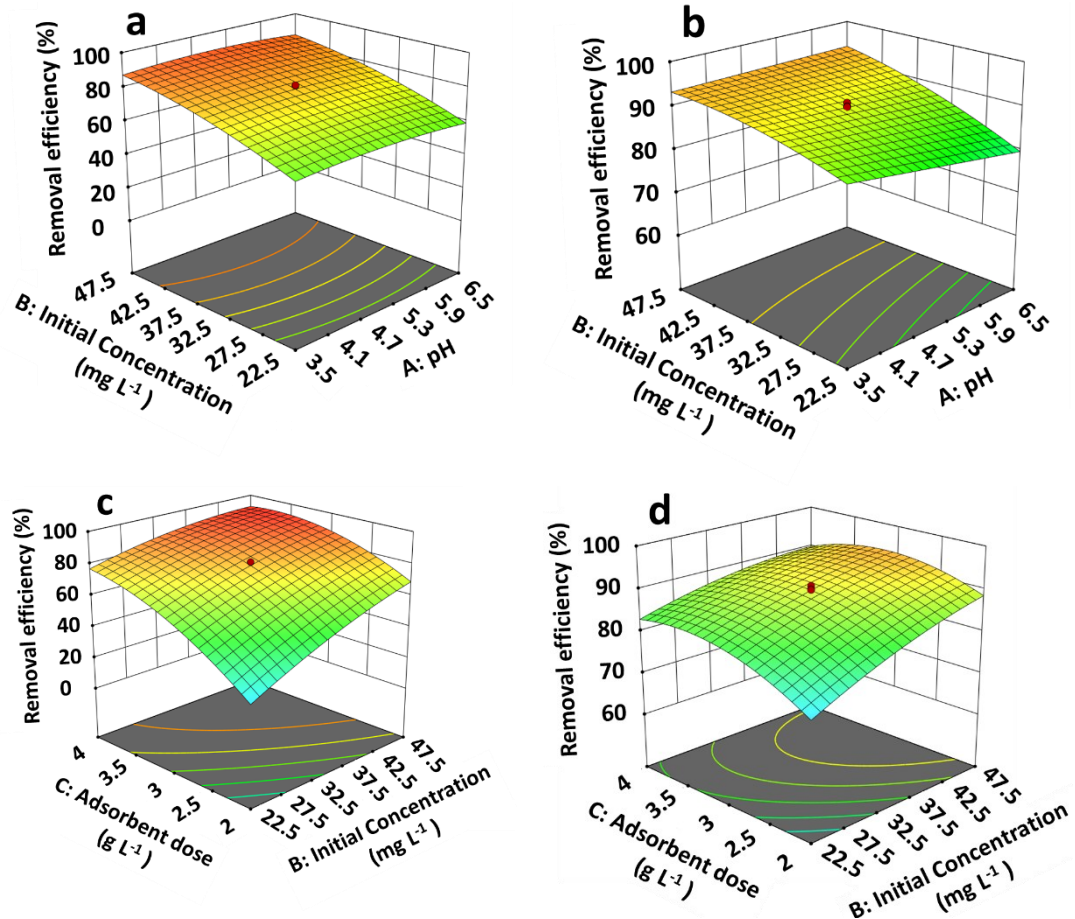


Figure 3-10 Effects of pH-initial concentration on (a) As(III), (b) As(V) removal efficiency; and initial concentrations- adsorbent dose on (c) As(III), and (d) As(V) removal efficiency. (Room temperature, rpm = 200).

3.3.3.2. Effect of adsorbent dose (A_d)

RSM-CCD modeling (Figure 3-10c and Figure 3-10d) also reveals a positive correlation between adsorbent dose and arsenic removal efficiency for both As(III) and As(V). In simpler terms, increasing the amount of IO-CMS used significantly enhances arsenic removal. The greater abundance of active sites on the modified mussel shells is likely the reason for the increased adsorption.

The results of this study conform to previous observations of the efficiency of Fe/Cu nanoparticles in removing As(III) and As(V) from aqueous solutions, which indicated that increasing the nanoparticles concentration up to 0.1 g L^{-1} increased the arsenic removal (Babaei et al., 2018). Also, As(III) and As(V) adsorption by modified montmorillonite showed that increasing the adsorbent dose up to 4 g L^{-1} significantly enhanced As(III) and As(V) removal. Beyond this, there was little benefit, suggesting saturation of adsorption sites (Ren et al., 2014).

3.3.3.3. Effect of initial concentration (C_i)

The RSM-CCD modeling (Figures 3-10a-d) results indicate a direct correlation between the initial concentration of arsenic and its removal efficiency by IO-CMS. In other words, as the starting concentration of arsenic (As(III) and As(V)) increases within the studied range, the removal efficiency also rises. The observed enhancement can be ascribed to the presence of a force that promotes increased interaction between the arsenic ions and the vacant sites on the IO-CMS. This study's results are consistent with observations from other studies. Research on perilla leaf biochar (Niazi et al., 2018) demonstrated a similar trend, where As(III) and As(V) sorption increased with higher initial concentrations from 0.05 to 7.0 mg L^{-1} . Additionally, magnetic gelatin-modified biochar (Zhou et al., 2017) exhibited improved As(V) adsorption capacity with increasing initial concentration from 0.2 to 50 mg L^{-1} .

3.3.3.4. Effect of contact time (t_c)

Optimization results suggest that contact time has a small impact on arsenic removal efficiency for As(III) and As(V). Arsenic removal increased slightly with extended contact time, with an optimum observed at approximately 4.4 h for As(III) and 4.9 h for As(V). The Arsenic adsorption process often exhibits an initial rapid uptake within 20 min (Karimi et al., 2019), followed by a gradual rise until a state of

equilibrium is achieved, at which point the rate of adsorption and desorption is equal. Another study reported that arsenic adsorption reaches equilibrium an hour (Rahdar et al., 2019). Therefore, the minimal impact of contact time within the tested range (1-5 h) could be due to the experiment focusing on a period after equilibrium has already been established.

To facilitate comparisons between different materials for arsenic removal, Table 3-7 summarizes results from various studies. Utilizing IO-CMS as the adsorbent showcases its promising potential for effectively removing arsenic from water.

Regeneration studies indicated a decrease in arsenic removal efficiency for both As(III) and As(V) following the first cycle. Specifically, the efficiency for As(III) decreased from 95.16% to 64.91%, and for As(V), it dropped from 99.05% to 56.50%. This initial decline in efficiency suggests that the regenerant (0.1 M NaOH) may not have been fully effective in desorbing arsenic from certain binding sites on the adsorbent. These sites may have a stronger affinity for arsenic, preventing full desorption during the regeneration process. As a result, these sites remain occupied, leading to a decrease in available capacity for subsequent cycles. However, after the first cycle, the removal efficiency stabilized and remained consistent across the following cycles, indicating that the adsorbent had reached a steady-state performance. To improve regeneration, it may be beneficial to explore alternative desorption agents or optimize the desorption conditions, such as increasing the NaOH concentration, extending the desorption time, or modifying the stirring speed. These adjustments could enhance the removal of arsenic from more tightly bound sites and improve the overall regeneration efficiency. The trend of removal efficiency over the cycles is clearly shown in Figure 3-11.

Table 3-7 Summary of arsenic adsorption performance of different adsorbents.

Adsorbent	Adsorbate	C _i (mg L ⁻¹)	Adsorbent dose (g L ⁻¹)	pH	Contact time (h)	Temperature (°C)	RE (%)/ AC (mg g ⁻¹)	Reference
IO-CMS	As(III)	57.9	3.4	6.4	4.4	R.T.	94.9%, 14.62	This study
	As(V)	59.9	2.7	5.7	4.9		98.5%, 18.76	
Fe/Cu nanoparticles	As(III)	1.0	0.1	7.0	1.0	R.T.	69%, 19.68	(Babae et al., 2018)
	As(V)						89%, 21.32	
Cellulose nanocomposite	As(V)	6.0	1.0	3.0	5	40	99%	(Santra & Sarkar, 2016)
Lettuce flour	As(III)	48.1	5.0	8.0	24	20	4.8	(Vieira et al., 2018)
Aluminum-Impregnated Tea Waste	As(V)	0.1	20	6.0	1	RT	0.099	(Sawood et al., 2021)
Biochar								
Nano-bentonite	As(V)	10.0	0.1	5.5	0.08	RT	55.5%, 2.08	(Mutar & Saleh, 2022)
Azadirachta indica (neem) bark powder	As(III)	0.1	20.0	6.0	0.3	30	89.96 %, 0.167	(Roy et al., 2017)
Tea waste	As(V)	100	10	6	1	25	72%	(Cheraghi et al., 2014)
Alginate beads	As(III)	10	1	6	7d	23	~55%	(Sigdel et al., 2016)
	As(V)						~30%	
Chitosan beads	As(III)	10	3.3	5	24	25	1.83	(C.-C. Chen & Chung, 2006)
	As(V)						1.94	
Saccharomyces cerevisiae	As(III)	0.132	48.5×10 ⁷ CFU	5	24	25	66.2%	(Hadiani et al., 2019)
	As(V)	0.133	47.5×10 ⁷ CFU				15.8%	
Rice straw-derived biochar	As(V)	0.1	2	6	2	R.T.	>60%	(Mukherjee et al., 2021)
							5.6 µg g ⁻¹	
Macromolecule-carbonized rice husks	As(V)	0.1	2	6	1.1	-	85%	(Babazad et al., 2021)

C_i = initial concentration; RE = removal efficiency; AC = adsorption capacity; IO-CMS = calcined mussel shells modified by Iron oxide nanoparticles, RT = room temperature

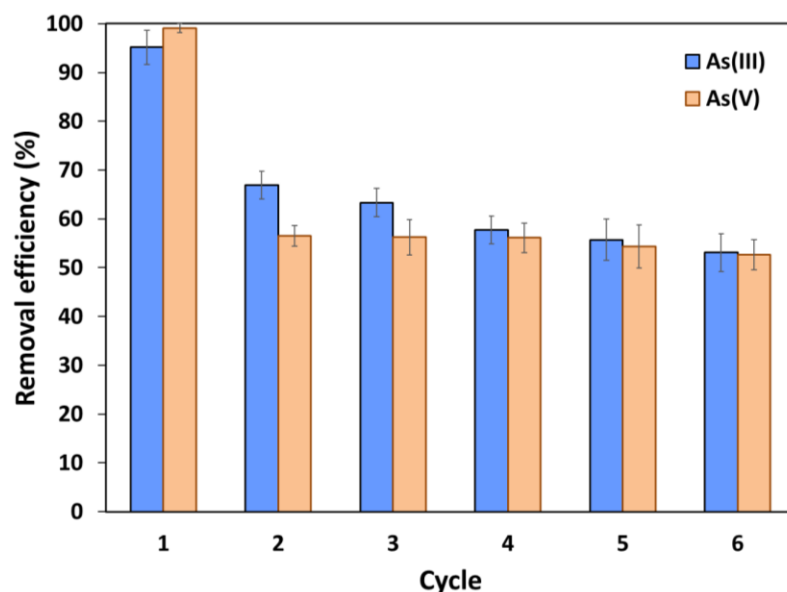


Figure 3-11 Regeneration of the adsorbent over multiple cycles for As(III) and As(V) removal.

3.3.4. Kinetics studies

Table 3-8 summarizes the parameters and coefficients derived from the PFO, PSO, intra-particle diffusion, and Elovich kinetic models. These values are obtained by analyzing the corresponding plots presented in Figure 3-12a and Figure 3-12b. According to R^2 values, the PSO model ($R^2(\text{As(III)}) = 0.99$, $R^2(\text{As(V)}) = 0.99$) provides a better fit to the data compared to PFO model for both As(III) and As(V) and indicates that chemisorption accounted for the majority of the adsorption process. (Cheraghipour & Pakshir, 2020). The intra-particle diffusion model results indicated a multi-step adsorption process, as shown by the distinct phases in Figure 3-12c. The second stage of intra-particle diffusion shows a lower slope compared to the first stage, indicating that the adsorption rate decreases as the process progresses. This slower diffusion suggests that the adsorbate molecules are moving slower within the pores of the adsorbent material, while the first stage corresponds to the rapid adsorption of contaminants onto the outer surface of the adsorbent. The Elovich (Figure 3-12d) model also closely matched the adsorption data, with a correlation coefficient ($R^2(\text{As(III)}) = 0.91$, $R^2(\text{As(V)}) = 0.98$), demonstrating a strong alignment with the experimental results.

Table 3-8 Adsorption parameters from isotherm, kinetic, and thermodynamic models.

Models		Parameters	As(III)	As(V)
Isotherm	Langmuir	b (l/mg)	0.082114	0.279788
		q_m (mg g ⁻¹)	28.73	31.54
		R^2	0.8692	0.9761
	Freundlich	K_f (mg g ⁻¹) (L mg ⁻¹) ^{1/n}	4.1899	8.0954
		n	2.2292	2.1839
		R^2	0.7014	0.8832
	Temkin	kt (L mg ⁻¹)	1.3367	2.9321
		B (J mol ⁻¹)	4.9024	6.7127
		R^2	0.7631	0.9365
	D-R	q_m (mol g ⁻¹)	0.00128	0.00208
		B (mol ² kJ ⁻²)	0.0042	0.0039
		R^2	0.7342	0.9098
Kinetic	PFO	k_l (min ⁻¹)	0.0114	0.0076
		q_e (mg g ⁻¹)	2.77	4.69
		R^2	0.65	0.94
	PSO	k_2 (g mg ⁻¹ min ⁻¹)	0.0226	0.0135
		q_e (mg g ⁻¹)	14.62	18.76
		R^2	0.99	0.99
		k_1d (g mg ⁻¹ min ^{-0.5})	0.7372	0.71
		k_1d (g mg ⁻¹ min ^{-0.5})	0.3804	0.1796
		k_1d (g mg ⁻¹ min ^{-0.5})	-0.0126	0.263
	Intra-particle diffusion	C_1 (mg g ⁻¹)	9.2436	12.945
		C_2 (mg g ⁻¹)	10.861	15.878
		C_3 (mg g ⁻¹)	14.464	15.276
		R_1^2	0.8117	0.9632
		R_2^2	0.7368	0.9619
		R_3^2	0.7072	0.9769
	Elovich	α (mg g ⁻¹ min ⁻¹)	4016.77	85622.15
		β (g mg ⁻¹)	0.8933	0.8853
		R^2	0.9118	0.9806
Thermodynamic	Van's Hoff	ΔH° (kJ mol ⁻¹)	187.248	118.233
		ΔS° (J mol ⁻¹ K ⁻¹)	651.884	447.385
			-6.152	-15.858
			(298.15 K)	(298.15 K)
		ΔG° (kJ mol ⁻¹)	-15.332	-18.383
			(308.15 K)	(308.15 K)
			-22.656	-26.890
			(323.15 K)	(323.15 K)

3.3.5. Isotherm studies

Table 3-8 compiles the calculated isotherm parameters alongside their corresponding correlation coefficients for all models employed in this study.

The visual representations (Figure 3-13) associated with these models effectively capture the trends observed in the experimental data. As shown by the straight lines in Figure 3-13 and confirmed by strong linear regression coefficients ($R^2 = 0.87\text{--}0.98$) for As(III) and As(V), the linear Langmuir model better fits the experimental data indicating arsenic adsorption by IO-CMS was monolayer adsorption (López-Luna et al., 2019). This also suggests that the entire surface has a uniform adsorption capacity, and there is minimal interaction between the adsorbed ions (X. Chen et al., 2022). It is noteworthy that the heterogeneity factor in Freundlich model, $1/n$, reflects the favourability of adsorption. Typically, $0 < 1/n < 1$ suggests favorable adsorption, which aligns with this research findings. This observation indicates a strong tendency for the ions to be adsorbed by the adsorbent. Conversely, values greater than 1 ($1/n > 1$) indicate unfavorable adsorption, and a value of 1 ($1/n = 1$) corresponds to irreversible adsorption (Debnath & Das, 2023). From the D-R isotherm, the calculated E values for As(III) and As(V) were $10.91 \text{ kJ mol}^{-1}$ and $11.32 \text{ kJ mol}^{-1}$, respectively. These values suggest that the adsorption of both As(III) and As(V) onto the adsorbent involves a chemisorption mechanism.

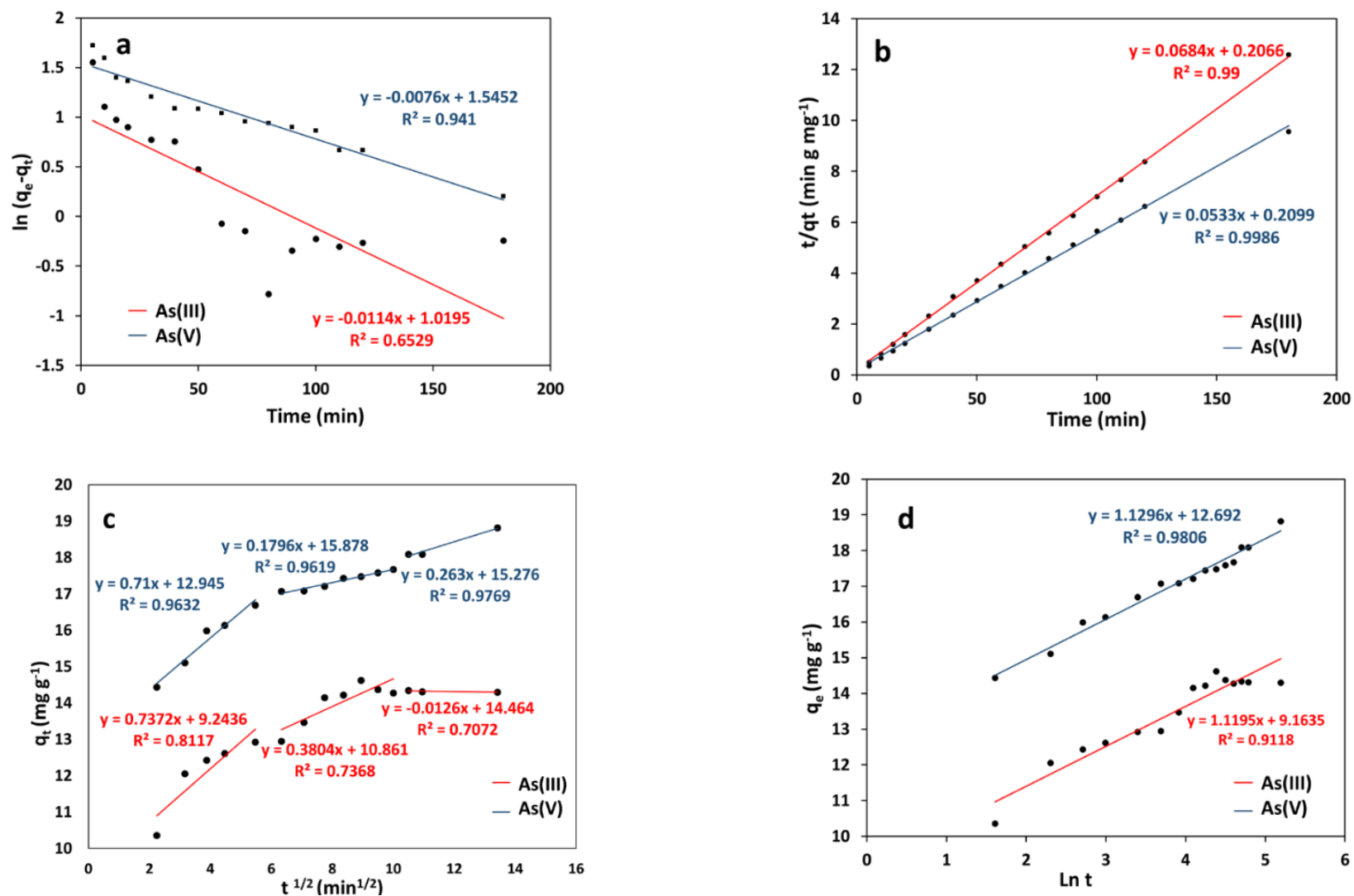


Figure 3-12 Arsenic adsorption kinetic models (a) PFO, (b) PSO, intra-particle diffusion (c), and Elovich models for the arsenic adsorption using IO-CMS.

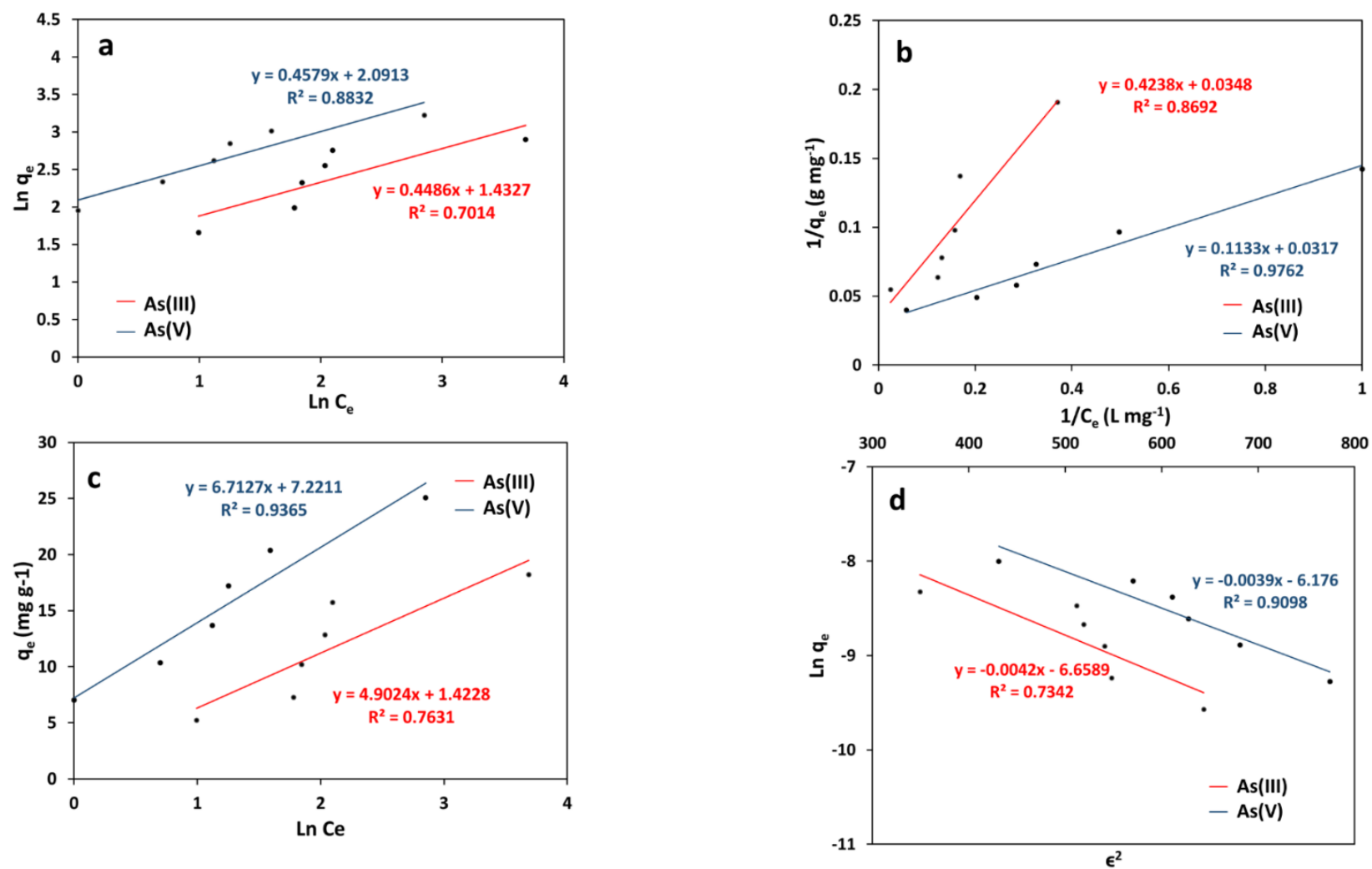


Figure 3-13 Arsenic adsorption isotherm models (a) Freundlich, (b) Langmuir, (c) Temkin, and (d) D-R models for the arsenic adsorption using IO-CMS.

3.3.6. Thermodynamic studies

Thermodynamic parameters are employed to understand As(III) and As(V) adsorption onto IO-CMS. Table 3-8 provides the entropy (ΔS°), enthalpy (ΔH°), and Gibbs free energy (ΔG°) values determined at different temperatures (298, 308, and 323 K) using Eq. (3-14) (Figure 3-14a) and Eq. (3-15) and a linear fit of $\log(q_e/C_e)$ vs. $1/T$ (Figure 3-14b).

The negative ΔG° values across all temperatures for As(III) and As(V) indicate a spontaneous adsorption process (Sahmoune, 2019). Notably, the increasingly negative ΔG° values with rising temperature suggest a growing favorability for adsorption in high temperatures

. The positive ΔH° values (187.248, and 118.233 kJ mol⁻¹) signifies that arsenic adsorption on IO-CMS is endothermic (Sahmoune, 2019). This aligns with the expected increase in enthalpy as temperature rises. The magnitude of the enthalpy change (ΔH°), corresponding to sorption energy, indicates the binding mechanism, differentiating between physical and chemical adsorption. Due to weak interactions, physical adsorption is characterized by a low ΔH° value (<8 kJ mol⁻¹). Conversely, chemical sorption exhibits a significantly higher ΔH° (> 40 kJ mol⁻¹), signifying a higher affinity between the adsorbate and the adsorbent (Gubbuk, 2011). The observed high ΔH° values for As(III) (187.248 kJ mol⁻¹) and As(V) (118.233 kJ mol⁻¹) strongly suggest that the primary process is chemisorption for these metal ions.

Furthermore, the positive ΔS° value (651.884 and 447.385 J mol⁻¹ K⁻¹) suggests an increase in randomness at the solid adsorbent-solution interface during arsenic adsorption (Sahmoune, 2019).

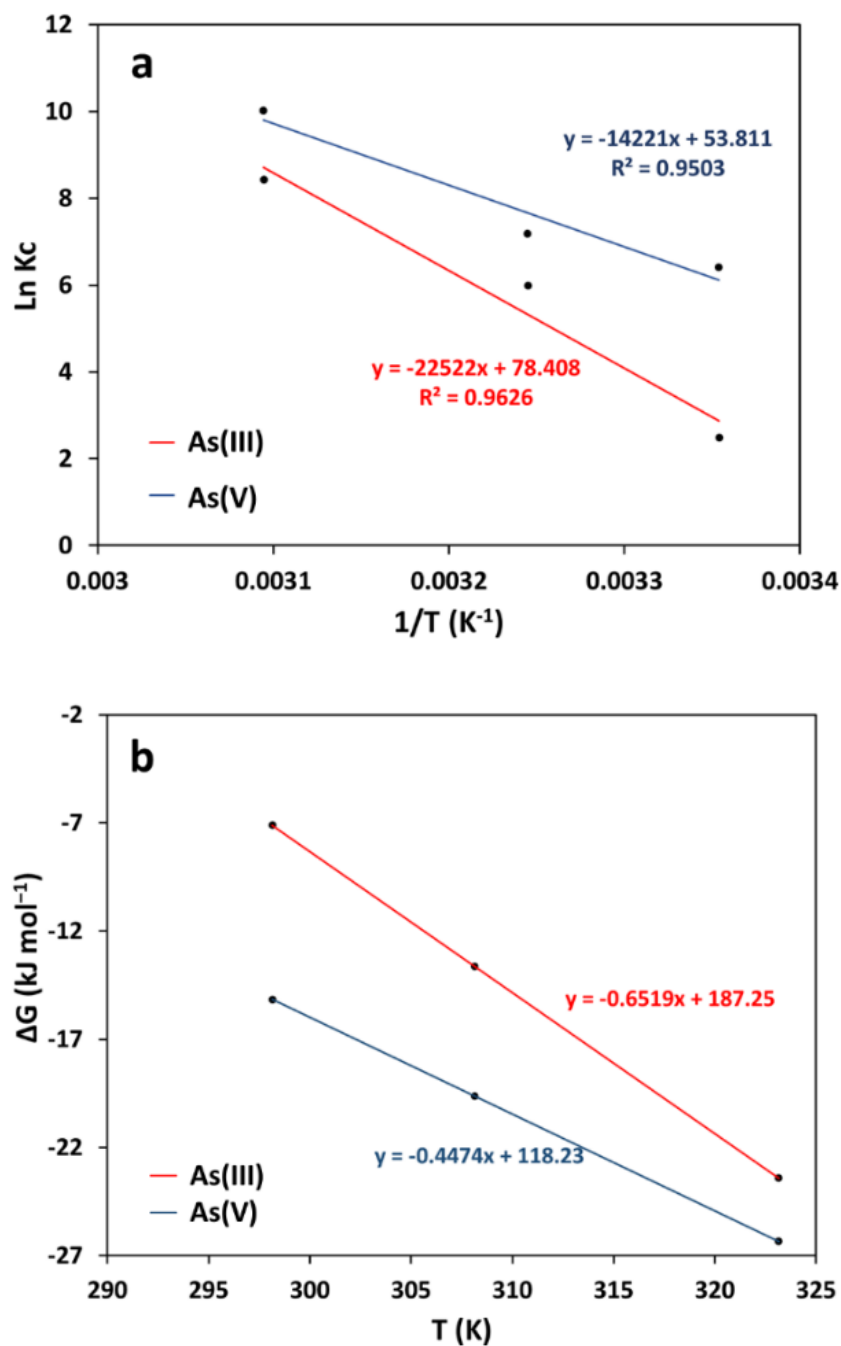


Figure 3-14 (a) Van't Hoff plot; and (b) Gibbs free energy for the arsenic adsorption using IO-CMS.

3.3.7. The potential and practicalities of calcined mussel shells

Mussel shells, a byproduct of the seafood industry, present a valuable opportunity for upcycling in water treatment applications. Compared to some conventional arsenic removal adsorbents, calcined mussel shells could be a more cost-effective solution,

particularly in regions with readily available mussel resources. Beyond arsenic removal, calcined mussel shells may also remove other contaminants from water. This could potentially simplify water treatment processes and reduce the overall environmental footprint of treatment plants.

On the other hand, the process of calcining mussel shells requires high temperatures to ensure the transformation into effective adsorbents. Scaling up this process demands high energy and infrastructure investments. The collection and calcination process may have environmental implications, such as carbon emissions from the calcination process. It's important to evaluate and minimize the environmental footprint. While lab-scale studies may show promising results, the real-world performance can vary. The adsorption capacity in actual water systems, which may contain various contaminants and fluctuating arsenic levels, needs thorough validation. While using calcined mussel shells for arsenic removal offers a promising sustainable solution, addressing these challenges and limitations is vital for successful large-scale implementation.

3.4. Conclusion

This study investigated the efficiency of modified calcined mussel shells (IO-CMS) as an adsorbent for removing arsenic (As(III) and As(V)) from water. By employing a comprehensive approach that combined optimization, kinetics, and equilibrium studies, optimal conditions were successfully identified for arsenic removal. For As(III) removal, the highest efficiency (94.9%) was achieved at pH 6.4, initial concentration of 57.9 mg L⁻¹, and adsorbent dose of 3.4 g L⁻¹. As(V) removal was optimal at pH 5.7, initial concentration of 59.9 mg L⁻¹, and adsorbent dose of 2.7 g L⁻¹, with a removal efficiency of 98.5%. The results of this research demonstrate the remarkable potential of IO-CMS as an inexpensive and ecologically-friendly adsorbent for arsenic

remediation applications. Kinetic investigation revealed that the arsenic adsorption aligned well with the prediction of PSO model (As(III): $R^2 = 0.99$, $k_2 = 0.00226 \text{ g mg}^{-1} \text{ min}^{-1}$, and $q_e = 14.6199 \text{ mg g}^{-1}$, As(V): $R^2 = 0.99$, $k_2 = 0.0135 \text{ g mg}^{-1} \text{ min}^{-1}$, and $q_e = 18.7617 \text{ mg g}^{-1}$), indicating chemisorption as the primary mechanism. Furthermore, Langmuir model fit of equilibrium isotherm data was strong ($R^2 = 0.87\text{--}0.98$), suggesting monolayer adsorption on the homogeneous surface of IO-CMS. Thermodynamic analysis using the determined parameters affirmed that the arsenic (both As(III) and As(V)) adsorption process is spontaneous and endothermic. Further research could explore the effectiveness of IO-CMS in real-world contaminated water sources, and potential modifications to enhance its adsorption capacity.

3.5. References

- Açıkgöz, Ç., Dandıl, S., & Akın Şahbaz, D. (2017). Investigation on surface characteristics of uncalcinated and calcinated mussel shells. *New Trends and Issues Proceedings on Advances in Pure and Applied Sciences*.
- Adebayo, G. B., Adegoke, H. I., Jamiu, W., Balogun, B. B., & Jimoh, A. A. (2015). Adsorption of Mn (II) and Co (II) ions from aqueous solution using Maize cob activated carbon: kinetics and Thermodynamics Studies. *Journal of Applied Sciences and Environmental Management*, 19(4), 737–748.
- Ahuja, I., Dauksas, E., Remme, J. F., Richardsen, R., & Løes, A.-K. (2020). Fish and fish waste-based fertilizers in organic farming—With status in Norway: A review. *Waste Management*, 115, 95–112.
- Al-mahbashi, N. M. Y., Kutty, S. R. M., Jagaba, A. H., Al-nini, A., Sholagberu, A. T., Aldhawi, B. N. S., & Rathnayake, U. (2023). Sustainable sewage sludge biosorbent activated carbon for remediation of heavy metals: Optimization by response surface methodology. *Case Studies in Chemical and Environmental*

Engineering, 8, 100437.

An, W., Liu, Y., Chen, H., Wang, Q., Hu, X., & Di, J. (2024). Oyster shell-modified lignite composite in globular shape as a low-cost adsorbent for the removal of Pb²⁺ and Cd²⁺ from AMD: Evaluation of adsorption properties and exploration of potential mechanisms. *Arabian Journal of Chemistry*, 17(5), 105732.

Arabkhani, P., Asfaram, A., & Sadegh, F. (2023). Green and low-temperature synthesis of the magnetic modified biochar under the air atmosphere for the adsorptive removal of heavy metal ions from wastewater: CCD-RSM experimental design with isotherm, kinetic, and thermodynamic studies.

Environmental Science and Pollution Research, 30(57), 120085–120102.

Azara, A., Castiglia, P., Piana, A., Masia, M. D., Palmieri, A., Arru, B., Maida, G., & Dettori, M. (2018). SHORT PAPER Derogation from drinking water quality standards in Italy according to the European Directive 98/83/EC and the Legislative Decree 31/2001-a look at the recent past. *Ann Ig*, 30, 517–526.

Azcarate, S. M., Teglia, C. M., Chiappini, F. A., & Goicoechea, H. C. (2023). Fundamentals of Design of Experiments and Optimization: Experimental Designs in Response Surface Methodology. In *Introduction to Quality by Design in Pharmaceutical Manufacturing and Analytical Development* (pp. 47–66). Springer.

Babae, Y., Mulligan, C. N., & Rahaman, M. S. (2017). Stabilization of Fe/Cu nanoparticles by starch and efficiency of arsenic adsorption from aqueous solutions. *Environmental Earth Sciences*, 76, 1–12.

Babae, Y., Mulligan, C. N., & Rahaman, M. S. (2018). Removal of arsenic (III) and arsenic (V) from aqueous solutions through adsorption by Fe/Cu nanoparticles. *Journal of Chemical Technology & Biotechnology*, 93(1), 63–71.

- Babazad, Z., Kaveh, F., & Ebadi, M. (2021). *Efficient removal of lead and arsenic using macromolecule-carbonized rice husks. Heliyon 7: e06631.*
- Baskan, M. B., & Pala, A. (2011). Removal of arsenic from drinking water using modified natural zeolite. *Desalination*, 281, 396–403.
- Benni, S. D., Munnolli, R. S., Katagi, K. S., & Kadam, N. S. (2021). Mussel shells as sustainable catalyst: synthesis of liquid fuel from non edible seeds of Bauhinia malabarica and Gymnosporia montana. *Current Research in Green and Sustainable Chemistry*, 4, 100124.
- Cardell, C., Herrera, A., Guerra, I., Navas, N., Simón, L. R., & Elert, K. (2017). Pigment-size effect on the physico-chemical behavior of azurite-tempera dosimeters upon natural and accelerated photo aging. *Dyes and Pigments*, 141, 53–65.
- Caruso, G., Floris, R., Serangeli, C., & Di Paola, L. (2020). Fishery wastes as a yet undiscovered treasure from the sea: Biomolecules sources, extraction methods and valorization. *Marine Drugs*, 18(12), 622.
- Chen, C.-C., & Chung, Y.-C. (2006). Arsenic removal using a biopolymer chitosan sorbent. *Journal of Environmental Science and Health, Part A*, 41(4), 645–658.
- Chen, X., Hossain, M. F., Duan, C., Lu, J., Tsang, Y. F., Islam, M. S., & Zhou, Y. (2022). Isotherm models for adsorption of heavy metals from water-a review. *Chemosphere*, 307, 135545.
- Cheraghi, M., Lorestani, B., Merrikhpour, H., & Mosaed, H. P. (2014). Assessment efficiency of tea wastes in arsenic removal from aqueous solution. *Desalination and Water Treatment*, 52(37–39), 7235–7240.
- Cheraghipour, E., & Pakshir, M. (2020). Process optimization and modeling of Pb (II) ions adsorption on chitosan-conjugated magnetite nano-biocomposite using

- response surface methodology. *Chemosphere*, 260, 127560.
- Chong, W. C., Choo, Y. L., Koo, C. H., Pang, Y. L., & Lai, S. O. (2019). Adsorptive membranes for heavy metal removal—A mini review. *AIP Conference Proceedings*, 2157(1).
- Chowdhury, S. R., Yanful, E. K., & Pratt, A. R. (2011). Arsenic removal from aqueous solutions by mixed magnetite–maghemite nanoparticles. *Environmental Earth Sciences*, 64, 411–423.
- Dandil, S., Sahbaz, D. A., & Acikgoz, C. (2019). High performance adsorption of hazardous triphenylmethane dye-crystal violet onto calcinated waste mussel shells. *Water Quality Research Journal*, 54(3), 249–256.
- de Alvarenga, R. A. F., Galindro, B. M., de Fátima Helpa, C., & Soares, S. R. (2012). The recycling of oyster shells: An environmental analysis using Life Cycle Assessment. *Journal of Environmental Management*, 106, 102–109.
- Debnath, S., & Das, R. (2023). Strong adsorption of CV dye by Ni ferrite nanoparticles for waste water purification: Fits well the pseudo second order kinetic and Freundlich isotherm model. *Ceramics International*, 49(10), 16199–16215.
- Derkani, M. H., Fletcher, A. J., Fedorov, M., Abdallah, W., Sauerer, B., & Anderson, J. (n.d.). *Mechanisms of surface charge modification of carbonates in aqueous electrolyte solutions. Colloids Interfaces*. 2019; 3 (4): 62.
- Dong, Y., Gao, M., Song, Z., & Qiu, W. (2020). As (III) adsorption onto different-sized polystyrene microplastic particles and its mechanism. *Chemosphere*, 239, 124792.
- Egbosiuba, T. C., Egwunyenga, M. C., Tijani, J. O., Mustapha, S., Abdulkareem, A. S., Kovo, A. S., Krikstolaityte, V., Veksha, A., Wagner, M., & Lisak, G. (2022).

- Activated multi-walled carbon nanotubes decorated with zero valent nickel nanoparticles for arsenic, cadmium and lead adsorption from wastewater in a batch and continuous flow modes. *Journal of Hazardous Materials*, 423, 126993.
- Fan, Y., Zheng, C., Liu, H., He, C., Shen, Z., & Zhang, T. C. (2020). Effect of pH on the adsorption of arsenic (V) and antimony (V) by the black soil in three systems: Performance and mechanism. *Ecotoxicology and Environmental Safety*, 191, 110145.
- Faria, D. N., Cipriano, D. F., Schettino Jr, M. A., Neto, A. C., Cunha, A. G., & Freitas, J. C. C. (2020). Na, Ca-based catalysts supported on activated carbon for synthesis of biodiesel from soybean oil. *Materials Chemistry And Physics*, 249, 123173.
- Feng, L., Cao, M., Ma, X., Zhu, Y., & Hu, C. (2012). Superparamagnetic high-surface-area Fe₃O₄ nanoparticles as adsorbents for arsenic removal. *Journal of Hazardous Materials*, 217, 439–446.
- Frisbie, S. H., & Mitchell, E. J. (2022). Arsenic in drinking water: An analysis of global drinking water regulations and recommendations for updates to protect public health. *PLoS One*, 17(4), e0263505.
- Genchi, G., Lauria, G., Catalano, A., Carocci, A., & Sinicropi, M. S. (2022). Arsenic: a review on a great health issue worldwide. *Applied Sciences*, 12(12), 6184.
- Ghelich, R., Jahannama, M. R., Abdizadeh, H., Torknik, F. S., & Vaezi, M. R. (2019). Central composite design (CCD)-Response surface methodology (RSM) of effective electrospinning parameters on PVP-B-Hf hybrid nanofibrous composites for synthesis of HfB₂-based composite nanofibers. *Composites Part B: Engineering*, 166, 527–541.

- Gubbuk, I. H. (2011). Isotherms and thermodynamics for the sorption of heavy metal ions onto functionalized sporopollenin. *Journal of Hazardous Materials*, 186(1), 416–422.
- Hadiani, M. R., Khosravi-Darani, K., & Rahimifard, N. (2019). Optimization of As (III) and As (V) removal by *Saccharomyces cerevisiae* biomass for biosorption of critical levels in the food and water resources. *Journal of Environmental Chemical Engineering*, 7(2), 102949.
- Hossain, M. S., Jahan, S. A., & Ahmed, S. (2023). Crystallographic characterization of bio-waste material originated CaCO_3 , green-synthesized CaO and $\text{Ca}(\text{OH})_2$. *Results in Chemistry*, 5, 100822.
- Huh, J.-H., Choi, Y.-H., Ramakrishna, C., Cheong, S. H., & Ahn, J. W. (2016). Use of calcined oyster shell powders as CO_2 adsorbents in algae-containing water. *Journal of the Korean Ceramic Society*, 53(4), 429–434.
- Iribarren, D., Moreira, M. T., & Feijoo, G. (2010). Implementing by-product management into the life cycle assessment of the mussel sector. *Resources, Conservation and Recycling*, 54(12), 1219–1230.
- Karimi, P., Javanshir, S., Sayadi, M. H., & Arabyarmohammadi, H. (2019). Arsenic removal from mining effluents using plant-mediated, green-synthesized iron nanoparticles. *Processes*, 7(10), 759.
- Kim, U. J., Furtado, C. A., Liu, X., Chen, G., & Eklund, P. C. (2005). Raman and IR spectroscopy of chemically processed single-walled carbon nanotubes. *Journal of the American Chemical Society*, 127(44), 15437-15445.
- Liang, Z., Wang, Q., Dong, B., Jiang, B., & Xing, F. (2018). Ion-triggered calcium hydroxide microcapsules for enhanced corrosion resistance of steel bars. *RSC Advances*, 8(69), 39536–39544.

- Linggawati, A. (2016). Preparation and characterization of calcium oxide heterogeneous catalyst derived from *Anadara granosa* shell for biodiesel synthesis. *KnE Engineering*.
- López-Luna, J., Ramírez-Montes, L. E., Martínez-Vargas, S., Martínez, A. I., Mijangos-Ricardez, O. F., González-Chávez, M. del C. A., Carrillo-González, R., Solís-Domínguez, F. A., Cuevas-Díaz, M. del C., & Vázquez-Hipólito, V. (2019). Linear and nonlinear kinetic and isotherm adsorption models for arsenic removal by manganese ferrite nanoparticles. *SN Applied Sciences*, *1*, 1–19.
- Luo, M., Lin, H., He, Y., Li, B., Dong, Y., & Wang, L. (2019). Efficient simultaneous removal of cadmium and arsenic in aqueous solution by titanium-modified ultrasonic biochar. *Bioresource Technology*, *284*, 333–339.
- Ma, X., Tao, S., Fu, S., Yang, H., Lin, B., Lou, Y., & Li, Y. (2023). Adsorption of Pyrethroids in Water by Calcined Shell Powder: Preparation, Characterization, and Mechanistic Analysis. *Materials*, *16*(7), 2802.
- Mamindy-Pajany, Y., Hurel, C., Marmier, N., & Roméo, M. (2011). Arsenic (V) adsorption from aqueous solution onto goethite, hematite, magnetite and zero-valent iron: Effects of pH, concentration and reversibility. *Desalination*, *281*, 93–99.
- Mane, P. V, Rego, R. M., Yap, P. L., Losic, D., & Kurkuri, M. D. (2024). Unveiling cutting-edge advances in high surface area porous materials for the efficient removal of toxic metal ions from water. *Progress in Materials Science*, 101314.
- Mass, T., Drake, J. L., Haramaty, L., Rosenthal, Y., Schofield, O. M. E., Sherrell, R. M., & Falkowski, P. G. (2012). Aragonite precipitation by “proto-polyps” in coral cell cultures. *PLoS One*, *7*(4), e35049.
- Medunić, G., Fiket, Ž., & Ivanić, M. (2020). Arsenic contamination status in Europe,

- Australia, and other parts of the world. *Arsenic in Drinking Water and Food*, 183–233.
- Métral, J., Charlet, L., Bureau, S., Mallik, S. B., Chakraborty, S., Ahmed, K. M., Rahman, M. W., Cheng, Z., & van Geen, A. (2008). Comparison of dissolved and particulate arsenic distributions in shallow aquifers of Chakdaha, India, and Araihaazar, Bangladesh. *Geochemical Transactions*, 9, 1–18.
- Mititelu, M., Stanciu, G., Drăgănescu, D., Ioniță, A. C., Neacșu, S. M., Dinu, M., Stefan-van Staden, R.-I., & Moroșan, E. (2021). Mussel shells, a valuable calcium resource for the pharmaceutical industry. *Marine Drugs*, 20(1), 25.
- Mohadi, R., Anggraini, K., Riyanti, F., & Lesbani, A. (2016). Preparation calcium oxide from chicken eggshells. *Sriwijaya Journal of Environment*, 1(2), 32–35.
- Mukherjee, S., Thakur, A. K., Goswami, R., Mazumder, P., Taki, K., Vithanage, M., & Kumar, M. (2021). Efficacy of agricultural waste derived biochar for arsenic removal: Tackling water quality in the Indo-Gangetic plain. *Journal of Environmental Management*, 281, 111814.
- Mutar, R. F., & Saleh, M. A. (2022). Optimization of arsenic ions adsorption and removal from hospitals wastewater by nano-bentonite using central composite design. *Materials Today: Proceedings*, 60, 1248–1256.
- Neisan, R. S., Saady, N. M. C., Bazan, C., Zendehboudi, S., Al-nayili, A., Abbassi, B., & Chatterjee, P. (2023). Arsenic Removal by Adsorbents from Water for Small Communities' Decentralized Systems: Performance, Characterization, and Effective Parameters. *Clean Technologies*, 5(1), 352–402.
<https://doi.org/10.3390/cleantechnol5010019>
- Neisan, R. S., Saady, N. M. C., Bazan, C., Zendehboudi, S., & Albayati, T. M. (2023). Adsorption of copper from water using TiO₂-modified activated carbon derived

- from orange peels and date seeds: Response surface methodology optimization. *Heliyon*, 9(11).
- Niazi, N. K., Bibi, I., Shahid, M., Ok, Y. S., Burton, E. D., Wang, H., Shaheen, S. M., Rinklebe, J., & Lüttge, A. (2018). Arsenic removal by perilla leaf biochar in aqueous solutions and groundwater: an integrated spectroscopic and microscopic examination. *Environmental Pollution*, 232, 31–41.
- Ogundiran, A. A., Ofudje, E. A., Ogundiran, O. O., & Adewusi, A. M. (2022). Cationic dye adsorptions by eggshell waste: kinetics, isotherms and thermodynamics studies. *Desalin Water Treat*, 280, 157–167.
- Onyeaka, H., & Hart, A. (2021). Eggshell and Seashells Biomaterials Sorbent for Carbon Dioxide Capture. *Chapters*.
- Rahdar, S., Taghavi, M., Khaksefidi, R., & Ahmadi, S. (2019). Adsorption of arsenic (V) from aqueous solution using modified saxaul ash: isotherm and thermodynamic study. *Applied Water Science*, 9(4), 1–9.
- Read, R., Briefs, C. B., & Cases, C. C. C. (2001). National Primary Drinking Water Regulations; Arsenic and Clarifications to Compliance and New Source Contaminants Monitoring 66 Fed. Reg. 37617 (Jul. 19, 2001) Copy Cite. *Federal Register*.
- Ren, X., Zhang, Z., Luo, H., Hu, B., Dang, Z., Yang, C., & Li, L. (2014). Adsorption of arsenic on modified montmorillonite. *Applied Clay Science*, 97, 17–23.
- Resources), G. of newfoundland and labrador (Fisheries and L. (2022). *Seafood industry review*. <https://www.gov.nl.ca/ffa/files/publications-pdf-syir-2017.pdf>
- Roy, P., Dey, U., Chattoraj, S., Mukhopadhyay, D., & Mondal, N. K. (2017). Modeling of the adsorptive removal of arsenic (III) using plant biomass: a bioremedial approach. *Applied Water Science*, 7, 1307–1321.

- Sahmoune, M. N. (2019). Evaluation of thermodynamic parameters for adsorption of heavy metals by green adsorbents. *Environmental Chemistry Letters*, 17(2), 697–704.
- Salim, N. A. A., Fulazzaky, M. A., Puteh, M. H., Khamidun, M. H., Yusoff, A. R. M., Abdullah, N. H., Ahmad, N., Lazim, Z. M., & Nuid, M. (2021). Adsorption of phosphate from aqueous solution onto iron-coated waste mussel shell: Physicochemical characteristics, kinetic, and isotherm studies. *Biointerface Res. Appl. Chem*, 11, 12831–12842.
- Santoso, A., Hanindita, C. F. A., & Rachman, I. B. (2019). Synthesis of biodiesel from low-quality crude palm oil with heterogeneous catalyst Cao-ZnO. *IOP Conference Series: Materials Science and Engineering*, 515(1), 12082.
- Santra, D., & Sarkar, M. (2016). Optimization of process variables and mechanism of arsenic (V) adsorption onto cellulose nanocomposite. *Journal of Molecular Liquids*, 224, 290–302.
- Sawood, G. M., Mishra, A., & Gupta, S. K. (2021). Optimization of arsenate adsorption over aluminum-impregnated tea waste biochar using RSM–central composite design and adsorption mechanism. *Journal of Hazardous, Toxic, and Radioactive Waste*, 25(2), 4020075.
- Seo, J. H., Park, S. M., Yang, B. J., & Jang, J. G. (2019). Calcined oyster shell powder as an expansive additive in cement mortar. *Materials*, 12(8), 1322.
- Shaji, E., Santosh, M., Sarath, K. V, Prakash, P., Deepchand, V., & Divya, B. V. (2021). Arsenic contamination of groundwater: A global synopsis with focus on the Indian Peninsula. *Geoscience Frontiers*, 12(3), 101079.
- Sigdel, A., Park, J., Kwak, H., & Park, P.-K. (2016). Arsenic removal from aqueous solutions by adsorption onto hydrous iron oxide-impregnated alginate beads.

Journal of Industrial and Engineering Chemistry, 35, 277–286.

- Singh, K. P., Gupta, S., Singh, A. K., & Sinha, S. (2010). Experimental design and response surface modeling for optimization of Rhodamine B removal from water by magnetic nanocomposite. *Chemical Engineering Journal*, 165(1), 151–160.
- Smedley, P. L., & Kinniburgh, D. G. (2002). A review of the source, behaviour and distribution of arsenic in natural waters. *Applied Geochemistry*, 17(5), 517–568.
- Tang, Y., Wang, J., & Gao, N. (2010). Characteristics and model studies for fluoride and arsenic adsorption on goethite. *Journal of Environmental Sciences*, 22(11), 1689–1694.
- Tekin, K. (2015). Hydrothermal conversion of russian olive seeds into crude bio-oil using a CaO catalyst derived from waste mussel shells. *Energy & Fuels*, 29(7), 4382–4392.
- Ungureanu, E. L., Mocanu, A. L., Stroe, C. A., Panciu, C. M., Berca, L., Sionel, R. M., & Mustatea, G. (2023). Agricultural byproducts used as low-cost adsorbents for removal of potentially toxic elements from wastewater: a comprehensive review. *Sustainability*, 15(7), 5999.
- Ventruti, G., Ventura, G. Della, Bellatreccia, F., Lacalamita, M., & Schingaro, E. (2016). Hydrogen bond system and vibrational spectroscopy of the iron sulfate fibroferrite, $\text{Fe}(\text{OH})\text{SO}_4 \cdot 5\text{H}_2\text{O}$. *European Journal of Mineralogy*, 28(5), 943–952.
- Veríssimo, N. V., Mussagy, C. U., Oshiro, A. A., Mendonça, C. M. N., de Carvalho Santos-Ebinuma, V., Pessoa, A., de Souza Oliveira, R. P., & Pereira, J. F. B. (2021). From green to blue economy: Marine biorefineries for a sustainable ocean-based economy. *Green Chemistry*, 23(23), 9377–9400.

- Vieira, J. C., Soares, L. C., & Froes-Silva, R. E. S. (2018). Comparing chemometric and Langmuir isotherm for determination of maximum capacity adsorption of arsenic by a biosorbent. *Microchemical Journal*, 137, 324–328.
- Wang, J., & Guo, X. (2023). Adsorption kinetics and isotherm models of heavy metals by various adsorbents: An overview. *Critical Reviews in Environmental Science and Technology*, 53(21), 1837–1865.
- Wang, L., & Giammar, D. E. (2015). Effects of pH, dissolved oxygen, and aqueous ferrous iron on the adsorption of arsenic to lepidocrocite. *Journal of Colloid and Interface Science*, 448, 331–338.
- Wen, Z., Lu, J., Zhang, Y., Cheng, G., Huang, S., Chen, J., Xu, R., Ming, Y., Wang, Y., & Chen, R. (2020). Facile inverse micelle fabrication of magnetic ordered mesoporous iron cerium bimetal oxides with excellent performance for arsenic removal from water. *Journal of Hazardous Materials*, 383, 121172.
- Wu, F., Chen, L., Hu, P., Wang, Y., Deng, J., & Mi, B. (2021). Industrial alkali lignin-derived biochar as highly efficient and low-cost adsorption material for Pb (II) from aquatic environment. *Bioresource Technology*, 322, 124539.
- Yang, H., & Yan, N. (2018). Transformation of seafood wastes into chemicals and materials. *Encycl. Sustain. Sci. Technol*, 1–23.
- Yu, Y., Zhang, C., Yang, L., & Chen, J. P. (2017). Cerium oxide modified activated carbon as an efficient and effective adsorbent for rapid uptake of arsenate and arsenite: Material development and study of performance and mechanisms. *Chemical Engineering Journal*, 315, 630–638.
- Zhan, J., Lu, J., & Wang, D. (2022). Review of shell waste reutilization to promote sustainable shellfish aquaculture. *Reviews in Aquaculture*, 14(1), 477–488.
- Zhang, S., Li, X., & Chen, J. P. (2010). An XPS study for mechanisms of arsenate

adsorption onto a magnetite-doped activated carbon fiber. *Journal of Colloid and Interface Science*, 343(1), 232–238.

Zhang, Y., Wang, Y., Zhang, H., Li, Y., Zhang, Z., & Zhang, W. (2020). Recycling spent lithium-ion battery as adsorbents to remove aqueous heavy metals: Adsorption kinetics, isotherms, and regeneration assessment. *Resources, Conservation and Recycling*, 156, 104688.

Zhou, Z., Liu, Y., Liu, S., Liu, H., Zeng, G., Tan, X., Yang, C., Ding, Y., Yan, Z., & Cai, X. (2017). Sorption performance and mechanisms of arsenic (V) removal by magnetic gelatin-modified biochar. *Chemical Engineering Journal*, 314, 223–231.

CHAPTER FOUR

INVESTIGATING ARSENIC (III AND V) ADSORPTION WITH MODIFIED CALCINED MUSSEL SHELLS IN CONTINUOUS FLOW EXPERIMENTS³

Roya Sadat Neisan¹, Noori M. Cata Saady¹, Carlos Bazan², Sohrab Zendehboudi³

¹ Department of Civil Engineering, Memorial University, St. John's, NL A1B 3X5, Canada

² Faculty of Business Administration, Memorial University, St. John's, NL A1B 3X5, Canada

³ Department of Process Engineering, Memorial University, St. John's, NL A1B 3X5, Canada

Abstract

This study explores arsenic (III and V) adsorption using modified calcined mussel shells in continuous flow experiments, focusing on effectiveness and regeneration over multiple cycles. Initial arsenic concentrations of 10 and 50 mg L⁻¹ were used for breakthrough curve analysis, while reuse and co-ion interference (Cl⁻, SO₄²⁻, NO₃⁻, HCO₃⁻, PO₄³⁻) tests were conducted at 50 mg L⁻¹. Higher initial concentrations (10 to 50 mg L⁻¹), increased flow rates (5 to 10 mL min⁻¹), and reduced adsorbent mass (10 to 5 g) improved maximum adsorption capacities (As(III): 8.99 mg g⁻¹, As(V): 26.60 mg g⁻¹). However, higher flow rates and reduced adsorbent mass accelerated breakthrough. Reuse for five cycles reduced adsorption capacity by ~50%, highlighting the need for regeneration or replacement. Co-ions reduced arsenic adsorption capacity from 10.43 to 7.62 mg g⁻¹ and shortened the 50% breakthrough time from 417.11 to 304.92 min. Mussel shell powder (MP) demonstrated faster adsorption kinetics, whereas mussel shell-coated discs (MD) showed higher maximum capacities. These findings highlight the potential of CMS as a sustainable, low-cost adsorbent for arsenic removal in continuous flow systems. Further research should assess the long-term performance and shelf life of CMS-based cartridges.

³ This chapter has been published as a peer-reviewed journal article:

Neisan, R. S., Saady, N. M. C., Bazan, C., & Zendehboudi, S. (2025). Investigating arsenic (III and V) continuous flow adsorption by modified calcined mussel shells. *Journal of Water Process Engineering*, 72, 107488. <https://doi.org/10.1016/j.jwpe.2025.107488>.

4.1. Introduction

Arsenic, classified by the International Agency for Research on Cancer (IARC) as a Category 1 carcinogen, represents a significant danger to the environment and public health (Omar et al., 2023; Signes-Pastor et al., 2024). Unsafe levels of arsenic in drinking water from underground sources concern more than 500 million people worldwide (Boussouga et al., 2023). Arsenic exists in two prevalent oxidation states in natural waters: arsenite (AsO_3^{3-}) and arsenate (AsO_4^{3-}) (Mendizabal et al., 2023). It exists as arsenite in groundwater with reducing environments and a natural pH of 6 to 8. On the other hand, arsenate is typically present in shallow groundwater under oxidizing conditions (Shukla et al., 2023). Various treatment methods are employed to reduce arsenic levels in drinking water below the $10 \mu\text{g L}^{-1}$ maximum contamination level, which is set by the World Health Organization (WHO) based on a 1 in 10,000 cancer risk assessment. Therefore, there is still a non-zero cancer risk from arsenic even at values below $10 \mu\text{g L}^{-1}$ (Boussouga et al., 2023; Farsad et al., 2023). Adsorption is a promising technique among various treatment methods due to its simplicity, cost-effectiveness, and efficiency (Tony, 2022). Numerous materials have been investigated for their arsenic adsorption capabilities, including activated carbons (Tony, 2022), metal oxides (A. D. Gupta et al., 2021), and bio-sorbents (Thanki et al., 2021). Recently, attention has turned to using waste materials as adsorbents, aligning with the principles of sustainability and waste management (Koul et al., 2022). In similar studies investigating arsenic removal in continuous flow systems, various adsorbents have been employed with notable results. For instance, stainless steel slag demonstrated rapid adsorption kinetics in removing As(V), as shown in column loading tests where 80% of As(V) was removed from a 10 mg L^{-1} solution using 1.0 g of washed slag at a solution flowrate of 1 mL min^{-1} (Liem-Nguyen et al., 2020). A fixed-bed column adsorption

study was conducted to evaluate the efficiency of iron oxide-coated natural rock, for removing As from aqueous media at an up-flow rate of 8 mL min⁻¹. The study reported an adsorption capacity of 295.30 mg L⁻¹ for As(III) at an initial concentration of 0.6 mg L⁻¹ and a minimum bed depth of 0.104 cm, and 599.82 mg L⁻¹ for As(V) at an initial concentration of 3 mg L⁻¹ and a minimum bed depth of 6.27 cm (Maji et al., 2015). In another column experiment, bagasse fly ash achieved maximum removal efficiencies of 98.9% for arsenate and 95.6% for arsenite at a flowrate of 1 mL min⁻¹ (I. Ali et al., 2014). Similarly, optimal dynamic experiments with a fixed-bed arsenic adsorption column using chitosan material showed a maximum adsorption capacity of 50 mg g⁻¹ from a 120 mg L⁻¹ solution (Brion-Roby et al., 2018).

Mussel shells, an abundant by-product of the seafood industry, present a potential low-cost and environmentally friendly adsorbent (Detho et al., 2022). In 2022, shellfish production reached about 17.7 million tons, accounting for roughly 23–26% of global aquaculture output (FAO, 2022; Martínez-García et al., 2017). Shell waste from the seafood industry is a significant problem, causing environmental harm and economic losses. Discarded shells often accumulate in piles, leading to unpleasant odors, contamination from decomposing organic matter, and visual pollution (Summa et al., 2022). By 2023, over 40 countries reported mussel production, generating more than 15 million tons of waste, with over 4 million tons discarded at sea, contributing to environmental issues like visual pollution and the spread of pests (de Freitas et al., 2024). Their abundance makes them a readily accessible resource, and repurposing mussel shells reduces waste while addressing water contamination. This approach not only lowers environmental impact but also supports circular economy principles by transforming waste into a valuable product (Summa et al., 2022; Topić Popović et al., 2023). Composed primarily of calcium carbonate, mussel shells can be transformed

through calcination into a more reactive form, increasing their adsorption capacity (Mohamed et al., 2016; Paradelo et al., 2016). Further modification can enhance their surface properties (Nawar et al., 2021), making them suitable for targeting specific contaminants like arsenic. In their natural and modified forms, mussel shells have recently been utilized for contaminant removal; Table 4-1 summarizes relevant studies.

Point-of-use (POU) systems have emerged as a practical solution for addressing drinking water contamination, particularly in small, isolated, and remote communities where centralized water treatment systems may be inadequate or unavailable. A Canadian Broadcasting Corporation (CBC) investigation revealed that over 100 wells out of 1000 sampled wells in Newfoundland and Labrador (NL) contained levels of arsenic exceeding Health Canada's recommended safe limits ($10 \mu\text{g L}^{-1}$) (Mullin, 2023b). At a presumed 10 percent risk rate, as many as 4,000 households in the province could be consuming arsenic-contaminated water without any awareness, as the odourless, colourless contaminant (Mullin, 2023a). This underscores the need for accessible, affordable solutions like POU systems, which can serve as a practical means of arsenic removal for individual households in such at-risk regions. These systems are designed to treat water at the point of consumption, offering several advantages over centralized treatment methods (Papadimitriou et al., 2017).

Table 4-1 Results of mussel shell-based adsorbents for contaminant removal.

Adsorbent	Adsorbate	C_i (mg L ⁻¹)	Adsorbent dose (g L ⁻¹)	pH	Contact time (min)	RE (%)/ AC (mg g ⁻¹)	Reference
Calcined shell powder	Pb(II)	20–100	0.5-2.5	4–6	10-540	57.79	(Q. Wang et al., 2021) (El Haddad et al., 2014)
Calcined mussels shells	Rhodamine B Alizarin Red S Orange II	25-100	1-5	2-12	90	45.67 39.65 41.75	
Raw mussel shells	Methyl blue Methyl red Cr(VI) Cd Cu	100 100 50 50 50	0.5-20		7 d	~100% ~100% >98% >98% >98%	(Papadimitriou et al., 2017)
Calcined mussel shells	Basic Fuchsin	50-200	1-5	2-12	240	167.68	(El Haddad, 2016) (Abdullah et al., 2022)
Raw mussel shells Calcined mussel shells	PO ₄ ³⁻	10	20		30-5760	52% 97%	
Raw mussel shells Chitosan obtained from mussel shells	PO ₄ ³⁻ tetracycline	5 50–100	20-100 4-10	7	1-6 d 20–60	83.4% ~30%	(Salim et al., 2020) (Topal & Topal, 2020)

C_i = initial concentration; RE = removal efficiency; AC = adsorption capacity.

First, POU systems are cost-effective and relatively easy to install and maintain, making them accessible for households and communities in remote or underserved areas (Neisan, Saady, Bazan, Zendeboudi, Al-nayili, et al., 2023; Pooi & Ng, 2018). Second, they provide immediate access to safe drinking water, bypassing the complexities and costs associated with centralized infrastructure (Neisan, Saady, Bazan, Zendeboudi, Al-nayili, et al., 2023; Pooi & Ng, 2018). Third, POU systems can be tailored to specific contaminants (M. Wang, Mohanty, et al., 2019), such as arsenic. In contrast to the large-scale centralized water treatment plants, POU units function with lower water flow rates and are activated only when required by the consumer. Since they are managed by individual users, these systems need to be user-friendly and require minimal maintenance (Ewy et al., 2022). In 2020, the decentralized water treatment market was valued at USD 21.45 billion, with projections indicating it would grow at a compound annual growth rate (CAGR) of 10.70% between 2020 and 2026, ultimately reaching USD 39.48 billion (*Decentralized Water Treatment Market | Size, Growth | 2021-26*, n.d.).

In American Indian communities, The Strong Heart Water Study (SHWS) aimed to reduce arsenic exposure among private well users by installing point-of-use (POU) arsenic filters (Multipure® (Model CB-As-SB)) in kitchen sinks and providing health communication programs (Zacher et al., 2023). Over two years, 93% of the filters effectively reduced arsenic levels below the maximum contaminant level (MCL) of 10 $\mu\text{g L}^{-1}$ despite less than half of the households changing their filter cartridges within the recommended time frame (Zacher et al., 2023). Another study found that 43% of homeowners installed POU arsenic filters 3–7 years after being informed that their well water contained arsenic levels above 10 $\mu\text{g L}^{-1}$, while 30% adopted other mitigation strategies, and 27% took no action. A 15% of these treatment units failed to reduce

arsenic levels below the $10 \mu\text{g L}^{-1}$ threshold, suggesting that risks of exposure persist even after a decision is made to implement treatment (Flanagan et al., 2015). Researchers also demonstrated the effectiveness of household arsenic treatment systems in southern-central Maine and northern New Jersey, with point-of-use reverse-osmosis (POU RO) systems in Maine reducing arsenic levels from a mean of 105 to $14.3 \mu\text{g L}^{-1}$, and dual-tank point-of-entry (POE) systems in New Jersey lowering levels from a mean of 15.8 to $2.1 \mu\text{g L}^{-1}$. Although 19% of systems in Maine and 16% in New Jersey failed to meet regulatory standards, the reductions in arsenic led to a significant decrease in skin cancer risk—from 3765 to 514 per million in Maine and from 568 to 75 per million in New Jersey (Q. Yang et al., 2020). These results underscore that any improvement in arsenic removal significantly reduces cancer risk. This underscores the need for ongoing research to develop more effective POU systems for arsenic removal. This highlights a critical need for further research to develop more effective POU systems for arsenic removal.

This study investigates using modified calcined mussel shells for arsenic (III and V) removal in flow-through systems, with a focus on species-specific adsorption. This research emphasizes the different adsorption behaviors of arsenite (As(III)) and arsenate (As(V)) in continuous systems, which more accurately simulate real-world conditions, and offers a comprehensive view of the practical applications of these modified shells by analyzing breakthrough curves, reusability, and the impact of co-ions. Additionally, the research extends to point-of-use (POU) cartridges, assessing their effectiveness in treating groundwater. Thus, the primary objectives are to assess the adsorption of As(III) and As(V) in continuous flow systems, evaluate the reusability of the modified adsorbent, and analyze the effect of co-existing ions on arsenic adsorption, while comparing the performance of the developed adsorbent with that of commercial carbon

cartridges using natural groundwater. When introducing a new adsorbent, particularly for a well-established application like water treatment, it is crucial to compare it to existing, commonly used materials. This comparative analysis highlights the potential of modified calcined mussel shells as a viable alternative in real-world water treatment systems. The significance of this research lies in its potential to bridge the gap between laboratory research and field applications.

4.2. Materials and Methods

4.2.1. Materials

Calcined mussel shells modified with iron oxide nanoparticles (IO-CMS) were used as an adsorbent, and their preparation and characterization were detailed in chapter three. For the initial phase of the study, arsenic solutions were prepared using sodium hydrogen arsenate (A&C American Chemicals Ltd., Quebec, Canada) and sodium arsenite (Sigma-Aldrich, USA) dissolved in deionized water. Real water samples directly sourced from wells in a Newfoundland community were employed for part two of this study.

4.2.2. Part I: flow-through experiments in glass columns

The fixed-bed column studies were carried out at room temperature in a column made of Pyrex glass (Figure 4-1) with an internal diameter of 38 mm and a height of 300 mm. A known amount of the developed adsorbent (5 or 10 g) was packed in the column. Inert beads were placed at the bottom and top of the adsorbent. Glass wool and glass beads were employed at the bottom and top of the column to support the bed. First, deionized water was passed through the column, and then, A solution with a known initial concentration (10 or 50 mg L⁻¹) at pH 6 was passed through the bed at various flowrates (5 and 10 mL min⁻¹) regulated by the peristaltic pump. Samples were gathered

at various time intervals for up to 6 h. The ion concentration in the samples was measured by ICP-MS.

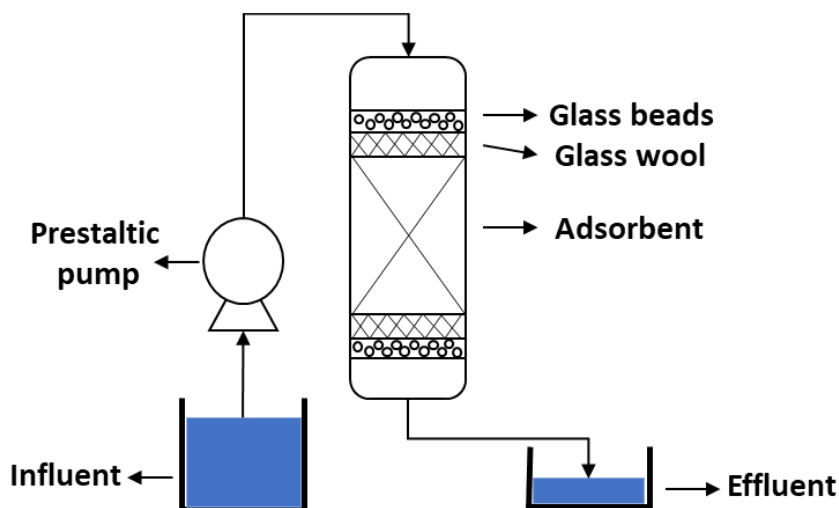


Figure 4-1 Schematic of the column apparatus.

4.2.2.1. Breakthrough curve Studies

The determination of the exhaustion capacity of the column was carried out by plotting a dimensionless number (C_t/C_0) as a function of time. C_t is the As concentration of the effluent at time t , while C_0 is the concentration of the feed solution (Mohsen & Ghanim, 2024). The breakthrough curves for two initial concentrations of 10 mg L^{-1} (As(III): 50%, As(V): 50%) and 50 mg L^{-1} (As(III): 50%, As(V): 50%), two different flowrates (5 and 10 mL min^{-1}), and two different adsorbent amounts (5 and 10 g) were plotted. The column is considered saturated when the effluent concentration is close to 100% of C_0 .

Thomas model is a widely used approach in adsorption studies, particularly for predicting the breakthrough behavior of adsorbates in a fixed-bed column. This model is based on the Langmuir isotherm and considers the kinetics of adsorption as a second-order reversible reaction. The Thomas model is described by Eq. (4-1) (López-

Cervantes et al., 2018; W. Wang, Li, et al., 2015).

$$\frac{C_t}{C_0} = \frac{1}{1 + e^{(K_{Th}(q_0 M - C_0 t)/F)}} \quad (4-1)$$

where C_t is the effluent concentration at time t , C_0 is the initial concentration, K_{Th} is the Thomas rate constant, q_0 is the maximum adsorption capacity, M is the mass of the adsorbent, and F is the flowrate.

The Yoon-Nelson model is another empirical approach used to describe the adsorption breakthrough curves in fixed-bed adsorption systems. This model simplifies the prediction of the breakthrough time without needing detailed information about the adsorbent's characteristics or the adsorption mechanism. The Yoon-Nelson equation is given by Eq. (4-2) (Biswas & Mishra, 2015; Vera et al., 2019).

$$\frac{C_t}{C_0} = \frac{1}{1 + e^{(K_{YN}(t-\tau))}} \quad (4-2)$$

where C_t is the effluent concentration at time t , C_0 is the initial concentration, K_{YN} is the Yoon-Nelson rate constant, and τ is the time required for 50% of the adsorbate to be adsorbed (Ansari et al., 2021). This model assumes that the rate of decrease in the probability of adsorption for each adsorbate molecule is proportional to the probability of adsorption (S. Mohan et al., 2017).

4.2.2.2. Arsenic uptake in the presence of co-ions

The effectiveness of the adsorbent in multi-ion systems was investigated to determine its selectivity, as single-ion systems are typically uncommon. The most common anions found in water, such as Cl^- , SO_4^{2-} , NO_3^- , HCO_3^- , and PO_4^{3-} , were used for this test. Water (pH 6) containing 50 mg L⁻¹ of arsenic and co-ions, each equal to the total arsenic concentration, was passed through the column to evaluate the effect of co-ions. The initial equal quantities of coexisting ions and arsenic were selected to

assess the impact of competition. A higher concentration of one ion would have resulted in greater interaction with the adsorbent. This experiment was conducted at 5 mL min^{-1} using 10 g of adsorbent. The concentration of arsenic ions in the treated solution was measured over time for up to 6 h.

4.2.2.3. Adsorbent reusability

To conduct reusability tests, the adsorbent containing absorbed arsenic ions was treated with 0.1 N NaOH, which was passed through the column at a flowrate of 5 mL min^{-1} for 6 h. Afterward, the column was washed with distilled water at the same flowrate for an additional 8 h. The exhaustion capacity was measured after each cycle of the reusability tests, which were carried out five times. This experiment was conducted at 5 mL min^{-1} using 10 g of adsorbent while solutions containing 50 mg L^{-1} arsenic were passed through the column.

4.2.3. Part II: comparative arsenic removal in point of use cartridges

4.2.3.1. Preparation of cartridges

Figure 4-2 depicts the preparation of three different cartridges for part II of the study. Filter cartridges for water, measuring $9\text{-}3/4"$ (247.65 mm) high, $2\text{-}1/2"$ (63.5 mm) OD, and $2\text{-}3/8"$ (60.325 mm) ID, were used to prepare three different cartridges. A 3-Stage Under Sink Water Filtration System for drinking was purchased, and the carbon block filter was cut into 0.5 cm discs, with 10 g of these used in the test, referred to as the carbon (AC) cartridge. The sediment filter was cut into 0.5 cm discs to be coated with 10 g of mussel shell powder adsorbent (MD cartridge). Additionally, 10 g of the developed adsorbent from mussel shell powder, without further processing, was placed in another filter cartridge (MP cartridge). Each cartridge was filled with inert material to ensure a consistent volume and facilitate adsorption. The cartridge was placed in the

water filtration system without any prior or further filtration units, while the other two units of the filtration system were kept empty.

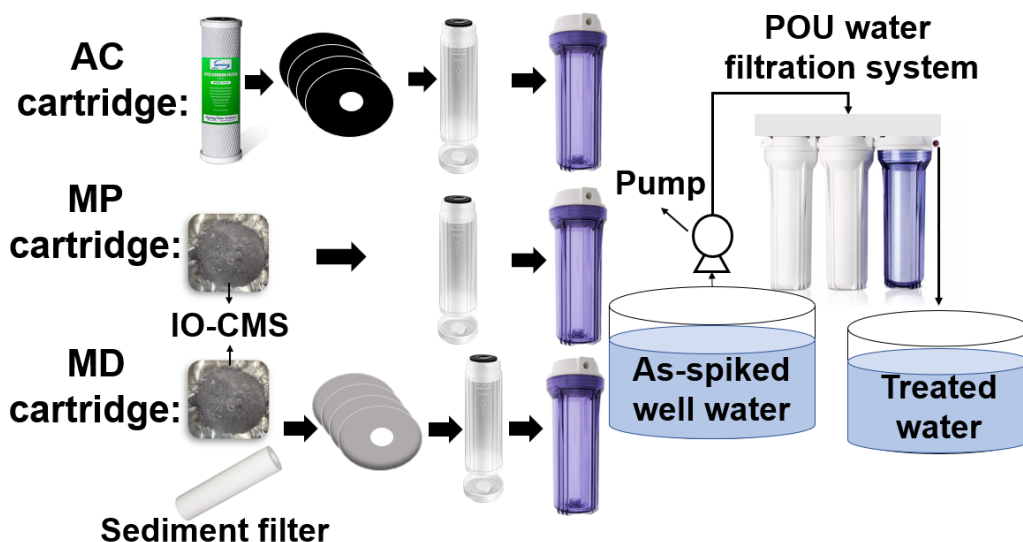


Figure 4-2 Preparation of three different cartridges (AC=Activated Carbon, MP= Mussel shell Powder, and MD= Mussel shell-coated Disc) for Part II of the study.

4.2.3.2. Adsorption-desorption

The water flowrate was set to 1 L h^{-1} . Each cartridge treated a maximum of 10 L of arsenic-spiked well water with an initial concentration of 300 ug L^{-1} . Table 4-2 provides the well water characteristics. Treated water samples were collected every hour during the filtration process to monitor the arsenic concentration over time. After 10 h of adsorption, a 0.1 M NaOH solution was employed for the desorption process. Desorption was conducted for 10 h, with samples taken every hour. For the analysis of both adsorption and desorption processes, graphs depicting the breakthrough curves will be generated by plotting the ratio of the concentration (C_e) to the initial concentration (C_i) against the bed volume.

Table 4-2 Well water characteristics (in mg L⁻¹ unless indicated otherwise).

Parameter	Concentration	Parameter	Concentration
Conductivity ($\mu\text{S cm}^{-1}$)	250	Turbidity (NTU)	0.17
Alkalinity	96	Sulphate	4.9
Hardness	85	Aluminum	0.0057
pH	8.08	Dissolved organic carbon	0.91
Total dissolved solids	140	Arsenic	0.028
Potassium	0.57	Barium	0.42
Calcium	27	Copper	0.021
Chloride	17	Magnesium	4.1
Sodium	18	Uranium	0.0071

4.3. Results and Discussion

4.3.1. Part I: flow-through experiments in glass columns

4.3.1.1. Breakthrough curve studies

Breakthrough curves illustrate the concentration of adsorbate in the effluent relative to the time or volume of influent passed through the adsorption system, allowing us to evaluate the adsorbent's efficiency and capacity. The breakthrough point is typically defined as the time or volume at which the effluent concentration reaches a predetermined fraction of the influent concentration, indicating that the adsorbent is becoming saturated and is no longer effectively removing the adsorbate from the solution (Apiratikul & Chu, 2021; Futralan & Wan, 2022).

This study investigated the breakthrough curves for arsenic adsorption at two different initial concentrations: 10 mg L⁻¹ (Figure 4-3a, Figure 4-3d, and Figure 4-3g) and 50 mg L⁻¹ (Figure 4-4a, Figure 4-4d, and Figure 4-4g). The effects of varying flowrates and adsorbent masses were also examined.

For initial arsenic concentrations of 10 and 50 mg L⁻¹, the breakthrough curves (Figure 4-3g, and Figure 4-4g) for an adsorbent mass of 10 g and a flow rate of 5 mL min⁻¹ displayed more gradual slopes and a broader saturation zone compared to other conditions. This suggests that a higher adsorbent mass and lower flowrate allow for

more effective arsenic removal due to increased contact time between the arsenic solution and the adsorbent and a larger surface area for adsorption. Similarly, a study of Mn(II) ion removal from wastewater using Mangosteen (*Garcinia mangostana*) peel-based granular-activated carbon found that a low flowrate and high bed height resulted in a longer time to reach breakthrough and exhaustion (Apiratikul & Chu, 2021). Conversely, the breakthrough (Figure 4-3g, and Figure 4-4g) for 5 g adsorbent mass at a flowrate of 10 mL min⁻¹ occurred much earlier, indicating rapid saturation of the adsorbent and less efficient arsenic removal. This can be attributed to the reduced adsorbent surface area and shorter contact time under these conditions (X. Lin et al., 2017). This finding aligns with a study that investigated bed heights from 3 to 9 cm, using optimal pH, a constant arsenate concentration of 1,000 µg L⁻¹, and a flow rate of 3.0 mL min⁻¹. The breakthrough curves for As(V) adsorption on iron-loaded *Azadirachta indica* (Fe-AIR) demonstrated that larger bed heights allow more time for Fe-AIR to interact with As(V), enhancing the diffusion of As(V) ions and increasing the adsorption capacity. Additionally, the study explored the influence of flow rate by varying it from 3.0 to 9.0 mL min⁻¹ while keeping the arsenate concentration, bed height, and pH constant. It was observed that higher flow rates resulted in quicker breakthrough times (Sawood & Gupta, 2020). While the breakthrough curves for total arsenic provide valuable insights, it is important to consider the speciation of arsenic in the adsorption process. Arsenic exists primarily in two oxidation states: As(III) and As(V) (X. Lin et al., 2017). The affinity of the adsorbent for each species can vary, and the possibility of arsenic oxidation during the experiment cannot be ruled out, as research indicates that As(III) can slowly oxidize to As(V) in the presence of air (G. Ungureanu et al., 2015). For instance, arsenite oxidation with oxygen and air was examined in groundwater containing 46–62 µg L⁻¹ of total dissolved arsenic, 100–1130

$\mu\text{g L}^{-1}$ of iron, and 9–16 $\mu\text{g L}^{-1}$ of manganese. After five days, 57% of As(III) was oxidized with pure oxygen and 54% with air (Kim & Nriagu, 2000). Similarly, 25% oxidation occurred within five days, when a solution containing 200 $\mu\text{g L}^{-1}$ of As(III) was purged with air (Clifford et al., 1983). In another study, purging with pure oxygen resulted in 8% oxidation within 60 min (Frank & Clifford, 1986), and in another case, 19% of As(III) was oxidized within 15 min in water containing 69 $\mu\text{g L}^{-1}$ of As(III) using pure oxygen (Böckelen & Niessner, 1992). This oxidation could lead to changes in the speciation of arsenic, potentially affecting the adsorption behavior and the observed patterns in the breakthrough curves. For As(III), a similar trend was observed as that of total arsenic. The adsorbent mass of 10 g at a flowrate of 5 mL min^{-1} consistently outperformed the other configurations, while the 5 g adsorbent mass at a flowrate of 10 mL min^{-1} showed the poorest performance. However, the breakthrough curves for As(V) showed that the flowrates and adsorbent masses had a lower impact.

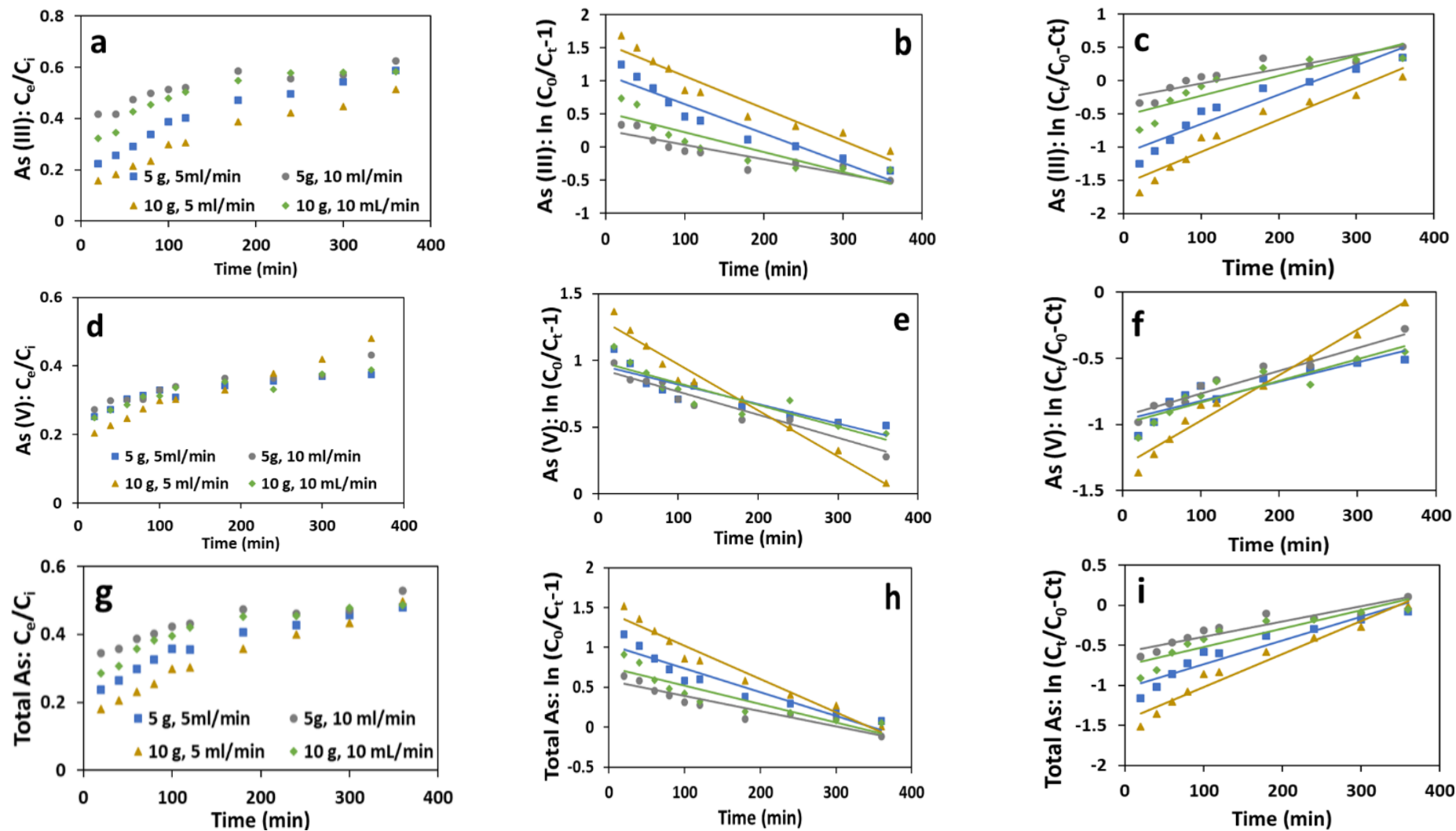


Figure 4-3 Breakthrough curves of a) As(III), d) As(V), and g) total As; Thomas linear plots of b) As(III), e) As(V), and h) total As; Yoon-Nelson plots of c) As(III), f) As(V), and i) total As (10 mg L⁻¹).

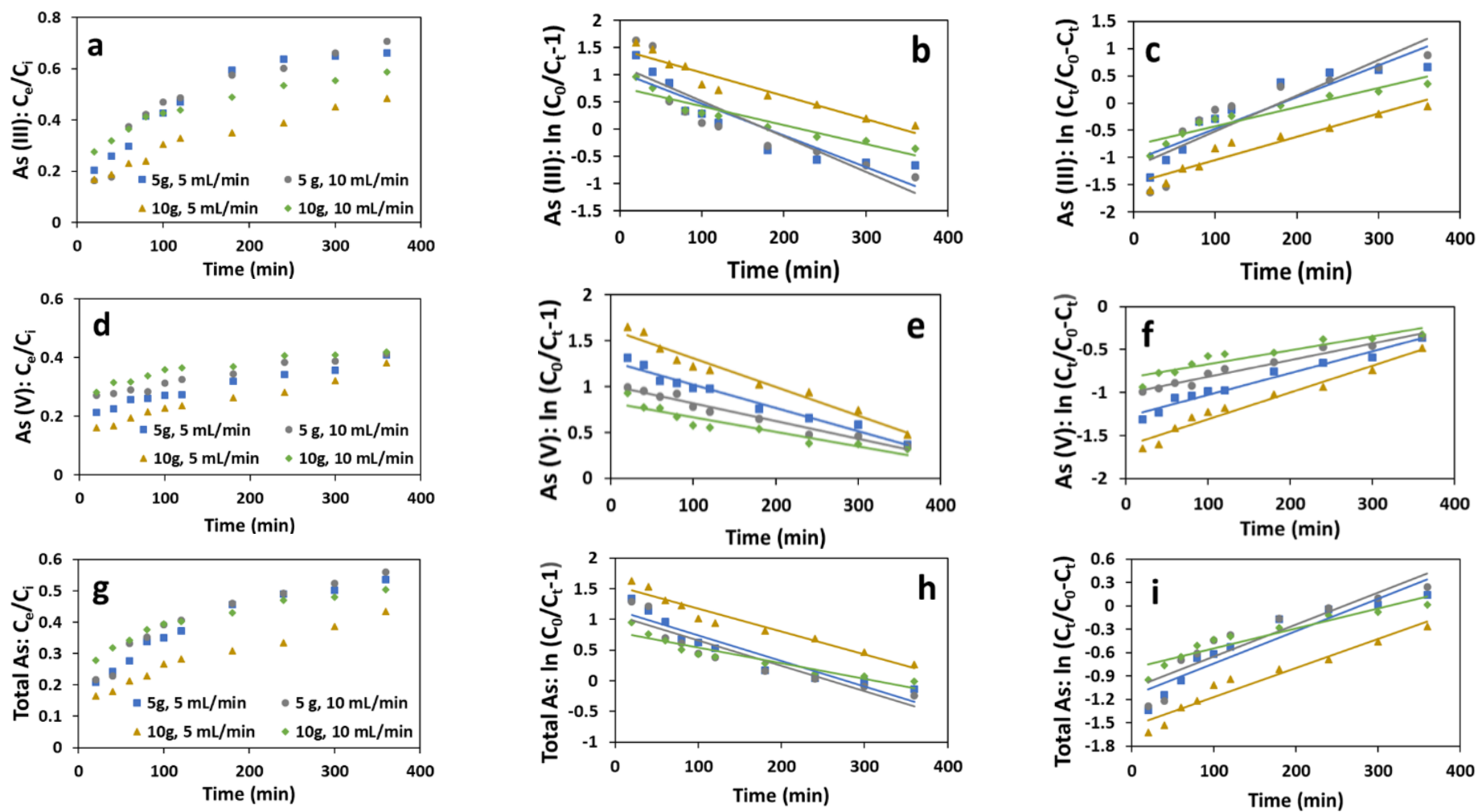


Figure 4-4 Breakthrough curves of a) As(III), d) As(V), and g) total As; Thomas linear plots of b) As(III), e) As(V), and h) total As; Yoon-Nelson plots of c) As(III), f) As(V), and i) total As (50 mg L⁻¹).

4.3.1.2. Thomas model

Figure 4-3b, Figure 4-3e, and Figure 4-3h (10 mg L⁻¹) and Figures Figure 4-4b, Figure 4-4e and Figure 4-4h (50 mg L⁻¹) illustrate fitting the breakthrough curves to Thomas model. The model provides a good fit for the experimental data, indicating that it can reliably describe the adsorption process under the tested conditions.

Table 4-3 presents the calculated Thomas model parameters, including the adsorption rate constant (K_{Th}) and the maximum adsorption capacity (q_0). The maximum adsorption capacity from the Thomas model (Table 4-3) indicates that the q_0 for As(V) (1.0–3.2 mg g⁻¹ and 6.5–26.6 mg g⁻¹ at initial concentrations of 10 and 50 mg L⁻¹, respectively) is higher than that for As(III) (0.8–1.2 mg g⁻¹ and 4.3–9.0 mg g⁻¹ at initial concentrations of 10 and 50 mg L⁻¹, respectively) under various conditions. This suggests that the adsorbent has a higher affinity and capacity for As(V) compared to As(III). The higher As(V) adsorption might be attributed to the electrostatic attraction between the positively charged adsorbent surface and negatively charged arsenate ($H_2AsO_4^-$, $HAsO_4^{2-}$) species. Arsenate (As(V)) exists as a negatively charged species in aqueous solutions across a wide pH range. Conversely, As(III) exists primarily as the neutral species $H_3AsO_3^\circ$ in the pH range of 3–10.5, making it less susceptible to electrostatic interactions (Kumar & Jiang, 2016).

Additionally, q_0 is higher for each species and total arsenic for the initial concentration of 50 mg L⁻¹ compared to 10 mg L⁻¹. This increase in q_0 with higher initial concentration indicates that the adsorption capacity of the adsorbent improves with increased arsenic concentration. This can be explained by the greater driving force for mass transfer at higher concentrations, which enhances the adsorption process (J. Fu et al., 2015). The higher concentration gradient between the solution and the adsorbent surface facilitates faster and more efficient adsorption until the adsorbent sites reach

saturation (W. Wang, Tian, et al., 2015). A similar trend was observed in arsenate adsorption from aqueous solutions using Fe-AIR root, where increasing the influent arsenic concentration enhanced the As(V) uptake capacity (Futalan & Wan, 2022).

An increase in flow rate resulted in a higher maximum adsorption capacity (q_0), likely due to improved mass transfer and reduced external film diffusion resistance (Futalan & Wan, 2022; Vasyliiev, 2015). Similarly, in the case of Cd(II), the adsorption capacity at the 50% breakpoint increased from 1.15×10^{-3} to 1.82×10^{-3} mmol g⁻¹ as the flow rate increased from 10 to 30 mL min⁻¹, with a comparable effect observed for Pb(II) sorption. In another study investigating the continuous flow sorption of heavy metals in a biomass (rice straw)-packed column (Soetaredjo et al., 2014), or in a different study, as the flow rate increased from 2.33 to 3 mL min⁻¹, a corresponding increase in adsorption capacity from 1.55 to 3.14 mg g⁻¹ was observed in the modeling of fixed-bed continuous column adsorption of amoxicillin onto a silver nanoparticle-maize leaf composite (Omitola et al., 2022).

On the other hand, increasing the adsorbent mass resulted in a reduction in q_0 . Similarly, in a study on the adsorption of hexavalent chromium (Cr(VI)) using modified corn stalks, the bed depth significantly affected the Cr(VI) uptake, with capacities of 175, 135, and 134 mg g⁻¹ at depths of 1.4, 2.2, and 2.9 cm, respectively (S. Chen et al., 2012). At higher bed heights, mass transfer limitations can prevent the adsorbate from effectively diffusing throughout the entire bed, leading to incomplete saturation of the adsorbent. This underutilization of active sites results in a decrease in the adsorption capacity, despite the larger amount of adsorbent material available.

Table 4-3 Thomas parameters for various configurations: Flowrates, adsorbent masses, and initial concentrations.

C_0	M (g)	F (mL min ⁻¹)	$K_{Th} \times 10^4$ (L mg ⁻¹ min ⁻¹)	q_0 (mg g ⁻¹)	R ²		
10	As(III)	5	5	8.80	1.2493	0.87	
		5	10	4.40	1.1623	0.83	
		10	5	9.80	0.7959	0.92	
		10	10	6.00	0.8808	0.83	
	As(V)	5	5	3.00	3.22765	0.82	
		5	10	3.40	5.5253	0.97	
		10	5	6.80	0.9669	0.82	
		10	10	3.20	3.1084	0.92	
	Total	5	5	3.00	3.44235	0.90	
		5	10	1.90	6.1116	0.95	
		10	5	4.10	1.74745	0.90	
		10	10	2.3	3.263	0.88	
	50	As(III)	5	5	2.32	4.54785	0.79
			5	10	2.60	8.9908	0.88
			10	5	1.72	4.3218	0.91
			10	10	1.40	5.525	0.79
As(V)		5	5	1.00	12.763	0.82	
		5	10	0.76	26.6079	0.86	
		10	5	1.24	6.53225	0.94	
		10	10	0.64	12.9547	0.96	
Total		5	5	0.82	14.05365	0.81	
		5	10	0.82	25.9732	0.91	
		10	5	0.74	10.4277	0.94	
		10	10	0.50	15.99	0.85	

M = adsorbent mass; F = flowrate.

4.3.1.3. Yoon-Nelson model

Figure 4-3c, Figure 4-3f, Figure 4-3i (10 mg L⁻¹) and Figure 4-4c, Figure 4-4f, and Figure 4-4i (50 mg L⁻¹) display the Yoon-Nelson plots. Table 4-4 provides Yoon-Nelson parameters for the various configurations studied.

Increasing the flowrate from 5 to 10 mL min⁻¹ resulted in a decrease in the kinetic rate constant (K_{YN}) and 50% breakthrough time (τ). A higher flowrate accelerates the fluid movement through the adsorption column, reducing the adsorbate-adsorbent contact time, and leading to a shorter breakthrough time (W. Zhang et al., 2011).

Likewise, in the microwave-assisted economic synthesis of multi-walled carbon nanotubes for arsenic species removal in water, increasing the flow rate from 30 to 40 mL min⁻¹ reduced the exhaustion time from 110 to 55 min (I. Ali, 2018).

Conversely, increasing the adsorbent mass from 5 to 10 g typically extended the breakthrough time. A larger adsorbent mass provides more adsorption sites for the adsorbate molecules. Similarly, in the study of arsenate adsorption from aqueous solutions using Fe-AIR, increasing the bed height from 3 to 9 cm extended the breakthrough time from 135.30 to 388.03 min (Sawood & Gupta, 2020).

Finally, an increase in initial concentration from 10 to 50 mg L⁻¹ decreased breakthrough time but increased K_{YN} . With a higher concentration, the adsorbent reached its saturation point more rapidly as the available adsorption sites were filled up quickly (Abbas et al., 2015). This resulted in a shorter breakthrough time compared to lower concentrations. This is consistent with a study that found the removal of arsenate and arsenite from aqueous solutions using organic-modified spent grains K_{YN} increased, while τ decreased with higher initial arsenic concentrations (Yunnen et al., 2017).

In comparing the results of this study with other flow-through studies on arsenic removal, the Thomas and Yoon-Nelson model parameters are summarized in Table 4-5. The q_0 values from our experiments, being comparable to those in other studies, along with favorable 50% breakthrough times (τ), demonstrate the effectiveness of the developed adsorbent.

Table 4-4 Yoon-Nelson parameters for various configurations: Flowrates, adsorbent masses, and initial concentrations.

C_0 (mg L ⁻¹)		M (g)	F (mL min ⁻¹)	$K_{YN} \times 10^3$ (min ⁻¹)	τ (min)	R ²
10	As(III)	5	5	4.4	249.86	0.92
		5	10	2.2	116.23	0.83
		10	5	4.9	318.37	0.93
		10	10	3.0	176.17	0.8
	As(V)	5	5	1.5	645.53	0.82
		5	10	1.7	552.53	0.92
		10	5	3.4	386.76	0.97
		10	10	1.6	621.75	0.82
	Total	5	5	3.0	344.23	0.9
		5	10	1.9	305.58	0.88
		10	5	4.1	349.49	0.95
		10	10	2.3	326.30	0.81
50	As(III)	5	5	5.8	181.91	0.85
		5	10	6.5	179.82	0.8
		10	5	4.3	345.74	0.91
		10	10	3.5	221	0.9
	As(V)	5	5	2.5	510.52	0.96
		5	10	1.9	532.16	0.96
		10	5	3.1	522.58	0.94
		10	10	1.6	518.19	0.87
	Total	5	5	4.1	281.07	0.89
		5	10	4.1	259.73	0.85
		10	5	3.7	417.11	0.94
		10	10	2.5	319.8	0.89

M = adsorbent mass; F = flowrate.

Table 4-5 Summary of Thomas and Yoon-Nelson model parameters from various flow-through studies on arsenic removal using different adsorbents.

Adsorbent	C_i (mg L ⁻¹)	F (mL min ⁻¹)	H (cm)/ M (g)	$K_{Th} \times 10^4$ (L mg ⁻¹ min ⁻¹)	q_0 (mg g ⁻¹)	$K_{YN} \times 10^3$ (min ⁻¹)	τ (min)	Reference
IO-CMS	10	10	5 g	1.90	6.12	1.9	305.6	This study
	50	10		0.82	25.97	4.1	259.7	
Graphene oxide	10	1	16.5 cm	0.51	27.73	-	-	(Abbasi et al., 2021)
MnFe ₂ O ₄	0.05	1000	40 g	0.642	228.00	-	-	(Z. Qi et al., 2018)
Natural pozzolan	0.40	1.4	30 g	950	4.42	-	-	(Kofa et al., 2015)
Chitosan	120	2.0	13 cm	2.18	46.50	26.1	446.5	(Brion-Roby et al., 2018)
Copper-impregnated natural mineral tufa	0.989	2.3	12 cm	451	55.40	36.9	129.0	(Pantić et al., 2019)
Iron-Zirconium Binary Oxide- Coated Sand	125	4	5 g	1.336	25.09	16.7	250.9	(Chaudhry et al., 2017)
Granular chitosan	0.15	5	27.5 g	16	52.70	33.5	6.4	(Zeng et al., 2021)
K-OMS2-ceramic	1	10	45.5 g	0.051	11.97	6.3	393.5	(Khamdahsag et al., 2021)
Chitosan-Magnetite Hydrogel Beads	5	0.22	13 cm	0.079	104.00	3.5	1152.5	(Mendizabal et al., 2023)

C_i = initial concentration; F = flowrate; H = bed height; M = adsorbent mass.

4.3.1.4. Arsenic uptake in the presence of co-ions

The impact of co-ions on arsenic adsorption was evaluated by examining the breakthrough curves and Thomas and Yoon models, as shown in Figure 4-5. The breakthrough curves for the total arsenic with and without co-ions are not significantly different, suggesting that while co-ions have some impact on total arsenic adsorption, this impact is not substantial. A study on the competitive effects of various anions on arsenic (As(V)) adsorption using Mg-Fe-(CO₃) LDH (layered double hydroxide) indicated that nitrate (NO₃⁻) had a minimal inhibitory effect on As(V) removal, while chloride (Cl⁻) and sulfate (SO₄²⁻) exhibited more significant negative impacts (Yadav et al., 2021). Phosphate (PO₄³⁻) and carbonate (CO₃²⁻) posed the most substantial challenges to As(V) adsorption. The overall inhibitory order was determined as NO₃⁻ < Cl⁻ < SO₄²⁻ < CO₃²⁻ < PO₄³⁻ (Yadav et al., 2021).

At pH 6, the surface charge of adsorbents like Iron Oxide Nanoparticles (Fe₃O₄) and Calcined Mussel Shells (CMS) is positive, primarily due to the protonation of surface hydroxyl groups. For Fe₃O₄, the hydroxyl groups (Fe-OH) on the surface become protonated to form Fe-OH₂⁺ at lower pH, giving the surface a positive charge. Similarly, in CMS, which is predominantly made of calcium oxide (CaO), the surface contains calcium hydroxide groups (Ca-OH). These groups are also protonated at pH 6, forming Ca-OH₂⁺ and contributing to a positively charged surface. This protonation and the positive surface charge facilitate electrostatic interactions with negatively charged species in the solution, including coexisting ions and contaminants like arsenate. Coexisting ions in the solution influence arsenic adsorption based on their charge properties. Chloride (Cl⁻) and nitrate (NO₃⁻), both monovalent anions, remain negatively charged at pH 6. Bicarbonate (HCO₃⁻) ions, also negatively charged at pH 6, carry a charge of -1. Sulfate (SO₄²⁻), a divalent anion, carries a charge of 2-.

Phosphate (PO_4^{3-}), a polyatomic anion, carries a charge of 3- at pH 6, making it more highly charged compared to the other ions in the solution. Additionally, NO_3^- and Cl^- are monovalent and have a lower ionic potential, leading to weaker competition with As(V) for adsorption (Hongtao et al., 2018; Yadav et al., 2021). Furthermore, the ionic radius of phosphate (0.17 Å) is considerably smaller than that of As(V) (0.36 Å), resulting in a stronger charge density driving force that enhances phosphate's competitive ability for adsorption sites (Lee et al., 2018).

Phosphate (PO_4^{3-}) and arsenate (As(V)) share similar structural characteristics, both having a tetrahedral configuration (Bazán et al., 2003) with a central atom (P or As) surrounded by four oxygen atoms, as shown in Figure 6. This structural similarity, combined with their high charge density (both ions carry a charge of -3), enables phosphate and arsenate to form strong electrostatic interactions with the positively charged surface sites on the adsorbents, particularly the Fe-O and Ca-O groups. The high charge density of these ions allows them to form stable surface complexes (Ding et al., 2019), and this strong interaction gives phosphate and arsenate a higher affinity for the adsorbent surface compared to other coexisting ions. In terms of complexation, phosphate ions compete directly with arsenate ions for adsorption sites on the surface. Both ions can form strong surface complexes with metal oxide surfaces (Dixit & Hering, 2003; Huang et al., 2014; Zeng et al., 2008), such as Fe-O and Ca-O, through ligand exchange and coordination. This results in a significant competition between phosphate and arsenate for available sites on the adsorbent. The XPS results and findings from our previous research (Neisan et al., 2024) further support this, showing shifts in the O 1s and Ca 2p spectra, indicating the formation of surface complexes between both arsenate and phosphate with the metal oxide sites. On the other hand, ions like chloride (Cl^-) and nitrate (NO_3^-), with lower charge densities and different

structural characteristics interact less strongly with the adsorbent surface. Sulfate, while divalent, does not possess the similar charge that matches arsenate or phosphate, and its surface binding is weaker. Nitrate, with its planar structure (Y. Wang et al., 2022), has even less affinity for the surface and competes with arsenate mainly through weaker electrostatic interactions. Despite their negative charge, bicarbonate ions interact weakly with the adsorbent surface due to their ability to form only weak complexes with metal oxides. Chloride ions, as simple monovalent anions (Rudolph & Irmer, 2013), primarily interact with the surface through electrostatic forces and do not form strong complexes. Therefore, their competition with arsenate for adsorption sites is minimal compared to phosphate.

Table 4-6 presents the Thomas and Yoon-Nelson parameters for As adsorption, both with and without co-ions. Thomas model parameters reveal that the q_0 value for total arsenic decreased by 26.94% (from 10.43 to 7.62 mg g⁻¹). For As(V), however, the impact of co-ions is more pronounced. The impact on As(III) adsorption was minimal, with the q_0 decreasing slightly (16.20%) from 4.32 to 3.62 mg g⁻¹. Despite the presence of co-ions, the q_0 value for As(V) remains higher than that for As(III), consistent with the higher affinity of the adsorbent for As(V). The q_0 value decreased significantly (36.18%) from 6.53 to 4.17 mg g⁻¹. This greater reduction can be attributed to the greater affinity of co-ions like SO₄²⁻ and PO₄³⁻ to the adsorption sites, which competes more effectively with As(V) compared to As(III). This effect is also reflected in the trend of decreasing τ with the presence of co-ions. The value of τ for total arsenic decreased from 417.11 to 304.92 min, for As(V) from 522.58 to 333.63 min, and for As(III) from 345.74 to 289.32 min. These reductions, particularly the significant decrease for As(V), highlight the competitive effect of co-ions, which is more pronounced for As(V). Similarly, it was found that none of the anions (Cl⁻, NO₃⁻, SO₄²⁻, HCO₃⁻) significantly

interfered with the removal of As(III) and As(V) by nanocomposites named CCA and CZA that were prepared by the incorporation of cellulose (CL) in the Ca/Al and Zn/Al layered double hydroxide (LDH). However, PO_4^{3-} reduced the removal efficiency of As(III) and As(V) to 8% and 15% for CCA, and 10% and 19% for CZA, respectively (Bessaies et al., 2020).

Table 4-6 Thomas and Yoon-Nelson parameters for arsenic adsorption with or without co-ions (Cl^- , SO_4^{2-} , NO_3^- , HCO_3^- , and PO_4^{3-}).

Process parameters	Species		$K_{Th} \times 10^4$ ($\text{L mg}^{-1} \text{ min}^{-1}$)	q_0 (mg g^{-1})	R^2
$C_i = 50 \text{ mg L}^{-1}$, $M = 10 \text{ g}$, $F = 5 \text{ mL min}^{-1}$	As(III)	Blank	1.72	4.32	0.91
		Co-ions	3.12	3.62	0.83
	As(V)	Blank	1.24	6.53	0.94
		Co-ions	1.28	4.17	0.92
	Total	Blank	0.74	10.43	0.94
		Co-ions	1.02	7.62	0.9
Process parameters			$K_{YN} \times 10^3$ (min^{-1})	τ (min)	R^2
$C_i = 50 \text{ mg L}^{-1}$, $M = 10 \text{ g}$, $F = 5 \text{ mL min}^{-1}$	As(III)	Blank	4.3	345.74	0.91
		Co-ions	7.8	289.32	0.83
	As(V)	Blank	3.1	522.58	0.94
		Co-ions	3.2	333.63	0.92
	Total	Blank	3.7	417.11	0.94
		Co-ions	5.1	304.92	0.9

C_i = initial concentration, M = adsorbent mass; F = flowrate.

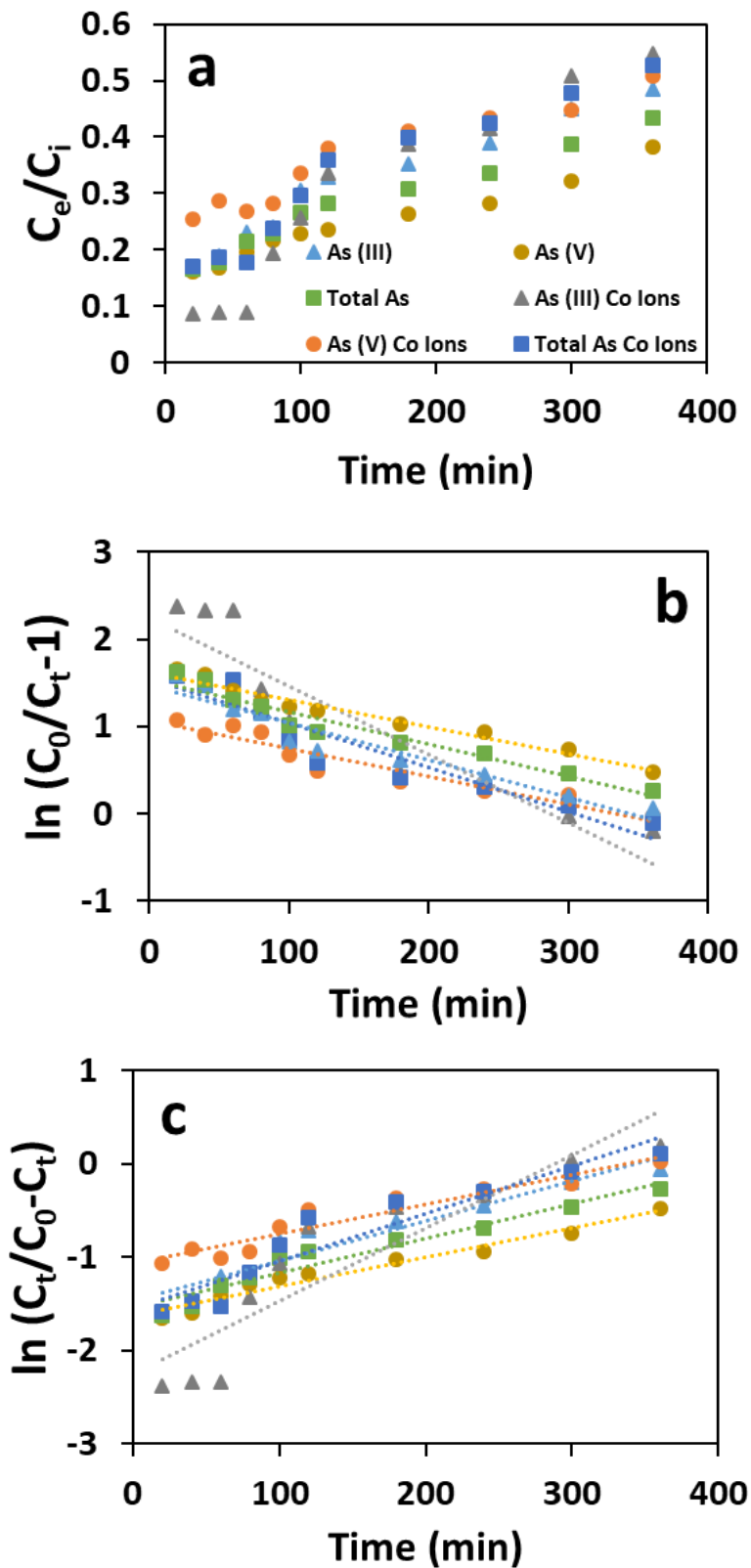


Figure 4-5 Arsenic adsorption with or without co-ions (Cl^- , SO_4^{2-} , NO_3^- , HCO_3^- , and PO_4^{3-}). a)

Breakthrough curves; b) Thomas linear plots; and c) Yoon-Nelson plots.

Iron oxide modification of calcined mussel shells increases the surface affinity of the adsorbent for anions like As(V). The iron oxide provides more active sites that preferentially bind with negatively charged species. Co-ions with similar charges (such as SO_4^{2-} and PO_4^{3-}) can compete effectively for these sites, leading to greater competition for As(V). Co-ions with similar or higher charge densities can, therefore, compete more effectively for adsorption sites, reducing the adsorption efficiency for As(V). Iron oxide can form strong complexes with As(V), enhancing its adsorption. However, co-ions such as phosphate and sulfate can also form strong complexes with iron oxide (Hinkle et al., 2015; J. Liu et al., 2021), leading to significant competition for these complexation sites. Overall, the competition for adsorption sites on the adsorbent surface is strongly influenced by the ions' charge density and structural similarity. Phosphate (PO_4^{3-}) and arsenate (As(V)), with their high charge densities and tetrahedral structures, exhibit the strongest affinity for adsorption sites on the positively charged Fe-O and Ca-O sites of the adsorbent. These ions form stable surface complexes, competing directly with each other. As a result, the presence of these co-ions can substantially reduce the available sites for As(V) adsorption. The Yoon model parameters further support these findings.

Competition from coexisting ions, particularly phosphate (PO_4^{3-}), is a common challenge in arsenic removal since phosphate shares similar chemical properties with arsenate (As(V)) and competes for the same adsorption sites. While phosphate (PO_4^{3-}) can indeed compete with arsenic for binding sites on the adsorbent, it is crucial to recognize that phosphate is a significant pollutant in groundwater (Abdelwaheb et al., 2019). Phosphate contamination is often associated with agricultural runoff, and its presence in well water can lead to issues like eutrophication and reduced water quality, even if concentrations are not as high as in surface water. Increasing the adsorbent dose

would be an effective solution in real-world groundwater resources with elevated phosphate levels, which could compete with arsenic for adsorption. This approach can ensure the simultaneous removal of arsenic and phosphate. By enhancing the IO-CMS dose, we can address arsenic and phosphate pollution, thereby providing cleaner and safer drinking water. Therefore, while phosphate may reduce the adsorption efficiency of arsenic in certain cases, its removal is equally important for ensuring water safety. Another effective approach is pre-treatment to selectively remove phosphate before arsenic adsorption. This can be achieved through chemical precipitation by adding calcium or aluminum salts to precipitate phosphate or using materials with a higher affinity for phosphate. Also, note that the same concentration of co-existing ions, including phosphate, was used for the tests in this study. In real-world conditions, phosphate concentrations may not be as high as 50 mg/L, but should they approach this level.

4.3.1.5. Adsorbent reusability

General decreases in adsorbent capacity over regeneration are caused by physical wear and tear can lead to physical degradation of the adsorbent material, such as fragmentation or loss of surface area. Additionally, adsorbate particles or regeneration chemicals might clog the adsorbent's pores, reducing its adsorption capacity. The adsorbent may also undergo chemical changes during regeneration that alter its adsorption properties. Regeneration may not fully restore the active sites of the adsorbent, leading to reduced capacity in subsequent cycles. To evaluate the reusability of the adsorbent, breakthrough curves were obtained after four cycles of regeneration (Cycle 1 - Cycle 5). The results (Figure 4-6), indicate that the adsorbent can maintain its capacity over multiple regeneration cycles. The breakthrough curves for each cycle are similar, showing that the adsorbent retains its performance even after repeated use.

The decrease in adsorbent efficiency after regeneration was investigated, and SEM analysis (Figure S4-1) revealed that the regenerated adsorbent's particle size is significantly larger than the virgin material. The scale bar in the SEM image before regeneration is in the micrometer (10 μm) range, whereas after regeneration, it extends to the hundreds of micrometers (up to 500 μm). Since the characterization of the same virgin adsorbent (Figure 3-3) showed that its particle size is around 100 μm , this significant increase in size clearly indicates agglomeration, which likely contributes to the reduction in adsorption efficiency. The agglomeration is attributed to the electrostatic destabilization of the iron oxide nanoparticles in the alkaline medium (0.1 M NaOH). The deprotonation of surface hydroxyl groups in the NaOH solution reduces the repulsive forces between nanoparticles, promoting van der Waals attraction and facilitating their aggregation into larger clusters (Illés & Tombácz, 2006; Shrestha et al., 2020). This results in a reduced surface area and a loss in adsorption capacity. In addition, NaOH exposure impacts the calcined mussel shell matrix, which is composed mainly of calcium oxide and calcium carbonate. The alkaline conditions cause the dissolution of calcium species, converting CaCO_3 into soluble calcium hydroxide (Ca(OH)_2) (Simoni et al., 2022; Whittington, 1996), weakening the structural integrity of the shells and reducing their mechanical strength. The dissolved calcium may reprecipitate, altering the surface structure and further diminishing the material's porosity. If this is the case, the structure of the adsorbent has likely changed, which might be the reason for the reduction in capacity. SEM images indicated a decrease in porosity, suggesting that some pores may have been clogged or collapsed during regeneration, contributing to the diminished efficiency of the adsorbent. These combined effects, including particle agglomeration, structural degradation, and reduced porosity, significantly impact the adsorbent's overall performance.

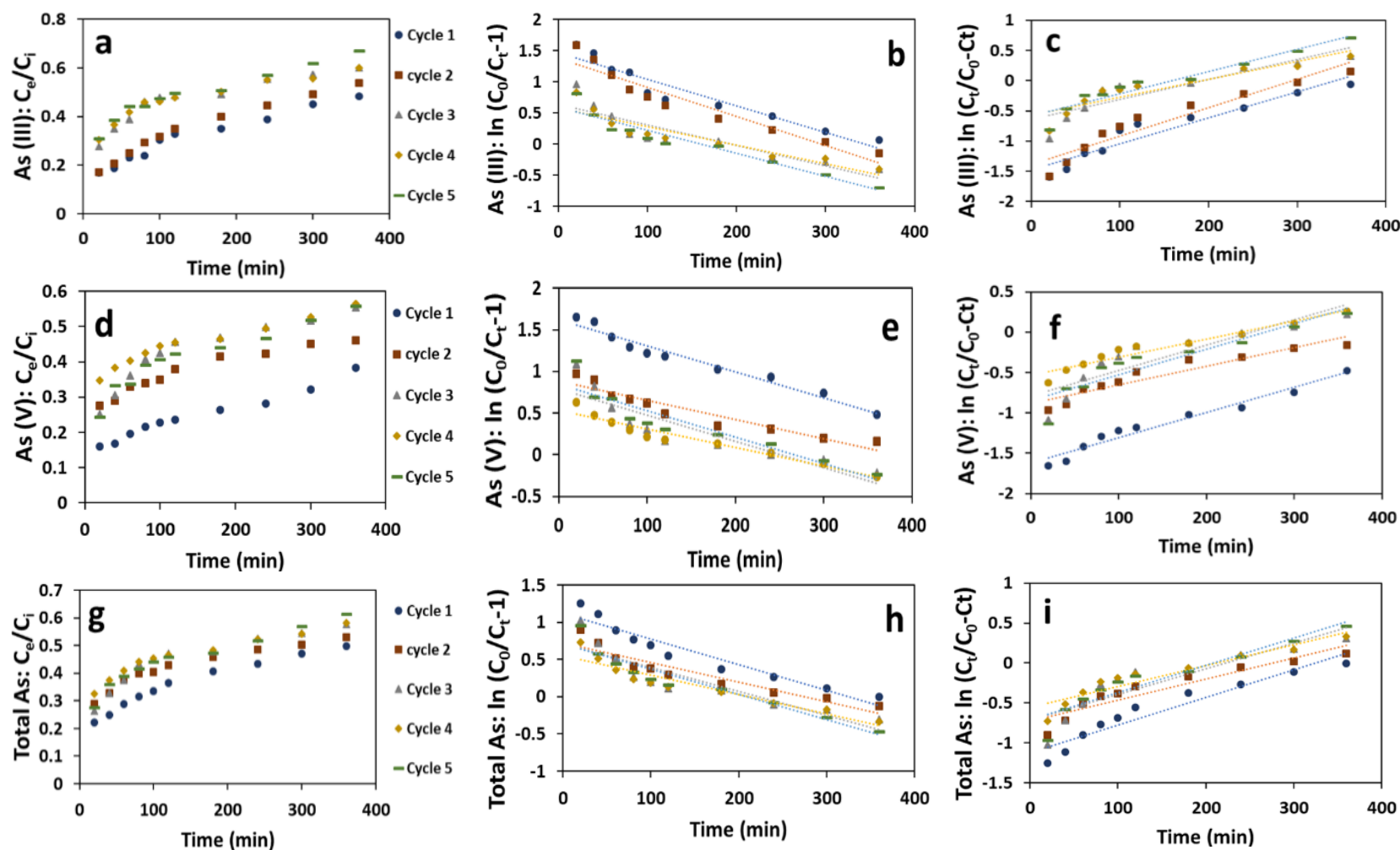


Figure 4-6 Breakthrough curves in five adsorption-desorption cycles of a) As(III), d) As(V), and g) total As; with Thomas linear plots for b) As(III), e) As(V), and h) total As; and Yoon-Nelson plots for c) As(III), f) As(V), and i) total As.

Table 4-7 shows the Thomas and Yoon-Nelson parameters for As adsorption over five adsorption consecutive cycles. The maximum adsorption capacity (q_0) value for As(V) decreases by approximately 49.46% from Cycle 1 to Cycle 5. For As(III), the q_0 value decreases by approximately 53.94% from Cycle 1 to Cycle 5. The q_0 for total arsenic decreases from 10.43 mg g⁻¹ in Cycle 1 to 5.24 mg g⁻¹ in Cycle 5, a reduction of approximately 49.76%. The Thomas constant exhibited negligible change following multiple regeneration cycles. These findings are consistent with the literature which also reported decreased adsorption capacities after multiple desorption cycles (Akinhanmi et al., 2020; H. Chen et al., 2022; Gu et al., 2024; Kumari & Bhaumik, 2015). Desorption of metals adsorbed on zeolite and Iron-coated zeolite (ICZ) columns using 0.1 M HCl removed 62–90% and 58–85% of metals in the first and second adsorption/desorption cycles, respectively. Despite this significant desorption, adsorption capacities declined in the second cycle, particularly for ICZ, with reductions in capacity from 1.03 to 0.61 mg g⁻¹ for Pb, 0.89 to 0.53 mg g⁻¹ for Cu, 0.93 to 0.54 mg g⁻¹ for Cd, 0.83 to 0.48 mg g⁻¹ for Zn, and 0.76 to 0.47 mg g⁻¹ for Cr (T. C. Nguyen et al., 2015).

Several strategies can be implemented to enhance the regeneration efficiency and maintain the adsorbent's capacity over multiple cycles: Instead of using 0.1 M NaOH, a more concentrated NaOH solution can be employed to improve the desorption efficiency of arsenic species from the adsorbent. Higher concentrations may break the bonds between the adsorbent and the adsorbed arsenic species more effectively, as demonstrated in studies. Pb(II) desorption from *Vitis vinifera* (the common grape vine) leaves improved with higher HNO₃ concentrations, with 1 M being the most effective among 0.25 M, 0.50 M, 0.75 M, and 1 M (Ghangale Sharmila et al., 2019).

Table 4-7 Thomas and Yoon-Nelson parameters for arsenic adsorption over five consecutive cycles.

Parameters	Cycle	$K_{Th} \times 10^4$ (L mg ⁻¹ min ⁻¹)	q_0 (mg g ⁻¹)	R ²
C _i = 50 mg L ⁻¹ , M = 10 g, F = 5 mL min ⁻¹	As(III)	1	1.72	0.91
		2	1.88	0.92
		3	1.32	0.8
		4	1.20	0.85
		5	1.48	0.93
	As(V)	1	1.24	0.94
		2	0.92	0.9
		3	1.24	0.8
		4	0.88	0.94
		5	1.28	0.86
	Total	1	0.74	0.94
		2	0.52	0.88
		3	0.64	0.8
		4	0.52	0.89
		5	0.68	0.9
parameters	Cycle	$K_{YN} \times 10^3$ (min ⁻¹)	τ (min)	R ²
C _i = 50 mg L ⁻¹ , M = 10 g, F = 5 mL min ⁻¹	As(III)	1	4.3	0.91
		2	4.7	0.92
		3	3.3	0.8
		4	3.0	0.85
		5	3.7	0.93
	As(V)	1	3.1	0.94
		2	2.3	0.9
		3	3.1	0.8
		4	2.2	0.94
		5	3.2	0.86
	Total	1	3.7	0.94
		2	2.6	0.88
		3	3.2	0.8
		4	2.6	0.89
		5	3.4	0.9

C_i = initial concentration; M = adsorbent mass; F = flowrate.

Additionally, testing other regenerants like HCl or a combination of acids and bases might yield better results. In the desorption of metals from Thiol-lignocellulose sodium bentonite (TLSB) nanocomposites, six eluents were tested: HCl, HNO₃, H₃PO₄, and H₂SO₄ as proton exchangers, along with NaOH and EDTA as complexing and chelating agents. The study showed that peak desorption of Zn(II) and Cd(II) was achieved with HCl, while HNO₃ was most effective for Hg(II) (W. Zhang et al., 2020). These eluents could be promising candidates for desorption testing in future experiments for this study.

Multi-step elution processes can also enhance regeneration efficiency. For instance, in a study comparing two methods for silver recovery from base metal-chloride solutions, the first used HCl, water rinse, EDTA, and thiourea, while the second replaced HCl with NaCl and thiourea with thiosulfate. The NaCl-thiosulfate method proved more stable, increasing silver purity from 61% to 72% (Virolainen et al., 2015).

Additionally, sonication can enhance desorption efficiency by generating localized heat and ultrasound-induced vortices, which provide metal ions with the energy to escape from desorption sites. Though the increase in desorption capacity for metal-loaded TLSB was modest, it remains a promising method for improving desorption in future experiments (W. Zhang et al., 2020).

Introducing aeration during the regeneration process can facilitate the oxidation of As(III) to As(V), which is generally easier to desorb. Aeration can also help physically disrupt the bond between the adsorbent and the adsorbate. A study showed that without aeration, the remaining adsorption capacity of chitosan-alginate hybrid adsorbent after four As(III) desorption cycles using NaOH was 60%, while adjusting the pH to 9-10 and aerating at 1 L min⁻¹ improved the process, increasing the remaining adsorption capacity to about 80% (Zeng et al., 2020).

Furthermore, agitating or shaking the adsorbent in the regenerant solution can enhance mass transfer and ensure better contact between the regenerant and the adsorbed species, leading to more efficient desorption. The experimental investigation of cadmium desorption from riverbed sediments revealed that increasing the agitation rate (flow turbulence) slightly increased the Cd desorption (Nasrabadi et al., 2022).

Finally, optimizing the flowrate of the regenerant solution through the column can ensure adequate contact time and prevent channeling, thereby improving the desorption efficiency. For example, various airflow rates were tested in microwave desorption and regeneration of activated carbon with adsorbed radon—1.3, 1.5, 2.0, and 2.6 L min⁻¹. It was found that when the airflow rate exceeded 2 L min⁻¹, radon concentration at the outlet decreased (H. Yang et al., 2019).

According to Yoon -Nelson model, the 50% breakthrough time (τ) for As(III) decreases from 345.74 min in Cycle 1 to 159.16 min in Cycle 5, showing a significant shortening after several cycles. For As(V), the 50% breakthrough time decreases from 522.58 min in Cycle 1 to 264.31 min in Cycle 5. The 50% breakthrough time for total arsenic decreases from 417.11 min in Cycle 1 to 209.559 min in Cycle 5, representing a reduction of approximately 49.76%, indicating a moderate decrease in the overall 50% breakthrough time across cycles. Similarly, a continuous fixed-bed column study evaluated rGO/ZrO₂ as an effective adsorbent for fluoride removal from water and regenerated the exhausted column with 10% NaOH, showed a decrease in breakthrough time from 4200 min in the first cycle to 1900 min in the third (S. Mohan et al., 2017).

4.3.2. Part II: comparative arsenic removal in point of use (POU) cartridges

4.3.2.1. Adsorption-desorption experiments

The breakthrough curves (Figure 4-7a) for three cartridges (carbon block filter, mussel shell powders, and mussel shells coated on sediment filter discs) highlight significant differences in their arsenic adsorption capabilities.

The experimental results show that the activated carbon (AC) block filter was not successful in removing arsenic. Activated carbon is highly effective in adsorbing organic compounds but has limited efficiency in removing inorganic contaminants such as arsenic. The pore structure and surface chemistry of activated carbon do not favor the adsorption of arsenic.

In contrast, the mussel shell powder and the mussel shell-coated disc demonstrated superior performance, with the mussel shell-coated disc outperforming the mussel shell powder. The higher performance of the mussel shell-coated disc can be attributed to several factors. First, the disc form allows for a more uniform flow distribution through the filter, enhancing the contact between arsenic ions and the adsorbent surface. Additionally, the structured form of the disc might facilitate better mechanical stability and prevent channeling effects, which can occur in loose powder forms. This uniform flow and mechanical stability can enhance the overall adsorption efficiency.

While both mussel shell powder and mussel shell-coated discs demonstrated similar performance in arsenic removal, as indicated by their closely similar exhaustion curves (C_e/C_i over time), the disc form offers several practical advantages. The disc form provides easier handling and implementation in water treatment systems, reducing the risk of clogging and ensuring consistent performance over time. Furthermore, the disc can be integrated into existing filtration systems without significant modifications, making it a versatile and convenient option for arsenic removal.

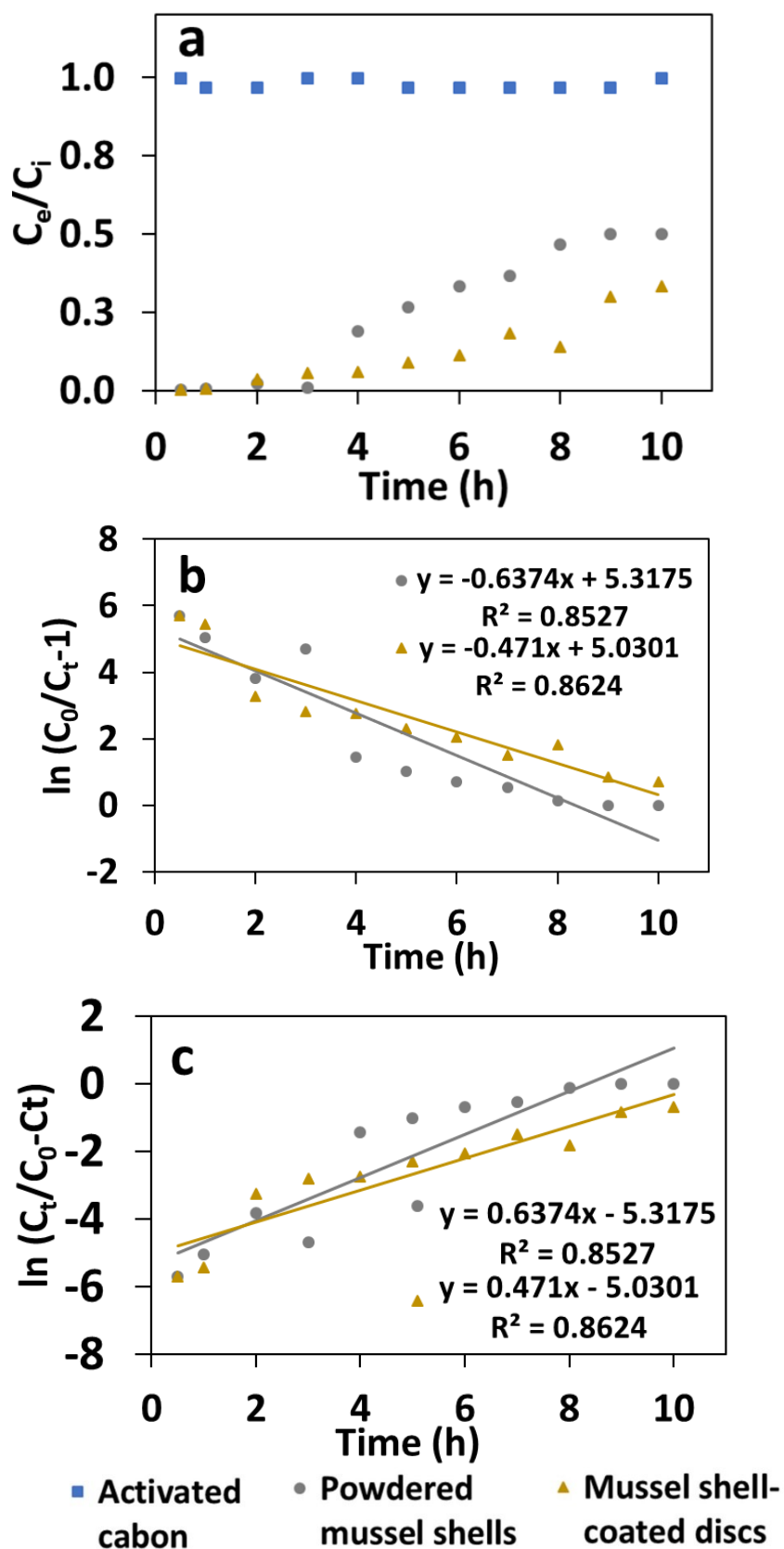


Figure 4-7 a) Breakthrough curves of; b) Thomas linear plots; c) Yoon-Nelson plots of three cartridges (activated carbon, powdered mussel shells, mussel shell-coated disc).

The Thomas and Yoon-Nelson models (Figure 4-7b) parameters for both cartridges are summarized in Table 4-8. The results validate the experimental findings, with the mussel shell powder (MP) exhibiting the higher Thomas rate constant (K_{Th}) ($2.12 \text{ L mg}^{-1} \text{ h}^{-1}$) compared to the mussel shell-coated disc (MD) ($1.57 \text{ L mg}^{-1} \text{ h}^{-1}$). This indicates that the MP cartridge has a faster adsorption rate; however, MD cartridge has a higher maximum adsorption capacity (0.32 mg g^{-1}) compared to MP (0.25 mg g^{-1}). Similarly, according to the Yoon-Nelson (Figure 4-7c) model, the MP cartridge exhibits a higher adsorption rate constant (0.64 h^{-1}) compared to the MD cartridge (0.47 h^{-1}), but the mussel shell-coated disc (MD) has a higher 50% breakthrough time (10.68 h). This implies that the disc maintains its adsorption capacity over a longer period before a breakthrough occurs.

For POU systems, the mussel shell-coated disc (MD) is recommended due to its higher capacity, longer breakthrough time, and stability. These characteristics make it a better fit for continuous use with less frequent replacement or regeneration. The mussel shell powder (MP) might be considered for scenarios where rapid initial adsorption is crucial, but practical limitations like handling and maintenance should be carefully evaluated.

Table 4-8 Thomas and Yoon-Nelson parameters for arsenic adsorption using three cartridges.

Parameters	Cartridge	R^2	K_{Th} ($\text{L mg}^{-1} \text{ h}^{-1}$)	q_0 (mg g^{-1})
Total arsenic $C_i = 0.3 \text{ mg L}^{-1}$, $M = 10 \text{ g}$, $F = 1 \text{ L h}^{-1}$	Powdered mussel shell	0.85	2.12	0.25
	Mussel shell-coated discs	0.86	1.57	0.32
	Cartridge	R^2	K_{YN} (h^{-1})	τ (h)
	Powdered mussel shell	0.85	0.64	8.34
	Mussel shell-coated discs	0.86	0.47	10.68

The effectiveness of 0.1 M NaOH in regenerating the As-loaded cartridges was shown in Figure 4-8, and in the initial hours, a substantial arsenic release was observed.

The desorption rate was notably rapid within the first three hours, resulting in a significant concentration of arsenic in the effluent. Similarly, column elution experiments for Congo red and cadmium using Neem leaf powder (NLP) and activated charcoal from Neem leaf powder (AC-NLP) with 0.1 M hydrochloric acid and 0.1 M sodium hydroxide solutions demonstrated that desorption was faster during the first hour (Patel, 2022). Initially, the desorption rate is high because the adsorbent is saturated with adsorbate, increasing the reaction probability. Over time, the desorption rate slows as equilibrium is established between the desorbed adsorbate and the remaining adsorbate on the adsorbent (Vakili et al., 2019). The higher peak observed for mussel shell powder compared to mussel shell discs can be attributed to several factors. The powder form offers a greater surface area and enhanced diffusion of NaOH, allowing for more efficient contact and interaction with the arsenic ions. Additionally, the finer particle size exposes more reactive sites, reducing mass transfer resistance and facilitating quicker arsenic release. This combination of increased surface area, improved diffusion, higher reactivity, and better interaction with the desorbing agent results in a more effective desorption process for the mussel shell powder.

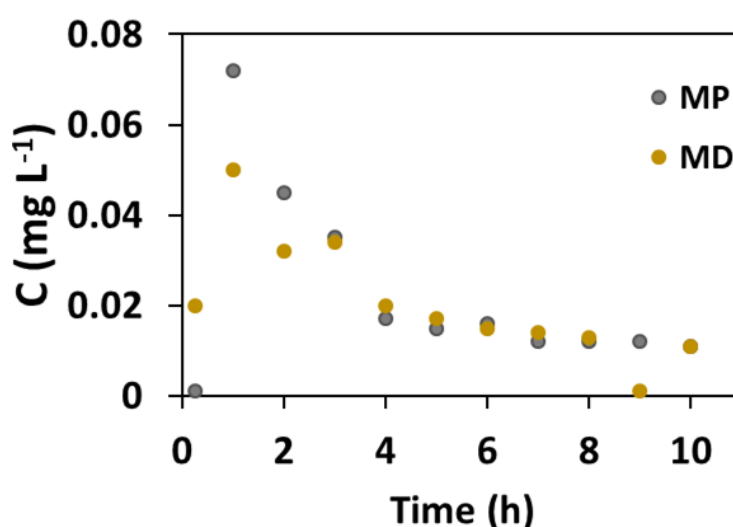


Figure 4-8 Desorption profiles for mussel shell-based adsorbents using 0.1 M NaOH.

4.4. Conclusion

This study highlights the promise of modified calcined mussel shells for effective arsenic removal from drinking water in point-of-use (POU) applications, with successful flow-through experimentation and testing in cartridges paving the way for future implementation in POU systems. The modified adsorbent shows high initial adsorption capacities, indicating its potential as a reliable solution for addressing arsenic contamination in drinking water. While performance is reduced over successive regeneration cycles, careful management of regeneration strategies may help mitigate capacity loss and enhance long-term usability. Increasing the initial adsorbate concentration from 10 to 50 mg L⁻¹, the flow rate from 5 to 10 mL min⁻¹, and reducing the adsorbent mass from 10 to 5 g increased the maximum adsorption capacity, reaching 25.97 mg g⁻¹ for total arsenic. However, the interplay between flowrate and adsorbent mass was critical in determining breakthrough time, with higher flowrates and lower adsorbent masses leading to earlier breakthrough.

Competing ions, including Cl⁻, SO₄²⁻, NO₃⁻, HCO₃⁻, and PO₄³⁻, influenced the adsorption performance, as reflected in the Thomas model parameters, where the q_0 value for total arsenic showed a decline from 10.43 to 7.62 mg g⁻¹. The experimental results highlight the significant contribution of this study, demonstrating that while the activated carbon (AC) block filter was ineffective in removing arsenic, both the mussel shell powder (MP) and mussel shell-coated disc (MD) outperformed it. Notably, MP exhibited a higher adsorption rate, whereas MD demonstrated a superior maximum adsorption capacity, emphasizing the enhanced potential of mussel shell-derived adsorbents in arsenic removal. These findings suggest that the optimal adsorbent choice depends on specific application requirements. Compared to other bio-based adsorbents, such as activated carbon derived from agricultural waste, CMS offers notable

advantages in terms of stability, consistent performance, and availability as a waste by-product from local shellfish industries. These characteristics support its potential as a scalable and practical solution for arsenic removal. Future studies should focus on enhancing the stability and regeneration efficiency of the adsorbent, as well as exploring the effects of other modifications on its performance. Additionally, scaling up the process and conducting long-term field tests will be essential to fully establish the feasibility of this method for large-scale applications.

4.5. Reference

- Abbas, S. H., Sulaymon, A. H., Hossien, Y. K., & Ismail, I. M. (2015). Breakthrough curves for adsorption/biosorption of Pb (II), Cu (II), Cd (II) and Co (II) ions from wastewater using granular activated carbon/fungal waste biomass: A comparative study. *Journal of Chemical and Pharmaceutical Research*, 7(4), 615–633.
- Abbasi, M., Safari, E., Baghdadi, M., & Janmohammadi, M. (2021). Enhanced adsorption of heavy metals in groundwater using sand columns enriched with graphene oxide: Lab-scale experiments and process modeling. *Journal of Water Process Engineering*, 40, 101961.
- Abdullah, N. H., Liom, S. L., Zainudin, A. H., Huzil, M. A. I., Yaacob, M. S. S., Salim, N. A. A., Kaamin, M., & Talaiekhazani, A. (2022). Waste Mussel Shells as an Adsorbent for Phosphate Removal in Solution: Kinetic and Isotherm Model. *International Journal of Nanoelectronics & Materials*, 15.
- Akinhanmi, T. F., Ofudje, E. A., Adeogun, A. I., Aina, P., & Joseph, I. M. (2020). Orange peel as low-cost adsorbent in the elimination of Cd (II) ion: kinetics, isotherm, thermodynamic and optimization evaluations. *Bioresources and*

Bioprocessing, 7, 1–16.

- Ali, I. (2018). Microwave assisted economic synthesis of multi walled carbon nanotubes for arsenic species removal in water: batch and column operations. *Journal of Molecular Liquids*, 271, 677–685.
- Ali, I., Al-Othman, Z. A., Alwarthan, A., Asim, M., & Khan, T. A. (2014). Removal of arsenic species from water by batch and column operations on bagasse fly ash. *Environmental Science and Pollution Research*, 21(5), 3218–3229.
- Ansari, W. R., Harahap, H., & Husin, A. (2021). Fixed-bed column adsorption performance for ammonia removal using adsorbent from zeolite. *IOP Conference Series: Materials Science and Engineering*, 1122(1), 12076.
- Apiratikul, R., & Chu, K. H. (2021). Improved fixed bed models for correlating asymmetric adsorption breakthrough curves. *Journal of Water Process Engineering*, 40, 101810.
- Bessaies, H., Iftekhhar, S., Doshi, B., Kheriji, J., Ncibi, M. C., Srivastava, V., Sillanpää, M., & Hamrouni, B. (2020). Synthesis of novel adsorbent by intercalation of biopolymer in LDH for the removal of arsenic from synthetic and natural water. *Journal of Environmental Sciences*, 91, 246–261.
- Biswas, S., & Mishra, U. (2015). Continuous fixed-bed column study and adsorption modeling: removal of lead ion from aqueous solution by charcoal originated from chemical carbonization of rubber wood sawdust. *Journal of Chemistry*, 2015(1), 907379.
- Böckelen, A., & Niessner, R. (1992). Removal of arsenic from mineral water. *Vom Wasser*, 78, 355–362.
- Boussouga, Y.-A., Tantish, F., & Schäfer, A. I. (2023). Microporous Hematite-Loaded Composite Membrane for Arsenic (III) and Arsenic (V) Removal. *ACS*

Applied Engineering Materials, 1(4), 1164–1175.

- Brion-Roby, R., Gagnon, J., Deschênes, J.-S., & Chabot, B. (2018). Investigation of fixed bed adsorption column operation parameters using a chitosan material for treatment of arsenate contaminated water. *Journal of Environmental Chemical Engineering*, 6(1), 505–511.
- Chaudhry, S. A., Zaidi, Z., & Siddiqui, S. I. (2017). Isotherm, kinetic and thermodynamics of arsenic adsorption onto Iron-Zirconium Binary Oxide-Coated Sand (IZBOCS): Modelling and process optimization. *Journal of Molecular Liquids*, 229, 230–240.
- Chen, H., Xu, J., Lin, H., Wang, Z., & Liu, Z. (2022). Multi-cycle aqueous arsenic removal by novel magnetic n/s-doped hydrochars activated via one-pot and two-stage schemes. *Chemical Engineering Journal*, 429, 132071.
- Chen, S., Yue, Q., Gao, B., Li, Q., Xu, X., & Fu, K. (2012). Adsorption of hexavalent chromium from aqueous solution by modified corn stalk: a fixed-bed column study. *Bioresource Technology*, 113, 114–120.
- Clifford, D., Ceber, L., & Chow, S. (1983). Arsenic (III)/Arsenic (V) separation by chloride-form ion-exchange resins. *Proceedings of the XI AWWA WQTC*.
- de Freitas, J. J. G., Vieira, C. M. F., Natalli, J. F., Lavander, H. D., de Azevedo, A. R. G., & Marvila, M. T. (2024). Cleaner Production of Cementitious Materials Containing Bioaggregates Based on Mussel Shells: A Review. *Sustainability*, 16(13), 5577.
- Decentralized Water Treatment Market | Size, Growth | 2021-26*. (n.d.). Retrieved December 13, 2022, from <https://www.arizton.com/market-reports/decentralized-water-treatment-market>
- Detho, A., Daud, Z., Almohana, A. I., Almojil, S. F., Alali, A., Din, M. F. M., Rosli,

- M. A., Memon, A. A., Awang, H., & Ridzuan, M. B. (2022). Adsorption of chemical oxygen demand and ammoniacal nitrogen removal from leachate using seafood waste (green mussel shell) as low-cost adsorbent. *Desalination and Water Treatment*, 260, 102–110.
- El Haddad, M. (2016). Removal of Basic Fuchsin dye from water using mussel shell biomass waste as an adsorbent: Equilibrium, kinetics, and thermodynamics. *Journal of Taibah University for Science*, 10(5), 664–674.
- El Haddad, M., Regti, A., Laamari, M. R., Slimani, R., Mamouni, R., El Antri, S., & Lazar, S. (2014). Calcined mussel shells as a new and eco-friendly biosorbent to remove textile dyes from aqueous solutions. *Journal of the Taiwan Institute of Chemical Engineers*, 45(2), 533–540.
- Ewy, W., Bahr, C., & Kellmann, S. (2022). Removal Of Arsenic in drinking water treatment with granular ferric hydroxide (GEH®). *XI Congreso Nacional de AIDIS*.
- FAO, R. (2022). The state of world fisheries and aquaculture 2022. Towards blue transformation. In *The State of World Fisheries and Aquaculture (SOFIA)* (p. 266). Food and Agriculture Organization of the United Nations Rome, Italy.
- Farsad, A., Marcos-Hernandez, M., Sinha, S., & Westerhoff, P. (2023). Sous Vide-Inspired Impregnation of Amorphous Titanium (Hydr) Oxide into Carbon Block Point-of-Use Filters for Arsenic Removal from Water. *Environmental Science & Technology*, 57(48), 20410–20420.
- Flanagan, S. V, Marvinney, R. G., Johnston, R. A., Yang, Q., & Zheng, Y. (2015). Dissemination of well water arsenic results to homeowners in Central Maine: influences on mitigation behavior and continued risks for exposure. *Science of the Total Environment*, 505, 1282–1290.

- Frank, P., & Clifford, D. A. (1986). *Arsenic (III) oxidation and removal from drinking water* (Vol. 86, Issue 158607). Water Engineering Research Laboratory, Office of Research and Development
- Fu, J., Chen, Z., Wang, M., Liu, S., Zhang, J., Zhang, J., Han, R., & Xu, Q. (2015). Adsorption of methylene blue by a high-efficiency adsorbent (polydopamine microspheres): kinetics, isotherm, thermodynamics and mechanism analysis. *Chemical Engineering Journal*, 259, 53–61.
- Futalan, C. M., & Wan, M.-W. (2022). Fixed-bed adsorption of lead from aqueous solution using chitosan-coated bentonite. *International Journal of Environmental Research and Public Health*, 19(5), 2597.
- Ghangale Sharmila, S., Bholay, A. D., & Saler, R. S. (2019). Biosorption and desorption of heavy metal lead (II) from aqueous solution using *Vitis vinifera* leaves as an agro waste biomass. *Journal of Information and Computational Science*, 12(6), 62–73.
- Gu, X., Jiang, L., Zhou, Z., Ling, C., Lu, D., Zhong, K., & Zhang, C. (2024). Mechanism of efficient adsorption for arsenic in aqueous solution by zeolitic imidazolate framework-8. *Environmental Science and Pollution Research*, 1–14.
- Gupta, A. D., Rene, E. R., Giri, B. S., Pandey, A., & Singh, H. (2021). Adsorptive and photocatalytic properties of metal oxides towards arsenic remediation from water: A review. *Journal of Environmental Chemical Engineering*, 9(6), 106376.
- Hinkle, M. A. G., Wang, Z., Giammar, D. E., & Catalano, J. G. (2015). Interaction of Fe (II) with phosphate and sulfate on iron oxide surfaces. *Geochimica et Cosmochimica Acta*, 158, 130–146.

- Hongtao, L., Shuxia, L., Hua, Z., Yanling, Q., Daqiang, Y., Jianfu, Z., & Zhiliang, Z. (2018). Comparative study on synchronous adsorption of arsenate and fluoride in aqueous solution onto MgAlFe-LDHs with different intercalating anions. *RSC Advances*, 8(58), 33301–33313.
- Khamdahsag, P., Yan, D. Y. S., Poompang, P., Supannafai, N., & Tanboonchuy, V. (2021). Continuous fixed-bed column studies of arsenite removal via oxidation and adsorption coprocesses. *Journal of Water Process Engineering*, 42, 102176.
- Kim, M. J., & Nriagu, J. (2000). Oxidation of arsenite in groundwater using ozone and oxygen. *Science of the Total Environment*, 247(1), 71–79.
[https://doi.org/10.1016/S0048-9697\(99\)00470-2](https://doi.org/10.1016/S0048-9697(99)00470-2)
- Kofa, G. P., NdiKoungou, S., Kayem, G. J., & Kamga, R. (2015). Adsorption of arsenic by natural pozzolan in a fixed bed: determination of operating conditions and modeling. *Journal of Water Process Engineering*, 6, 166–173.
- Koul, B., Yakoob, M., & Shah, M. P. (2022). Agricultural waste management strategies for environmental sustainability. *Environmental Research*, 206, 112285.
- Kumar, A. S. K., & Jiang, S.-J. (2016). Chitosan-functionalized graphene oxide: A novel adsorbent an efficient adsorption of arsenic from aqueous solution. *Journal of Environmental Chemical Engineering*, 4(2), 1698–1713.
- Kumari, V., & Bhaumik, A. (2015). Mesoporous ZnAl₂O₄: an efficient adsorbent for the removal of arsenic from contaminated water. *Dalton Transactions*, 44(26), 11843–11851.
- Lee, S.-H., Choi, H., & Kim, K.-W. (2018). Removal of As (V) and Sb (V) in water using magnetic nanoparticle-supported layered double hydroxide

- nanocomposites. *Journal of Geochemical Exploration*, 184, 247–254.
- Liem-Nguyen, V., Sjöberg, V., Dinh, N. P., Huy, D. H., & Karlsson, S. (2020). Removal mechanism of arsenic (V) by stainless steel slags obtained from scrap metal recycling. *Journal of Environmental Chemical Engineering*, 8(4), 103833.
- Lin, X., Huang, Q., Qi, G., Shi, S., Xiong, L., Huang, C., Chen, X., Li, H., & Chen, X. (2017). Estimation of fixed-bed column parameters and mathematical modeling of breakthrough behaviors for adsorption of levulinic acid from aqueous solution using SY-01 resin. *Separation and Purification Technology*, 174, 222–231.
- Liu, J., Zhu, R., Ma, L., Fu, H., Lin, X., Parker, S. C., & Molinari, M. (2021). Adsorption of phosphate and cadmium on iron (oxyhydr) oxides: A comparative study on ferrihydrite, goethite, and hematite. *Geoderma*, 383, 114799.
- López-Cervantes, J., Sánchez-Machado, D. I., Sánchez-Duarte, R. G., & Correa-Murrieta, M. A. (2018). Study of a fixed-bed column in the adsorption of an azo dye from an aqueous medium using a chitosan–glutaraldehyde biosorbent. *Adsorption Science & Technology*, 36(1–2), 215–232.
- Maji, S. K., Kao, Y. H., Wang, Y. Bin, & Liu, C. W. (2015). Dynamic column adsorption of As on iron-oxide-coated natural rock (IOCNR) and sludge management. *Desalination and Water Treatment*, 55(8), 2171–2182. <https://doi.org/10.1080/19443994.2014.928912>
- Martínez-García, C., González-Fontboa, B., Martínez-Abella, F., & Carro-López, D. (2017). Performance of mussel shell as aggregate in plain concrete. *Construction and Building Materials*, 139, 570–583.

- Mendizabal, E., Ríos-Donato, N., Jasso-Gastinel, C. F., & Verduzco-Navarro, I. P. (2023). Removal of arsenate by fixed-bed columns using chitosan-magnetite hydrogel beads and chitosan hydrogel beads: Effect of the operating conditions on column efficiency. *Gels*, 9(10), 825.
- Mohamed, M., Yusup, S., & Bustam, M. A. (2016). Synthesis of CaO-based sorbent from biomass for CO₂ capture in series of calcination-carbonation cycle. *Procedia Engineering*, 148, 78–85.
- Mohan, S., Singh, D. K., Kumar, V., & Hasan, S. H. (2017). Effective removal of Fluoride ions by rGO/ZrO₂ nanocomposite from aqueous solution: fixed bed column adsorption modelling and its adsorption mechanism. *Journal of Fluorine Chemistry*, 194, 40–50.
- Mohsen, H. A., & Ghanim, A. N. (2024). Efficient Removal of Zinc and Copper from Wastewater Using Activated Carbon Derived from Date Pits in a Continuous Fixed-Bed Column. *Journal of Composite & Advanced Materials/Revue Des Composites et Des Matériaux Avancés*, 34(2).
- Mullin, M. (2023a). *High levels of arsenic detected in 112 wells across N.L. — and hundreds more could be at risk | CBC News*.
<https://www.cbc.ca/news/canada/newfoundland-labrador/arsenic-test-results-1.6920066>
- Mullin, M. (2023b). *No Title*. CBC News.
<https://www.cbc.ca/news/canada/newfoundland-labrador/arsenic-test-results-1.6920066>
- Nasrabadi, M., Omid, M. H., & Mazdeh, A. M. (2022). Experimental Study of Flow Turbulence Effect on Cadmium Desorption Kinetics from Riverbed Sands. *Environmental Processes*, 9(1), 10.

- Nawar, A., Ali, M., Khoja, A. H., Waqas, A., Anwar, M., & Mahmood, M. (2021). Enhanced CO₂ capture using organic acid structure modified waste eggshell derived CaO sorbent. *Journal of Environmental Chemical Engineering*, 9(1), 104871.
- Neisan, R. S., Saady, N. M. C., Bazan, C., Zendehboudi, S., Al-nayili, A., Abbassi, B., & Chatterjee, P. (2023). Arsenic Removal by Adsorbents from Water for Small Communities' Decentralized Systems: Performance, Characterization, and Effective Parameters. *Clean Technologies*, 5(1), 352–402.
<https://doi.org/10.3390/cleantechnol5010019>
- Nguyen, T. C., Loganathan, P., Nguyen, T. V., Vigneswaran, S., Kandasamy, J., & Naidu, R. (2015). Simultaneous adsorption of Cd, Cr, Cu, Pb, and Zn by an iron-coated Australian zeolite in batch and fixed-bed column studies. *Chemical Engineering Journal*, 270, 393–404.
- Omar, N. M. A., Othman, M. H. D., Tai, Z. S., Amhamed, A. O. A., Kurniawan, T. A., Puteh, M. H., & Sokri, M. N. M. (2023). Recent progress, bottlenecks, improvement strategies and the way forward of membrane distillation technology for arsenic removal from water: A review. *Journal of Water Process Engineering*, 52, 103504.
- Omitola, O. B., Abonyi, M. N., Akpomie, K. G., & Dawodu, F. A. (2022). Adams-Bohart, Yoon-Nelson, and Thomas modeling of the fix-bed continuous column adsorption of amoxicillin onto silver nanoparticle-maize leaf composite. *Applied Water Science*, 12(5), 94.
- Pantić, K., Bajić, Z. J., Veličković, Z. S., Nešić, J. Z., Đolić, M. B., Tomić, N. Z., & Marinković, A. D. (2019). Arsenic removal by copper-impregnated natural mineral tufa part II: a kinetics and column adsorption study. *Environmental*

Science and Pollution Research, 26, 24143–24161.

- Papadimitriou, C. A., Krey, G., Stamatis, N., & Kallianiotis, A. (2017). The use of waste mussel shells for the adsorption of dyes and heavy metals. *Journal of Chemical Technology & Biotechnology*, 92(8), 1943–1947.
- Paradelo, R., Conde-Cid, M., Cutillas-Barreiro, L., Arias-Estévez, M., Nóvoa-Muñoz, J. C., Álvarez-Rodríguez, E., Fernández-Sanjurjo, M. J., & Núñez-Delgado, A. (2016). Phosphorus removal from wastewater using mussel shell: Investigation on retention mechanisms. *Ecological Engineering*, 97, 558–566.
- Patel, H. (2022). Elution profile of cationic and anionic adsorbate from exhausted adsorbent using solvent desorption. *Scientific Reports*, 12(1), 1665.
- Pooi, C. K., & Ng, H. Y. (2018). Review of low-cost point-of-use water treatment systems for developing communities. *Npj Clean Water*, 1(1), 11.
- Qi, Z., Joshi, T. P., Liu, R., Li, Y., Liu, H., & Qu, J. (2018). Adsorption combined with superconducting high gradient magnetic separation technique used for removal of arsenic and antimony. *Journal of Hazardous Materials*, 343, 36–48.
- Salim, N. A. A., Puteh, M. H., Yusoff, A. R. M., Abdullah, N. H., Fulazzaky, M. A., Rudie Arman, M. A. Z., & Zainuddin, N. A. (2020). Adsorption isotherms and kinetics of phosphate on waste mussel shell. *Malaysian Journal of Fundamental and Applied Sciences*, 16(3), 393–399.
- Sawood, G. M., & Gupta, S. K. (2020). Arsenate adsorption from aqueous solution using iron-loaded *Azadirachta indica* roots: batch and fixed-bed column study. *Desalination and Water Treatment*, 203, 292–308.
- Shukla, P. K., Deshpande, V., & Raychoudhury, T. (2023). In-situ groundwater treatment for arsenic removal: Laboratory pilot scale study with 3-D tank

- packed porous media as subsurface. *Environmental Technology*, 1–14.
- Signes-Pastor, A. J., Wu, F., Farzan, S. F., Chen, Y., & Karagas, M. R. (2024). Arsenic Exposure in Children. *Textbook of Children's Environmental Health*, 437.
- Soetaredjo, F. E., Kurniawan, A., Ong, L. K., Widagdyo, D. R., & Ismadji, S. (2014). Investigation of the continuous flow sorption of heavy metals in a biomass-packed column: revisiting the Thomas design model for correlation of binary component systems. *RSC Advances*, 4(95), 52856–52870.
- Summa, D., Lanzoni, M., Castaldelli, G., Fano, E. A., & Tamburini, E. (2022). *Trends and Opportunities of Bivalve Shells' Waste Valorization in a Prospect of Circular Blue Bioeconomy. Resources 2022*, 11, 48. s Note: MDPI stays neutral with regard to jurisdictional claims in published
- Thanki, A., Thanki, A., Singh, R., & Sohal, K. S. (2021). The Application of Low-Cost Natural Bio-Adsorbents for the Removal of Heavy Metals—A Review. *Sustainable Development Through Engineering Innovations: Select Proceedings of SDEI 2020*, 355–371.
- Tony, M. A. (2022). Low-cost adsorbents for environmental pollution control: a concise systematic review from the prospective of principles, mechanism and their applications. *Journal of Dispersion Science and Technology*, 43(11), 1612–1633.
- Topal, M., & Topal, E. I. A. (2020). Optimization of tetracycline removal with chitosan obtained from mussel shells using RSM. *Journal of Industrial and Engineering Chemistry*, 84, 315–321.
- Topić Popović, N., Lorencin, V., Strunjak-Perović, I., & Čož-Rakovac, R. (2023). Shell waste management and utilization: Mitigating organic pollution and

- enhancing sustainability. *Applied Sciences*, 13(1), 623.
- Ungureanu, G., Santos, S., Boaventura, R., & Botelho, C. (2015). Arsenic and antimony in water and wastewater: Overview of removal techniques with special reference to latest advances in adsorption. *Journal of Environmental Management*, 151, 326–342.
- Vakili, M., Deng, S., Cagnetta, G., Wang, W., Meng, P., Liu, D., & Yu, G. (2019). Regeneration of chitosan-based adsorbents used in heavy metal adsorption: A review. In *Separation and Purification Technology* (Vol. 224, pp. 373–387). <https://doi.org/10.1016/j.seppur.2019.05.040>
- Vasyliiev, G. S. (2015). The influence of flow rate on corrosion of mild steel in hot tap water. *Corrosion Science*, 98, 33–39.
- Vera, L. M., Bermejo, D., Uguña, M. F., Garcia, N., Flores, M., & González, E. (2019). Fixed bed column modeling of lead (II) and cadmium (II) ions biosorption on sugarcane bagasse. *Environmental Engineering Research*, 24(1), 31–37.
- Virolainen, S., Tyster, M., Haapalainen, M., & Sainio, T. (2015). Ion exchange recovery of silver from concentrated base metal-chloride solutions. *Hydrometallurgy*, 152, 100–106.
- Wang, M., Mohanty, S. K., & Mahendra, S. (2019). Nanomaterial-supported enzymes for water purification and monitoring in point-of-use water supply systems. *Accounts of Chemical Research*, 52(4), 876–885.
- Wang, Q., Jiang, F., Ouyang, X.-K., Yang, L.-Y., & Wang, Y. (2021). Adsorption of Pb (II) from aqueous solution by mussel shell-based adsorbent: Preparation, characterization, and adsorption performance. *Materials*, 14(4), 741.
- Wang, W., Li, M., & Zeng, Q. (2015). Adsorption of chromium (VI) by strong

- alkaline anion exchange fiber in a fixed-bed column: experiments and models fitting and evaluating. *Separation and Purification Technology*, 149, 16–23.
- Wang, W., Tian, G., Zhang, Z., & Wang, A. (2015). A simple hydrothermal approach to modify palygorskite for high-efficient adsorption of Methylene blue and Cu (II) ions. *Chemical Engineering Journal*, 265, 228–238.
- Yadav, M. K., Gupta, A. K., Ghosal, P. S., & Mukherjee, A. (2021). Effect of coexisting ions on adsorptive removal of arsenate by Mg-Fe-(CO₃) LDH: multi-component adsorption and ANN-based multivariate modeling. *Journal of Environmental Science and Health, Part A*, 56(5), 572–584.
- Yang, H., Shan, J., Li, J., & Jiang, S. (2019). Microwave desorption and regeneration methods for activated carbon with adsorbed radon. *Adsorption*, 25, 173–185.
- Yang, Q., Flanagan, S. V, Chillrud, S., Ross, J., Zeng, W., Culbertson, C., Spayd, S., Backer, L., Smith, A. E., & Zheng, Y. (2020). Reduction in drinking water arsenic exposure and health risk through arsenic treatment among private well households in Maine and New Jersey, USA. *Science of the Total Environment*, 738, 139683.
- Yunnen, C., Ye, W., Chen, L., Lin, G., Jinxia, N., & Rushan, R. (2017). Continuous Fixed-Bed Column Study and Adsorption Modeling: Removal of Arsenate and Arsenite in Aqueous Solution by Organic Modified Spent Grains. *Polish Journal of Environmental Studies*, 26(4).
- Zacher, T., Endres, K., Richards, F., Robe, L. B., Powers, M., Yracheta, J., Harvey, D., Best, L. G., Cloud, R. R., & Bear, A. B. (2023). Evaluation of a water arsenic filter in a participatory intervention to reduce arsenic exposure in American Indian communities: The Strong Heart Water Study. *Science of the Total Environment*, 862, 160217.

- Zeng, H., Sun, S., Yu, Y., Zhang, J., & Li, D. (2021). Column studies on the adsorption of As (V) by granular chitosan adsorbent prepared with backwashing iron-containing sludge. *Colloids and Surfaces A: Physicochemical and Engineering Aspects*, 627, 127247.
- Zeng, H., Wang, F., Xu, K., Zhang, J., & Li, D. (2020). Optimization and regeneration of chitosan-alginate hybrid adsorbent embedding iron-manganese sludge for arsenic removal. *Colloids and Surfaces A: Physicochemical and Engineering Aspects*, 607, 125500.
- Zhang, W., An, Y., Li, S., Liu, Z., Chen, Z., Ren, Y., Wang, S., Zhang, X., & Wang, X. (2020). Enhanced heavy metal removal from an aqueous environment using an eco-friendly and sustainable adsorbent. *Scientific Reports*, 10(1), 16453.
- Zhang, W., Dong, L., Yan, H., Li, H., Jiang, Z., Kan, X., Yang, H., Li, A., & Cheng, R. (2011). Removal of methylene blue from aqueous solutions by straw based adsorbent in a fixed-bed column. *Chemical Engineering Journal*, 173(2), 429–436.

CHAPTER FIVE

REMOVAL OF ARSENIC FROM WATER USING RENEWABLE ADSORBENTS DERIVED FROM ORANGE PEELS ⁴

Roya Sadat Neisan¹, Noori M. Cata Saady¹, Carlos Bazan², Sohrab Zendehboudi³

¹ Department of Civil Engineering, Memorial University, St. John's, NL A1B 3X5, Canada

² Faculty of Business Administration, Memorial University, St. John's, NL A1B 3X5, Canada

³ Department of Process Engineering, Memorial University, St. John's, NL A1B 3X5, Canada

Abstract

This study developed titanium dioxide (TiO₂)-modified activated carbon from orange peels (OP-TiO₂) to optimize its arsenic adsorption capacity from water. The adsorbent was characterized using SEM, EDX, FT-IR, XRD, BET surface area analysis, and elemental analysis. BET analysis revealed a 2.55 times increase in surface area compared to unmodified carbon. Adsorption experiments were conducted with synthetic aqueous As(V) solutions, and Response Surface Methodology (RSM) incorporating Central Composite Design (CCD) was used for optimization. The study identified optimal conditions at pH 4.2, initial arsenic concentration of 50 mg L⁻¹, adsorbent dose of 3.3 g L⁻¹, and contact time of 4.8 hours, achieving a maximum adsorption capacity of 10.91 mg g⁻¹. Results indicated that increasing the adsorbent dose (0.5–8 g L⁻¹) enhanced removal efficiency, while higher initial concentrations correlated with increased adsorption capacity. Contact time (0.4–6 h) had minimal influence within the tested range. Adsorption followed the intra-particle diffusion kinetic model and Temkin isotherm. This study demonstrates the potential of agricultural waste-derived adsorbents as a sustainable and economical solution for arsenic removal from water.

⁴ This chapter has been published as a peer-reviewed journal article: Neisan, R. S., Saady, N. M. C., Bazan, C., & Zendehboudi, S. (2025). Optimization of arsenic removal from water using novel renewable adsorbents derived from orange peels. *Waste Management Bulletin*, 3(2), 21-35. <https://doi.org/10.1016/j.wmb.2025.02.006>.

5.1. Introduction

Arsenic is a naturally occurring element found in the Earth's crust, and its presence in water sources can pose a significant threat to human health (Masuda, 2018; Raju, 2022). It is categorized as a metalloid, exhibiting properties of both metals and non-metals (Bowell et al., 2014). Arsenic contamination in water typically arises from geological sources, where minerals containing arsenic dissolve over time, releasing the element into groundwater (Garellick et al., 2008). This contamination can also result from industrial processes, mining activities, and agricultural runoff (Li et al., 2020). Arsenic concentration in drinking water has affected more than 300 million people worldwide (Dilpazeer et al., 2023).

Arsenic exists in two primary forms: inorganic arsenic, which is more toxic and poses a greater health risk, and organic arsenic, which is generally less harmful (Rehman et al., 2021). Ingesting water with elevated levels of arsenic over extended periods can lead to serious health problems, including skin lesions, various cancers (such as skin, bladder, and lung cancer), and adverse effects on the nervous system (Palma-Lara et al., 2020; Prakash & Verma, 2021). Given the severe health implications, understanding and mitigating arsenic contamination in water sources is important for public health and environmental protection (Siddique et al., 2020).

Several methods have been developed to mitigate arsenic contamination in water sources. These approaches include a range of physical, chemical, and biological techniques (Mahimairaja et al., 2005). Common strategies include coagulation-flocculation, precipitation, ion exchange, membrane filtration, and adsorption treatment (Bayuo, Rwiza, Mtei, et al., 2024). Among these techniques, adsorption has emerged as a particularly effective and widely applied method for arsenic removal (Siddiqui & Chaudhry, 2017). Adsorption offers notable advantages, including simplicity in

operation, convenient waste management, lack of additional chemicals, high efficiency, and lower operational costs (Bayuo et al., 2023; Habuda-Stanić & Nujić, 2015; Siddiqui et al., 2019). A diverse range of adsorbents, including activated alumina, activated carbon, silica gel, zeolites, metal oxide/hydroxide, nanomaterials, and low-cost options such as sand, biomaterials, and clay minerals have been utilized for arsenic removal in water treatment (Islam et al., 2021; Mondal & Garg, 2017; Rahidul Hassan, 2023). Activated alumina has been reported to effectively capture arsenic at different capacities (mg g^{-1}) such as 0.03 (Majumder, 2018), 0.05 (Singh & Pant, 2004), and 36.6 (Han et al., 2013).

In recent years, increasing interest has been in utilizing renewable and low-cost adsorbents derived from agricultural waste for water treatment applications (Dai et al., 2018). For instance, activated carbon showed good adsorption potential, with a capacity of 0.18 mg mg^{-1} (Lee, 2010), and 1.01 mg g^{-1} (Budinova et al., 2009) for arsenic removal. Activated carbon is recognized for its exceptional ability to bind a wide range of water contaminants, making it a popular choice for adsorption. Due to environmental and economic concerns, researchers are exploring low-cost alternatives prepared from waste materials (Jjagwe et al., 2021).

Among the renewable resources to produce biochar, orange peels have shown promising potential as an adsorbent due to their high content of pectin (25%), cellulose (22%), and hemicellulose (11%) (Ayala et al., 2021). From a sustainability point of view, orange peels, which account for 50–60% of the total mass of orange fruit, currently represent a significant waste management challenge (Alalm et al., 2016; Teigiserova et al., 2021). The improper disposal of orange peel waste poses significant environmental and socioeconomic challenges. Incineration contributes to air pollution and health risks, while dumping contaminates land and water resources (Koiri & Das,

2024). In 2022/2023, the global orange production reached approximately 46.88 million metric tons, highlighting its significance as a major crop economically and nutritionally. Accordingly, the mass of waste orange peel was between 23.44 and 28.13 million metric tons in 2022/2023. Brazil remains the largest producer in the 2023-2024 season, contributing around 34% of the global output. China follows, accounting for about 15.5% of total production, while the United States and the European Union also play significant roles in the global market (*United States Department of Agriculture, 2024*). Producing biochar from orange peel is an effective way to manage and reduce waste (Lam et al., 2018). This process not only recycles organic waste but also transforms it into a valuable material with applications in environmental management.

The addition of Titanium dioxide (TiO_2) to activated carbon from orange peels for surface modification is specifically aimed at enhancing the material's properties for arsenic removal. Incorporating TiO_2 nanoparticles can enhance the surface area and porosity of the activated carbon, creating more sites for arsenic interaction (Alalm et al., 2016; Vajedi & Dehghani, 2019). Titanium dioxide is a highly promising material for enhancing the surface properties of activated carbon due to its exceptional stability, insolubility in water, and non-toxicity (Ali et al., 2019; Eshaghi & Moradi, 2018; Jain et al., 2019).

Response Surface Methodology (RSM) is a statistical technique widely used in experimental design and optimization (Bashir et al., 2015). The RSM's capability to develop multivariate regression models surpasses the limitations of conventional approaches, which involve keeping variables constant and restricting their range during optimization to determine the optimal conditions (Khoshraftar et al., 2023).

The most commonly employed response surface design is the Central Composite Design (CCD). This design enables the extension of factorial experiments by

incorporating axial and center points (Veza et al., 2023). The CCD involves selecting factorial points to capture main effects, axial points to model curvature, and center points to estimate pure error and validate the model (Beg & Rahman, 2021). This balanced arrangement enables researchers to explore the experimental space efficiently, providing insights into the optimal operating conditions for a desired outcome.

Previous studies have demonstrated the potential of various agricultural waste-based adsorbents for arsenic removal. However, limited research has been conducted on using orange peels as an adsorbent for arsenic removal. This study aims to investigate the efficiency of renewable adsorbents derived from orange peels in removing arsenic from synthetic aqueous solutions. It focuses on optimizing the adsorption capacity and evaluating the kinetics of the modified activated carbon derived from orange peels.

This research is important as it leverages the abundant by-product of orange peels, transforming it into a novel high-performance adsorbent through TiO_2 modification for arsenic removal from water. Addressing the environmental challenge of waste management and the critical issue of arsenic contamination in drinking water aligns with the circular economy principles and the United Nations Sustainable Development Goals (SDG), particularly SDG 6 (clean water and sanitation) and SDG 12 (responsible consumption and production). The approach exemplifies sustainability by turning waste into a valuable resource, providing an affordable and effective solution for arsenic removal, particularly in regions where both issues are prevalent. This dual benefit contributes to economic viability and environmental protection.

5.2. Materials and Methods

5.2.1. Preparation and characterization of the adsorbent

The Nanopowder used in this study was titanium dioxide (TiO_2 , anatase, 99.9%, particle size 18 nm), procured from U.S. Research Nanomaterials in Texas, USA. Sodium hydrogen arsenate (AsHNa_2O_4) was obtained from A&C American Chemicals Ltd. in QC, Canada. High-purity carbon dioxide and nitrogen (99.99%) were purchased from Praxair Canada Inc. An Arsenic solution (60 mg L^{-1}) was prepared by dissolving $\text{AsHNa}_2\text{O}_4 \cdot 7\text{H}_2\text{O}$ in deionized water.

The orange peels were sourced from markets in St. John's, Newfoundland and Labrador. The peels were washed with distilled water to remove dirt from their surface and oven-dried for 12 h at 80°C . The dried peels were crushed and sieved to the desired mesh size (0.595 mm). The dried and crushed peels were placed in ceramic combustion boats inside the quartz tube. The orange peels were carbonized under N_2 atmosphere (flow rate = $100 \text{ cm}^3 \text{ min}^{-1}$) in a tubular furnace (Lindberg/Blue M, Model TF55035A-1, USA) at 500°C for 2 h. The powdered orange peels before and after carbonization were subjected to elemental analysis. After that, for the activation of biochar, the N_2 flow was substituted for CO_2 (flow rate = $100 \text{ cm}^3 \text{ min}^{-1}$ at 500°C for 1 h). Afterward, 0.1 g of TiO_2 nanoparticles was added per each 1 g of the activated carbon from both materials in a flask containing 50 mL of distilled water; the solution was thoroughly ultrasonicated for 30 min at room temperature. The final mixture was filtered and washed with distilled water. The material retained on the filters was oven-dried overnight at 65°C and called OP- TiO_2 (Activated carbon from orange peels modified by titanium dioxide). Figure 5-1 illustrates the steps of synthesizing the OP- TiO_2 .

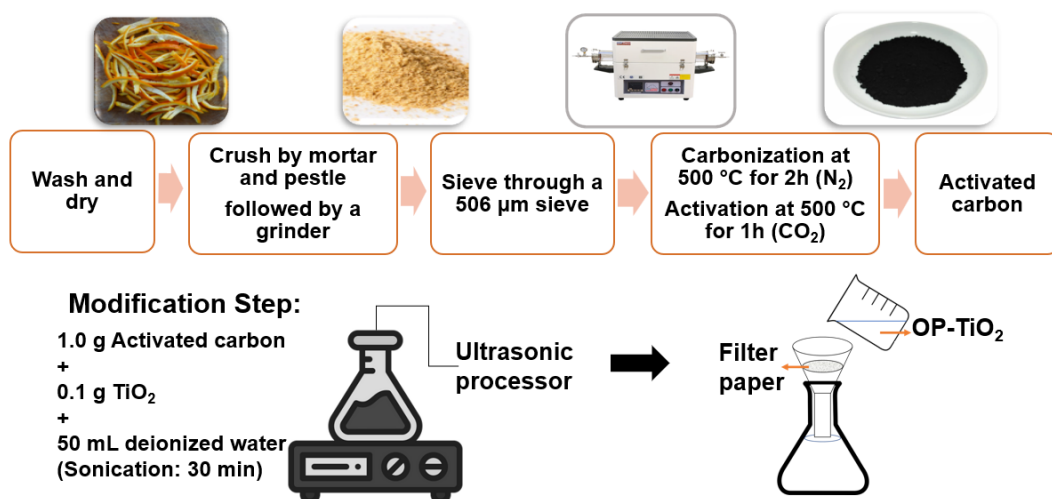


Figure 5-1 Preparation of activated carbon from orange peels modified by titanium dioxide (OP- TiO_2).

Characterization studies were conducted to investigate activated carbon's physical and chemical properties before and after modification with TiO_2 . These studies aimed to understand better the effectiveness of the adsorbent creation process and the adsorption mechanisms. The adsorbents' surface morphology and chemical composition were analyzed using a Field Emission Detector Scanning Electron Microscope (SEM) coupled with Energy-Dispersive X-ray Spectroscopy (EDX). This analysis involved using a Thermo EDX at 15.0 kV to perform particle elemental analysis (JSM-7100F, JEOL Ltd, Japan). A Bruker Tensor 27 FTIR instrument operating in the ZnSe Attenuated Total Reflection (ATR) mode was utilized to identify the functional surface groups. X-ray diffraction (XRD) analysis was performed using a Cu source and scintillation detector (Ultima-IV, 40 kV/44 mA, Rigaku, Japan) to determine structural composition. A surface area analyzer (Tristar II 3020, Micromeritics, US) was employed to measure the specific surface area through nitrogen adsorption-desorption at 77 K. Additionally, the pH of zero charge (pH_{pzc}) of the adsorbent was determined by adjusting 100 mL of distilled water to a pH range of 2 to 12 using HCl or NaOH. Then, 100 mg of the adsorbent was added to the solution and

stirred for 24 h. After this period, the final pH (pH_{final}) was measured. The pH_{pzc} was identified by plotting the final pH against the initial pH and locating the point where the final pH equaled the initial pH.

5.2.2. Adsorption experiments

The As(V) stock solution (60 mg L^{-1}) was prepared by dissolving $\text{HAsNa}_2\text{O}_4 \cdot 7\text{H}_2\text{O}$ and in deionized water, respectively. The stock solution was diluted to provide the required solutions. A known amount of adsorbent was added to 50 mL Erlenmeyer flasks containing As solution at the desired pH. The pH of the metal solutions was adjusted using 0.1 M and 1 M solution of hydrochloric acid (HCl) and sodium hydroxide (NaOH). The flasks were then placed on an orbital shaker at 200 rpm for a given time. All experiments were carried out at room temperature. The mixture was filtered and analyzed using an inductively coupled plasma–optical emission spectrometer, ICP-OES (Optima 5300 DV, PerkinElmer, USA).

Batch adsorption experiments were performed to remove arsenic ions (Sodium hydrogen arsenate (AsHNa_2O_4)) from water. The selection of factors and the operating range for the independent variables were established based on a thorough review of relevant literature, combined with the outcomes of preliminary experiments, including one-factor-at-a-time tests. Several factors influence heavy metal adsorption from water, impacting the efficiency and capacity of adsorbents. The most important parameters are pH, initial metal concentration, adsorbent dose, contact time, and temperature (Qiu et al., 2021; Tahooun et al., 2020). This study examined pH (A), initial metal concentration (B), adsorbent dose (C), and contact time (D). Various studies have widely used these four factors to optimize heavy metal adsorption (Baby et al., 2019; ElSayed, 2018; Pavithra et al., 2021). The study also discussed the effect of temperature in the

thermodynamics section since many studies have reported an optimum temperature of around 25 °C for heavy metal adsorption from aqueous samples (Aboli et al., 2020; Chai et al., 2020; Fakhre & Ibrahim, 2018). The central composite design (CCD) is a widely used experimental design in response surface methodology (RSM) to establish the relationship between process factors and the response, which is the adsorbent capacity (Lamidi et al., 2022; Sugashini & Begum, 2013). The central composite design in response surface methodology optimization is highly effective in reducing both operational time and cost, while minimizing the number of experimental runs. Furthermore, the results obtained through this approach are statistically reliable (Bayuo, Rwiza, Choi, et al., 2024). The design included factorial points at the corners of the experimental space to estimate main effects and interactions, axial points along the factor axes to capture curvature and quadratic effects, and center points at the midpoint to assess experimental error and detect any curvature (Bayuo et al., 2020; Beg & Rahman, 2021). The CCD created a matrix for four variables to determine the optimal pH values, metal ion concentration, biomass dosage, and contact time (Table 5-1). The experimental data can be fitted using a second-order polynomial response surface model (Eq. (5-1)) (Šumić et al., 2016):

$$R = \beta_0 + \sum_{i=1}^4 \beta_i x_i + \sum_{i=1}^3 \sum_{j=i+1}^4 \beta_{ij} x_i x_j + \sum_{i=1}^4 \beta_{ii} x_i^2 + \varepsilon \quad (5-1)$$

where, R represents the expected response (adsorbent capacity), while β_0 , β_i , β_{ii} , β_{ij} , and ε denote the offset, linear effect, squared effect, interaction impact, and residual term, respectively. The coded independent variables (pH, contact time, initial concentration, and adsorbent dose) are denoted by x_i and x_j . A total of 21 experiments consisting of 5 center points, 8 axial points, and 8 factorial points were designed using Design Expert software (version 12.0.8.0, Stat-Ease Inc., Minneapolis, MN, USA). Table 5-1

represents the experimental design for the adsorption of arsenic on OP-TiO₂.

Table 5-1 Experimental factors for optimization of arsenic adsorption using OP-TiO₂.

Parameter	Unit	- α	-1	0	+1	+ α
A-pH		1	2.2	4	5.8	7
B-Initial concentration	mg L ⁻¹	10	20	35	50	60
C-Adsorbent dose	g L ⁻¹	0.5	2	4.2	6.4	8
D-Contact time	h	0.4	1.25	3	4.8	6

5.2.3. Kinetic and isotherm experiments

Kinetic experiments were conducted under optimal conditions over 5 to 180 min to investigate the adsorption behavior of the orange peel-derived adsorbents for arsenic removal. The experimental data obtained from these kinetic studies were fitted to pseudo-first-order (Eq. (5-2)), pseudo-second-order (Eq. (5-3)), intra-particle diffusion (Eq. 5-4), and Elovich (Eq. (5-5)) models.

$$\log (q_e - q_t) = \log q_e - \left(\frac{k_1}{2.303} \right) t \quad (5-2)$$

In Eq. (5-2), q_e represents the adsorption capacity at equilibrium in milligrams per gram (mg g⁻¹), k_1 is the adsorption rate constant in grams per milligram per minute (g (mg·min)⁻¹).

$$t/q_t = 1/q_e^2 k_2 + t/q_e \quad (5-3)$$

In Eq. (5-3), k_2 is the reaction rate constant in grams per milligram per hour (g (mg·min)⁻¹), q_e is the amount of solute adsorbed at equilibrium in milligrams per gram (mg g⁻¹), and q_t is the amount of solute adsorbed at time t .

To determine k_2 and q_e , a plot of t/q_t versus t is created, and a straight line can be formed. The value of k_2 can be calculated using the slope and intercept of the graph as $k_2 = (\text{slope})^2 / \text{intercept}$. The q_e is determined as $1/\text{slope}$.

$$q_t = k_{id}t^{1/2} + C \quad (5-4)$$

where q_t is the amount of adsorbate adsorbed at time, k_{id} is the intra-particle diffusion rate constant, and C is the intercept, which gives an indication of the boundary layer thickness (Azha et al., 2015).

$$q_t = \frac{1}{\beta} \ln(\alpha\beta) + \frac{1}{\beta} \ln(t) \quad (5-5)$$

where q_t is the adsorbed amount at time (t), α is the initial adsorption rate, and β is related to the extent of surface coverage and activation energy.

Isotherm studies were conducted to examine the adsorption behavior of the selected OP-TiO₂ adsorbent for arsenic removal. The comparison of the calculated values with the experimental data helps to identify the most suitable model for describing the adsorption isotherms and provides insights into the adsorption mechanisms and surface properties of the OP-TiO₂ adsorbent. To determine the adsorption capacity and assess the adsorption isotherms, the obtained experimental data were fitted to Langmuir, Freundlich, Temkin, and Dubinin-Radushkevich (D-R) models.

The experiments were conducted at room temperature with a constant optimum initial ion concentration of 50 mg L⁻¹ and a pH of 4.2. Various adsorbent doses ranging from 0.5 to 4.5 g L⁻¹ were employed, and the contact time was set at 24 h.

The Langmuir model assumes monolayer adsorption onto a homogeneous surface, while the Freundlich model accounts for multilayer adsorption on a heterogeneous surface.

The Langmuir model is represented by Eq. (5-6).

$$\frac{C_e}{q_e} = \frac{1}{bq_{max}} + \frac{C_e}{q_{max}} \quad (5-6)$$

where C_e represents the equilibrium concentration of the adsorbate (mg L⁻¹), q_e is the

amount of adsorbate adsorbed at equilibrium (mg g^{-1}), q_{max} is the maximum adsorption capacity (mg g^{-1}), and b is the Langmuir constant related to the adsorption energy.

The Freundlich model is described by Eq. (5-7).

$$\ln q_e = \ln k_f + \frac{1}{n} \ln C_e \quad (5-7)$$

where k_f is the Freundlich constant representing adsorption capacity, and n is the Freundlich exponent related to adsorption intensity.

The Temkin model is expressed by Eq. (5-8) (X. Chen et al., 2022; Musah et al., 2022).

$$q_e = B \ln (k_t C_e) \quad (5-8)$$

where q_e is the amount of adsorbate adsorbed at equilibrium, C_e is the equilibrium concentration of the adsorbate in solution, k_t is the Temkin isotherm constant related to the maximum binding energy, and B is a constant related to the heat of adsorption (Adebayo et al., 2015).

The Dubinin-Radushkevich (D-R) isotherm is used to describe adsorption on heterogeneous surfaces and is expressed by Eq. (5-9) (X. Chen et al., 2022).

$$q_e = q_m e^{-\beta \epsilon^2} \quad (5-9)$$

where q_e is the amount of adsorbate adsorbed at equilibrium, q_m is the theoretical saturation capacity, β is a constant related to the adsorption energy, and ϵ is the Polanyi potential, calculated as (Eq. (5-10)):

$$\epsilon = RT \ln \left(1 + \frac{1}{C_e} \right) \quad (5-10)$$

where R is the gas constant, T is the absolute temperature, and C_e is the equilibrium

concentration. In the Dubinin-Radushkevich (D-R) isotherm, E represents the mean free energy of adsorption per adsorbate mole. E is calculated using the D-R isotherm constant β and is given by Eq. (5-11) (Abin-Bazaine et al., 2022; Amin et al., 2017):

$$E = \frac{1}{\sqrt{2\beta}} \quad (5-11)$$

where β is the D-R constant, related to the adsorption energy and determined from the isotherm fitting. The value of E provides insight into the type of adsorption process. When E is under 8 kJ mol^{-1} , it typically signifies physical adsorption, which is associated with weaker van der Waals forces. An E value ranging from 8 to 16 kJ mol^{-1} usually points to ion exchange processes. Values exceeding 16 kJ mol^{-1} indicate chemisorption, where stronger chemical bonds form between the adsorbate and the adsorbent (X. Chen et al., 2022).

5.2.4. Thermodynamic studies

The investigation into the thermodynamic aspects of the arsenic adsorption process included examining its favourability, reversibility, and energy characteristics.

Eqs. (5-12) and (5-13) provide a means to compute thermodynamic properties such as changes in entropy (ΔS°), standard enthalpy (ΔH°), and Gibbs free energy (ΔG°).

The relationship between these parameters is given by:

$$\Delta G^\circ = \Delta H^\circ - T\Delta S^\circ \quad (5-12)$$

$$\ln K_c = \frac{\Delta S^\circ}{R} - \frac{\Delta H^\circ}{RT} \quad (5-13)$$

where R is the ideal gas constant ($8.314 \text{ J} \cdot \text{K}^{-1} \cdot \text{mol}^{-1}$) and T represents the temperature in Kelvin.

The equilibrium constant (K_c) is expressed by the equation $K_c = q_e/C_e$. The thermodynamic properties, ΔS° , ΔH° , and ΔG° , can all be determined from the slopes

and intercepts of the plot $\ln K_c$ versus $1/T$.

5.3. Results and Discussion

5.3.1. Adsorbent characterization

5.3.1.1. Elemental analysis

Table 5-2 provides a detailed overview of the properties of powdered orange peels before and after carbonization. Carbon content increased significantly from 41.38% in the original orange peels to 73.09% in the activated carbon. Conversely, hydrogen and oxygen levels decreased, dropping from 6.19% to 3.10% and 47.45% to 14.25%, respectively, while Sulfur and nitrogen levels remained relatively unchanged. A previous study found that carbonization significantly increased the carbon content of orange peels from 41% to 86%, while reducing oxygen and hydrogen levels from 52% to 14% and 6% to 2%, respectively (Malesic-Eleftheriadou et al., 2022). These changes are consistent with the removal of volatile components and the breakdown of oxygen-containing functional groups during carbonization (H. Liu et al., 2022), confirming the significant impact of activation on the structure of the final product.

Table 5-2 Properties of powdered orange peels before and after carbonization (wt.% by dry basis).

Parameter	Powdered orange peels	Charred orange peels
pH	5.71	8.75
Ash (%)	4.11	7.95
C (%)	41.38	73.09
H (%)	6.19	3.10
N (%)	0.84	1.61
S (%)	0.03	0.00
O* (%)	47.45	14.25
Molecular formula	$C_{57}H_{102}O_{50}N$	$C_{55}H_{28}O_8N$

C = Carbon; H = Hydrogen; N = Nitrogen; S = Sulfur; and O = Oxygen.

*Calculated by difference ($O\% = 100\% - (C\% + H\% + N\% + S\% + \text{Ash}\%)$).

5.3.1.2. X-ray diffraction crystallography (XRD)

Figure 5-2 depicts the XRD patterns of activated carbon derived from orange peels

before and after being modified with TiO₂ nanoparticles. A peak at $2\theta = 22^\circ$ corresponding to the (002) planes confirms the presence of activated carbon, as supported by previous studies (Kakavandi et al., 2019; Sarioğlu, 2013), while the diffraction peaks observed at small angles ($< 30^\circ$) indicate a broadening diffusion pattern, suggesting that the structure of the activated carbon is amorphous with a heterogeneous surface (Okamura et al., 2006). The peaks observed at 25° (101), 36° (004), 48° (200), 52° (105), 54° (211), 62° (204), 69° (220), and 75° (215) indicate the attachment of TiO₂ to the activated carbon. These diffraction peaks align well with the characteristic pattern of anatase, as indicated by the standard JCPDS card no. 89-492 (Selvaraj et al., 2019).

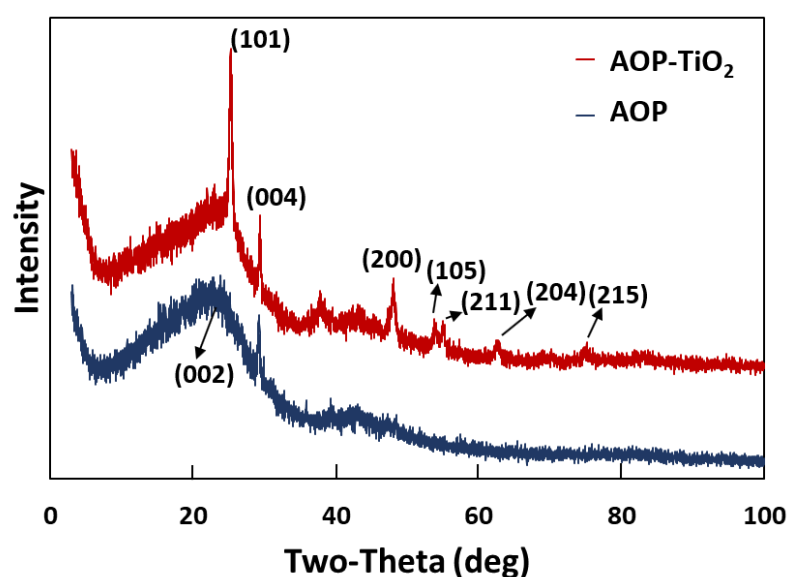


Figure 5-2 X-ray diffraction crystallography (XRD) patterns for activated carbon before and after modification by TiO₂.

5.3.1.3. Brunauer-Emmett-Teller (BET) surface area analysis

As indicated in Table 5-3, introducing TiO₂ modification to the surface of activated carbon obtained from orange peels resulted in a remarkable 255.68% increase in the surface area and 265.91% in the pore volume of the orange peel-based adsorbent. This

augmentation in surface area is attributed to the deposition of TiO₂ nanoparticles onto the activated carbon surface, facilitating the generation of extra active sites and surface roughness. An increase in pore volume typically indicates that the modification with TiO₂ has led to the creation of additional pores or the expansion of existing ones. This can be attributed to the deposition of TiO₂ nanoparticles on the surface of the activated carbon, contributing to forming more active sites and potentially enhancing the material's adsorption capacity.

Table 5-3 Results of the Brunauer-Emmett-Teller (BET) analysis for activated carbon before and after modification.

Characteristic of activated carbon	Before modification	After modification
BET surface area (m ² g ⁻¹)	2.3962	8.5182
Pore volume (cm ³ g ⁻¹)	0.000701	0.002561

5.3.1.4. Scanning electron microscopy (SEM)

The comparison of the modified activated carbon (OP-TiO₂) and activated carbon derived from orange peels SEM results (Figure 5-3a, Figure 5-3c) revealed that aggregates were present on the particle surface of modified activated carbon. In contrast, the unmodified materials displayed a smooth surface.

The Energy dispersive X-ray spectroscopy (EDX) analysis demonstrated that carbon is the most abundant element in activated carbon derived from orange peels before and after modification (Figure 5-3b, Figure 5-3d). The presence of TiO₂ was confirmed by EDX analysis for both adsorbents, as depicted in Figure 5-3.

5.3.1.5. *Fourier-transform infrared spectroscopy (FTIR)*

The FTIR spectra of OP-TiO₂ and As loaded-OP-TiO₂ is shown in Figure 5-4. The peak observed at 666.7 cm⁻¹ confirmed the successful creation of titanium dioxide nanoparticles loaded onto activated carbon since this peak indicates the presence of oxygen-metal-oxygen bonds (Neisan et al., 2023; Parvathiraja et al., 2022).

The peak at 1565.8 cm⁻¹ can be attributed to the asymmetric stretching vibration of the C=O bond (Afolabi et al., 2022; Beyan et al., 2021; Yang et al., 2022). Additionally, the peak at 2325 cm⁻¹ was attributed to –NH stretching, while the peak at 1372 cm⁻¹ was believed to be due to O–H and C–O stretching vibrations (Alam et al., 2018; Beyan et al., 2022; Ramesh et al., 2019).

The adsorption peaks before and after As adsorption were nearly identical across the wavelength ranges. This indicates that the same functional groups are present on the OP-TiO₂ surface before and after adsorption. However, there is a significant change in the peak intensities of the spectrum (Afolabi et al., 2022). The absorption band observed at approximately 2325 cm⁻¹ is more likely attributed to the asymmetric stretching vibration of atmospheric CO₂, which is commonly detected in FTIR spectra due to background interference during measurements. Additionally, the shift in the peak at 1564 cm⁻¹ to 1568 cm⁻¹ and the decreased intensity of the peak at 1372 cm⁻¹ suggest the involvement of hydroxyl and carboxyl groups in the adsorption of arsenic and the formation of surface complexes (Afolabi et al., 2022; Alam et al., 2018; Beyan et al., 2022; Ramesh et al., 2019).

The observed changes suggest that As(V) adsorption is primarily driven by electrostatic and surface complexation involving oxygen-containing functional groups. These results align with the findings reported by previous studies (Beyan et al., 2022; Dehghan et al., 2021; Mudzielwana et al., 2020; Ramesh et al., 2019).

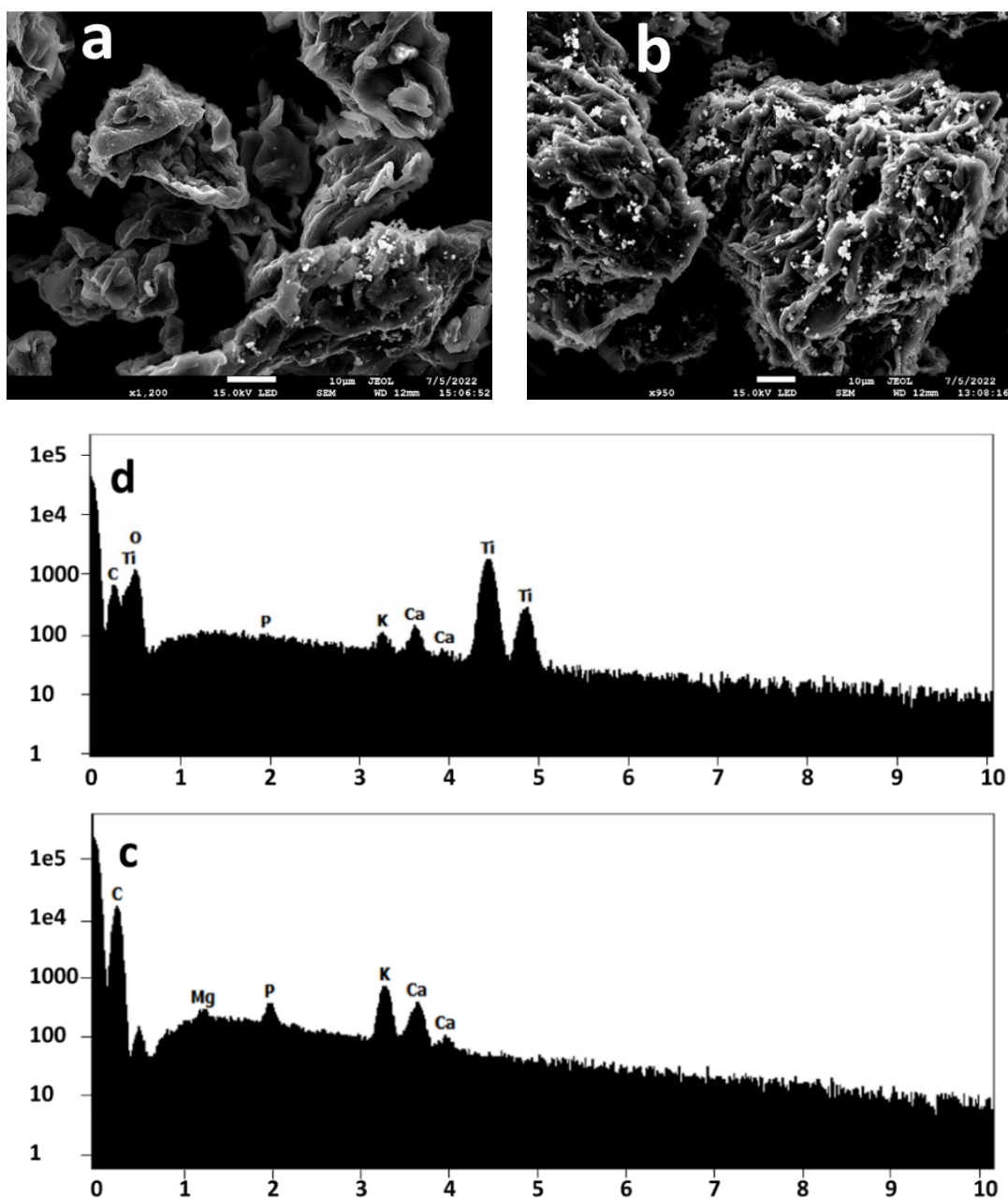


Figure 5-3 Scanning electron microscopy (SEM) of the activated carbon (a) before and (b) after modification by TiO_2 ; energy dispersive X-ray spectroscopy (EDX) of the activated carbon (c) before and (d) after modification by TiO_2 .

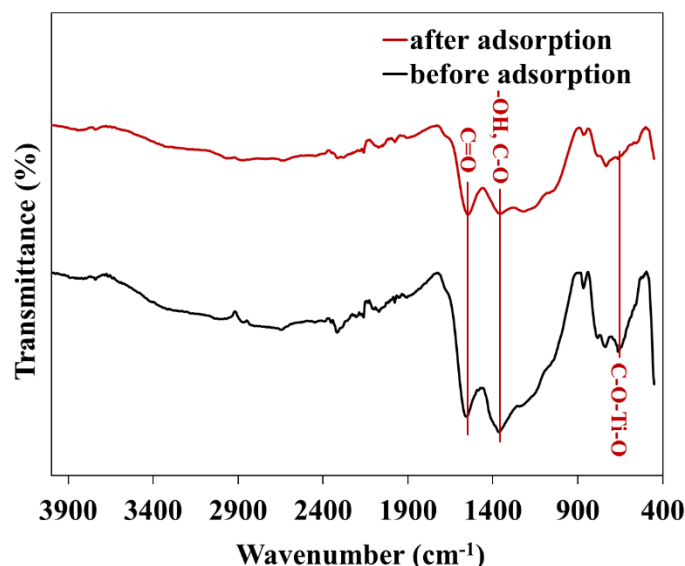


Figure 5-4 Fourier-transform infrared spectroscopy (FTIR) spectra of modified orange peel activated carbon (OP-TiO₂).

5.3.2. Optimization of arsenic removal

The analysis of variance (ANOVA) was utilized to evaluate the statistical significance of the quadratic model. The F and p values determine the significance of each coefficient. A higher F-value and a smaller p-value indicate a greater level of significance for the corresponding coefficients (Peng et al., 2020). Lack-of-fit p-values greater than 0.05 were considered insignificant, and the term model is significant ($p < 0.05$) (Khoshnamvand et al., 2018), indicating that the proposed model accurately described the relationship between the experimental variables and adsorption capacity.

According to Table 5-4, the linear effects of initial ion concentration (B) and adsorbent dosage (C) were significant ($p < 0.0001$), and the linear effects of contact time (D) and pH (A) were moderately significant. The squared terms of C^2 and D^2 were insignificant, with all other factors (initial ion concentration (B), adsorbent dosage (C), A^2 , B^2 , AB, AC, AD, BC, BD, and CD being significant ($p < 0.0001$). The regression equations were employed to determine the OP-TiO₂ capacity, which was dependent on the initial As ion concentration, pH, adsorbent dosage, and contact time. The empirical

relationship between As ion removal (Y) and the variables was represented by reduced polynomial equations (Table 5-5). Table 5-6 provides the optimal values of each factor to achieve maximum adsorption efficiency.

Table 5-4 ANOVA for reduced quadratic modeling of arsenic removal.

Adsorbent capacity					
Source	Sum of Squares	df	Mean Square	F-value	p-value
Model	132.01	12	11.00	538.71	< 0.0001
A- pH	0.0590	1	0.0590	2.89	0.1402
B- initial concentration	30.33	1	30.33	1485.40	< 0.0001
C- adsorbent dose	13.80	1	13.80	675.66	< 0.0001
D- contact time	0.0310	1	0.0310	1.52	0.2642
AB	6.01	1	6.01	294.47	< 0.0001
AC	10.62	1	10.62	520.02	< 0.0001
AD	8.20	1	8.20	401.73	< 0.0001
BC	2.00	1	2.00	98.06	< 0.0001
BD	7.66	1	7.66	374.99	< 0.0001
CD	10.35	1	10.35	506.97	< 0.0001
A ²	1.77	1	1.77	86.76	< 0.0001
B ²	0.1588	1	0.1588	7.77	0.0316
C ²					
Residual	0.1225	6	0.0204		
Lack of Fit	0.0005	2	0.0003	0.0087	0.9914
Pure Error	0.1220	4	0.0305		
Cor Total	132.13	18			
Predicted R ²	0.894		Adjusted R ²		0.996

Table 5-5 Coefficients in terms of coded factors.

Factor	Coefficient
Intercept	+5.59
A-pH	+0.1031
B-initial concentration	+2.32
C-adsorbent dose	-1.68
D-contact time	+0.0741
AB	-1.70
AC	+1.81
AD	+2.01
BC	+0.7790
BD	+1.93
CD	-1.78
A ²	-0.3631
B ²	-0.1069
C ²	0
D ²	0

Table 5-6 Optimal solutions for highest arsenic adsorption.

Adsorbent	pH	C_i (mg L ⁻¹)	A_d (g L ⁻¹)	t_c (h)	Desirability	RE (%)	AC (mg g ⁻¹)
OP-TiO ₂	4.2	50	3.3	4.8	0.885	75.250	10.916

C_i = initial concentration; A_d = adsorbent dose; t_c = contact time; RE = removal efficiency; AC = adsorption capacity.

Figure 5-5 presents the model's 3D plots for adsorption capacity as a function of various factors. In Figure 5-5a, with adsorbent dose (4.25 g L⁻¹) and contact time (3.2 h), increasing pH and initial concentration leads to a higher adsorption capacity. Similar trends were observed in other heavy metal removal studies. For instance, Pb, Cu, Cd, Zn, and Cr adsorption from water on blast furnace slag and fly ash increased with rising pH, showing a sharp increase between pH 4.0-7.0 (T. C. Nguyen et al., 2018). Similarly, removal rates of polyacrylamide-modify-chitosan magnetic composite nanoparticles for metal ions increased significantly when pH rose from 2.0 to 3.0, then improved more gradually with higher pH. At pH > 3.0, removal rates remained high (>86% for Cu(II) and >75% for Ni(II) (Zheng et al., 2020). Additionally, As the pH increased from 2 to 6, the adsorption capacity of sultone-modified magnetic activated carbon for Pb(II), As(III), and Cd(II) metal ions improved (Nejadshafiee & Islami, 2019).

Similarly, in Figure 5-5d, at a fixed pH (4) and contact time (3.2 h), increasing the initial concentration also increases adsorption capacity, while decreasing the adsorbent dose boosts adsorption capacity. In Figure 5-5e, where pH (4) and adsorbent dose (4.25 g L⁻¹) are held constant, increasing the initial concentration enhances adsorption capacity. This is supported by findings from other research on heavy metal adsorption. It was reported that agricultural waste materials (peanut shell and sawdust) were used to replace activated carbon for removing heavy metal ions from aqueous solutions. As the initial concentration of ions (lead, copper, and cadmium) increased (5-400mg L⁻¹),

adsorption also increased, since higher initial concentrations provide a driving force for ions to move from the solution to the adsorbent surface (X. Liu et al., 2020).

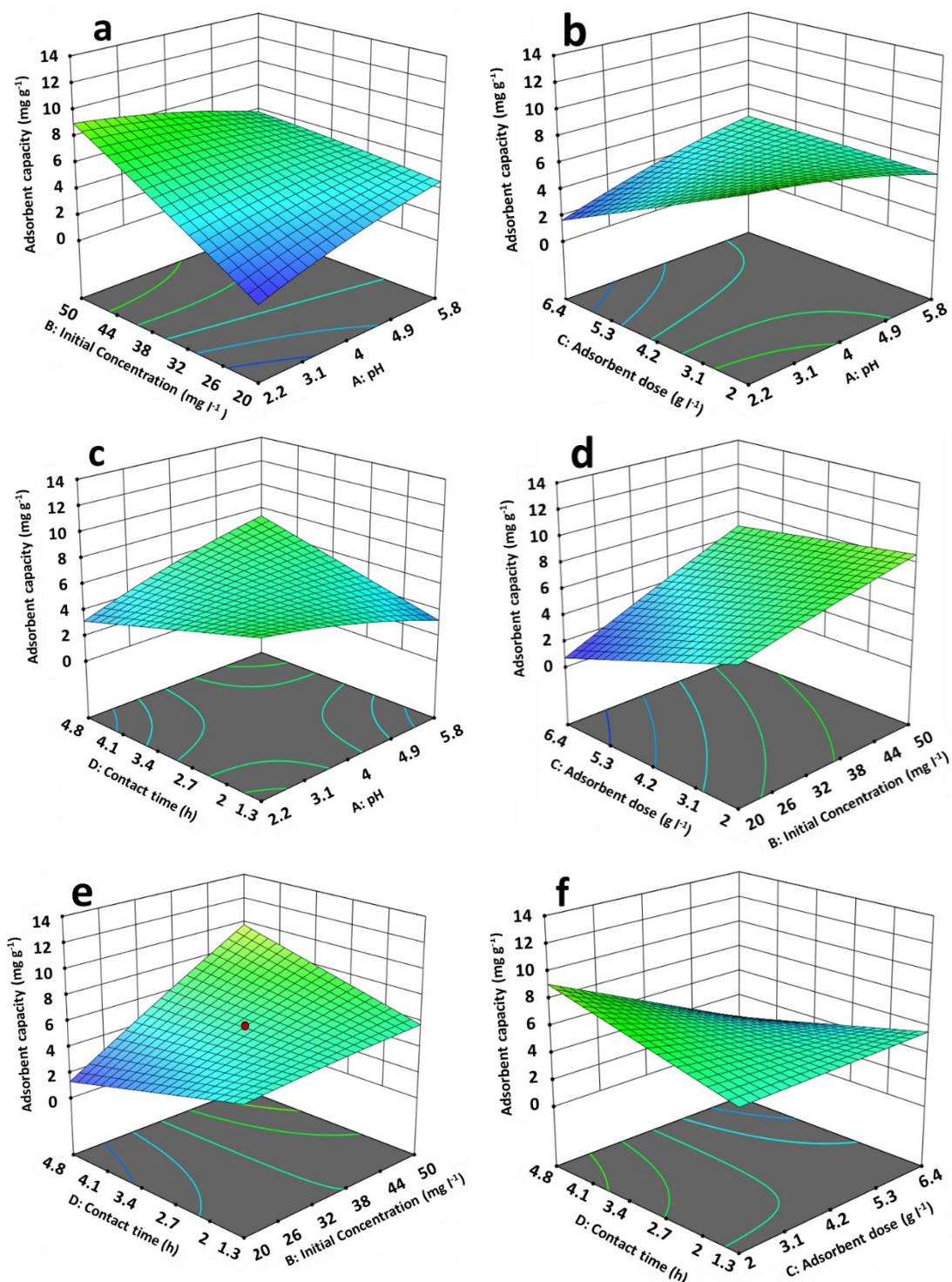


Figure 5-5 Combined influence of (a) pH and initial concentration; (b) pH and adsorbent dose; (c) pH and contact time; (d) initial concentration and adsorbent dose; (e) initial concentration and contact time; and (f) adsorbent dose and contact time on adsorbent capacity.

Additionally, in the removal percentages of Ni(II), Cu(II), Zn(II), Cd(II), and Pb(II) using chemically modified cellulose, as the initial concentrations increased from 2 to 12 mg L⁻¹, the adsorption efficiency of the metals rose (Fakhre & Ibrahim, 2018).

On the other hand, Figure 5-5b, which holds the initial concentration (35 mg L⁻¹) and contact time (3.2 h) constant, shows that increasing the adsorbent dose decreases adsorption capacity. This trend aligns with the findings of other studies. For instance, for copper adsorption on rubber (*Hevea brasiliensis*) leaf powder, the adsorption capacity decreased from 5.63 mg g⁻¹ to 0.23 mg g⁻¹ as the adsorbent dosage increased from 0.4 g L⁻¹ to 20 g L⁻¹ (Rukayat et al., 2021). Moreover, for a polysaccharide composite hydrogel, in a 50 mL solution of 100 mg L⁻¹ M²⁺ (where M = Cu, Co, Ni, Pb, Cd), the adsorption capacity decreases as the amount of hydrogel exceeds 0.02 g (Jiang et al., 2019). Figure 5-5f, however, with a fixed pH (4) and initial concentration (35 mg L⁻¹), demonstrates that increasing the contact time improves the adsorption capacity. This is supported by studies that found that extending contact time improved the adsorption capacity of various adsorbents in heavy metal removal. For instance, using 0.12 g L⁻¹ of 200 µm date pits, Cu²⁺, Zn²⁺, and Ni²⁺ were removed from solutions (10–110 ppm) at pH 5.5. The metal uptake increased with time and stabilized after 72 h, with efficiency remaining constant thereafter (Hummadi, 2021).

Furthermore, the effect of contact time on the biosorption capacity of Moringa pods for heavy metal ions (Cu, Ni, and Cr) at initial concentrations of 25–100 mg L⁻¹ at 10-minute intervals was investigated. It was found that further increases in contact time did not enhance biosorption removal after 40 min for copper, 30 min for nickel, and 40 mins for chromium (Matouq et al., 2015). Additionally, in the adsorption of Pb(II) on chemically oxidized mesoporous carbon (COMC), the rate of Pb(II) uptake was rapid

initially, with 80% of adsorption completed within 1–2 h on COMC. Equilibrium adsorption was achieved in 5 h (Baniamerian et al., 2009).

The adsorption of heavy metals is typically very rapid within the first hour (Ayob et al., 2021; Chakraborty et al., 2022), which is why no significant changes were observed within this timeframe in the experiment. Diagnostic plots were examined to assess the suitability of the regression model. Figure 5-6b displays the actual and predicted removal efficiency and adsorbent capacity values, illustrating that the linear regression fit successfully predicts the experimental data. The reliability of the model was assessed using the residuals versus fits plot (Figure 5-6a), which indicated no discernible trends of rising or dropping points, rising or dropping residuals with increasing fits, or a majority of positive or negative residuals. These findings indicate the reliability of the model.

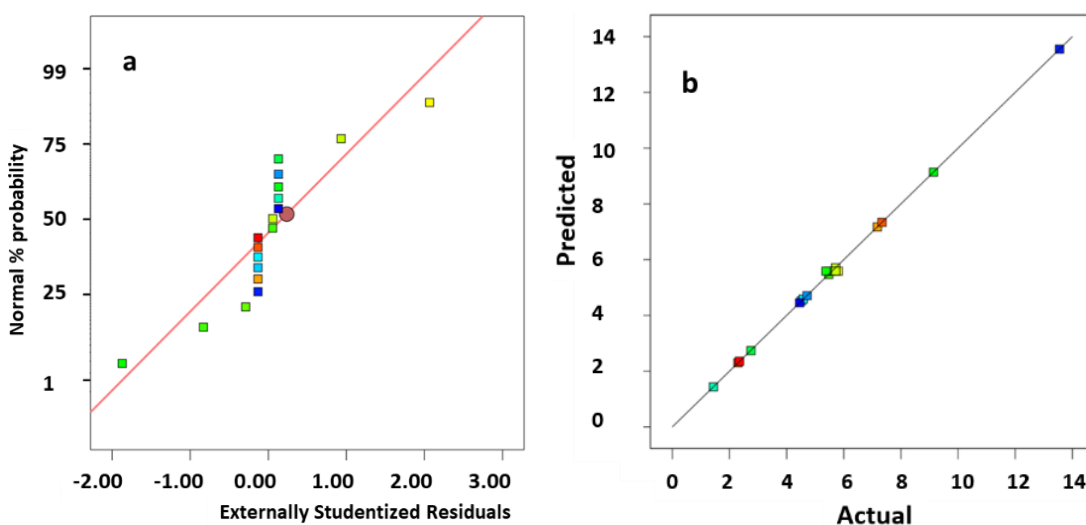


Figure 5-6 plots of the adsorbent capacity model (a) normal probability versus residual; (b) correlation between the predicted and actual experiment values.

5.3.2.1. Effect of pH

Within the range of the experimental conditions, the effect of pH on the adsorbent capacity of OP-TiO₂ was statistically insignificant, and the optimal pH for maximizing

these parameters was approximately 4.2. The interactions between pH, initial concentration, adsorbent dose, and contact time were visualized in Figure 5-5c, Figure 5-5d, and Figure 5-5e. Similar trends have been observed in previous studies. For example, in the removal of As(V) using zirconium-based nanoparticle-doped activated carbon fiber, it was found that the maximum uptake of As(V) occurred at pH 3.0, while the uptake decreased with increasing pH due to competition between hydroxide ions and arsenic species (D. Zhao et al., 2016). Another study reported that the adsorption capacity of composite material for arsenic gradually reduced as the initial pH of the solution increased, with an optimal initial pH of 4.0 (Ma et al., 2018).

5.3.2.2. Effect of adsorbent dose

The effect of the adsorbent dose on the adsorption process was investigated, and it was observed that increasing the OP-TiO₂ dosage enhanced the adsorption efficiency. This improvement can be attributed to the increased availability of active sites on the surface of the adsorbent, facilitating the adsorption of heavy metal ions. However, it was observed that beyond a certain point within the experimental range, further increases in the adsorbent dose resulted in a decrease in adsorbent capacity. Similar findings have been reported in other studies, such as the adsorption of As(V) using nanoscale zero-valent iron supported by activated carbon, where increasing the dose of NZVI/AC from 0.5 to 2.0 g L⁻¹ resulted in an increase in the removal rate of As(V) from approximately 63.6% to 100% (Zhu et al., 2020). In the study of As(III) and As(V) removal using rubber tire-derived activated carbon modified with alumina composite at room temperature, experiments were conducted at pH 7 with initial arsenic concentrations ranging from 20 to 100 mg L⁻¹. The effect of adsorbent dose on adsorption was investigated. For As(III), the percentage removal increased rapidly with an adsorbent dose up to 4 g L⁻¹, then showed a slower increase up to 8 g L⁻¹. For As(V),

a sharp increase in removal was observed up to 2 g L^{-1} , followed by a slower increase. However, the adsorptive capacity (q_e) decreased significantly as the adsorbent dose increased from 1 to 8 g L^{-1} in all cases (Karmacharya et al., 2016).

5.3.2.3. Effect of initial concentration

Increasing As initial concentration were found to increase the adsorbent capacity. Models predicted the optimum C_i was around 50 mg L^{-1} . The available active sites on the adsorbent are easily occupied with metal ions at low initial concentrations. Figure 5-5f and Figure 5-5g show the mutual effect of initial concentration, adsorbent dose, and contact time. Similarly, in the biosorption study of toxic heavy metals using activated carbon derived from the algae species *Ulva lactuca*, the impact of initial metal concentration was examined at pH 5 with a biosorbent dosage of 0.6 g L^{-1} over 60 min. Metal concentrations from 5 to 80 mg L^{-1} were tested. It was found that the initial metal ion concentration significantly affected metal uptake. Maximum removal percentages of 87.5% and 100% were achieved at 60 mg L^{-1} for *Ulva lactuca* and its activated carbon, respectively. The high removal efficiency at this concentration was attributed to the availability of vacant active sites. However, removal efficiency decreased at higher metal concentrations due to the saturation of binding sites on the adsorbent's surface (Ibrahim et al., 2016).

5.3.2.4. Effect of contact time

The duration of the contact time had minimal effect on the adsorbent capacity. A slight improvement was observed within the experimental timeframe for the desired outcome. Figure 5-5e, Figure 5-5g, and Figure 5-5h illustrate the combined influence of contact time and other variables. The maximum adsorption capacity was achieved after approximately 4.8 h of contact, and no significant additional increase was observed beyond that point. Likewise, The effect of contact time on date palm fiber activated

carbon (AC-DPF) adsorption for Pb(II) and Cu(II) was studied between 0–180 minutes (pH ~5.5, 20 mg L⁻¹, and 1.5 g L⁻¹). in two stages: initial rapid adsorption occurred due to abundant active sites, followed by slower adsorption as sites filled. Equilibrium was reached at 90 minutes for Pb(II) and 120 minutes for Cu(II) (Melliti et al., 2023).

As the literature shows, heavy metal adsorption typically involves three stages: fast, slow, and equilibrium. Initially, adsorption is rapid due to the abundance of vacant sites on the activated carbon surface. Over time, the adsorption rate slows as the heavy metal concentration decreases and these sites fill up. Eventually, the adsorbent nears saturation, signaling the transition to the equilibrium stage after a certain period of time (Zhang et al., 2023).

5.3.3. Comparison with other studies

In order to provide a comprehensive overview and comparison of the effectiveness of various adsorbents for arsenic removal, Table 5-7 was compiled to present a summary of the results obtained from different studies. This table includes details on the adsorbents used, experimental conditions, and the corresponding removal efficiency or adsorbent capacity achieved in each study. The results of the experiments conducted using OP-TiO₂ adsorbent demonstrated its promising capacity for arsenic removal.

Table 5-8 presents various biochar adsorbents derived from sources such as agricultural, food, animal, forestry, and aquacultural waste, along with their highest adsorption capacities as reported in similar studies. A visual representation of this data is shown in Figure 5-7. The figure demonstrates that our adsorbent performed exceptionally well in arsenic removal, surpassing many other similar adsorbents.

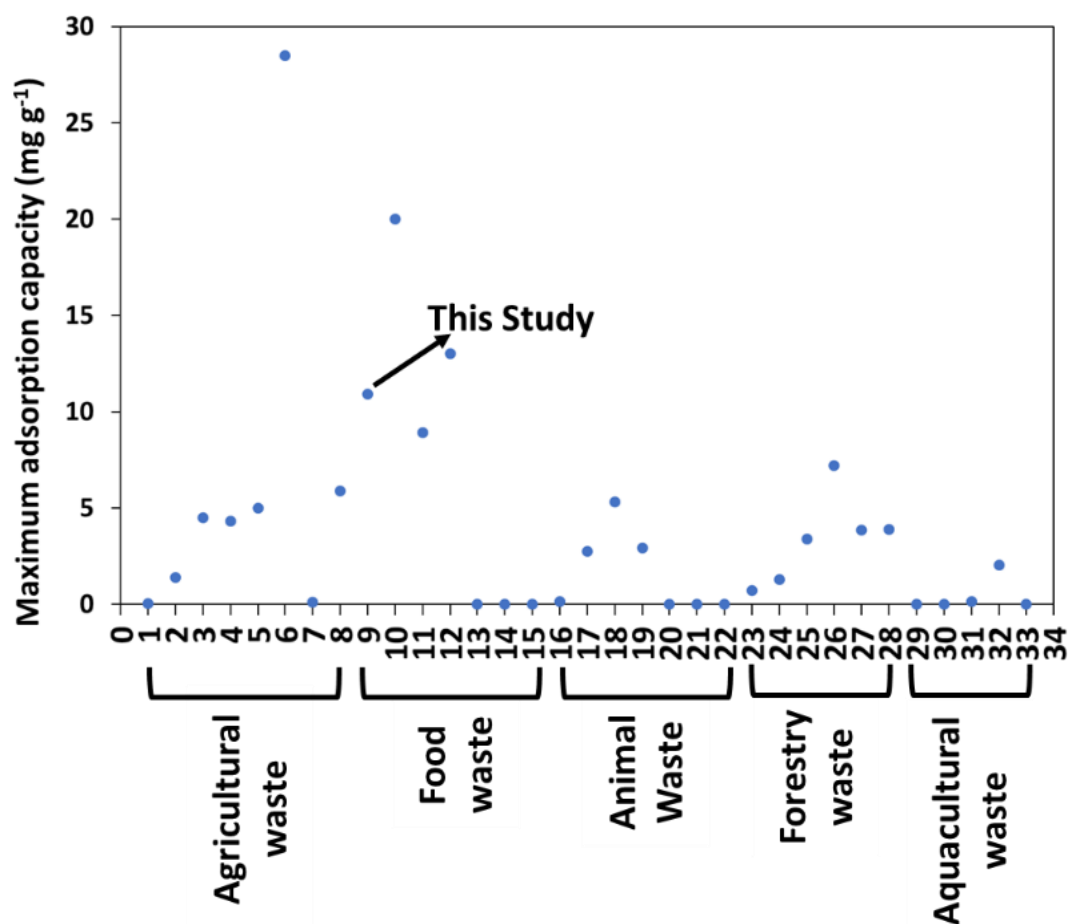


Figure 5-7 Comparison of arsenic adsorption capacities of the biochar adsorbent developed in this research and similar biochars from various sources.

Table 5-7 Summary of adsorptive removal of arsenic by various adsorbents.

Adsorbent	Adsorbate	C _i (mg L ⁻¹)	Adsorbent dose (g L ⁻¹) Unless indicated otherwise	pH	Contact time (h)	Other Info	RE (%)/ AC (mg g ⁻¹)	Reference
OP-TiO ₂	As(v)	50	3.3	4.2	4.8	room temperature 200 rpm	75.25% 10.91	This study
Rice straw-derived biochar	As(V)	0.1	2	6	2	room temperature 250 rpm	>60% 5.6 µg g ⁻¹	(Mukherjee et al., 2021)
Tea waste	As(V)	100	10	6	1	25 ± 1 °C	72%	(Cheraghi et al., 2014)
Alginate beads	As(III) As(V)	10	1	6	7d	23 ± 1 °C 100 rpm	~55% ~30%	(Sigdel et al., 2016)
Aluminum-Impregnated Tea waste Biochar	As(V)	0.1	10	6	1	room temperature 120 rpm	99.6 µg g ⁻¹	(Sawood et al., 2021)
Chitosan beads	As(III) As(V)	10	3.3	5	24	25 ± 2 °C 50 rpm	1.83 1.94	(C.-C. Chen & Chung, 2006)
FeOOH/CuO-water bamboo cellulose	As(III)	150		3.5	24	20 ± 2	76.1 mg g ⁻¹	(H. Liu et al., 2020)
Saccharomyces cerevisiae	As(III) As(V)	0.132 0.133	48.5×10 ⁷ CFU 47.5×10 ⁷ CFU	5	24	100 rpm 25 °C	66.2% 15.8%	(Hadiani et al., 2019)
Macromolecule-carbonized rice husks	As(V)	0.1	2	6	1.1	300 rpm	85%	(Babazad et al., 2021)
PAN Fiber	As(III) As(V)	0.05	10	7	2	150 rpm	80% 98%	(Bhatti et al., 2020)
Fe/Cu nanoparticles	As(III) As(V)	1	0.1	7	1	room temperature 200 rpm	69% 89%	(Babae et al., 2018)
Iron-coated seaweeds	As(III) As(V)	25	10	7	4	20 °C 200 rpm	4.2 7.3	(Vieira et al., 2017)

C_i = initial concentration; RE = removal efficiency; AC = adsorption capacity; OP-TiO₂ = activated carbon from orange peels modified by TiO₂.

Table 5-8 Overview of biochar adsorbents derived from different waste sources (agricultural, food, animal, forestry, and aquacultural) and their highest reported adsorption capacities for arsenic removal from similar studies.

	Biochar source (waste)	Adsorbent	Adsorbent capacity (mg g ⁻¹)	Surface area (m ² g ⁻¹)	Pore volume (cm ³ g ⁻¹)	Reference
1	Agricultural	Rice straw-derived biochar	0.0256	133	0.043–0.048	(Mukherjee et al., 2021)
2	Agricultural	ZnO-impregnated coffee husk biochar	1.4	3	-	(Cruz et al., 2020)
3	Agricultural	Base modified cotton stalk biochar	4.48	(60.3	-	(Hussain et al., 2020)
4	Agricultural	Acid-modified cotton stalk biochar	4.32	47.3	-	(Hussain et al., 2020)
5	Agricultural	Peanut shell biochar	5.01	-	-	(Sattar et al., 2019)
6	Agricultural	Rice straw iron-modified biochar	28.49	-	-	(T. H. Nguyen et al., 2019)
7	Agricultural	Iron-impregnated banana pith biochar	0.12	31.59	-	(Lata et al., 2019)
8	Agricultural	Red mud-modified rice straw	5.9	186.95	-	(Wu et al., 2017)
9	Food	Iron oxide-modified calcined mussel shells	10.91	8.5182	0.002561	This study
10	Food	Biochar sugarcane bagasse Fe modified	20	-	-	(Montero et al., 2018)
11	Food	FeCl ₃ /Coffee ground under CO ₂	8.9	512	0.249	(Cho et al., 2017)
12	Food	FeCl ₃ /Coffee ground under N ₂	13	8.3	0.018	(Cho et al., 2017)
13	Food	Kitchen Waste	11.3	2.57	-	(Kumar et al., 2021)
14	Food	Orange peel	6.5	1.5	0.002–0.093	(Kumar et al., 2023)
15	Food	Pomelo peel biochar coated with iron	11.77	5.43	0.0289	(T. H. Nguyen et al., 2022)
16	Animal	Cattle bone char	0.13	100	0.225	(Begum et al., 2016)
17	Animal	Crayfish shell biochar	2.76	28.64	0.11	(Sun et al., 2022)

Table 5-8 continued.

	Biochar source (waste)	Adsorbent	Adsorbent capacity (mg g ⁻¹)	Surface area (m ² g ⁻¹)	Pore volume (cm ³ g ⁻¹)	Reference
18	Animal	Magnetic dairy cattle manure biochar	5.3	21.35	-	(Akyürek et al., 2022)
19	Animal	Yak dung	2.926	37.944	0.0782	(Chunhui et al., 2018)
20	Animal	Pristine hydrochar from dairy cattle manure	19.05	0.935	0.001	(H. Chen et al., 2021)
21	Animal	Thiourea-activated manure hydrochar	38.77	7.34	0.02	(H. Chen et al., 2021)
22	Animal	Thiourea-Fe(NO ₃) ₃ -activated manure hydrochar	44.80	33.45	0.095	(H. Chen et al., 2021)
23	Forestry	Lagerstroemia leaves biochar	0.71	6.18	0.0499	(Verma & Singh, 2019)
24	Forestry	Tectona leaves Biochar	1.3	34.55	0.1929	(Verma & Singh, 2019)
25	Forestry	Japanese oak wood biochar	3.38	475	0.2	(Niazi, Bibi, Shahid, Ok, Shaheen, et al., 2018)
26	Forestry	Perilla leaf derived biochar (700 °C)	7.21	473.4	0.1	(Niazi, Bibi, Shahid, Ok, Burton, et al., 2018)
27	Forestry	Perilla leaf derived biochar (300 °C)	3.85	3.2	0.4734	(Niazi, Bibi, Shahid, Ok, Burton, et al., 2018)
28	Forestry	<i>L. camara</i>	3.9	1.5–148.1	0.002–0.093	(Kumar et al., 2023)
29	Aquacultural	Green seaweed (<i>Ulva reticulata</i>)	7.67	-	-	(Senthilkumar et al., 2020)
30	Aquacultural	Bone char	0.124	-	-	(CONG et al., 2019)
31	Aquacultural	Pleco fish bone chars	0.1321	154	0.381	(Cruz-Briano et al., 2024)
32	Aquacultural	Crayfish shell biochar	2.03	25.46, 63.79	32.67, -	(Xiao et al., 2017)
33	Aquacultural	Modified algal-based biochars	62.5–80.7	-	-	(Johansson et al., 2016)

5.3.4. Kinetics studies

Table 5-9 presents the kinetics parameters, while Figure 5-8 illustrates the kinetic plot for the pseudo-first-order, pseudo-second-order, intra-particle diffusion, and Elovich models, respectively. The kinetics studies were conducted at pH 4.2, initial concentration 50 mg L⁻¹, and adsorbent dose 3.3 g L⁻¹.

Based on the R^2 values, the intra-particle diffusion model is the most suitable model for describing As adsorption by OP-TiO₂. This model's results revealed a multi-stage adsorption process, which was evident from the distinct phases observed in Figure 5-8c. The first stage exhibited the highest slope, indicating rapid adsorption due to external surface diffusion, where the adsorbate quickly adheres to the outer surface of the adsorbent. This phase is driven by boundary layer diffusion and is marked by the immediate availability of active sites on the adsorbent surface. The second stage showed a lower slope, suggesting a slower adsorption process, controlled by intra-particle diffusion. During this phase, the adsorbate molecules penetrate into the internal pores of the adsorbent, and the adsorption rate decreases as the molecules encounter more resistance within the adsorbent structure. The third stage, with the lowest slope, represented the final equilibrium phase, where diffusion into the micropores is nearly complete, and the adsorption rate is minimal. The presence of these distinct stages confirms that intra-particle diffusion was involved in the overall adsorption process, but it was not the sole rate-limiting step (Taha et al., 2016; J. Zhao et al., 2016).

The Elovich model also provided a good fit for the adsorption data, with a correlation coefficient ($R^2 = 0.924$). The relatively high α value suggests a rapid initial adsorption rate, while the β value indicates a gradual decrease in adsorption rate over time, which is consistent with the behavior observed for chemisorption on heterogeneous surfaces (Baniamerian et al., 2009; Matouq et al., 2015).

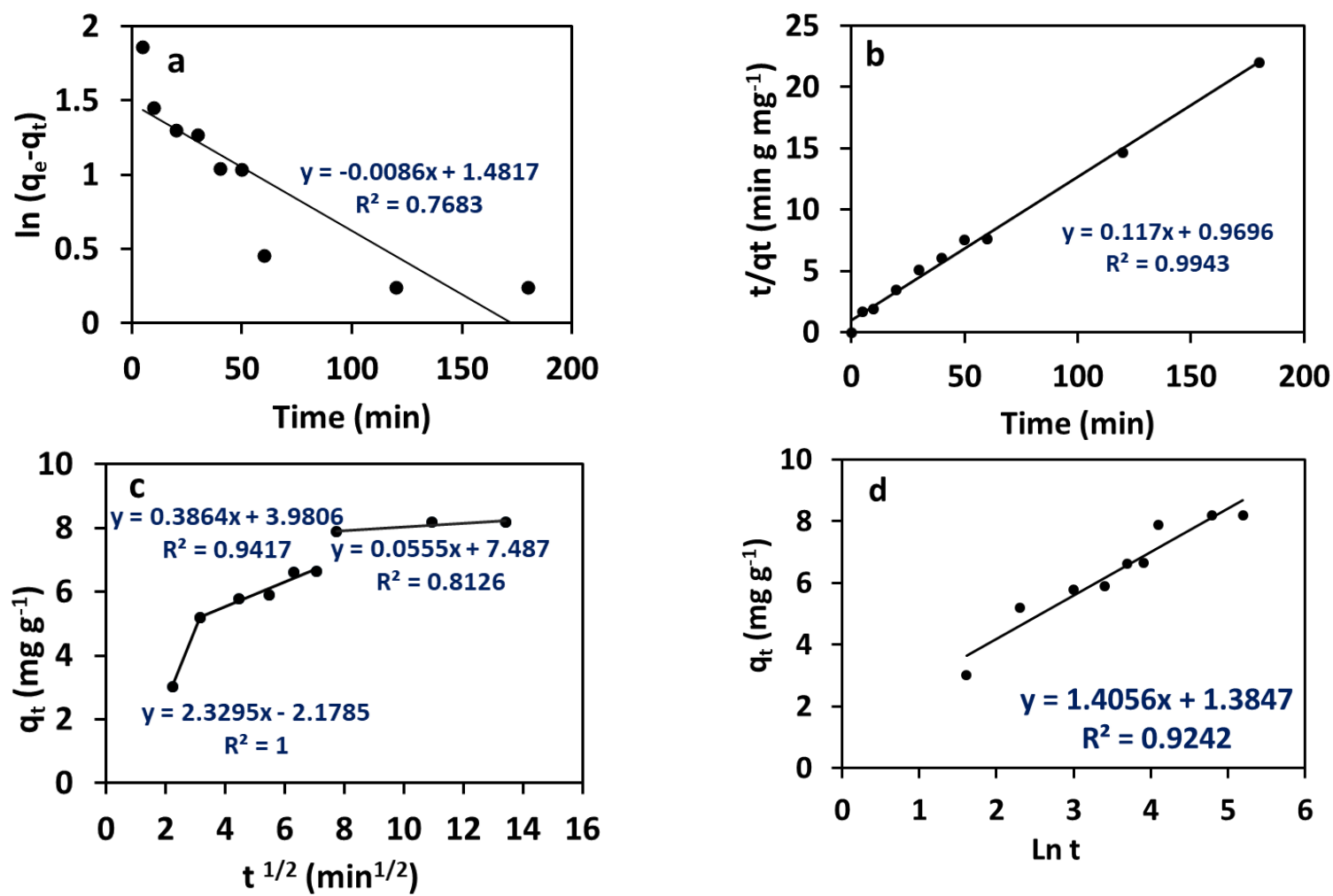


Figure 5-8 Arsenic adsorption kinetic studies: (a) pseudo-first-order, (b) pseudo-second-order, (c) intra-particle diffusion, and (d) Elovich models. All at pH = 4.2, $C_i = 50 \text{ mg L}^{-1}$, and room temperature.

Table 5-9 Kinetic parameters for the pseudo-first-order, pseudo-second-order, Elovich, and intra-particle diffusion models.

Parameter	Pseudo-first-order	Pseudo-second-order	Elovich	Intra-particle diffusion
1st parameter (adsorption rate constant)	$k_1 = 0.00005 \text{ min}^{-1}$	$k_2 = 0.222 \text{ g mg}^{-1} \text{ min}^{-1}$	$\alpha = 3.764 \text{ mg g}^{-1} \text{ min}^{-1}$	$k_{1d} = 2.330$ $k_{2d} = 0.386$ $k_{3d} = 0.056 \text{ g mg}^{-1} \text{ min}^{-0.5}$
2nd parameter (mg g^{-1}) Unless indicated otherwise	$q_e = 9.46$	$q_e = 6.215$	$\beta = 0.711 \text{ g mg}^{-1}$	$C_1 = -2.179$ $C_2 = 3.981$ $C_3 = 7.487$
R^2	0.002	0.998	0.924	$R_1^2 = 1$ $R_2^2 = 0.942$ $R_3^2 = 0.813$

R^2 = coefficient of determination.

5.3.5. Isotherm studies

Table 5-10 provides the parameters obtained from fitting the experimental data to the isotherm models. It was observed that the Temkin isotherm model provided a better fit to the experimental data compared to the other isotherm models for the adsorption of arsenic onto the OP-TiO₂ adsorbent. Furthermore, the R^2 value for Temkin isotherm was the closest to 1, confirming its strong predictive accuracy. A better fit to the Temkin isotherm suggests that the adsorption process is likely influenced by factors such as surface heterogeneity, non-ideal adsorption, and interactions between adsorbate molecules (Jawad et al., 2016). Figure 5-9 illustrates the fitting of various adsorption isotherm models (Freundlich, Langmuir, Temkin, and D-R) to the experimental data for arsenic adsorption onto OP-TiO₂. In the Freundlich isotherm model, a parameter value of $1/n < 1$ indicates that the adsorption process is favorable and suggests chemisorption. Additionally, when n lies between 1 and 10, it suggests that the adsorbent surface is heterogeneous (Bayuo et al., 2019).

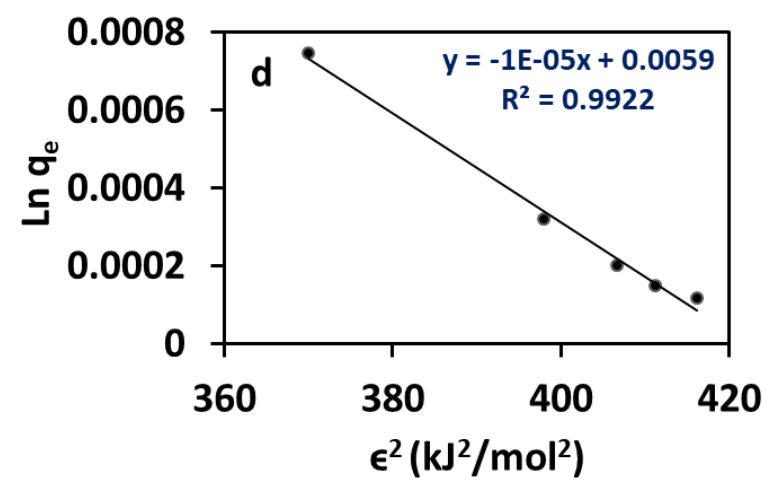
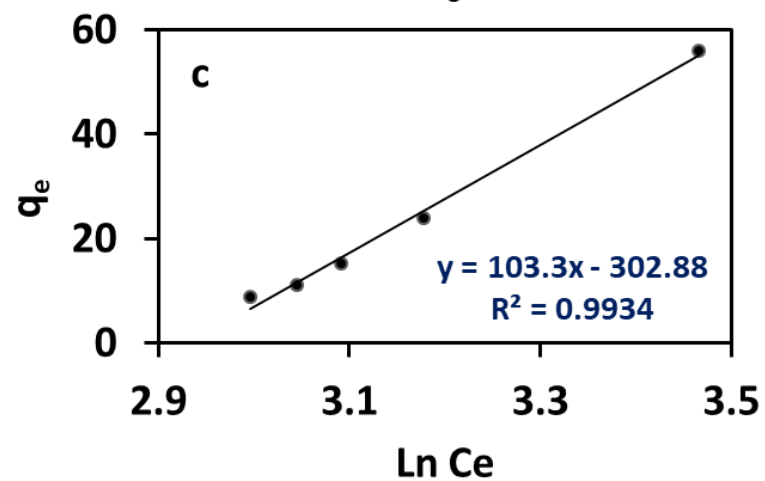
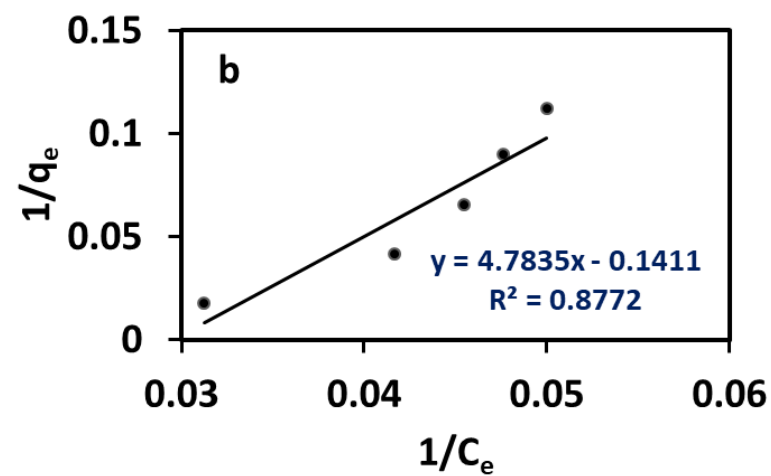
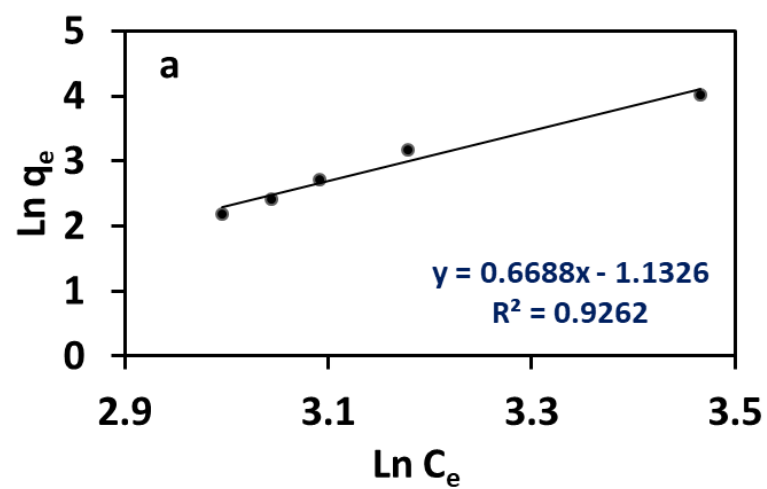


Figure 5-9 Adsorption isotherm models fitted to the experimental data for arsenic adsorption onto OP-TiO₂: (a) Freundlich (b) Langmuir (c) Temkin, and (d) D-R models.

Table 5-10 Isotherm parameters of Langmuir, Freundlich, Temkin, and D-R models.

Parameter	Langmuir	Freundlich	Temkin	D-R
Model 1st parameter	$b = 33.902$ L mg^{-1}	$k_f = 0.322$ $\text{L mg}^{(1-(1/n))} \text{g}^{-1}$	$k_t = 0.0533$ L mg^{-1}	$q_m = 1.0059$ mol g^{-1}
Model 2 nd parameter	$q_m = 0.209$ mg g^{-1}	$n = 1.495$	$B = 103.3$	$\beta = 0.0000$ $1 \text{ mol}^2 \text{ kJ}^{-2}$
R^2	0.887	0.926	0.993	0.992

R^2 = coefficient of determination

5.3.6. Thermodynamic studies

The entropy (ΔS°) and enthalpy (ΔH°) values for adsorption were determined by fitting a linear plot (Figure 5-10) of $\log(q_e/C_e)$ against $1/T$ within three distinct temperature ranges: 298 K, 308 K, and 323 K (Table 5-11). The computed free energy (ΔG°) was negative, indicating that the adsorption is spontaneous at these temperatures. The increasing magnitude of the negative values indicates a progressively more spontaneous reaction as the temperature rises.

The positive ΔH° value ($13.59 \text{ kJ mol}^{-1}$) for OP-TiO₂ suggests that arsenic adsorption by OP-TiO₂ is endothermic. This is consistent with an increase in enthalpy as the temperature rises. Additionally, the positive value of ΔS° ($46.39 \text{ J mol}^{-1} \text{ K}^{-1}$) indicates the increased randomness at the solid/solution interface during As(V) adsorption on the adsorbent.

Table 5-11 Thermodynamic parameters for removal of arsenic at different temperatures.

Adsorbent	Temperature (K)	ΔH° (kJ mol^{-1})	ΔS° ($\text{J mol}^{-1} \text{ K}^{-1}$)	ΔG° (kJ mol^{-1})
OP-TiO ₂	298.15	13.5884	46.39	-0.32473
	308.15			-0.54764
	323.15			-1.46529

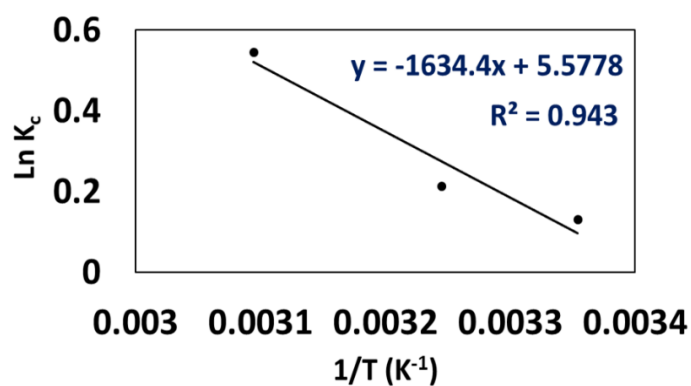


Figure 5-10 Thermodynamic studies for arsenic adsorption onto OP-TiO₂.

5.4. Conclusion

A novel adsorbent material was successfully developed by incorporating TiO₂ nanoparticles into activated carbon derived from orange peels. This modification resulted in a significant increase in the surface area of the activated carbon. The experimental results highlight the highest arsenic removal capacity of OP-TiO₂ (10.91 mg g⁻¹), with pH optimization at 4.2, optimum As initial concentration of 50 mg L⁻¹, adsorbent dose of 3.3 g L⁻¹. While contact time exhibited minimal impact on removal efficiency, a slight improvement was observed within the experimental timeframe (0.4-6 h) after 4.8 h. Applying statistical models for experimental design contributed to a systematic approach to process optimization. The experimental data were fitted to four kinetic models, and the results indicated that the intra-particle kinetic model provided a better description of As sorption onto OP-TiO₂. Moreover, the Temkin isotherm model was found to be a more suitable description of the experimental data for arsenic adsorption onto the OP-TiO₂ adsorbent, compared to the other isotherm models. The thermodynamics studies of arsenic adsorption on OP-TiO₂ indicated that the reaction is spontaneous and endothermic, confirmed by the negative free energy (ΔG°) and positive ΔH° . The findings of this research not only underscore the potential of OP-

TiO₂ but also pave the way for further exploration of renewable adsorbents for broader applications in water treatment.

5.5. References

- Abin-Bazaine, A., Trujillo, A. C., & Olmos-Marquez, M. (2022). Adsorption isotherms: enlightenment of the phenomenon of adsorption. *Wastewater Treatment*, 1–15.
- Aboli, E., Jafari, D., & Esmaeili, H. (2020). Heavy metal ions (lead, cobalt, and nickel) biosorption from aqueous solution onto activated carbon prepared from Citrus limetta leaves. *Carbon Letters*, 30, 683–698.
- Adebayo, G. B., Adegoke, H. I., Jamiu, W., Balogun, B. B., & Jimoh, A. A. (2015). Adsorption of Mn (II) and Co (II) ions from aqueous solution using Maize cob activated carbon: kinetics and Thermodynamics Studies. *Journal of Applied Sciences and Environmental Management*, 19(4), 737–748.
- Afolabi, F. O., Musonge, P., & Bakare, B. F. (2022). Adsorption of copper and lead ions in a binary system onto orange peels: Optimization, equilibrium, and kinetic study. *Sustainability*, 14(17), 10860.
- Akyürek, Z., Çelebi, H., Çakal, G. Ö., & Turgut, S. (2022). Enhanced Arsenic (V) Removal from Aqueous Solution by a Novel Magnetic Biochar Derived from Dairy Cattle Manure. *Korean Chemical Engineering Research*, 60(3), 423–432.
- Alalm, M. G., Tawfik, A., & Ookawara, S. (2016). Enhancement of photocatalytic activity of TiO₂ by immobilization on activated carbon for degradation of pharmaceuticals. *Journal of Environmental Chemical Engineering*, 4(2), 1929–1937.

- Alam, M. A., Shaikh, W. A., Alam, M. O., Bhattacharya, T., Chakraborty, S., Show, B., & Saha, I. (2018). Adsorption of As (III) and As (V) from aqueous solution by modified *Cassia fistula* (golden shower) biochar. *Applied Water Science*, 8, 1–14.
- Ali, S., Li, Z., Chen, S., Zada, A., Khan, I., Khan, I., Ali, W., Shaheen, S., Qu, Y., & Jing, L. (2019). Synthesis of activated carbon-supported TiO₂-based nano-photocatalysts with well recycling for efficiently degrading high-concentration pollutants. *Catalysis Today*, 335, 557–564.
- Amin, M. T., Alazba, A. A., & Shafiq, M. (2017). Effective adsorption of methylene blue dye using activated carbon developed from the rosemary plant: isotherms and kinetic studies. *Desalination and Water Treatment*, 74, 336–345.
- Ayala, J. R., Montero, G., Coronado, M. A., García, C., Curiel-Alvarez, M. A., León, J. A., Sagaste, C. A., & Montes, D. G. (2021). Characterization of orange peel waste and valorization to obtain reducing sugars. *Molecules*, 26(5), 5.
<https://doi.org/10.3390/molecules26051348>
- Ayob, S., Othman, N., Altowayti, W. A. H., Khalid, F. S., Bakar, N. A., Tahir, M., & Soedjono, E. S. (2021). A review on adsorption of heavy metals from wood-industrial wastewater by oil palm waste. *Journal of Ecological Engineering*, 22(3).
- Azha, S. F., Ahmad, A. L., & Ismail, S. (2015). Thin coated adsorbent layer: characteristics and performance study. *Desalination and Water Treatment*, 55(4), 956–969.
- Babae, Y., Mulligan, C. N., & Rahaman, M. S. (2018). Removal of arsenic (III) and arsenic (V) from aqueous solutions through adsorption by Fe/Cu nanoparticles. *Journal of Chemical Technology & Biotechnology*, 93(1), 63–71.

- Babazad, Z., Kaveh, F., & Ebadi, M. (2021). *Efficient removal of lead and arsenic using macromolecule-carbonized rice husks. Heliyon 7: e06631.*
- Baby, R., Saifullah, B., & Hussein, M. Z. (2019). Palm Kernel Shell as an effective adsorbent for the treatment of heavy metal contaminated water. *Scientific Reports*, 9(1), 18955.
- Baniamerian, M. J., Moradi, S. E., Noori, A., & Salahi, H. (2009). The effect of surface modification on heavy metal ion removal from water by carbon nanoporous adsorbent. *Applied Surface Science*, 256(5), 1347–1354.
- Bashir, M. J. K., Amr, S. S. A., Aziz, S. Q., Aun, N. C., & Sethupathi, S. (2015). Wastewater treatment processes optimization using response surface methodology (RSM) compared with conventional methods: Review and comparative study. *Middle-East Journal of Scientific Research*, 23(2), 244–252.
- Bayuo, J., Abukari, M. A., & Pelig-Ba, K. B. (2020). Optimization using central composite design (CCD) of response surface methodology (RSM) for biosorption of hexavalent chromium from aqueous media. *Applied Water Science*, 10(6), 1–12.
- Bayuo, J., Pelig-Ba, K. B., & Abukari, M. A. (2019). *Adsorptive removal of chromium (VI) from aqueous solution unto groundnut shell. Appl Water Sci 9: 107.*
- Bayuo, J., Rwiza, M. J., Choi, J. W., Sillanpää, M., & Mtei, K. M. (2024). Optimization of desorption parameters using response surface methodology for enhanced recovery of arsenic from spent reclaimable activated carbon: Eco-friendly and sorbent sustainability approach. *Ecotoxicology and Environmental Safety*, 280, 116550.
- Bayuo, J., Rwiza, M. J., Mtei, K. M., & Choi, J. W. (2024). Adsorptive Removal of

- Heavy Metals from Wastewater Using Low-Cost Adsorbents Derived from Agro-based Materials. In *Heavy Metal Remediation: Sustainable Nexus Approach* (pp. 237–271). Springer.
- Bayuo, J., Rwiza, M., & Mtei, K. (2023). *Applicability of bio-adsorbents synthesized from maize/corn plant residues for heavy metals removal from aquatic environments: an insight review*.
- Beg, S., & Rahman, Z. (2021). Central composite designs and their applications in pharmaceutical product development. *Design of Experiments for Pharmaceutical Product Development: Volume I: Basics and Fundamental Principles*, 63–76.
- Begum, S. A., Golam Hyder, A. H. M., & Vahdat, N. (2016). Adsorption isotherm and kinetic studies of As (V) removal from aqueous solution using cattle bone char. *Journal of Water Supply: Research and Technology—AQUA*, 65(3), 244–252.
- Beyan, S. M., Amibo, T. A., Prabhu, S. V., & Ayalew, A. G. (2021). Production of nanocellulose crystal derived from enset fiber using acid hydrolysis coupled with ultrasonication, isolation, statistical modeling, optimization, and characterizations. *Journal of Nanomaterials*, 2021(1), 7492532.
- Beyan, S. M., Prabhu, S. V., Ambio, T. A., & Gomadurai, C. (2022). A statistical modeling and optimization for Cr (VI) adsorption from aqueous media via teff straw-based activated carbon: isotherm, kinetics, and thermodynamic studies. *Adsorption Science & Technology*, 2022, 7998069.
- Bhatti, Z. A., Qureshi, K., Maitlo, G., & Ahmed, S. (2020). Study of PAN fiber and iron ore adsorbents for arsenic removal. *Civil Engineering Journal*, 6(3), 548–562.

- Bowell, R. J., Alpers, C. N., Jamieson, H. E., Nordstrom, D. K., & Majzlan, J. (2014). The environmental geochemistry of arsenic—an overview—. *Reviews in Mineralogy and Geochemistry*, 79(1), 1–16.
- Budinova, T., Savova, D., Tsyntsarski, B., Ania, C. O., Cabal, B., Parra, J. B., & Petrov, N. (2009). Biomass waste-derived activated carbon for the removal of arsenic and manganese ions from aqueous solutions. *Applied Surface Science*, 255(8), 4650–4657.
- Chai, J.-B., Au, P.-I., Mubarak, N. M., Khalid, M., Ng, W. P.-Q., Jagadish, P., Walvekar, R., & Abdullah, E. C. (2020). Adsorption of heavy metal from industrial wastewater onto low-cost Malaysian kaolin clay-based adsorbent. *Environmental Science and Pollution Research*, 27(12), 13949–13962.
- Chakraborty, R., Asthana, A., Singh, A. K., Jain, B., & Susan, A. B. H. (2022). Adsorption of heavy metal ions by various low-cost adsorbents: a review. *International Journal of Environmental Analytical Chemistry*, 102(2), 342–379.
- Chen, C.-C., & Chung, Y.-C. (2006). Arsenic removal using a biopolymer chitosan sorbent. *Journal of Environmental Science and Health, Part A*, 41(4), 645–658.
- Chen, H., Xu, J., Lin, H., Zhao, X., Shang, J., & Liu, Z. (2021). Arsenic removal via a novel hydrochar from livestock waste co-activated with thiourea and $\gamma\text{-Fe}_2\text{O}_3$ nanoparticles. *Journal of Hazardous Materials*, 419, 126457.
- Chen, X., Hossain, M. F., Duan, C., Lu, J., Tsang, Y. F., Islam, M. S., & Zhou, Y. (2022). Isotherm models for adsorption of heavy metals from water-a review. *Chemosphere*, 307, 135545.
- Cheraghi, M., Lorestani, B., Merrikhpour, H., & Mosaed, H. P. (2014). Assessment

efficiency of tea wastes in arsenic removal from aqueous solution.

Desalination and Water Treatment, 52(37–39), 7235–7240.

Cho, D.-W., Yoon, K., Kwon, E. E., Biswas, J. K., & Song, H. (2017). Fabrication of magnetic biochar as a treatment medium for As (V) via pyrolysis of FeCl₃-pretreated spent coffee ground. *Environmental Pollution*, 229, 942–949.

Chunhui, L., Jin, T., Puli, Z., Bin, Z., Duo, B., & Xuebin, L. (2018). Simultaneous removal of fluoride and arsenic in geothermal water in Tibet using modified yak dung biochar as an adsorbent. *Royal Society Open Science*, 5(11), 181266.

CONG, V. O. T., DO QUY, D., & VAN SON, N. (2019). The study of adsorption capacity on bone char in wastewater treatment contained arsenic ion. *Journal of Science and Technology-IUH*, 39(03).

Cruz, G. J. F., Mondal, D., Rimaycuna, J., Soukup, K., Gómez, M. M., Solis, J. L., & Lang, J. (2020). Agrowaste derived biochars impregnated with ZnO for removal of arsenic and lead in water. *Journal of Environmental Chemical Engineering*, 8(3), 103800.

Cruz-Briano, S. A., Medellin-Castillo, N. A., Delgado-Sanchez, P., Castro-Larragoitia, G. J., Leyva-Ramos, R., Cortina-Rangel, M. A., Labrada-Delgado, G. J., Villela-Martinez, D. E., Flores-Rojas, A. I., & Gonzalez-Fernandez, L. A. (2024). Binary fluoride and As (V) adsorption in water using pleco fish bone chars. *Environmental Science and Pollution Research*, 31(28), 40156–40173.

Dai, Y., Sun, Q., Wang, W., Lu, L., Liu, M., Li, J., Yang, S., Sun, Y., Zhang, K., & Xu, J. (2018). Utilizations of agricultural waste as adsorbent for the removal of contaminants: A review. *Chemosphere*, 211, 235–253.

Dehghan, P., Abbasi, M., Mofarahi, M., & Azari, A. (2021). Adsorption of synthetic

- and real Kinetic Hydrate Inhibitors (KHI) wastewaters on activated carbon: adsorption kinetics, isotherms, and optimized conditions. *Separation Science and Technology*, 56(13), 2266–2277.
- Dilpazeer, F., Munir, M., Baloch, M. Y. J., Shafiq, I., Iqbal, J., Saeed, M., Abbas, M. M., Shafique, S., Aziz, K. H. H., & Mustafa, A. (2023). A comprehensive review of the latest advancements in controlling arsenic contaminants in groundwater. *Water*, 15(3), 478.
- ElSayed, E. E. (2018). Natural diatomite as an effective adsorbent for heavy metals in water and wastewater treatment (a batch study). *Water Science*, 32(1), 32–43.
- Eshaghi, A., & Moradi, H. (2018). Optical and photocatalytic properties of the Fe-doped TiO₂ nanoparticles loaded on the activated carbon. *Advanced Powder Technology*, 29(8), 1879–1885.
- Fakhre, N. A., & Ibrahim, B. M. (2018). The use of new chemically modified cellulose for heavy metal ion adsorption. *Journal of Hazardous Materials*, 343, 324–331.
- Garelick, H., Jones, H., Dybowska, A., & Valsami-Jones, E. (2008). Arsenic pollution sources. *Reviews of Environmental Contamination Volume 197: International Perspectives on Arsenic Pollution and Remediation*, 17–60.
- Habuda-Stanić, M., & Nujić, M. (2015). Arsenic removal by nanoparticles: a review. *Environmental Science and Pollution Research*, 22(11), 8094–8123.
<https://doi.org/10.1007/s11356-015-4307-z>
- Hadiani, M. R., Khosravi-Darani, K., & Rahimifard, N. (2019). Optimization of As (III) and As (V) removal by *Saccharomyces cerevisiae* biomass for biosorption of critical levels in the food and water resources. *Journal of Environmental Chemical Engineering*, 7(2), 102949.

- Han, C., Li, H., Pu, H., Yu, H., Deng, L., Huang, S., & Luo, Y. (2013). Synthesis and characterization of mesoporous alumina and their performances for removing arsenic (V). *Chemical Engineering Journal*, 217, 1–9.
- Hummadi, K. K. (2021). Optimal operating conditions for adsorption of heavy metals from an aqueous solution by an agriculture waste. *Iraqi Journal of Chemical and Petroleum Engineering*, 22(2), 27–35.
- Hussain, M., Imran, M., Abbas, G., Shahid, M., Iqbal, M., Naeem, M. A., Murtaza, B., Amjad, M., Shah, N. S., & Ul Haq Khan, Z. (2020). A new biochar from cotton stalks for As (V) removal from aqueous solutions: its improvement with H₃PO₄ and KOH. *Environmental Geochemistry and Health*, 42, 2519–2534.
- Islam, A., Teo, S. H., Ahmed, M. T., Khandaker, S., Ibrahim, M. L., Vo, D.-V. N., Abdulkreem-Alsultan, G., & Khan, A. S. (2021). Novel micro-structured carbon-based adsorbents for notorious arsenic removal from wastewater. *Chemosphere*, 272, 129653.
- Jain, P., Kumar, A., Verma, N., & Gupta, R. K. (2019). In-situ synthesis of TiO₂ nanoparticles in ACF: Photocatalytic degradation under continuous flow. *Solar Energy*, 189, 35–44.
- Jawad, A. H., Abd Rashid, R., Mahmuod, R. M. A., Ishak, M. A. M., Kasim, N. N., & Ismail, K. (2016). Adsorption of methylene blue onto coconut (Cocos nucifera) leaf: optimization, isotherm and kinetic studies. *Desalination and Water Treatment*, 57(19), 8839–8853.
- Jiang, C., Wang, X., Wang, G., Hao, C., Li, X., & Li, T. (2019). Adsorption performance of a polysaccharide composite hydrogel based on crosslinked glucan/chitosan for heavy metal ions. *Composites Part B: Engineering*, 169, 45–54.

- Jjagwe, J., Olupot, P. W., Menya, E., & Kalibbala, H. M. (2021). Synthesis and application of granular activated carbon from biomass waste materials for water treatment: A review. *Journal of Bioresources and Bioproducts*, 6(4), 292–322.
- Johansson, C. L., Paul, N. A., de Nys, R., & Roberts, D. A. (2016). Simultaneous biosorption of selenium, arsenic and molybdenum with modified algal-based biochars. *Journal of Environmental Management*, 165, 117–123.
- Kakavandi, B., Bahari, N., Kalantary, R. R., & Fard, E. D. (2019). Enhanced sono-photocatalysis of tetracycline antibiotic using TiO₂ decorated on magnetic activated carbon (MAC@ T) coupled with US and UV: A new hybrid system. *Ultrasonics Sonochemistry*, 55, 75–85.
- Khoshnamvand, N., Kord Mostafapour, F., Mohammadi, A., & Faraji, M. (2018). Response surface methodology (RSM) modeling to improve removal of ciprofloxacin from aqueous solutions in photocatalytic process using copper oxide nanoparticles (CuO/UV). *Amb Express*, 8, 1–9.
- Khoshraftar, Z., Taheri, F. S., Nezami, S., & Ghaemi, A. (2023). Using halloysite nanotubes modified by tetraethylenepentamine for advanced carbon capture: Experimental and modeling via RSM and ANNs. *Chemical Engineering Journal Advances*, 16, 100543.
- Koiri, P., & Das, S. (2024). Agri-Food Waste Management and Treatment Approaches for Environmental Sustainability. In *Environmental Engineering and Waste Management: Recent Trends and Perspectives* (pp. 343–373). Springer.
- Kumar, A., Bhattacharya, T., Shaikh, W. A., Roy, A., Mukherjee, S., & Kumar, M. (2021). Performance evaluation of crop residue and kitchen waste-derived

- biochar for eco-efficient removal of arsenic from soils of the Indo-Gangetic plain: A step towards sustainable pollution management. *Environmental Research*, 200, 111758.
- Kumar, A., Bhattacharya, T., & Vithanage, M. (2023). Valorization of waste biomass for biochar production and arsenic removal: a comparative assessment. *Groundwater for Sustainable Development*, 22, 100972.
- Lam, S. S., Liew, R. K., Cheng, C. K., Rasit, N., Ooi, C. K., Ma, N. L., Ng, J.-H., Lam, W. H., Chong, C. T., & Chase, H. A. (2018). Pyrolysis production of fruit peel biochar for potential use in treatment of palm oil mill effluent. *Journal of Environmental Management*, 213, 400–408.
- Lamidi, S., Olaleye, N., Bankole, Y., Obalola, A., Aribike, E., & Adigun, I. (2022). *Applications of response surface methodology (RSM) in product design, development, and process optimization*. IntechOpen.
- Lata, S., Prabhakar, R., Adak, A., & Samadder, S. R. (2019). As (V) removal using biochar produced from an agricultural waste and prediction of removal efficiency using multiple regression analysis. *Environmental Science and Pollution Research*, 26, 32175–32188.
- Lee, S. (2010). Application of activated carbon fiber (ACF) for arsenic removal in aqueous solution. *Korean Journal of Chemical Engineering*, 27, 110–115.
- Li, Z., Yang, Q., Yang, Y., Xie, C., & Ma, H. (2020). Hydrogeochemical controls on arsenic contamination potential and health threat in an intensive agricultural area, northern China. *Environmental Pollution*, 256, 113455.
- Liu, H., Li, P., Qiu, F., Zhang, T., & Xu, J. (2020). Controllable preparation of FeOOH/CuO@ WBC composite based on water bamboo cellulose applied for enhanced arsenic removal. *Food and Bioproducts Processing*, 123, 177–187.

- Liu, H., Wang, Y., Li, Q., Yang, N., Wang, Z., & Wang, Q. (2022). Research on the evolution characteristics of oxygen-containing functional groups during the combustion process of the torrefied corn stalk. *Biomass and Bioenergy*, 158, 106343.
- Liu, X., Xu, X., Dong, X., & Park, J. (2020). Competitive adsorption of heavy metal ions from aqueous solutions onto activated carbon and agricultural waste materials. *Pol. J. Environ. Stud*, 29(1), 749–761.
- Ma, M.-D., Wu, H., Deng, Z.-Y., & Zhao, X. (2018). Arsenic removal from water by nanometer iron oxide coated single-wall carbon nanotubes. *Journal of Molecular Liquids*, 259, 369–375.
- Mahimairaja, S., Bolan, N. S., Adriano, D. C., & Robinson, B. (2005). Arsenic contamination and its risk management in complex environmental settings. *Advances in Agronomy*, 86, 1–82.
- Majumder, C. (2018). Arsenic (V) removal using activated alumina: Kinetics and modeling by response surface. *Journal of Environmental Engineering*, 144(3), 4017115.
- Malesic-Eleftheriadou, N., Liakos, E. V, Evgenidou, E., Kyzas, G. Z., Bikiaris, D. N., & Lambropoulou, D. A. (2022). Low-cost agricultural wastes (orange peels) for the synthesis and characterization of activated carbon biosorbents in the removal of pharmaceuticals in multi-component mixtures from aqueous matrices. *Journal of Molecular Liquids*, 368, 120795.
- Masuda, H. (2018). Arsenic cycling in the Earth's crust and hydrosphere: interaction between naturally occurring arsenic and human activities. *Progress in Earth and Planetary Science*, 5(1), 1–11.
- Matouq, M., Jildeh, N., Qtaishat, M., Hindiyeh, M., & Al Syouf, M. Q. (2015). The

- adsorption kinetics and modeling for heavy metals removal from wastewater by Moringa pods. *Journal of Environmental Chemical Engineering*, 3(2), 775–784.
- Melliti, A., Yılmaz, M., Sillanpää, M., Hamrouni, B., & Vurm, R. (2023). Low-cost date palm fiber activated carbon for effective and fast heavy metal adsorption from water: Characterization, equilibrium, and kinetics studies. *Colloids and Surfaces A: Physicochemical and Engineering Aspects*, 672, 131775.
- Mondal, M. K., & Garg, R. (2017). A comprehensive review on removal of arsenic using activated carbon prepared from easily available waste materials. *Environmental Science and Pollution Research*, 24(15), 13295–13306.
- Montero, J. I. Z., Monteiro, A. S. C., Gontijo, E. S. J., Bueno, C. C., de Moraes, M. A., & Rosa, A. H. (2018). High efficiency removal of As (III) from waters using a new and friendly adsorbent based on sugarcane bagasse and corncob husk Fe-coated biochars. *Ecotoxicology and Environmental Safety*, 162, 616–624.
- Mudzielwana, R., Gitari, M. W., & Ndungu, P. (2020). Enhanced As (III) and As (V) adsorption from aqueous solution by a clay based hybrid sorbent. *Frontiers in Chemistry*, 7, 913.
- Mukherjee, S., Thakur, A. K., Goswami, R., Mazumder, P., Taki, K., Vithanage, M., & Kumar, M. (2021). Efficacy of agricultural waste derived biochar for arsenic removal: Tackling water quality in the Indo-Gangetic plain. *Journal of Environmental Management*, 281, 111814.
- Musah, M., Azeh, Y., Mathew, J. T., Umar, M. T., Abdulhamid, Z., & Muhammad, A. I. (2022). Adsorption kinetics and isotherm models: a review. *CaJoST*, 4(1), 20–26.

- Neisan, R. S., Saady, N. M. C., Bazan, C., Zendehboudi, S., & Albayati, T. M. (2023). Adsorption of copper from water using TiO₂-modified activated carbon derived from orange peels and date seeds: Response surface methodology optimization. *Heliyon*, 9(11).
- Nejadshafiee, V., & Islami, M. R. (2019). Adsorption capacity of heavy metal ions using sultone-modified magnetic activated carbon as a bio-adsorbent. *Materials Science and Engineering: C*, 101, 42–52.
- Nguyen, T. C., Loganathan, P., Nguyen, T. V., Kandasamy, J., Naidu, R., & Vigneswaran, S. (2018). Adsorptive removal of five heavy metals from water using blast furnace slag and fly ash. *Environmental Science and Pollution Research*, 25, 20430–20438.
- Nguyen, T. H., Loganathan, P., Nguyen, T. V., Vigneswaran, S., Nguyen, T. H. H., Tran, H. N., & Nguyen, Q. B. (2022). Arsenic removal by pomelo peel biochar coated with iron. *Chemical Engineering Research and Design*, 186, 252–265.
- Nguyen, T. H., Pham, T. H., Nguyen Thi, H. T., Nguyen, T. N., Nguyen, M.-V., Tran Dinh, T., Nguyen, M. P., Do, T. Q., Phuong, T., & Hoang, T. T. (2019). Synthesis of Iron-Modified Biochar Derived from Rice Straw and Its Application to Arsenic Removal. *Journal of Chemistry*, 2019(1), 5295610.
- Niazi, N. K., Bibi, I., Shahid, M., Ok, Y. S., Burton, E. D., Wang, H., Shaheen, S. M., Rinklebe, J., & Lüttge, A. (2018). Arsenic removal by perilla leaf biochar in aqueous solutions and groundwater: an integrated spectroscopic and microscopic examination. *Environmental Pollution*, 232, 31–41.
- Niazi, N. K., Bibi, I., Shahid, M., Ok, Y. S., Shaheen, S. M., Rinklebe, J., Wang, H., Murtaza, B., Islam, E., & Nawaz, M. F. (2018). Arsenic removal by Japanese oak wood biochar in aqueous solutions and well water: Investigating arsenic

- fate using integrated spectroscopic and microscopic techniques. *Science of the Total Environment*, 621, 1642–1651.
- Okamura, M., Takagaki, A., Toda, M., Kondo, J. N., Domen, K., Tatsumi, T., Hara, M., & Hayashi, S. (2006). Acid-catalyzed reactions on flexible polycyclic aromatic carbon in amorphous carbon. *Chemistry of Materials*, 18(13), 3039–3045.
- Palma-Lara, I., Martínez-Castillo, M., Quintana-Pérez, J. C., Arellano-Mendoza, M. G., Tamay-Cach, F., Valenzuela-Limón, O. L., García-Montalvo, E. A., & Hernández-Zavala, A. (2020). Arsenic exposure: A public health problem leading to several cancers. *Regulatory Toxicology and Pharmacology*, 110, 104539.
- Parvathiraja, C., Katheria, S., Siddiqui, M. R., Wabaidur, S. M., Islam, M. A., & Lai, W.-C. (2022). Activated Carbon-Loaded Titanium Dioxide Nanoparticles and Their Photocatalytic and Antibacterial Investigations. *Catalysts*, 12(8), 834.
- Pavithra, S., Thandapani, G., Sugashini, S., Sudha, P. N., Alkhamis, H. H., Alrefaei, A. F., & Almutairi, M. H. (2021). Batch adsorption studies on surface tailored chitosan/orange peel hydrogel composite for the removal of Cr (VI) and Cu (II) ions from synthetic wastewater. *Chemosphere*, 271, 129415.
- Peng, Y., Khaled, U., Al-Rashed, A. A. A. A., Meer, R., Goodarzi, M., & Sarafraz, M. M. (2020). Potential application of Response Surface Methodology (RSM) for the prediction and optimization of thermal conductivity of aqueous CuO (II) nanofluid: A statistical approach and experimental validation. *Physica A: Statistical Mechanics and Its Applications*, 554, 124353.
- Prakash, S., & Verma, A. K. (2021). Arsenic: It's toxicity and impact on human health. *International Journal of Biological Innovations, IJBI*, 3(1), 38–47.

- Qiu, B., Tao, X., Wang, H., Li, W., Ding, X., & Chu, H. (2021). Biochar as a low-cost adsorbent for aqueous heavy metal removal: A review. *Journal of Analytical and Applied Pyrolysis*, 155, 105081.
- Rahidul Hassan, H. (2023). A review on different arsenic removal techniques used for decontamination of drinking water. *Environmental Pollutants and Bioavailability*, 35(1), 2165964.
- Raju, N. J. (2022). Arsenic in the geo-environment: A review of sources, geochemical processes, toxicity and removal technologies. *Environmental Research*, 203, 111782.
- Ramesh, S., Sundararaju, P., Banu, K. S. P., Karthikeyan, S., Doraiswamy, U., & Soundarapandian, K. (2019). Hydrothermal carbonization of arecanut husk biomass: fuel properties and sorption of metals. *Environmental Science and Pollution Research*, 26, 3751–3761.
- Rehman, M. U., Khan, R., Khan, A., Qamar, W., Arafah, A., Ahmad, A., Ahmad, A., Akhter, R., Rinklebe, J., & Ahmad, P. (2021). Fate of arsenic in living systems: Implications for sustainable and safe food chains. *Journal of Hazardous Materials*, 417, 126050.
- Rukayat, O. O., Usman, M. F., Elizabeth, O. M., Abosede, O. O., & Faith, I. U. (2021). Kinetic adsorption of heavy metal (Copper) on rubber (Hevea Brasiliensis) leaf powder. *South African Journal of Chemical Engineering*, 37, 74–80.
- Sarioğlu, Ş. (2013). Recovery of palladium from spent activated carbon-supported palladium catalysts. *Platinum Metals Review*, 57(4), 289–296.
- Sattar, M. S., Shakoor, M. B., Ali, S., Rizwan, M., Niazi, N. K., & Jilani, A. (2019). Comparative efficiency of peanut shell and peanut shell biochar for removal of

- arsenic from water. *Environmental Science and Pollution Research*, 26, 18624–18635.
- Sawood, G. M., Mishra, A., & Gupta, S. K. (2021). Optimization of arsenate adsorption over aluminum-impregnated tea waste biochar using RSM–central composite design and adsorption mechanism. *Journal of Hazardous, Toxic, and Radioactive Waste*, 25(2), 4020075.
- Selvaraj, P., Roy, A., Ullah, H., Sujatha Devi, P., Tahir, A. A., Mallick, T. K., & Sundaram, S. (2019). Soft-template synthesis of high surface area mesoporous titanium dioxide for dye-sensitized solar cells. *International Journal of Energy Research*, 43(1), 523–534.
- Senthilkumar, R., Reddy Prasad, D. M., Govindarajan, L., Saravanakumar, K., & Naveen Prasad, B. S. (2020). Synthesis of green marine algal-based biochar for remediation of arsenic (V) from contaminated waters in batch and column mode of operation. *International Journal of Phytoremediation*, 22(3), 279–286.
- Siddique, T. A., Dutta, N. K., & Choudhury, N. R. (2020). Nanofiltration for arsenic removal: Challenges, recent developments, and perspectives. In *Nanomaterials* (Vol. 10, Issue 7). <https://doi.org/10.3390/nano10071323>
- Siddiqui, S. I., & Chaudhry, S. A. (2017). Iron oxide and its modified forms as an adsorbent for arsenic removal: a comprehensive recent advancement. *Process Safety and Environmental Protection*, 111, 592–626.
- Siddiqui, S. I., Naushad, M., & Chaudhry, S. A. (2019). Promising prospects of nanomaterials for arsenic water remediation: A comprehensive review. *Process Safety and Environmental Protection*, 126, 60–97.
- Sigdel, A., Park, J., Kwak, H., & Park, P.-K. (2016). Arsenic removal from aqueous

- solutions by adsorption onto hydrous iron oxide-impregnated alginate beads. *Journal of Industrial and Engineering Chemistry*, 35, 277–286.
- Singh, T. S., & Pant, K. K. (2004). Equilibrium, kinetics and thermodynamic studies for adsorption of As(III) on activated alumina. *Separation and Purification Technology*, 36(2), 139–147. [https://doi.org/10.1016/S1383-5866\(03\)00209-0](https://doi.org/10.1016/S1383-5866(03)00209-0)
- Sugashini, S., & Begum, K. M. M. S. (2013). Optimization using central composite design (CCD) for the biosorption of Cr (VI) ions by cross linked chitosan carbonized rice husk (CCACR). *Clean Technologies and Environmental Policy*, 15, 293–302.
- Šumić, Z., Vakula, A., Tepić, A., Čakarević, J., Vitas, J., & Pavlić, B. (2016). Modeling and optimization of red currants vacuum drying process by response surface methodology (RSM). *Food Chemistry*, 203, 465–475.
- Sun, T., Pei, P., Sun, Y., Xu, Y., & Jia, H. (2022). Performance and mechanism of As (III/V) removal from aqueous solution by novel positively charged animal-derived biochar. *Separation and Purification Technology*, 290, 120836.
- Taha, A. A., Shreadah, M. A., Ahmed, A. M., & Heiba, H. F. (2016). Multi-component adsorption of Pb (II), Cd (II), and Ni (II) onto Egyptian Na-activated bentonite; equilibrium, kinetics, thermodynamics, and application for seawater desalination. *Journal of Environmental Chemical Engineering*, 4(1), 1166–1180.
- Tahoon, M. A., Siddeeg, S. M., Salem Alsaiani, N., Mnif, W., & Ben Rebah, F. (2020). Effective heavy metals removal from water using nanomaterials: A review. *Processes*, 8(6), 645.
- Teigiserova, D. A., Tiruta-Barna, L., Ahmadi, A., Hamelin, L., & Thomsen, M. (2021). A step closer to circular bioeconomy for citrus peel waste: A review of

- yields and technologies for sustainable management of essential oils. *Journal of Environmental Management*, 280, 111832.
- United States Department of Agriculture. (2024).
<https://apps.fas.usda.gov/psdonline/app/index.html#/app/home>
- Vajedi, F., & Dehghani, H. (2019). The characterization of TiO₂-reduced graphene oxide nanocomposites and their performance in electrochemical determination for removing heavy metals ions of cadmium (II), lead (II) and copper (II). *Materials Science and Engineering: B*, 243, 189–198.
- Verma, L., & Singh, J. (2019). Synthesis of novel biochar from waste plant litter biomass for the removal of Arsenic (III and V) from aqueous solution: A mechanism characterization, kinetics and thermodynamics. *Journal of Environmental Management*, 248, 109235.
- Veza, I., Spraggon, M., Fattah, I. M. R., & Idris, M. (2023). Response surface methodology (RSM) for optimizing engine performance and emissions fueled with biofuel: Review of RSM for sustainability energy transition. *Results in Engineering*, 101213.
- Vieira, B. R. C., Pintor, A. M. A., Boaventura, R. A. R., Botelho, C. M. S., & Santos, S. C. R. (2017). Arsenic removal from water using iron-coated seaweeds. *Journal of Environmental Management*, 192, 224–233.
- Wu, C., Huang, L., Xue, S.-G., Huang, Y.-Y., Hartley, W., Cui, M., & Wong, M.-H. (2017). Arsenic sorption by red mud-modified biochar produced from rice straw. *Environmental Science and Pollution Research*, 24, 18168–18178.
- Xiao, Y., Xue, Y., Gao, F., & Mosa, A. (2017). Sorption of heavy metal ions onto crayfish shell biochar: effect of pyrolysis temperature, pH and ionic strength. *Journal of the Taiwan Institute of Chemical Engineers*, 80, 114–121.

- Yang, Y., Zhang, R., Chen, S., Zhu, J., Wu, P., Huang, J., & Qi, S. (2022). Arsenic (iii) removal from aqueous solution using TiO₂-loaded biochar prepared by waste Chinese traditional medicine dregs. *RSC Advances*, 12(13), 7720–7734.
- Zhang, X., Wu, S., Liu, Y., Wang, Z., Zhang, H., & Xiao, R. (2023). Removal of Cr (VI) from aqueous solution by Rice-husk-based activated carbon prepared by Dual-mode heating method. *Carbon Resources Conversion*, 6(2), 76–84.
- Zhao, D., Yu, Y., & Chen, J. P. (2016). Fabrication and testing of zirconium-based nanoparticle-doped activated carbon fiber for enhanced arsenic removal in water. *RSC Advances*, 6(32), 27020–27030.
- Zhao, J., Liu, J., Li, N., Wang, W., Nan, J., Zhao, Z., & Cui, F. (2016). Highly efficient removal of bivalent heavy metals from aqueous systems by magnetic porous Fe₃O₄-MnO₂: Adsorption behavior and process study. *Chemical Engineering Journal*, 304, 737–746.
- Zheng, X., Zheng, H., Xiong, Z., Zhao, R., Liu, Y., Zhao, C., & Zheng, C. (2020). Novel anionic polyacrylamide-modify-chitosan magnetic composite nanoparticles with excellent adsorption capacity for cationic dyes and pH-independent adsorption capability for metal ions. *Chemical Engineering Journal*, 392, 123706.
- Zhu, H., Shi, M., Zhang, X., Liu, B., & Yao, D. (2020). Adsorption kinetics of arsenic (V) on nanoscale zero-valent iron supported by activated carbon. *Nanomaterials*, 10(9), 1791.

CHAPTER SIX

ADSORPTION OF COPPER FROM WATER USING TiO₂-MODIFIED ACTIVATED CARBON DERIVED FROM ORANGE PEELS AND DATE SEEDS: RESPONSE SURFACE METHODOLOGY OPTIMIZATION ⁵

Roya Sadat Neisan¹, Noori M. Cata Saady¹, Carlos Bazan², Sohrab Zendehboudi³, Talib M. Albayati⁴

¹ Department of Civil Engineering, Memorial University, St. John's, NL A1B 3X5, Canada

² Faculty of Business Administration, Memorial University, St. John's, NL, A1B 3X5, Canada

³ Department of Process Engineering, Memorial University, St. John's, NL A1B 3X5, Canada

⁴ Department of Chemical Engineering, University of Technology - Iraq, 52 Alsinaa St., PO Box 35010, Baghdad, Iraq

Abstract

This study evaluated the efficiency of titanium dioxide (TiO₂)-modified activated carbon for copper (Cu) removal from synthetic aquatic samples. Activated carbon derived from orange peel (AC-OP) and date seeds (AC-DS) was modified with TiO₂ (OP-TiO₂, and DS-TiO₂), increasing the surface area of AC-OP from 2.40 to 6.06 m² g⁻¹ and AC-DS from 51.10 to 81.37 m² g⁻¹. Response Surface Methodology (RSM) with Central Composite Design (CCD) was used to optimize conditions, including pH (1–7), initial concentration (10–60 mg L⁻¹), adsorbent dose (0.5–8 g L⁻¹), and contact time (0.4–6 h). The optimal conditions for OP-TiO₂ were pH 5, initial concentration 24.6 mg L⁻¹, adsorbent dose 4.9 g L⁻¹, and contact time 3.6 h, achieving 99.90% Cu removal and a maximum adsorption capacity of 13.34 mg g⁻¹. For DS-TiO₂, optimal conditions were pH 6.4, initial concentration 21.2 mg L⁻¹, adsorbent dose 5 g L⁻¹, and contact time 3.0 h, achieving 97.40% Cu removal and a maximum adsorption capacity of 13.96 mg g⁻¹. Kinetic data were best described by the pseudo-second-order model (R² > 98%).

⁵ This chapter was published as a peer-reviewed journal article:

Neisan, R. S., Saady, N. M. C., Bazan, C., Zendehboudi, S., & Albayati, T. M. (2023). Adsorption of copper from water using TiO₂-modified activated carbon derived from orange peels and date seeds: Response surface methodology optimization. *Heliyon*, 9(11). e21420. <https://doi.org/10.1016/j.heliyon.2023.e21420>.

6.1. Introduction

Pollution of water sources by heavy metals has increased globally as a result of rising industrial activity and improper water and wastewater treatment. Drinking water contamination is the main route exposing humans to heavy metals. Drinking water contaminated with heavy metals has been linked to several harmful consequences on human metabolism. The formation of reactive oxygen species, i.e., oxidative damage, is the main mechanism of adverse effects on people's health, leading to high rates of disease and fatalities worldwide (Z. Fu & Xi, 2020; Joseph et al., 2019).

Copper (Cu, molecular weight: 63.5 g mol⁻¹ and oxidation state +1, +2) (Joseph et al., 2019) is one of the most toxic metals which is irresponsibly released into the environment by various activities, such as metal processing, coal combustion, Copper photogravure, and tire manufacturing. The World Health Organization (WHO) has determined the maximum copper concentration in drinking water at 2 mg L⁻¹ due to health risks caused by copper exposure. High Cu consumption may result in gastrointestinal issues, liver or kidney damage, nervous system disorders acute hemolytic anaemia, capillary damage, and in severe cases, even death. Considering such toxic effects in human health and aquatic systems, Cu removal from drinking water sources and wastewater before discharge is critical (Lenka et al., 2021; Stala et al., 2022).

Among the common heavy metal removing technologies such as coagulation–flocculation, ion exchange, and membrane technologies, the most popular one, absorption, is widely used because of abundant low-cost and renewable materials that can be converted to adsorbents, easy operation, low cost, removal and energy efficiency, and ability to remove various contaminants (Stala et al., 2022; Y. Zhang et al., 2019).

Various adsorbents have been used to remove Cu from water and wastewater, including polymeric fibers (Deng et al., 2003), nanomaterials (Azzam et al., 2016), modified natural materials (J. Lin et al., 2011), agricultural waste (Asim et al., 2020), industrial waste (Méndez et al., 2009) and carbon-based materials (Elkady et al., 2015). However, activated carbon has long been the preferred adsorbent in heavy metal removal due to its excellent adsorption capacity, rate, porosity and high surface area (Hydari et al., 2012).

The need for developing more affordable and effective adsorbents from renewable sources has been prompted by the high cost of commercial activated carbon (Tan et al., 2015). Biochar is a type of carbon-rich substance made by pyrolyzing biomass at high temperatures in an inert environment. However, it has generally poor adsorption capability. Surface chemical modification could solve this problem because it enhances the functional groups, active sites, and surface structure of biochar (Y. Zhang et al., 2019). Recently, agricultural waste such as orange peels and date seeds have been used to remove heavy metals from aquatic sources. Table 6-1 summarizes the removal efficiency and adsorbent capacity of recently developed adsorbents from orange peels and date seeds.

Despite the extensive research on the adsorption of heavy metals from water using various adsorbents, limited attention has been given to removing copper from water using TiO₂-modified activated carbon derived from agricultural waste materials such as orange peels and date seeds. This study's primary objective is to investigate copper adsorption from water using modified activated carbon derived from orange peels and date seeds. By modifying the activated carbon through the incorporation of TiO₂ nanoparticles (NPs), we aim to enhance its adsorption capacity and efficiency for copper removal.

Table 6-1 Summary of adsorptive removal of heavy metals by relevant adsorbents.

Adsorbent	Adsorbate	C _i (mg L ⁻¹)	Adsorbent dose (g L ⁻¹)	pH	Contact time (min)	Other Info	RE (%) or/ and AC (mg g ⁻¹)	Reference
Modified Orange peel	Cd(II)	50	30	6	180	25 °C	91.0 %	(Faisal et al., 2020)
	Ni(II)		25			200 rpm	93.4%	
Fe(II)/Fe(III) modified Orange peel	As(V)	40	200	6	300	300 rpm	81.3 mg g ⁻¹	(Meng et al., 2017)
Chitosan/ orange peel hydrogel composite	Cr(VI)	100	40	4	360	200 rpm	80.4%	(Pavithra et al., 2021)
	Cu(II)			5		room temperature	82.5%	
Orange peels modified with magnetic nanoparticles	As(III)	40	1	7	720	180 rpm	10.3 mg g ⁻¹ 98.5%	(Shehzad et al., 2018)
Orange peel modified with mercaptoacetic acid	As(V)	80	2	6	120	220 rpm	34.0 mg g ⁻¹	(Amin et al., 2017)
	Cu(II)						50.0 mg g ⁻¹	
	Pb(II)						43.5 mg g ⁻¹	
Date seeds powder	Ni(II)	50	6	7	30	150 rpm 25°C	90%	(Elkhaleefa et al., 2020)
Activated carbon from date seeds	Cr(VI)	50	2	2	60	30 °C	42.6mg g ⁻¹	(Rambabu et al., 2019)
Carbonized date seeds	Pb(II)	5	6	5	2	25 °C 120 rpm	88.5%	(Azmi et al., 2020)
Microwave-assisted modified Date seed Husk	As(III)	25	10	4	45	250 rpm	85% 1.3 mg g ⁻¹	(T. M. Khan et al., 2019)
Date seeds biochar	Cd(II), Cr(III), Co(II), Cu(II), Pb(II), Mn(II)	2	2	NA	overnight	200 rpm	93.3%, 71.1% 92.1%, 97.0% 95.9%, 36.1%	(Juma Mohamed et al., 2019)

C_i = initial concentration; RE = removal efficiency; AC = adsorption capacity.

Recently, there has been a growing interest in utilizing TiO₂ for various applications, including environmental purification and adsorption processes (Gan et al., 2019). TiO₂ excellent physical and chemical properties, including its large surface area, and abundant active sites make it particularly attractive for removing heavy metals and organic pollutants (Gan et al., 2019; Vajedi & Dehghani, 2019). However, the practical application of TiO₂ NPs faces challenges such as agglomeration, reduced surface area, and difficulties in recovery (Ajala et al., 2022). To overcome these limitations, combining nanostructured materials, such as TiO₂, with carbon-based materials has been shown to enhance the overall efficiency of adsorption processes in water (Vajedi & Dehghani, 2019).

The significance of this research is in its potential contribution to addressing the pressing challenges associated with copper contamination in water. Understanding the factors influencing the adsorption process and optimizing the conditions for maximum copper removal are crucial aspects of this study. By exploring the effects of various process variables and employing response surface methodology (RSM) for optimization, we aim to achieve improved adsorption efficiency while minimizing resource consumption.

Emerging research has demonstrated the effectiveness of RSM as a potent statistical tool in optimizing process parameters (Abdulhameed et al., 2021; Jawad et al., 2017; Jawad, Bardhan, et al., 2020). The application of RSM entails an empirical modeling approach aimed at evaluating the correlation between process variables and corresponding outputs (Abdulhameed et al., 2021). The utilization of RSM for optimizing the conditions offers notable advantages, such as time and chemical savings. Additionally, it contributes to a deeper comprehension of the factors influencing the performance of the adsorbent (Bessegato et al., 2019)

The central composite design (CCD) includes axial star points in its design, enabling improved estimation of RSM curves. RSM-CCD provides more flexibility in exploring the response space and capturing the behavior at extreme cases, such as the corners or edges of the design space (Chaware & Khobragade, n.d.; Ghahri et al., 2011; Pantazis et al., 2023; Salari et al., 2022). Although the Box- Behnken (BBD) statistical method offers benefits in terms of process optimization by smaller number of experiments and reducing operational costs (Jawad et al., 2021), the CCD allows for more levels per factor, with five different levels for each factor, including points both within and outside the specified limits (Chaware & Khobragade, n.d.; Ghahri et al., 2011; Pantazis et al., 2023; Salari et al., 2022).

In addition to optimization studies, comprehensive kinetic studies have been conducted to examine the dynamic behavior of copper removal using the modified activated carbon derived from orange peels and date seeds. By investigating the adsorption kinetics, valuable insights were obtained regarding the rate of copper ion adsorption onto the adsorbent surface and the time required to achieve equilibrium. Adsorption kinetics were performed and compared to Pseudo-first-order and second-order kinetic models. Several physiochemical characterizations were used to study the modified activated carbon's surface and functional groups.

6.2. Materials and Methods

6.2.1. Preparation and procedures

The titanium dioxide Nanopowder (TiO_2 , anatase, 99.9%, 18 nm) and copper (II) sulfate pentahydrate ($\text{CuSO}_4 \cdot 5\text{H}_2\text{O}$) were purchased from US Research Nanomaterials (Texas, U.S) and Acros Organics (New Jersey, U.S), respectively. Carbon dioxide and nitrogen of 99.99% purity were purchased from Praxair Canada Inc. The orange peels

and dates were collected from local markets in St John's, NL. Cu(II) solution (60 mg L⁻¹) has been prepared by dissolving CuSO₄.5H₂O in deionized water. The stock solution has been diluted to provide the required solutions.

The physical and chemical characteristics of materials are investigated through characterization studies to understand better the efficacy of the procedure used to create the adsorbents and the adsorption mechanisms. The surface morphology and the chemical elements of all adsorbents were studied using a Field emission detector Scanning Electron Microscope (SEM) coupled to an energy-dispersive X-ray spectroscopy (EDX) to perform particle elemental analysis (JSM-7100F, JEOL Ltd, Japan). A Bruker Tensor 27 Fourier transform infrared spectrometer (FTIR) working in the ZnSe ATR mode in the range of 4000–650 cm⁻¹ at a spectral resolution of 4 cm⁻¹ for 32 scans has been used to identify the functional surface groups. The elements in the materials and the structural composition have been characterized using an X-ray diffraction (XRD) with Cu source and scintillation detector (Ultima-IV, 40 kV/44 mA, Rigaku, Japan). A surface area analyzer (Tristar II 3020, Micromeritics, US) has been used for nitrogen adsorption–desorption at 77 K for measuring specific surface area.

6.2.2. Preparation of adsorbents

Date seeds and orange peels have been converted to activated carbon using the following procedure. The biomass was washed with distilled water and oven-dried at 80 °C for 6 h. The dried biomass was ground using a mortar and pestle followed by a grinder. Once ground, it was passed through a 506 µm sieve. The carbonization and activation experiments were conducted in a tubular furnace reactor (Carbolite Gero, Germany). The carbonization temperature was controlled at 500 °C for orange peels and seed dates powders. During the carbonation process, the reactor was heated to the target temperature at 10 °C min⁻¹ heating rate, under nitrogen gas (N₂), and the flow rate

was controlled at 100 mL min⁻¹. The samples have been kept at the target temperature for 2 h. After 2 h, the nitrogen gas valve is closed and carbon dioxide (CO₂) gas is connected. The sample is kept under CO₂ gas for 1 h at 100 mL min⁻¹.

Titanium dioxide NPs were fabricated using ultrasonication methodology. For every 1.0 g of activated carbon from each material, 0.1 g of TiO₂ NPs were added to a flask containing 50 mL of distilled water. Then, the flask was ultrasonicated for 30 min at room temperature. The resultant suspensions were filtered and washed 4–5 times with distilled water. Finally, the resulting wet material was oven-dried overnight at 65 °C.

6.2.3. Experimental design

The CCD, a common experimental design of RSM, was utilized to develop the relationship between the process factors and response which is the removal efficiency. To determine the optimum values of pH, metal ion concentration, biomass dosage, and contact time, the CCD created an experimental design matrix for four variables (Table 6-2).

Table 6-2 The ranges and levels of independent parameters.

Parameter	Unit	-1	+1	- α	+ α
A-pH		2.2	5.8	1.0	7.0
B-Initial concentration	mg l ⁻¹	20.0	50.0	10.0	60.0
C-Adsorbent dose	g l ⁻¹	2.0	6.4	0.5	8.0
D-Contact time	h	1.3	4.8	0.4	6.0

The investigation on the impacts of four factors on the removal of Cu (%) was carried out through a total of 21 runs. Table 6-3 presents the CCD matrix used for evaluating the removal efficiency (%) of Cu with OP-TiO₂ and DS-TiO₂. A second-order polynomial response surface model can be used to fit the experimental data (Eq. (6-1)):

$$R = \beta_0 + \sum_{i=1}^4 \beta_i x_i + \sum_{i=1}^3 \sum_{j=i+1}^4 \beta_{ij} x_i x_j + \sum_{i=1}^4 \beta_{ii} x_i^2 + \varepsilon \quad (6-1)$$

where R stands for the expected response (removal efficiency (%)), and β_0 , β_i , β_{ii} , β_{ij} ,

and ε represent the offset, the linear effect, the squared effect, the interaction impact, and the residual term, respectively. The coded independent variables (pH, contact time, initial concentration, and adsorbent dose) are represented by x_i and x_j . A total number of 21 experiments have been designed by Design expert software (version 12.0.8.0, Stat-Ease Inc., Minneapolis, MN, USA).

Table 6-3 The four-factors CCD matrix for Cu removal.

Run	pH	C _i (mg L ⁻¹)	Adsorbent dose (g L ⁻¹)	Contact time (h)
1	4	35	4.2	3
2	1	35	4.2	3
3	4	35	8	3
4	5.8	20	2	4.8
5	2.2	50	2	4.8
6	4	35	0.5	3
7	5.8	20	6.4	4.8
8	5.8	50	2	1.25
9	4	10	4.2	3
10	4	35	4.2	6
11	5.8	50	6.4	1.25
12	4	35	4.2	0.04
13	2.2	20	6.4	1.25
14	4	60	4.2	3
15	4	35	4.2	3
16	2.2	20	2	1.25
17	4	35	4.2	3
18	2.2	50	6.4	4.8
19	4	35	4.2	3
20	4	35	4.2	3
21	7	35	4.2	3

6.2.4. Adsorption experiments

Adsorption batch tests were conducted based on the CCD design, and the impact of the adsorption factors on the removal of Cu(II) from aqueous solution was investigated. Different concentrations of Cu solution were prepared and a known amount of adsorbents were added to 50 mL Erlenmeyer flasks containing Cu solution at the desired pH. The pH of the metal solutions has been adjusted using 0.1 M and 1 M solution of hydrochloric acid (HCl) and sodium hydroxide (NaOH). The flasks were

then placed on an orbital shaker with a speed of 200 rpm for a given time. All experiments were carried out at room temperature. The mixture was filtered and analyzed using inductively coupled plasma–optical emission spectrometer, ICP-OES (Optima 5300 DV, Perkin-Elmer, US).

The adsorption efficiency or removal percentage of contaminants and the adsorption capacity of the adsorbents were calculated using Eq. (6-2) and Eq. (6-3), respectively.

$$\% \text{ Adsorption} = \frac{C_0 - C_t}{C_0} \times 100 \quad (6-2)$$

$$q_t = (C_0 - C_t)V/m \quad (6-3)$$

where C_0 and C_t are initial and final (at time t) concentrations of the metal ions, respectively, q_t (mg g⁻¹) is the mass of adsorbate per mass of adsorbent at time t , V is the volume of the solution (L), and m is the mass of adsorbent (g) (Vunain et al., 2017).

6.2.5. Kinetic studies

The adsorption mechanism of Cu(II) was studied using four different kinetic models. The kinetic study was conducted for the time span of 5–240 min under optimum condition at room temperature.

Pseudo-first-order model (Eq. (6-4)) describes the adsorption of adsorbate onto surface of the adsorbent and follows the first order mechanism.

$$\log (q_e - q_t) = \log q_e - \left(\frac{k_1}{2.303} \right) t \quad (6-4)$$

where q_e is the adsorption capacity at equilibrium (mg g⁻¹), k_1 is the adsorption rate constant (g mg⁻¹ min⁻¹).

Based on pseudo-second-order kinetics, the adsorption kinetics can be described as the following equation (Eq. (6-5)):

$$t/q_t = 1/q_e^2 k_2 + t/q_e \quad (6-5)$$

where k_2 is the reaction rate constant ($\text{g mg}^{-1} \text{ min}^{-1}$), q_e is the amount of solute adsorbed at equilibrium (mg g^{-1}), and q_t is the amount of solute adsorbed at time t (ALothman et al., 2016). A straight line from a t/q_t vs. t plot is used to determine k_2 and q_e . The value of k_2 is calculated from the interception and slope of the graph as $k_2 = (\text{Slop})^2 / \text{Intercept}$ and q_e is determined by $1/\text{slope}$ (Mishra et al., 2012).

In addition to Pseudo-first-order and Pseudo-second-order models, the intra-particle diffusion (Eq. (6-6)) and Elovich (Eq. (6-7)) models were also used to describe the adsorption kinetics and to provide insights into the mechanisms and rate-controlling steps of the adsorption process.

$$q_t = k_i t^{0.5} + C \quad (6-6)$$

where k_i is the intra-particle diffusion rate constant ($\text{mg g}^{-1} \text{ min}^{-0.5}$), and C is the intercept which reflects the thickness of the boundary layer. The plot of q_t against $t^{0.5}$ can provide insights into the involvement of intra-particle diffusion in the adsorption process.

$$q_t = \left(\frac{1}{\beta}\right) \ln(\alpha\beta) + \left(\frac{1}{\beta}\right) \ln(t) \quad (6-7)$$

where α is the initial sorption rate ($\text{mg g}^{-1} \text{ min}^{-1}$), and β (g mg^{-1}) is the desorption constant related to the extent of surface coverage and activation energy.

6.3. Results and Discussion

6.3.1. Adsorbent characterization

6.3.1.1. Scanning electron microscopy (SEM)

The results obtained from the SEM images of OP-TiO₂ and DS-TiO₂ (Figure 6-1b and Figure 6-1d, respectively) indicated the presence of aggregates on the surface of the particles while in the unmodified materials (Figure 6-1a and Figure 6-1c), the images exhibited a smooth surface. The EDX analysis revealed that the AC-OP and AC-DS (Figure 6-2a and Figure 6-2c) have similar chemical composition, with carbon the most abundant. The EDX test confirmed the presence of TiO₂ for both adsorbents as shown in Figure 6-2b and Figure 6-2d.

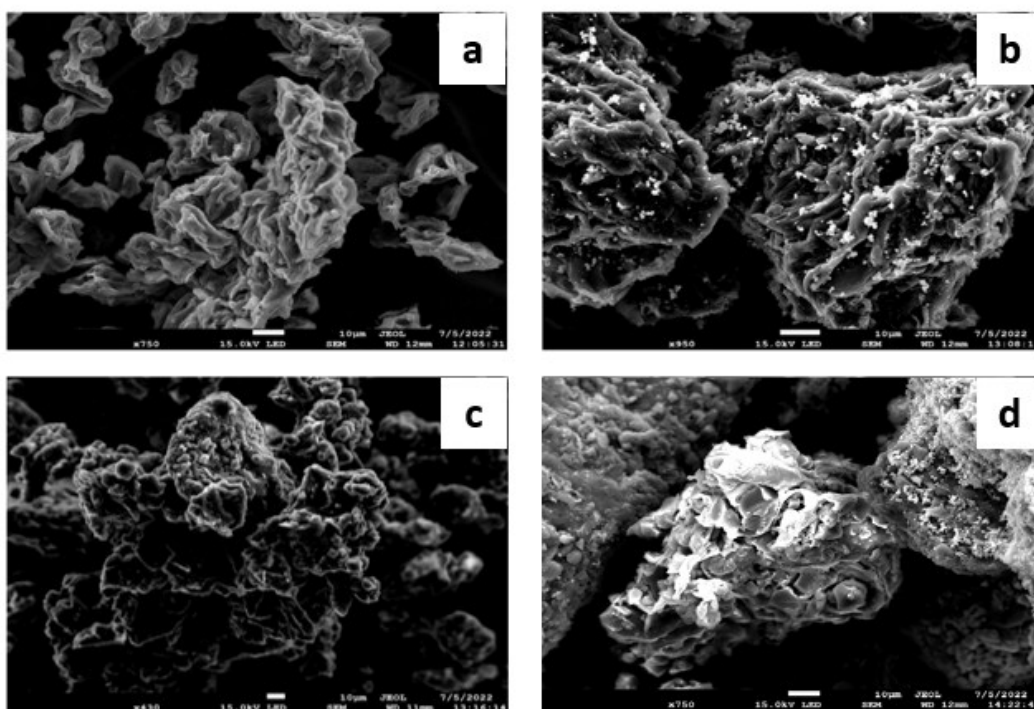


Figure 6-1 SEM image of (a) AC-OP, (b) OP-TiO₂, (c) AC-DS and d) DS-TiO₂.

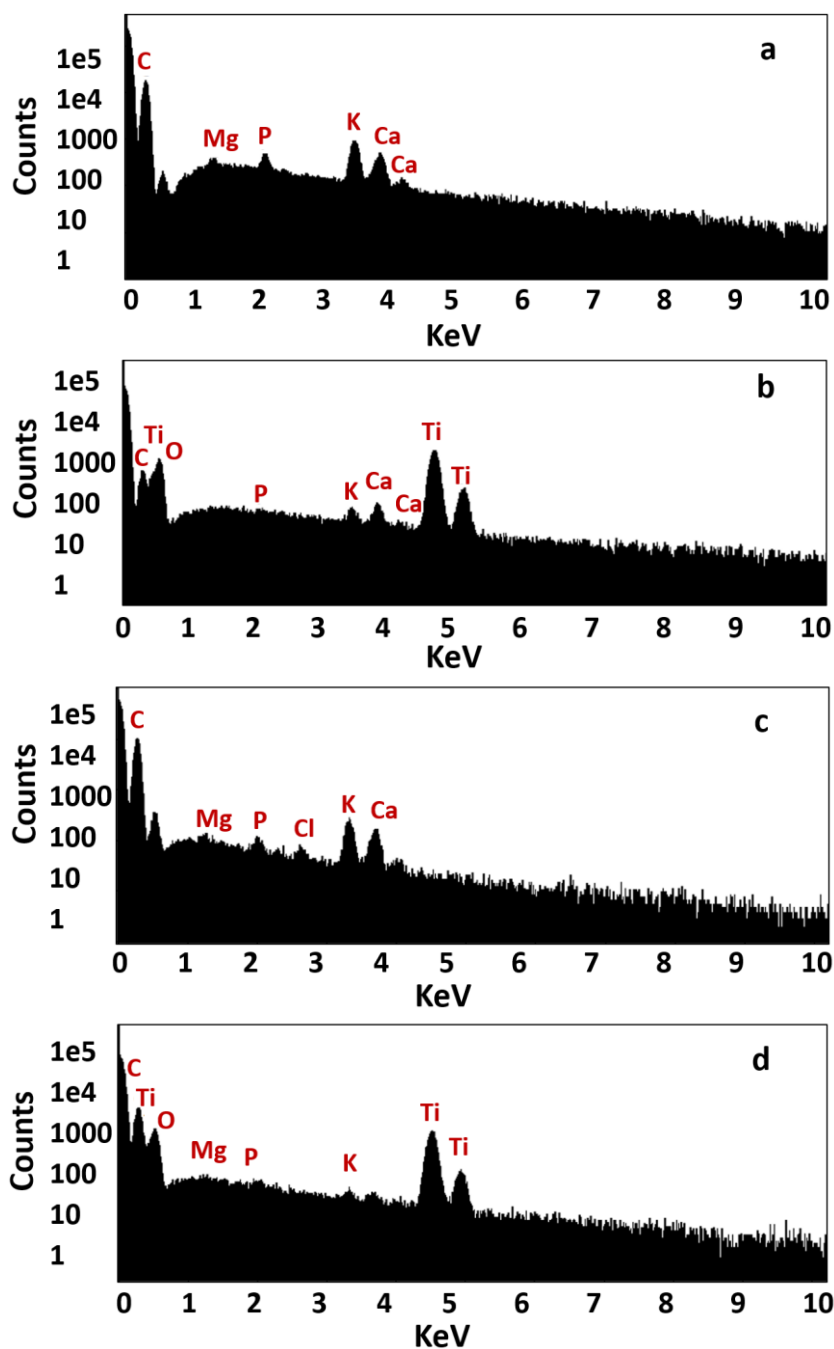


Figure 6-2 (a) EDX graph of AC-OP, (b) EDX graph of OP-TiO₂, (c) EDX graph of AC-DS, and (d) EDX graph of DS-TiO₂.

6.3.1.2. X-ray diffraction crystallography (XRD) analysis

Figure 6-3a and Figure 6-3b shows the XRD patterns for the activated carbon from orange peels and date seeds after modification with TiO₂ NPs. In both adsorbents, $2\theta=25^\circ$ validated the activated carbon existence (Parvathiraja et al., 2022). The broadening diffusion peaks are depicted at small angles ($<20^\circ$), which reveals that the

activated carbon structure is amorphous with a heterogeneous surface (Pujiono et al., 2019). The sharp peak at 30° confirmed that quartz was formed (SiO_2). The peaks at 25° , $36\text{--}38^\circ$, 48° , 52° , 54° , 62° , 69° and 75° indicate the presence and attachment of TiO_2 to activated carbon. All these diffractions peaks are well in accordance with typical pattern of anatase according to standard JCPDS card no. 89-492 (F. Ahmed et al., 2019).

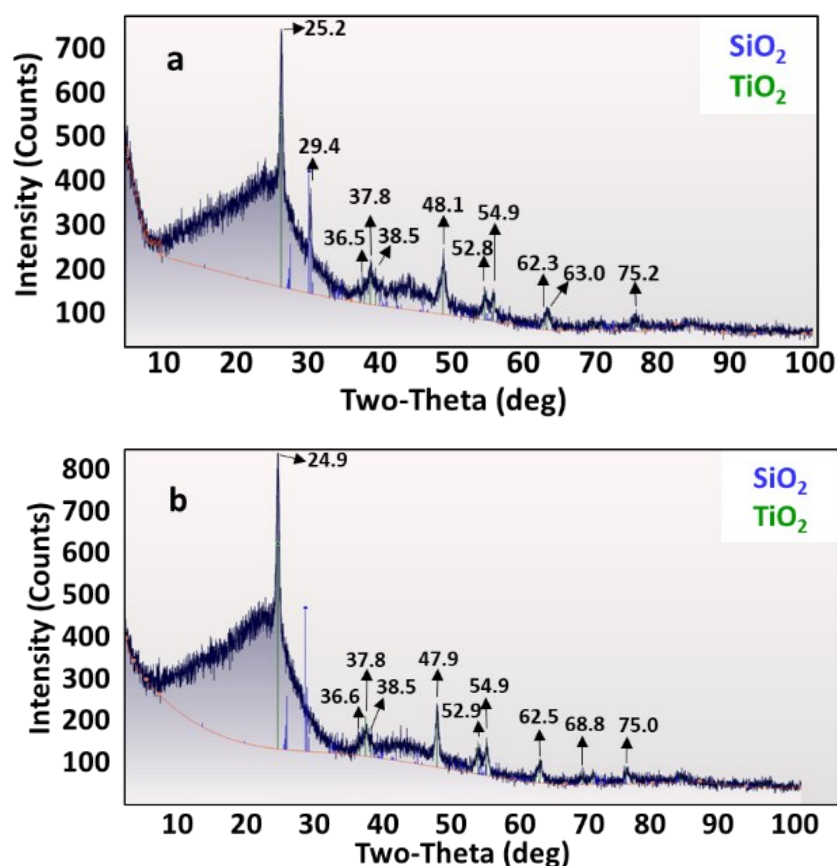


Figure 6-3 XRD patterns of (A) OP- TiO_2 and (B) DS- TiO_2 .

6.3.1.3. Fourier transformed infrared radiation (FTIR)

The FTIR analysis in Figure 6-4 represents the wavelength of modified activated date seed and orange peels by performing Fourier Transformed Infrared characterization technique AC-OP with TiO_2 . Main peaks observed in the plots are explained in Table 6-4. According to the literature, the peaks around 800 cm^{-1} have been attributed to the Ti-O stretching bands and C-O-Ti-O bonding which indicated the

attachment of titanium dioxide NPs to activated carbon (Parvathiraja et al., 2022). An -OH bending of alcoholic or carboxylic groups, or C-H bending vibrations, causes the peak to appear about 1473 cm^{-1} for OP-TiO₂ and 1480 cm^{-1} for DS-TiO₂ (Taoufik et al., 2019). C=O bonds of the carboxyl acid groups were created and confirmed by peaks around 1725 cm^{-1} . An aromatic ring vibration at the C=C stretching peak was found at 1660 and 1664 cm^{-1} for OP-TiO₂ and DS-TiO₂, respectively (Bamdad, 2019; V. K. Gupta & Nayak, 2012; Parvathiraja et al., 2022).

Table 6-4 FTIR spectra of OP-TiO₂ and DS-TiO₂.

Group	FTIR peak of	
	OP-TiO ₂ (cm^{-1})	DS-TiO ₂ (cm^{-1})
C-O-Ti-O bonding	850	772
C-H bending vibrations or O-H bending	1473	1480
C=C stretching in aromatic ring vibration or alkene	1660	1664
C=O stretching	1725	1725

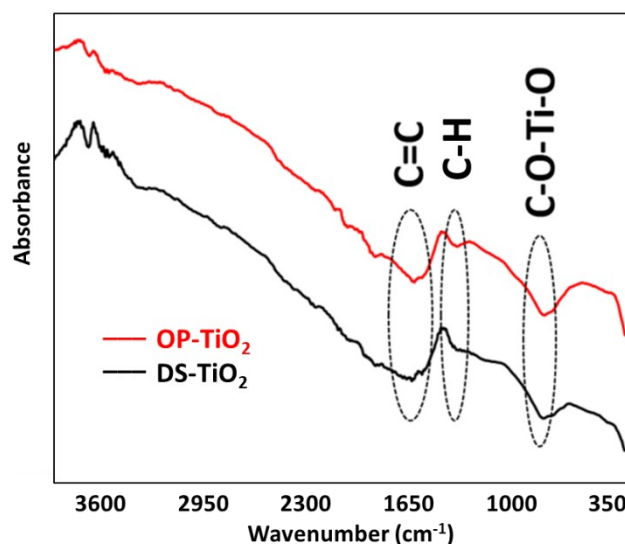


Figure 6-4 FTIR spectra of OP-TiO₂ and DS-TiO₂.

6.3.1.4. Brunauer-Emmett-Teller (BET) Theory

The surface area of the adsorbents was measured using the Brunauer–Emmett–Teller (BET) technique. As shown in Table 6-5, when the surface of activated carbon

derived from orange peels and date seeds was modified with TiO₂, the surface area of the orange peel-based adsorbent increased by approximately 150%, while the date seed-based adsorbent showed an increase of about 60% compared to their respective original values. This increase in surface area can be attributed to the deposition of TiO₂ nanoparticles onto the surface of the activated carbon, leading to the creation of additional active sites and increased surface roughness.

It is worth noting that the initial surface area of the date seed-based adsorbent was higher than that of the orange peel-based adsorbent, which can be attributed to the structural and compositional differences between the two materials. However, the addition of TiO₂ resulted in a greater relative increase in the surface area of the orange peel-based adsorbent. This difference in enhancement can be explained by the specific interactions between TiO₂ nanoparticles and the activated carbon matrix, which may differ between orange peels and date seeds. These variations may influence the extent of surface area expansion, potentially due to the presence of different functional groups and surface characteristics in each material that affect the adsorption and deposition behavior of TiO₂ nanoparticles. The BET results highlight the importance of surface modification in enhancing the performance of adsorbents for pollution removal applications.

Table 6-5 Adsorbents results from BET analysis.

Samples	BET Surface area (m ² g ⁻¹)
AC-OP	2.40
OP-TiO ₂	8.52
AC-DS	51.10
DS-TiO ₂	81.37

6.3.2. Optimization of copper removal

According to the value of the coefficient of determination in Table 6-6 ($R^2 = 0.91$)

and $R^2 = 0.99$), the regressions generated a strong coefficient of determination, showing each regression's validity and a strong correlation between the actual and expected values (Jawad, Mohammed, et al., 2020). In addition, the experiments' accuracy and dependability are further indicated by the relatively low coefficient of variation ($CV = 4.78$). The analysis of variance (ANOVA; Table 6-7) was used to assess the statistical significance of the quadratic model. The F-values and p-values (Table 6-6), were used to assess each coefficient's significance. The greater the magnitude of the F-values and the smaller the p-values, the more significant the corresponding coefficients (Afshin et al., 2021; Dehghani et al., 2021).

Table 6-6 Fit statistics of response surface methodology model.

Adsorbent	Std. Dev.	Mean	C.V. %	R^2
OP-TiO ₂	5.91	85.91	6.88	0.91
DS-TiO ₂	1.46	38.94	3.74	0.99

For both adsorbents, the model's terms are significant. Moreover, the lack-of-fit p-values greater than 0.05 are insignificant, meaning that the proposed models in both cases managed to adequately describe the relation between the experimental variables and the adsorption efficiency (Reghioua et al., 2021; Yousefi et al., 2021).

According to Table 6-7, the linear effect of solution pH (A), initial ion concentration (B), and adsorbent dosage (C) were significant ($p < 0.0001$), and the contact time (D) linear effect was moderately significant ($p = 0.1280$) for DS-TiO₂; while for OP-TiO₂ the linear adsorbent dosage, and solution pH was significant ($p < 0.0001$) and the contact time and initial concentration linear effect was moderately significant. For DS-TiO₂, the effects of squared terms of B^2 , A^2 , and the interaction between AB, AC, and AD were significant; the effect of interaction between BD was slightly significant; however, the effects of interaction between other terms were not statistically significant. For OP-TiO₂, the effects of squared terms of C^2 , A^2 and the

interaction between BC was significant and for B² was slightly significant.

Cu ion removal was determined by the regression equation, which was a function of the initial Cu concentration, pH, adsorbent dosage, and contact time. Cu ion removal (Y) and the variables' empirical relationship based on reduced polynomial equations are in Table 6-8. The value of each factor to achieve the maximum adsorption efficiency reported in Table 6-9. Eqs. (6-8) and (6-9) give the relationship between the process variables and copper removal efficiency for the developed adsorbents.

$$\text{Cu removal (\%)} \text{ by OP-TiO}_2 = 89.47 + 2.91A - 1.25B + 8.49C + 3.19D + 5.02BC - 4.17A^2 + 2.81B^2 - 4.12C^2 \quad (6-8)$$

$$\text{Cu removal (\%)} \text{ by DS-TiO}_2 = 31.57 + 25.34A - 36.29B + 6.55C + 1.03D - 10.06AB + 4.37AC - 21.38AD + 1.67BD + 9.20A^2 - 3.62B^2 \quad (6-9)$$

Graphical methods were utilized to validate the CCD model by comparing the distribution of standardized residuals versus run plot and the correlation between experimental and model-predicted values for Cu adsorption (Abdulhameed et al., 2021; Ghelich et al., 2019). Figure 6-5a and Figure 6-5b display the actual and predicted removal efficiency values. The linear regression fit indicates that predicted values are in good agreement with the actual values. Figure 6-5c and Figure 6-5d illustrate scatter plots of residuals against the order of experimental runs, showing a uniform distribution of points without any discernible pattern or unusual structure, which indicates that the model is appropriate and fits the data adequately.

Table 6-7 ANOVA for reduced quadratic modelling of Cu removal.

Reduced Quadratic model (DS-TiO ₂)						Reduced Quadratic model (OP-TiO ₂)				
Source	Sum of squares	df	Mean Square	F-value	p-value	Sum of squares	df	Mean square	F-value	p-value
Model	14799.32	10	1479.93	697.78	< 0.0001	4246.09	8	530.76	15.21	< 0.0001
A- pH	3563.15	1	3563.15	1680.00	< 0.0001	2260.71	1	2260.71	64.80	< 0.0001
B- initial concentration	1464.82	1	1464.82	690.65	< 0.0001	21.45	1	21.45	0.61	0.4482
C- adsorbent dose	593.23	1	593.23	279.71	< 0.0001	995.50	1	995.50	28.53	0.0002
D- contact time	5.96	1	5.96	2.81	0.1280	138.93	1	138.93	3.98	0.0692
AB	340.34	1	340.34	160.47	< 0.0001					
AC	152.43	1	152.43	71.87	< 0.0001					
AD	440.94	1	440.94	207.90	< 0.0001					
BC						205.13	1	205.13	5.88	0.0320
BD	9.26	1	9.26	4.37	0.0662					
A ²	1068.21	1	1068.21	503.66	< 0.0001	253.06	1	253.06	7.25	0.0196
B ²	57.67	1	57.67	27.19	0.0006	118.95	1	118.95	3.41	0.0896
C ²						266.57	1	266.57	7.64	0.0171
Residual	19.09	9	2.12			418.67	12	34.89		
Lack of Fit	6.51	5	1.30	0.41	0.8200	359.72	8	44.97	3.05	0.1481
Pure Error	12.58	4	3.14			58.94	4	14.74		
Cor Total	14818.41	19				4664.75	20			

Table 6-8 Coefficients in terms of coded factors.

Factor	Coefficient Estimate	
	OP-TiO ₂	DS-TiO ₂
Intercept	89.47	31.57
A-pH	+12.91	+25.34
B-initial concentration	-1.25	-36.29
C-adsorbent dose	+8.49	+6.55
D-contact time	+3.19	+1.03
AB	0	-10.06
AC	0	+4.37
AD	0	-21.38
BC	+5.02	0
BD	0	+1.67
CD	0	0
A ²	-4.17	+9.20
B ²	+2.81	-3.62
C ²	-4.12	0
D ²	0	0

Table 6-9 Optimal solutions for highest Cu removal efficiency.

Adsorbent	pH	Initial concentration (mg g ⁻¹)	Adsorbent dose (g L ⁻¹)	Contact time (h)	Desirability
OP-TiO ₂	5.0	24.6	4.9	3.6	1.0
DS-TiO ₂	6.4	21.2	5.0	3.0	1.0

The model's three-dimensional plots for Cu removal (percentage) as a function of pH-initial concentration and initial concentration-adsorbent dose for OP-TiO₂ and pH-adsorbent dose and pH-contact time for DS-TiO₂ is shown in Figure 6-6. Figure 6-6a demonstrates a substantial increase in Cu removal (%) with an increase in the adsorbent dose from 2 to 5.8 and a decrease in the initial concentration from 50 to 20, while maintaining the other factors constant (pH = 5 and contact time = 3.6h). The plot Figure 6-6b illustrates that, the removal of Cu (%) increased significantly as the solution pH increased from 2.2 to 6.4 and the initial concentration decreased from 50 to 20, while the other factors were kept constant (adsorbent dose = 5 g L⁻¹, and contact time = 3h).

The interaction of pH and DS-TiO₂ dose, as depicted in Figure 6-6d, confirms that the removal efficiency slightly increased with the simultaneous increase of pH and

contact time, while the other fixed parameters are initial concentration (20 mg g^{-1}) and adsorbent dose (5 g L^{-1}). Figure 6-6C shows that the removal efficiency increased with an increase in the adsorbent dose from 2 to 6.4 g L^{-1} . This observation can be attributed to the higher number of active adsorption sites available at higher adsorbent doses.

Highest Cu adsorption efficiency and adsorption capacity were 99.90% and 13.34 mg g^{-1} for OP-TiO₂ and 97.40% and 13.96 mg g^{-1} for DS-TiO₂. The performance of modified activated carbons for the adsorption of heavy metals is promising, attaining adsorption efficiency of >80%, according to previous research (Azmi et al., 2020; Elkhaleefa et al., 2020; Faisal et al., 2020; T. M. Khan et al., 2019; Pavithra et al., 2021; Shehzad et al., 2018). The Comparison of the results of similar Cu adsorption studies using different adsorbents in Table 6-10 revealed that removal efficiency of the OP-TiO₂ and DS-TiO₂ in this study is comparable to other adsorbents. Immobilized fungi residues were less effective, with a removal rate of only 73.11% at a low concentration of 10 mg L^{-1} (X. Li et al., 2018). In terms of adsorbent dosage, the developed adsorbents in this study required a dosage of 5 g L^{-1} to achieve high removal rates, while peanut hull, and treated laterite required a much higher dosage of 20 g L^{-1} . However, compared to around 20 mg L^{-1} for Cu(II) in OP-TiO₂ and DS-TiO₂, the initial concentration for these experiments were also much higher at 150 mg L^{-1} and 200 mg L^{-1} , respectively (R. M. Ali et al., 2016; Rani et al., 2018). On the other hand, some of the other adsorbents, such as Luffa Actangula carbon, requires a lower adsorbent dose of 1 g L^{-1} (S. H. Siddiqui, 2018). While most of the adsorbents required a shorter contact time of around 1-2 hours (R. M. Ali et al., 2016; X. Li et al., 2018; X. Liu et al., 2018; Rani et al., 2018; S. H. Siddiqui, 2018; Teodoro et al., 2017), compared to this study, date seed biochar achieved a high removal rate of 96.96% overnight (Juma Mohamed et al., 2019). The optimum pH for OP-TiO₂ and DS-TiO₂ was found to be 5, and 6.4,

respectively, which is similar to other adsorbents ranging 4-6 (R. M. Ali et al., 2016; Juma Mohamed et al., 2019; X. Li et al., 2018; X. Liu et al., 2018; Rani et al., 2018; S. H. Siddiqui, 2018; Teodoro et al., 2017).

It is important to note, that the effectiveness of an adsorbent in removing Cu(II) ions can be affected by a variety of factors, including the surface area, porosity, and the chemical composition of the adsorbent, as well as the experimental conditions (Qiu et al., 2021). Additionally, other experimental conditions used such as temperature and agitation speed could also impact the adsorption efficiency of the adsorbents.

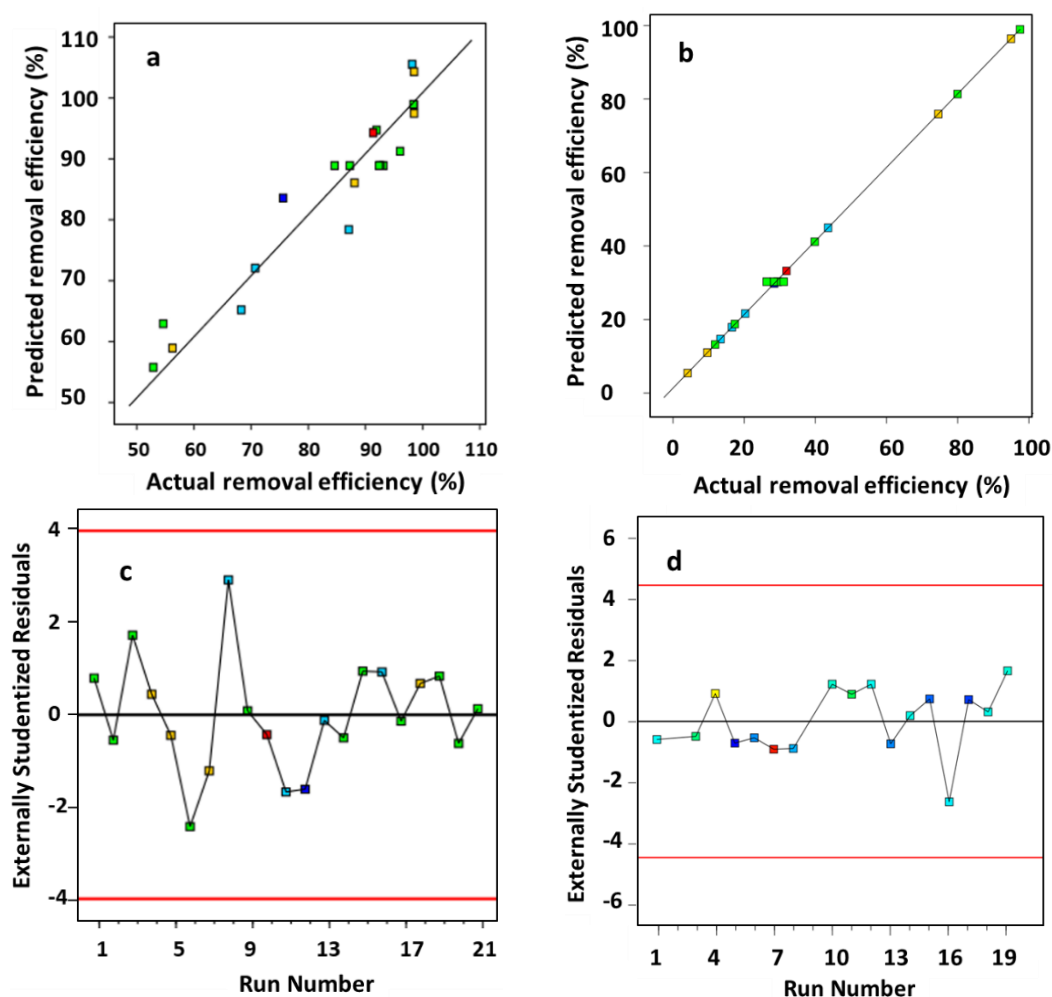


Figure 6-5 Predicted vs actual values of removal efficiency for (a) orange peel (OP-TiO₂); (b) date seeds (DS-TiO₂); and residuals vs runs for (c) OP-TiO₂; and (d) DS-TiO₂.

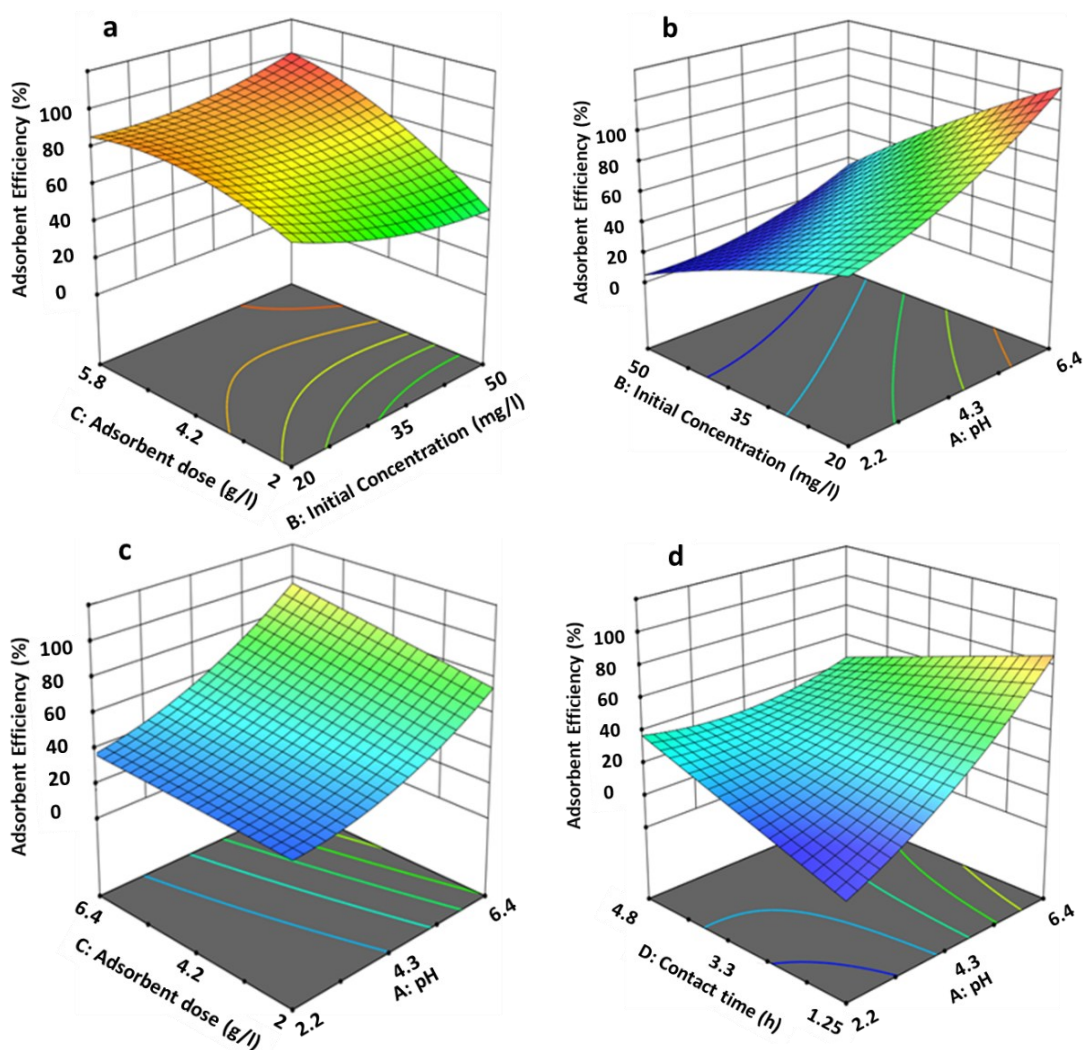


Figure 6-6 Response surface maps of the effects of (a) initial concentration-adsorbent dose on the removal efficiency using OP-TiO₂ and (b) pH-Cu initial concentrations, (c) pH-adsorbent dose and (d) pH-contact time on the removal efficiency using DS-TiO₂. (All at room temperature).

Table 6-10 Summary of adsorptive removal of copper by various adsorbents.

Adsorbent	Adsorbate	C _i (mg L ⁻¹) Unless indicated otherwise	A _d (g L ⁻¹)	pH	t _c (h)	Other Info	RE (%)	AC (mg g ⁻¹)	Reference
TiO ₂ modified-Activated carbon from orange peels (OP-TiO ₂)	Cu(II)	24.6	4.9	5.0	3.6	200 rpm 20 °C	99.9	13.34	This study
TiO ₂ modified-Activated carbon from date seeds (DS-TiO ₂)	Cu(II)	21.2	5.0	6.4	3.0	200 rpm 20 °C	97.4	13.96	This study
Date seeds biochar	Cu(II)	2.0	2.0		overnight	200 rpm	97.0		(Juma Mohamed et al., 2019)
Carboxylated cellulose derivative	Cu(II)-Co(II), Cu(II)-Ni(II)	0.8 mmol L ⁻¹	0.2	5.5	1.0	25 °C 130 rpm		Cu(II)-Co(II): 0.99-0.24 mmol g ⁻¹ Cu(II)-Ni(II): 1.13-0.3 mmol g ⁻¹	(Teodoro et al., 2017)
Peanut hull	Cu(II)	150.0	20.0	4.0	1.0	150 rpm 25 °C,		14.13	(R. M. Ali et al., 2016)
Sugarcane bagasse	Cu(II)	10.0	5.0	5.0	1.0	150 rpm, 25 °C	SG: 88.9	4.84	(M. Gupta et al., 2018)
Acid modified sugarcane bagasse (ASG)							ASG:96.9	5.35	
Base modified sugarcane bagasse (BSG)							BSG:94.8	2.06	
Activated carbon (AC)							AC: 98.5	5.62	
Luffa Actangula Carbon	Cu(II)	50.0	1.0	6.0	2.0	30 °C		12.50	(S. H. Siddiqui, 2018)
Groundnut seed cake power, sesame seed cake powder, coconut cake powders	Cu(II)	10.0	15.0	5.0	0.5	40 °C		4.24	(Pavan Kumar et al., 2019)
			20.0						
Immobilized fungi residues	Cu(II)	10.0	20.0	6.0	2.0	25 °C, 150 rpm	73.1	8.13	(X. Li et al., 2018)
Uncaria gambir	Cu(II)	10.0	1.2	5.0	1.5	60 °C, 150 rpm		9.95	(Tong et al., 2011)

C_i = initial concentration; A_d = adsorbent dose; t_c = contact time; RE = removal efficiency; AC = adsorption capacity.

6.3.2.1. Effect of pH

The optimum pH for OP-TiO₂ and DS-TiO₂ was 5, and 6.4, respectively. Figure 6-6b shows the mutual effect of pH and initial concentration for OP-TiO₂. The interaction of pH-adsorbent dose, and pH-contact time are presented in Figure 6-6c and Figure 6-6d for DS-TiO₂. In the range of the experiment, increasing the pH increased the removal efficiency for both adsorbents. Similar trends were observed in many past studies; for instance, 20 mg EDTA-functionalized bamboo activated carbon was added to 25 mL Pb(II) and Cu(II) solution and the findings showed that the adsorption capacities for Pb(II) and Cu(II) increased for both ions when pH increased from 2 to 6 (Lv et al., 2018). In another case, as the solution pH increased, activated carbon and activated carbon impregnated with iron(III) were more effective at removing Cu(II) and for both adsorbents, it was found that Cu(II) was almost completely removed above pH 7 (J.-K. Yang et al., 2009). Two other studies also revealed that the optimal pH range for adsorption performance is between 5 and 7. Guo et al. (2011) and Amin et al. (2017) reported that the highest adsorption capacity of adsorbents occurs between pH 5 and 7 (Amin et al., 2017; Fang et al., 2011).

6.3.2.2. Effect of adsorbent dose

The adsorption efficiency of OP-TiO₂ and DS-TiO₂ increased with increasing doses of adsorbents (Figure 6-6a, Figure 6-6c), since increasing the adsorbent dose provides more active sites for heavy metal adsorption. Similarly, another study showed that the adsorption of 5.30 mg L⁻¹ Pb(II) and 4.00 mg L⁻¹ Cu(II) ions from wastewater increased with increase in biosorbent dose (2-10 g) using activated carbon from cassava peels (Owamah, 2014). Amin et al. (2017) stated as the adsorbent dose rose from 0.1 g L⁻¹ to 2.0 g L⁻¹ the Cu(II) removal efficiency increased from 20% to 99.99% for orange peel, and from 12% to 96% for date palm at a same adsorbent dose (Amin et al., 2017).

6.3.2.3. Effect of initial concentration

Increasing Cu initial concentration decreased the removal efficiency, for OP-TiO₂ (Figure 6-6b) and DS-TiO₂, and models predicted the optimum C_i was around 20 mg L⁻¹. The available active sites on the adsorbent are easily occupied with metal ions at low initial concentrations. The effects of C_i on the Pb(II) and Cu(II) adsorption by EDTA-functionalized bamboo activated carbon was similar. The increased initial concentration of Pb(II) and Cu(II) led to improved equilibrium adsorption capacity before the active sites on the surface of the adsorbent were saturated (Lv et al., 2018).

6.3.2.4. Effect of contact time

Increasing the contact time to more than 3 h did not significantly impact the Cu removal efficiency despite that the removal efficiency increased with increasing the contact time up to 3 h. Similarly, in another study, the adsorption capacities for Cu(II) and Pb(II) removal at 100, 200, and 300 ppm, respectively, were studied as a function of the contact time and the adsorption capacity gradually increased with time. The maximum adsorption capacities were attained after 180 min of contact time, and there was no further substantial increase (ALothman et al., 2016).

6.3.3. Adsorption kinetic study

From the results, pseudo-second-order model was best fitted to Cu adsorption for the case of OP- TiO₂ and DS-TiO₂. This observation implies that the adsorption process is governed by chemisorption. However, it is important to approach the interpretation of these models with caution, as complex matrices may involve a combination of chemisorption and physisorption mechanisms in the adsorption process (Chopra et al., 2020; da Costa et al., 2023).

Table 6-11 gives the kinetic parameters, and Figure 6-7 (OP-TiO₂) and Figure 6-8 (DS-TiO₂) show the kinetic plots for the pseudo-first-order Figure 6-7a and Figure 6-8a),

pseudo-second-order (Figure 6-7b and Figure 6-8b), intra-particle diffusion (Figure 6-7c and Figure 6-8c) and Elovich models (Figure 6-7d and Figure 6-8d). The R^2 values are 0.99 and 0.98 for OP-TiO₂ and DS-TiO₂, respectively, in the case of pseudo-second-order. The Cu maximum adsorption capacities (q_e) for OP-TiO₂, and DS-TiO₂ are 9.98 mg g⁻¹ and 9.95 mg g⁻¹, respectively.

The results obtained from the fitting of the intra-particle diffusion model provide insights into the involvement of intra-particle diffusion in the adsorption process of Cu(II) onto OP-TiO₂ and DS-TiO₂. If the adsorption process is solely controlled by intra-particle diffusion, the plot should yield a linear relationship which passes through the origin (Z. Wu et al., 2014). However, in reality, the plot often exhibits multiple linear segments, indicating the involvement of other factors.

In this study, the fitting of the intra-particle diffusion model to the experimental data revealed that the plot of q_t against $t^{0.5}$ showed distinct linear segments. This suggests that the adsorption process of Cu(II) onto the modified activated carbon adsorbents involves multiple steps. The initial steep section of the line indicates film diffusion, followed by another section where diffusion becomes the rate-controlling factor. The final part represents the equilibrium stage, where intra-particle diffusion slows down due to the low concentration of the remaining substance in the solution (Claros et al., 2021; Malash & El-Khaiary, 2010). The adsorption rates for different stages were observed to exhibit the following order: the second stage > the third stage > the first stage for both adsorbents. Hence, the initial step (film diffusion) governs the overall rate of adsorption. The intercept (C) in the intra-particle diffusion model represents the thickness of the boundary layer. A higher intercept value indicates a thicker boundary layer, which could potentially hinder the diffusion process and affect the overall adsorption rate (Q. Du et al., 2014).

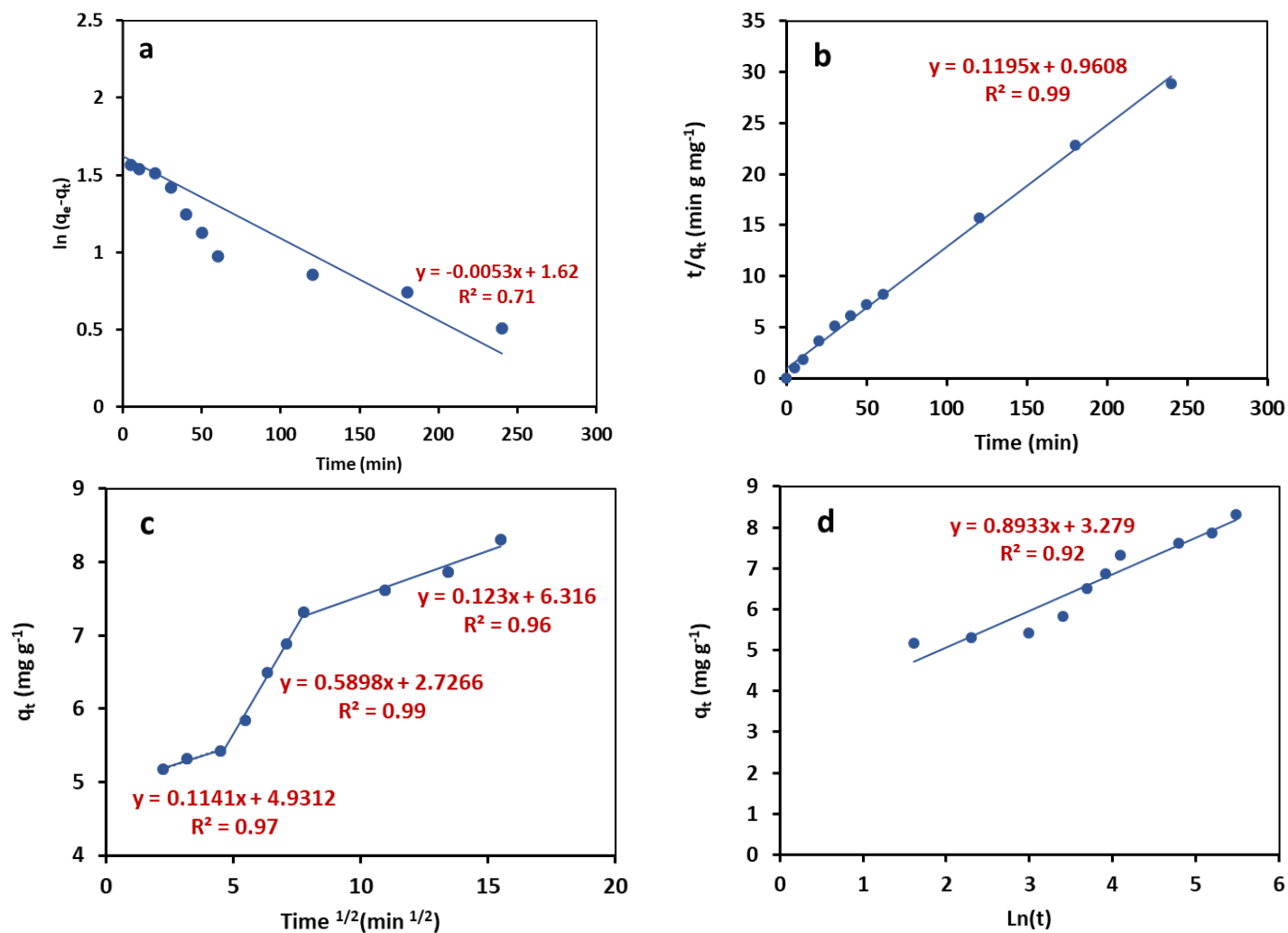


Figure 6-7 Copper adsorption kinetic studies by OP-TiO₂ (a) pseudo-first-order, (b) pseudo-second-order, (c) intra-particle diffusion model (d) Elovich model.

(Room temperature, rpm = 200)

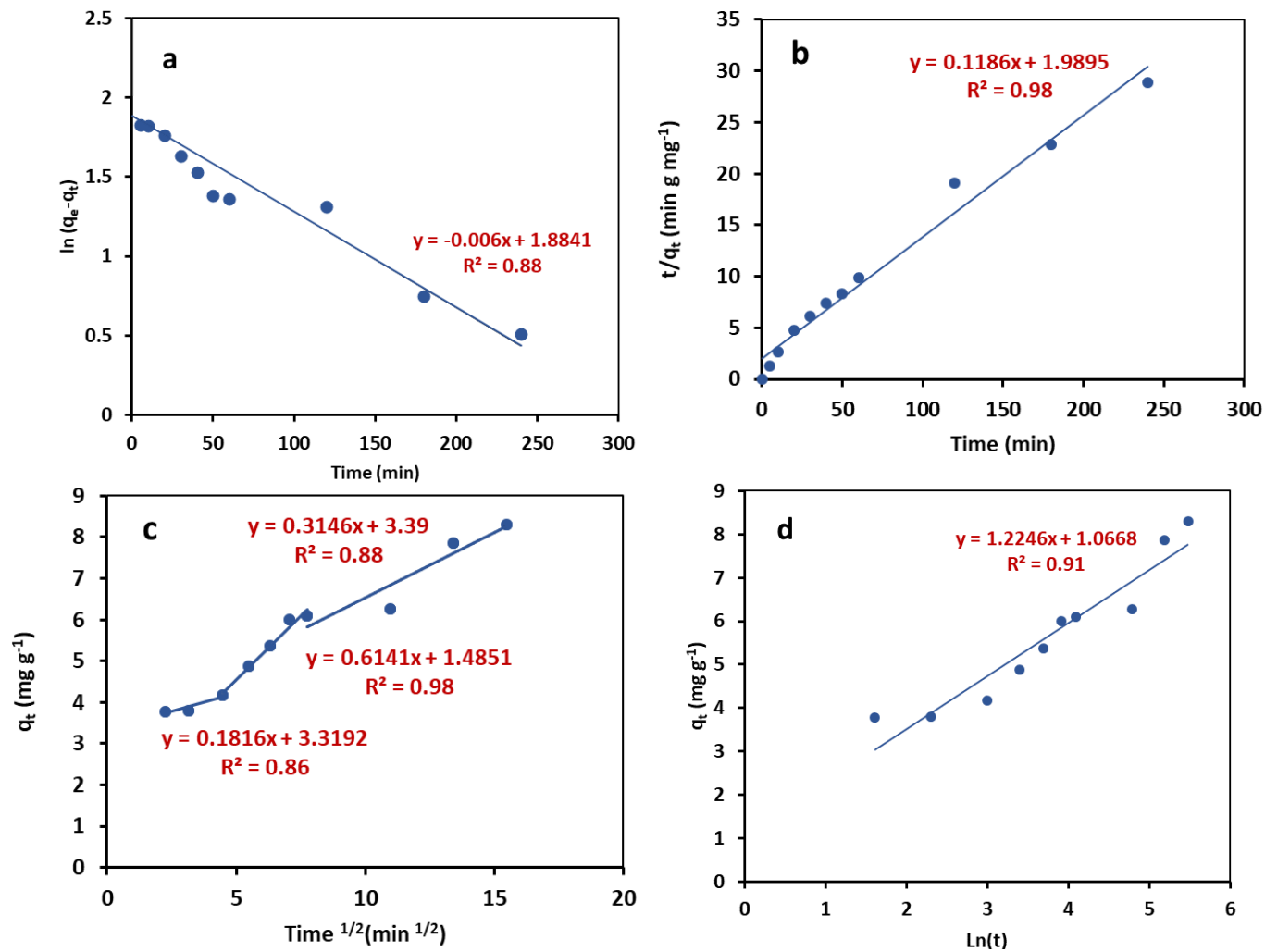


Figure 6-8 Copper adsorption kinetic studies by DS-TiO₂ (a) pseudo-first-order, (b) pseudo-second-order, (c) intra-particle diffusion model (d) Elovich model.

(Room temperature, rpm = 200)

Table 6-11 Kinetic parameters of pseudo-first-order and pseudo-second-order models.

Model	Parameter	OP-TiO ₂	DS-TiO ₂
Pseudo-first-order model	k_1 (min ⁻¹)	-2.94×10^{-5}	-3.33×10^{-5}
	q_e (mg g ⁻¹)	5.05	6.58
	R^2	0.71	0.88
Pseudo-second-order model	k_2 (g mg ⁻¹ min ⁻¹)	0.01	7.07×10^{-5}
	q_e (mg g ⁻¹)	8.37	8.43
	R^2	0.99	0.98
Intra-particle diffusion model	k_1 (mg g ⁻¹ min ^{-0.5})	0.11	0.18
	C_1	4.93	3.32
	R_1^2	0.97	0.86
	k_2 (mg g ⁻¹ min ^{-0.5})	0.59	0.61
	C_2	2.73	1.49
	R_2^2	0.99	0.98
	k_3 (mg g ⁻¹ min ^{-0.5})	0.12	0.31
	C_3	6.32	3.39
	R_3^2	.96	0.88
Elovich model	α (mg g ⁻¹ min ⁻¹)	0.82	1.12
	β (g mg ⁻¹)	35.09	2.93
	R^2	0.92	0.91

6.4. Strengths, Limitations, and Recommendations

One of the major strengths of this study is utilizing waste materials (orange peels and date seeds) as precursors for the modified activated carbon. This study adds value to waste and promotes sustainable practices by repurposing these abundant and easily accessible materials. Another notable strength of this study is using the RSM and CCD for optimization. Applying RSM allows for a systematic and efficient exploration of the process variables, and identifies the optimal conditions for copper removal. Additionally, the results from the batch Cu²⁺ adsorption experiments demonstrate the synthesized adsorbents effectiveness in removing copper from water.

A limitation of this study is the use of synthetic water instead of real water samples. While synthetic water provides controlled conditions for experimentation, it may not fully represent the complex composition of real-world water sources, which can contain various ions and contaminants. Future studies should consider investigating the adsorption performance of the developed adsorbents using real water samples to assess its efficacy in practical applications. Furthermore, it is recommended to conduct

continuous flow studies to evaluate the performance of the OP-TiO₂ and DS-TiO₂ under continuous operation. Continuous flow experiments can provide insights into the long-term stability and efficiency of the adsorbent in real-world scenarios. Furthermore, investigating the feasibility of adsorbent regeneration and assessing its stability and reusability would contribute to developing cost-effective and sustainable water treatment processes. Another important thing to consider is recovering the adsorbents after water treatment, which challenges their reusability. It is important to address the potential release of TiO₂ nanoparticles into the environment and investigate their behavior and long-term effects thoroughly. It is recommended that we focus on developing safe disposal methods and exploring the potential for recycling or reusing the spent adsorbents. These efforts will contribute to the overall sustainability and minimize any potential environmental impact.

6.5. Conclusion

A TiO₂ nanoparticles-modified activated carbon has been successfully developed from orange peels (OP) and date seeds (DS). Modifying the activated carbon with TiO₂ increased the surface area of both adsorbents. The developed adsorbent (OP-TiO₂ and DS-TiO₂) can significantly remove Cu ions from aquatic solutions with a removal efficiency of 99.90% and 97.40%, respectively, after about three hours. The highest adsorption efficiency for OP-TiO₂ was predicted at pH 5.0, adsorbent dose of 4.9 mg g⁻¹, contact time 3.6 h, and initial Cu concentration of 24.6 ppm, based on the RSM-CCD. A similar optimum condition has been found for DS-TiO₂ at pH 6.4, 5.0 mg g⁻¹, contact time 3.0 h, and initial Cu concentration of 21.2 ppm. The highest adsorption capacity was 13.34 mg g⁻¹ for OP-TiO₂ and 13.96 mg g⁻¹ for DS-TiO₂. The experimental data were fitted to several kinetic models, and the results revealed that the Cu sorption

on OP-TiO₂ ($R^2 = 0.99$, $k_2 = 0.01 \text{ g mg}^{-1} \text{ min}^{-1}$, and $q_e = 8.37 \text{ mg g}^{-1}$) and DS-TiO₂ ($R^2 = 0.98$, $k_2 = 7.07 \times 10^{-5} \text{ g mg}^{-1} \text{ min}^{-1}$, and $q_e = 8.43 \text{ mg g}^{-1}$) could be better described by the pseudo-second-order kinetic.

The exceptional heavy metal removal capability of these renewable, affordable adsorbents from locally accessible sources was proven. More research is required to replace commercial activated carbon with environmentally friendly adsorbents such as OP-TiO₂ and DS-TiO₂ to be successfully used in water and wastewater treatment plants.

6.6. References

- Abdulhameed, A. S., Hum, N. N. M. F., Rangabhashiyam, S., Jawad, A. H., Wilson, L. D., Yaseen, Z. M., Al-Kahtani, A. A., & AlOthman, Z. A. (2021). Statistical modeling and mechanistic pathway for methylene blue dye removal by high surface area and mesoporous grass-based activated carbon using K₂CO₃ activator. *Journal of Environmental Chemical Engineering*, 9(4), 105530.
- Afshin, S., Rashtbari, Y., Vosough, M., Dargahi, A., Fazlzadeh, M., Behzad, A., & Yousefi, M. (2021). Application of Box–Behnken design for optimizing parameters of hexavalent chromium removal from aqueous solutions using Fe₃O₄ loaded on activated carbon prepared from alga: Kinetics and equilibrium study. *Journal of Water Process Engineering*, 42, 102113.
- Ahmed, F., Awada, C., Ansari, S. A., Aljaafari, A., & Alshoaibi, A. (2019). Photocatalytic inactivation of Escherichia coli under UV light irradiation using large surface area anatase TiO₂ quantum dots. *Royal Society Open Science*, 6(12), 191444.
- Ajala, M. A., Abdulkareem, A. S., Tijani, J. O., & Kovo, A. S. (2022). Adsorptive

- behaviour of rutile phased titania nanoparticles supported on acid-modified kaolinite clay for the removal of selected heavy metal ions from mining wastewater. *Applied Water Science*, 12(2), 19.
- Ali, R. M., Hamad, H. A., Hussein, M. M., & Malash, G. F. (2016). Potential of using green adsorbent of heavy metal removal from aqueous solutions: adsorption kinetics, isotherm, thermodynamic, mechanism and economic analysis. *Ecological Engineering*, 91, 317–332.
- AlOthman, Z. A., Habila, M. A., Al-Shalan, N. H., Alfadul, S. M., Ali, R., & Alfarhan, B. (2016). Adsorptive removal of Cu (II) and Pb (II) onto mixed-waste activated carbon: kinetic, thermodynamic, and competitive studies and application to real wastewater samples. *Arabian Journal of Geosciences*, 9(4), 1–9.
- Amin, M. T., Alazba, A. A., & Amin, M. N. (2017). Absorption behaviours of copper, lead, and arsenic in aqueous solution using date palm fibres and orange peel: Kinetics and thermodynamics. *Polish Journal of Environmental Studies*, 26(2), 543–557. <https://doi.org/10.15244/pjoes/66963>
- Asim, N., Amin, M. H., Samsudin, N. A., Badiei, M., Razali, H., Akhtaruzzaman, M., Amin, N., & Sopian, K. (2020). Development of effective and sustainable adsorbent biomaterial from an agricultural waste material: Cu (II) removal. *Materials Chemistry and Physics*, 249, 123128.
- Azmi, S. N. H., Al-Balushi, M., Al-Siyabi, F., Al-Hinai, N., & Khurshid, S. (2020). Adsorptive removal of Pb (II) ions from groundwater samples in Oman using carbonized Phoenix dactylifera seed (Date stone). *Journal of King Saud University-Science*, 32(7), 2931–2938.
- Azzam, A. M., El-Wakeel, S. T., Mostafa, B. B., & El-Shahat, M. F. (2016). Removal

- of Pb, Cd, Cu and Ni from aqueous solution using nano scale zero valent iron particles. *Journal of Environmental Chemical Engineering*, 4(2), 2196–2206.
- Bamdad, H. (2019). *A theoretical and experimental study on biochar as an adsorbent for removal of acid gases (CO₂ and H₂S)*. Memorial University of Newfoundland.
- Bessegato, G. G., De Almeida, L. C., Ferreira, S. L. C., & Zanoni, M. V. B. (2019). Experimental design as a tool for parameter optimization of photoelectrocatalytic degradation of a textile dye. *Journal of Environmental Chemical Engineering*, 7(4), 103264.
- Chaware, C. Y., & Khobragade, M. U. (2022). Recent advancement in process optimization using rsm for adsorptive removal of dyes from aqueous solutions: a review. *International Journal of Mechanical Engineering*, 7(6).
- Chopra, I., Singh, P. K., & Singh, S. B. (2020). Kinetics and equilibrium studies for methylene blue removal from simulated wastewater effluents using agricultural waste, *Parthenium hysterophorus* L. *Indian Journal of Chemical Technology (IJCT)*, 27(4), 274–282.
- Claros, M., Kuta, J., El-Dahshan, O., Michalička, J., Jimenez, Y. P., & Vallejos, S. (2021). Hydrothermally synthesized MnO₂ nanowires and their application in Lead (II) and Copper (II) batch adsorption. *Journal of Molecular Liquids*, 325, 115203.
- da Costa, T. B., da Silva, T. L., da Silva, M. G. C., & Vieira, M. G. A. (2023). Efficient recovery of europium by biosorption and desorption using beads developed from sericin residues from silk yarns processing, sodium alginate and poly (ethylene glycol) diglycidyl ether. *Journal of Environmental Chemical Engineering*, 11(1), 109222.

- Dehghani, M. H., Hassani, A. H., Karri, R. R., Younesi, B., Shayeghi, M., Salari, M., Zarei, A., Yousefi, M., & Heidarinejad, Z. (2021). Process optimization and enhancement of pesticide adsorption by porous adsorbents by regression analysis and parametric modelling. *Scientific Reports*, *11*(1), 11719.
- Deng, S., Bai, R., & Chen, J. P. (2003). Aminated polyacrylonitrile fibers for lead and copper removal. *Langmuir*, *19*(12), 5058–5064.
- Du, Q., Sun, J., Li, Y., Yang, X., Wang, X., Wang, Z., & Xia, L. (2014). Highly enhanced adsorption of congo red onto graphene oxide/chitosan fibers by wet-chemical etching off silica nanoparticles. *Chemical Engineering Journal*, *245*, 99–106.
- Elkady, M. F., Hussein, M. M., & Atiaa, H. M. (2015). Preparation of nano-activated carbon from carbon based material for copper decontamination from wastewater. *American Journal of Applied Chemistry*, *3*(3–1), 31–37.
- Elkhaleefa, A., Ali, I. H., Brima, E. I., Elhag, A. B., & Karama, B. (2020). Efficient removal of Ni (II) from aqueous solution by date seeds powder biosorbent: adsorption kinetics, isotherm and thermodynamics. *Processes*, *8*(8), 1001.
- Faisal, M. L., Al-Najjar, S. Z., & Al-Sharif, Z. T. (2020). Modified orange peel as sorbent in removing of heavy metals from aqueous solution. *J Green Eng*, *10*(11), 10600–10615.
- Fang, J., Qin, G., Wei, W., & Zhao, X. (2011). Preparation and characterization of tubular supported ceramic microfiltration membranes from fly ash. *Separation and Purification Technology*, *80*(3), 585–591.
- Fu, Z., & Xi, S. (2020). The effects of heavy metals on human metabolism. *Toxicology Mechanisms and Methods*, *30*(3), 167–176.
- Gan, W., Shang, X., Li, X.-H., Zhang, J., & Fu, X. (2019). Achieving high adsorption

- capacity and ultrafast removal of methylene blue and Pb^{2+} by graphene-like $\text{TiO}_2@ \text{C}$. *Colloids and Surfaces A: Physicochemical and Engineering Aspects*, 561, 218–225.
- Ghahri, P., Jamiolahmady, M., & Sohrabi, M. (2011). A Thorough Investigation of Cleanup Efficiency of Hydraulic Fractured Wells Using Response Surface Methodology. *SPE European Formation Damage Conference and Exhibition*, SPE-144114.
- Ghelich, R., Jahannama, M. R., Abdizadeh, H., Torknik, F. S., & Vaezi, M. R. (2019). Central composite design (CCD)-Response surface methodology (RSM) of effective electrospinning parameters on PVP-B-Hf hybrid nanofibrous composites for synthesis of HfB_2 -based composite nanofibers. *Composites Part B: Engineering*, 166, 527–541.
- Gupta, M., Gupta, H., & Kharat, D. S. (2018). Adsorption of Cu (II) by low cost adsorbents and the cost analysis. *Environmental Technology & Innovation*, 10, 91–101.
- Gupta, V. K., & Nayak, A. (2012). Cadmium removal and recovery from aqueous solutions by novel adsorbents prepared from orange peel and Fe_2O_3 nanoparticles. *Chemical Engineering Journal*, 180, 81–90.
<https://doi.org/10.1016/j.cej.2011.11.006>
- Hydari, S., Sharififard, H., Nabavinia, M., & reza Parvizi, M. (2012). A comparative investigation on removal performances of commercial activated carbon, chitosan biosorbent and chitosan/activated carbon composite for cadmium. *Chemical Engineering Journal*, 193, 276–282.
- Jawad, A. H., Abdulhameed, A. S., Wilson, L. D., Syed-Hassan, S. S. A., ALOthman, Z. A., & Khan, M. R. (2021). High surface area and mesoporous activated

- carbon from KOH-activated dragon fruit peels for methylene blue dye adsorption: Optimization and mechanism study. *Chinese Journal of Chemical Engineering*, 32, 281–290.
- Jawad, A. H., Bardhan, M., Islam, M. A., Islam, M. A., Syed-Hassan, S. S. A., Surip, S. N., ALothman, Z. A., & Khan, M. R. (2020). Insights into the modeling, characterization and adsorption performance of mesoporous activated carbon from corn cob residue via microwave-assisted H₃PO₄ activation. *Surfaces and Interfaces*, 21, 100688.
- Jawad, A. H., Ishak, M. A. M., Farhan, A. M., & Ismail, K. (2017). Response surface methodology approach for optimization of color removal and COD reduction of methylene blue using microwave-induced NaOH activated carbon from biomass waste. *Water Treat*, 62, 208–220.
- Jawad, A. H., Mohammed, I. A., & Abdulhameed, A. S. (2020). Tuning of fly ash loading into chitosan-ethylene glycol diglycidyl ether composite for enhanced removal of reactive red 120 dye: optimization using the Box–Behnken design. *Journal of Polymers and the Environment*, 28, 2720–2733.
- Joseph, L., Jun, B. M., Flora, J. R. V., Park, C. M., & Yoon, Y. (2019). Removal of heavy metals from water sources in the developing world using low-cost materials: A review. *Chemosphere*, 229, 142–159.
<https://doi.org/10.1016/j.chemosphere.2019.04.198>
- Juma Mohamed, A. A., Vuai, L. A., Kombo, M., & Chukwuma, O. J. (2019). Removal of selected metal ions using powder of seeds of Ajwaa dates from aqueous solution. *Journal of Analytical & Pharmaceutical Research*, 8(6), 228–232. <https://doi.org/10.15406/japlr.2019.08.00343>
- Khan, T. M., Riaz, I., Hameed, S., & Khan, B. (2019). Lemon juice and microwave

- assisted modification of date seed husk for arsenic biosorption. *Journal of Innovative Sciences*, 5(2), 106–114.
- Lenka, S. P., Shaikh, W. A., Owens, G., Padhye, L. P., Chakraborty, S., & Bhattacharya, T. (2021). Removal of copper from water and wastewater using dolochar. *Water, Air, & Soil Pollution*, 232(5), 1–15.
- Li, X., Zhang, D., Sheng, F., & Qing, H. (2018). Adsorption characteristics of Copper (II), Zinc (II) and Mercury (II) by four kinds of immobilized fungi residues. *Ecotoxicology and Environmental Safety*, 147, 357–366.
- Lin, J., Zhan, Y., & Zhu, Z. (2011). Adsorption characteristics of copper (II) ions from aqueous solution onto humic acid-immobilized surfactant-modified zeolite. *Colloids and Surfaces A: Physicochemical and Engineering Aspects*, 384(1–3), 9–16.
- Liu, X., Chen, Z.-Q., Han, B., Su, C.-L., Han, Q., & Chen, W.-Z. (2018). Biosorption of copper ions from aqueous solution using rape straw powders: optimization, equilibrium and kinetic studies. *Ecotoxicology and Environmental Safety*, 150, 251–259.
- Lv, D., Liu, Y., Zhou, J., Yang, K., Lou, Z., Baig, S. A., & Xu, X. (2018). Application of EDTA-functionalized bamboo activated carbon (BAC) for Pb (II) and Cu (II) removal from aqueous solutions. *Applied Surface Science*, 428, 648–658.
- Malash, G. F., & El-Khaiary, M. I. (2010). Piecewise linear regression: A statistical method for the analysis of experimental adsorption data by the intraparticle-diffusion models. *Chemical Engineering Journal*, 163(3), 256–263.
- Méndez, A., Barriga, S., Fidalgo, J. M., & Gascó, G. (2009). Adsorbent materials from paper industry waste materials and their use in Cu (II) removal from water. *Journal of Hazardous Materials*, 165(1–3), 736–743.

- Meng, F., Yang, B., Wang, B., Duan, S., Chen, Z., & Ma, W. (2017). Novel dendrimerlike magnetic biosorbent based on modified orange peel waste: Adsorption–reduction behavior of arsenic. *ACS Sustainable Chemistry & Engineering*, 5(11), 9692–9700.
- Mishra, S., Achary, G., & Das, M. (2012). Adsorption of Cu (II) by used aqua guard carbon (UAC). *J Chem Pharm Res*, 4(2), 1207–1216.
- Owamah, H. I. (2014). Biosorptive removal of Pb (II) and Cu (II) from wastewater using activated carbon from cassava peels. *Journal of Material Cycles and Waste Management*, 16(2), 347–358.
- Pantazis, D., Pease, S. G., Goodall, P., West, A., & Conway, P. (2023). A design of experiments Cyber–Physical System for energy modelling and optimisation in end-milling machining. *Robotics and Computer-Integrated Manufacturing*, 80, 102469.
- Parvathiraja, C., Katheria, S., Siddiqui, M. R., Wabaidur, S. M., Islam, M. A., & Lai, W.-C. (2022). Activated Carbon-Loaded Titanium Dioxide Nanoparticles and Their Photocatalytic and Antibacterial Investigations. *Catalysts*, 12(8), 834.
- Pavan Kumar, G., Malla, K. A., Yerra, B., & Srinivasa Rao, K. (2019). Removal of Cu (II) using three low-cost adsorbents and prediction of adsorption using artificial neural networks. *Applied Water Science*, 9, 1–9.
- Pavithra, S., Thandapani, G., Sugashini, S., Sudha, P. N., Alkhamis, H. H., Alrefaei, A. F., & Almutairi, M. H. (2021). Batch adsorption studies on surface tailored chitosan/orange peel hydrogel composite for the removal of Cr (VI) and Cu (II) ions from synthetic wastewater. *Chemosphere*, 271, 129415.
- Pujiono, F. E., Mulyati, T. A., & Fizakia, M. N. (2019). Modification of activated carbon with titanium dioxide as a water treatment material. *Journal of Public*

Health in Africa, 10(s1).

- Qiu, B., Tao, X., Wang, H., Li, W., Ding, X., & Chu, H. (2021). Biochar as a low-cost adsorbent for aqueous heavy metal removal: A review. *Journal of Analytical and Applied Pyrolysis*, 155, 105081.
- Rambabu, K., Banat, F., Nirmala, G. S., Velu, S., Monash, P., & Arthanareeswaran, G. (2019). Activated carbon from date seeds for chromium removal in aqueous solution. *Desalin Water Treat*, 156, 267–277.
- Rani, K. S., Srinivas, B., GouruNaidu, K., & Ramesh, K. V. (2018). Removal of copper by adsorption on treated laterite. *Materials Today: Proceedings*, 5(1), 463–469.
- Reghioua, A., Barkat, D., Jawad, A. H., Abdulhameed, A. S., Al-Kahtani, A. A., & ALOthman, Z. A. (2021). Parametric optimization by Box–Behnken design for synthesis of magnetic chitosan-benzil/ZnO/Fe₃O₄ nanocomposite and textile dye removal. *Journal of Environmental Chemical Engineering*, 9(3), 105166.
- Salari, M., Nikoo, M. R., Al-Mamun, A., Rakhshandehroo, G. R., & Mooselu, M. G. (2022). Optimizing Fenton-like process, homogeneous at neutral pH for ciprofloxacin degradation: Comparing RSM-CCD and ANN-GA. *Journal of Environmental Management*, 317, 115469.
- Shehzad, K., Xie, C., He, J., Cai, X., Xu, W., & Liu, J. (2018). Facile synthesis of novel calcined magnetic orange peel composites for efficient removal of arsenite through simultaneous oxidation and adsorption. *Journal of Colloid and Interface Science*, 511, 155–164.
- Siddiqui, S. H. (2018). The removal of Cu²⁺, Ni²⁺ and methylene blue (MB) from aqueous solution using Luffa Actangula carbon: kinetics, thermodynamic and isotherm and response methodology. *Groundwater for Sustainable*

Development, 6, 141–149.

- Stala, Ł., Ulatowska, J., & Polowczyk, I. (2022). Copper (II) ions removal from model galvanic wastewater by green one-pot synthesised amino-hypophosphite polyampholyte. *Journal of Hazardous Materials*, 436, 129047.
- Tan, K. B., Vakili, M., Horri, B. A., Poh, P. E., Abdullah, A. Z., & Salamatina, B. (2015). Adsorption of dyes by nanomaterials: recent developments and adsorption mechanisms. *Separation and Purification Technology*, 150, 229–242.
- Taoufik, N., Elmchaouri, A., Anouar, F., Korili, S. A., & Gil, A. (2019). Improvement of the adsorption properties of an activated carbon coated by titanium dioxide for the removal of emerging contaminants. *Journal of Water Process Engineering*, 31, 100876.
- Teodoro, F. S., Adarme, O. F. H., Gil, L. F., & Gurgel, L. V. A. (2017). Synthesis and application of a new carboxylated cellulose derivative. Part II: Removal of Co^{2+} , Cu^{2+} and Ni^{2+} from bicomponent spiked aqueous solution. *Journal of Colloid and Interface Science*, 487, 266–280.
- Tong, K. S., Kassim, M. J., & Azraa, A. (2011). Adsorption of copper ion from its aqueous solution by a novel biosorbent *Uncaria gambir*: Equilibrium, kinetics, and thermodynamic studies. *Chemical Engineering Journal*, 170(1), 145–153.
- Vajedi, F., & Dehghani, H. (2019). The characterization of TiO_2 -reduced graphene oxide nanocomposites and their performance in electrochemical determination for removing heavy metals ions of cadmium (II), lead (II) and copper (II). *Materials Science and Engineering: B*, 243, 189–198.
- Vunain, E., Kenneth, D., & Biswick, T. (2017). Synthesis and characterization of low-cost activated carbon prepared from Malawian baobab fruit shells by H_3PO_4

activation for removal of Cu (II) ions: equilibrium and kinetics studies.

Applied Water Science, 7(8), 4301–4319.

Wu, Z., Zhong, H., Yuan, X., Wang, H., Wang, L., Chen, X., Zeng, G., & Wu, Y.

(2014). Adsorptive removal of methylene blue by rhamnolipid-functionalized graphene oxide from wastewater. *Water Research*, 67, 330–344.

Yang, J.-K., Park, H.-J., Lee, H.-D., & Lee, S.-M. (2009). Removal of Cu (II) by

activated carbon impregnated with iron (III). *Colloids and Surfaces A: Physicochemical and Engineering Aspects*, 337(1–3), 154–158.

Yousefi, M., Gholami, M., Oskoei, V., Mohammadi, A. A., Baziar, M., & Esrafil, A.

(2021). Comparison of LSSVM and RSM in simulating the removal of ciprofloxacin from aqueous solutions using magnetization of functionalized multi-walled carbon nanotubes: Process optimization using GA and RSM techniques. *Journal of Environmental Chemical Engineering*, 9(4), 105677.

Zhang, Y., Yue, X., Xu, W., Zhang, H., & Li, F. (2019). Amino modification of rice

straw-derived biochar for enhancing its cadmium (II) ions adsorption from water. *Journal of Hazardous Materials*, 379, 120783.

CHAPTER SEVEN

CONCLUSION AND RECOMMENDATION

7.1. Summary

This research reviewed various methods for removing arsenic from water, specifically focusing on decentralized systems, which are increasingly relevant for small communities that do not have access to centralized water treatment. The study first introduced arsenic's occurrence and structural properties, highlighting its toxic effects and the global concerns regarding its contamination of drinking water sources.

Traditional arsenic removal techniques such as ion exchange, coagulation-flocculation, and membrane filtration were discussed, emphasizing their limitations in decentralized systems, including high operational costs, complex infrastructure requirements, and maintenance challenges. Among these methods, adsorption emerged as a particularly effective and cost-efficient approach for arsenic removal in small-scale systems due to its simplicity, ease of implementation, and ability to work effectively at lower scales.

The thesis also provided a detailed discussion of adsorbent materials, including natural and industrial by-products, and their potential for use in arsenic removal. Various adsorbent characterization techniques such as surface area analysis, scanning electron microscopy (SEM), and X-ray diffraction (XRD) were reviewed to assess the properties of these materials. The importance of adsorption kinetics, including pseudo-first-order, pseudo-second-order, Elovich, and intra-particle diffusion models, was also highlighted to provide a framework for evaluating adsorbent performance.

Building on these foundational concepts, the experimental work conducted to assess the potential of modified mussel shells and other renewable adsorbents, along with the results achieved, are outlined below.

• Investigation of Mussel Shell Adsorbents for Arsenic Removal in Batch Systems

Then study then explored mussel shells as a potential adsorbent for arsenic removal (Chapter 3). Mussel shells, a waste material from the seafood industry, were calcined and modified with iron oxide nanoparticles (IO-CMS) to enhance their adsorption capacity and efficiency. A detailed methodology was provided for the preparation of the adsorbents, which included the calcination of mussel shells followed by functionalization with iron oxide nanoparticles to improve surface area and adsorption sites.

Batch adsorption experiments were carried out to evaluate the efficiency of these adsorbents in removing arsenic species, specifically As(III) and As(V), from aqueous solutions. The optimization of factors such as pH, contact time, and initial arsenic concentration was carried out using Response Surface Methodology (RSM) with Central Composite Design (CCD) to achieve higher adsorption efficiency and capacity. IO-CMS demonstrated significant potential for arsenic removal.

For As(III), the highest removal efficiency of 94.9% was achieved at pH 6.4, an initial concentration of 57.9 mg L⁻¹, and an adsorbent dose of 3.4 g L⁻¹. For As(V), 98.5% removal efficiency was achieved at pH 5.7, an initial concentration of 59.9 mg L⁻¹, and an adsorbent dose of 2.7 g L⁻¹. The maximum adsorption capacities were 14.62 mg g⁻¹ for As(III) and 18.76 mg g⁻¹ for As(V).

Four kinetic models (pseudo-first-order, pseudo-second-order, Elovich, and intra-particle diffusion) and four isotherm models (Langmuir, Freundlich, Temkin, and Dubinin-Radushkevich) were fitted to the experimental data for analyzing adsorption behavior. The kinetics of arsenic adsorption were well-described by the pseudo-second-order (PSO) model, which indicated that chemisorption was the primary mechanism.

Langmuir model fit of equilibrium isotherm data was strong, suggesting monolayer adsorption on the homogeneous surface of IO-CMS. Thermodynamic analysis revealed that the process is spontaneous and endothermic. These findings highlight the efficiency and practicality of IO-CMS for arsenic removal from contaminated water sources.

• **Application of Modified Mussel Shells for Arsenic Removal in Continuous Flow Systems**

This study then extended the investigation into continuous flow systems (Chapter 4), which mimicked real-world water treatment scenarios, and investigated the performance of modified calcined mussel shells (CMS) for arsenic (As(III) and As(V)) removal in continuous flow experiments. This section involved conducting breakthrough curve studies to evaluate the adsorbent's performance in a continuous flow system, by varying initial arsenic concentrations (from 10 to 50 mg L⁻¹), flow rate (from 5 to 10 mL min⁻¹) and adsorbent mass (from 10 to 5 g) the study tracked the efficiency of arsenic removal over time, which is crucial for understanding the long-term performance of the adsorbent in real-world applications.

The impact of co-ions (Cl⁻, SO₄²⁻, NO₃⁻, HCO₃⁻, and PO₄³⁻) on arsenic uptake was investigated. Moreover, the reusability of the modified mussel shells was assessed by subjecting the adsorbent to multiple cycles of adsorption and desorption.. The experimental results were analyzed using Thomas model and Yoon-Nelson model to evaluate the kinetics and performance of arsenic removal, providing a deeper understanding of the adsorption process in continuous flow systems.

Increasing the initial arsenic concentration and flow rate, while decreasing the adsorbent mass, improved the maximum adsorption capacity for As(III) (8.99 mg g⁻¹) and As(V) (26.60 mg g⁻¹).

Additionally, the study involved testing the adsorbent in point-of-use (POU)

cartridges designed for practical application to serve households impacted by arsenic contamination of their drinking water sources. The performance of these mussel shell-based cartridges was compared to that of commercial activated carbon cartridges, providing a benchmark for evaluating the effectiveness and potential advantages of using modified mussel shells in water treatment systems. The performance of the cartridges was analyzed through adsorption-desorption experiments, which provided insight into the reusability and effectiveness of the cartridges in real-world water treatment scenarios. While the commercial activated carbon cartridge did not remove arsenic effectively, mussel shell-based cartridges removed arsenic with high efficiency, demonstrating their superior performance for arsenic removal in point-of-use filtration systems. Mussel shell powder (MP) showed faster adsorption kinetics than mussel shell-coated discs (MD), although MD had a higher maximum adsorption capacity.

The findings from this study confirmed that modified mussel shells are effective for continuous arsenic removal in glass column and point-of-use cartridge setups. The study demonstrated that the mussel shell adsorbent maintained high efficiency over multiple cycles and showed resilience in the presence of co-ions. This research supports the potential of using modified mussel shells as a sustainable and cost-effective solution for decentralized water treatment, particularly in areas with limited access to centralized water purification systems.

• Utilizing Orange Peel-Derived Biochar for Arsenic Removal

The potential of using renewable and low-cost adsorbents derived from orange peels for arsenic removal were explored (Chapter 5). Biochar derived from agricultural waste (orange peels), was modified with TiO_2 nanoparticles (OP- TiO_2) to improve arsenic removal capacity. The thesis detailed the preparation process, including drying and grinding the peels into fine powder, followed by characterization techniques such

as SEM, FTIR, and surface area analysis to evaluate the properties of the adsorbent. The factors such as pH, contact time, and initial arsenic concentration were optimized using Response Surface Methodology (RSM) with Central Composite Design (CCD) to enhance adsorption efficiency and capacity. The OP-TiO₂ adsorbent exhibited a maximum arsenic removal capacity of 10.91 mg g⁻¹ under optimal conditions, which included a pH of 4.2, initial arsenic concentration of 50 mg L⁻¹, and an adsorbent dose of 3.3 g L⁻¹.

The experimental data were analyzed by fitting four kinetic models (pseudo-first-order, pseudo-second-order, Elovich, and intra-particle diffusion) and four isotherm models (Langmuir, Freundlich, Temkin, and Dubinin-Radushkevich) to evaluate the adsorption behavior. The adsorption process was best described by the intra-particle diffusion model, suggesting a complex multi-step adsorption process. Moreover, the Temkin isotherm model was found to be a more suitable description of the experimental data for arsenic adsorption onto the OP-TiO₂ adsorbent. Thermodynamic studies confirmed that arsenic adsorption on OP-TiO₂ was spontaneous and endothermic, making it a promising and renewable adsorbent for effective water treatment. This study provided significant contribution by showing how waste-derived materials, when modified and optimized, can serve as valuable resources for environmental remediation.

• Optimization of Biochar Adsorbents for Copper Removal from Water

Building on the success of using orange peel-derived adsorbents for arsenic removal, this chapter focused on the removal of copper ions from water using TiO₂-modified activated carbon derived from both orange peels and date seeds (Chapter 6). The goal of this study was to expand the potential of bio-based adsorbents for the removal of other heavy metals, and copper was selected as the target contaminant. TiO₂-modified biochar derived from both orange peels (OP-TiO₂) and date seeds (DS-TiO₂)

was evaluated for its effectiveness in copper removal. Response Surface Methodology (RSM) with Central Composite Design (CCD) was used to optimize parameters like pH, contact time, and initial copper concentration, aiming to improve adsorption efficiency. The optimal conditions for copper removal were identified as pH 5.0, adsorbent dose of 4.9 mg L⁻¹ for OP-TiO₂, and pH 6.4, adsorbent dose of 5.0 mg L⁻¹ for DS-TiO₂. The maximum adsorption capacities were 13.34 mg g⁻¹ for OP-TiO₂ and 13.96 mg g⁻¹ for DS-TiO₂. Four kinetic models (pseudo-first-order, pseudo-second-order, Elovich, and intraparticle diffusion) were applied to the experimental data to assess the adsorption behavior. The experimental data was best described by the pseudo-second-order kinetic model, indicating that copper adsorption involved chemisorption.

The results confirmed that TiO₂ modification enhanced the adsorption capacity, making the adsorbent more effective for copper removal, thereby contributing to the broader field of sustainable water treatment technologies.

7.2. Conclusion

This research highlights the potential of utilizing renewable materials, such as mussel shells and agricultural waste (orange peels and date seeds), as low-cost and sustainable adsorbents for arsenic and copper removal from water. These materials, which are often considered waste products, can be transformed into valuable resources through simple modification techniques. The study demonstrates that by modifying these materials with nanoparticles, their adsorption capacities were significantly enhanced, thus improving their efficiency for arsenic and copper removal. This modification not only boosts the performance of these adsorbents but also ensures that they can serve as viable and cost-effective alternatives to traditional adsorbents like commercial activated carbon, which are typically more expensive and less

environmentally sustainable.

The findings from this research offer a conceptual framework for tackling the issue of heavy metal contamination in water, a problem that is particularly pressing in regions with limited access to high-end technologies. By focusing on renewable and locally available materials, the study introduces a more accessible approach to water purification. This is of particular importance in decentralized water treatment systems, which are increasingly relevant for small communities and rural areas, where centralized water treatment infrastructure is often unavailable. The ability to scale up the use of these adsorbents means that they could play a significant role in reducing the public health risks associated with arsenic and copper contamination in drinking water.

On a broader scientific and intellectual level, this research contributes to the ongoing shift towards sustainable and green chemistry approaches in environmental remediation. The ability to convert waste biomass into effective water treatment materials aligns with global sustainability goals, such as reducing waste, lowering environmental impact, and promoting circular economy practices. Moreover, the use of nanoparticles for adsorbent modification opens avenues for exploring the nanotechnology's role in environmental applications, where it can significantly improve the performance of traditional materials without compromising environmental safety.

The work also underscores the importance of optimizing adsorption conditions through methods like Response Surface Methodology (RSM) with Central Composite Design (CCD), which was employed to optimize critical factors like pH, contact time, and initial contaminant concentration. These optimization techniques minimize the number of experiments compared to the traditional one-factor-at-a-time approach, while still providing high accuracy in predicting the optimal conditions.

Furthermore, the study's incorporation of flow-through and batch experiments provides a comprehensive understanding of the adsorption process under both controlled and more dynamic conditions. Moreover, by examining the kinetics and isotherms of the adsorption process, the study offers a deeper understanding of the interaction mechanisms between contaminants and adsorbents. This holistic approach contributes to the advancement of adsorption science, as it provides valuable insights into the real-world applicability of these materials in addressing water quality challenges.

In conclusion, the study demonstrates the potential of modified mussel shells and agricultural waste as effective and sustainable adsorbents for arsenic and copper removal. It also provides valuable guidance for the design and optimization of low-cost water treatment systems using renewable materials.

Beyond the experimental results, the research offers a practical framework for addressing global water contamination issues, emphasizing the need for scalable, environmentally friendly solutions that can be adapted to local needs and resources.

7.3. Research Contributions

This research advanced sustainable water treatment by developing innovative solutions for removing arsenic and copper from water using renewable and locally sourced waste materials. These findings are particularly significant for small, rural, and remote communities that face challenges in accessing conventional water treatment infrastructure. The feasibility of using these adsorbents for decentralized, point-of-use applications was highlighted, offering significant benefits for small, rural, and remote communities, not only in Newfoundland and Labrador but also in similar regions worldwide that face challenges in accessing conventional water treatment

infrastructure. The study focused on utilizing modified calcined mussel shells, orange peel-derived biochar, and date seed-derived biochar as effective adsorbents, addressing critical water quality challenges.

For arsenic removal, calcined mussel shells were modified with iron oxide nanoparticles, achieving high adsorption capacities for both As(III) and As(V) in both synthetic and real water matrices. The successful testing of this material in cartridge flow-through systems highlights its practical potential for on-site arsenic removal, particularly for households using private wells in areas where water sources are unregulated and vulnerable to contamination. The problem that this solution addresses is the global challenge of arsenic contamination in drinking water, which affects millions of people worldwide. The innovative use of mussel shells provides an accessible water treatment method, particularly for rural or underserved communities, where traditional water purification technologies are often too expensive or inaccessible. In Newfoundland and Labrador, approximately 15% of the population depend on private wells for their drinking water. These private water sources are often unregulated and susceptible to contamination, including arsenic. For these households, implementing point-of-use filtration systems using mussel shell-based adsorbents can provide an effective and affordable means of removing arsenic, ensuring access to safe drinking water without the need for expensive or complex infrastructure.

Orange peel-derived biochar, functionalized with TiO_2 , demonstrated enhanced adsorption properties, enabling efficient removal of arsenic from water. Additionally, both orange peel-derived and date seed-derived biochars proved effective for copper removal, exhibiting strong adsorption capabilities. The research showcased the value of agricultural waste in providing high-performance adsorbents for water treatment, which also contributes to waste management by repurposing organic byproducts.

The study underscored the environmental and economic advantages of repurposing local waste materials such as mussel shells, orange peels, and date seeds. The research provided a sustainable solution that integrates waste management with water treatment by turning these byproducts into high-performance adsorbents. Furthermore, the combined findings of these studies offer valuable insights into optimizing adsorbent performance under diverse water chemistries and operational conditions. This research represents a significant step toward scalable, eco-friendly water treatment technologies, promoting environmental sustainability and resource efficiency.

This research contributes to the growing body of knowledge on sustainable water treatment by offering effective, low-cost, and environmentally friendly solutions for addressing heavy metal contamination in water. By combining renewable materials, nanoparticles, and optimized adsorption strategies, this study represents a significant step toward achieving sustainable, decentralized water treatment technologies that can be adapted to meet the needs of both developed and developing regions.

7.4. Recommendations

Based on the findings of this research, the following recommendations are proposed to advance sustainable water treatment technologies further:

- **Scale-Up and Field Testing**

Future studies should focus on scaling up the production of the developed adsorbents, including modified calcined mussel shells, orange peel-derived and date seed-derived biochar, for pilot and full-scale applications. Field testing in diverse water systems, including those with varying water chemistries and contamination levels, will provide valuable insights into their real-world performance and operational feasibility.

- Economic and Environmental Analysis

A life cycle assessment (LCA) and cost analysis should be conducted to evaluate the environmental and economic impacts throughout the entire life cycle of the adsorbents. This includes examining the impacts from raw material production, transportation, and their application in point-of-use water treatment systems, as well as considering the disposal or regeneration of the adsorbents after use. Specifically, the LCA should focus on key environmental factors such as resource usage, energy consumption, greenhouse gas emissions, and waste generation throughout the adsorbent's life cycle, while also considering economic factors such as the cost of production, cost of deployment, and cost-benefit analysis. This analysis will help identify optimization opportunities and promote the adoption of these technologies in cost-sensitive regions.

- Optimization of Cartridge Design:

Further research is recommended to optimize the design and configuration of cartridge systems for point-of-use applications. Enhancements in flow dynamics, adsorbent packing, and regeneration techniques could improve their efficiency and lifespan, particularly for use in remote and small communities. Also, investigating the spent cartridge disposal and handling would provide utility to their domestic applications.

- Integration with Existing Water Treatment Systems

Research should explore how these adsorbents can be integrated into existing water treatment systems to create a hybrid approach that maximizes contaminant removal efficiency.

Implementation should focus on locally adaptable production and deployment strategies to enable the practical application of the developed technologies, especially

in decentralized settings. Utilizing waste materials such as mussel shells and agricultural by-products supports environmental sustainability and enables low-cost, community-based solutions that can be manufactured using local labor and resources. This can contribute to job creation, circular economy models, and reduced waste disposal burdens. Integrating the developed adsorbents into existing or stand-alone point-of-use systems could provide safe drinking water in underserved areas without the need for large-scale infrastructure. A broader socio-economic analysis, including cost-benefit assessments, user acceptance, and maintenance feasibility, will be essential to support policy adoption and long-term sustainability of these technologies in real-world applications.

APPENDIX 1

Supplementary Information for Chapter 3

Surface modification of calcined mussel shells with iron oxide nanoparticles

Materials and Quantities:

- Calcined Mussel Shell Powder: 3 g
- Iron Oxide Nanoparticles: 30 mg
- Deionized Water: 200 mL

Procedure:

1. Nanoparticle Dispersion: The 30 mg of iron oxide nanoparticles were first added to 200 mL deionized water. To ensure a homogeneous dispersion and break up any nanoparticle agglomerates, the nanoparticle–water suspension was ultrasonicated for 30 min.
2. Impregnation: After the dispersion step, 3 g of calcined mussel shell powder was introduced into the nanoparticle suspension. The combined mixture was then stirred continuously at 300 rpm for 10 h at room temperature. This prolonged stirring allowed the iron oxide nanoparticles to interact with and adhere to the porous surfaces of the mussel shell powder.
3. Separation and Drying: Following the 10-h stirring period, the modified particles were separated from the liquid phase by centrifugation. The collected solid was then subjected to lyophilization (freeze-drying) to remove residual water gently, preserving the structural integrity of the nanoparticle coating.

The final product, referred to as IO-CMS, consists of calcined mussel shell particles impregnated with a uniform distribution of iron oxide nanoparticles.

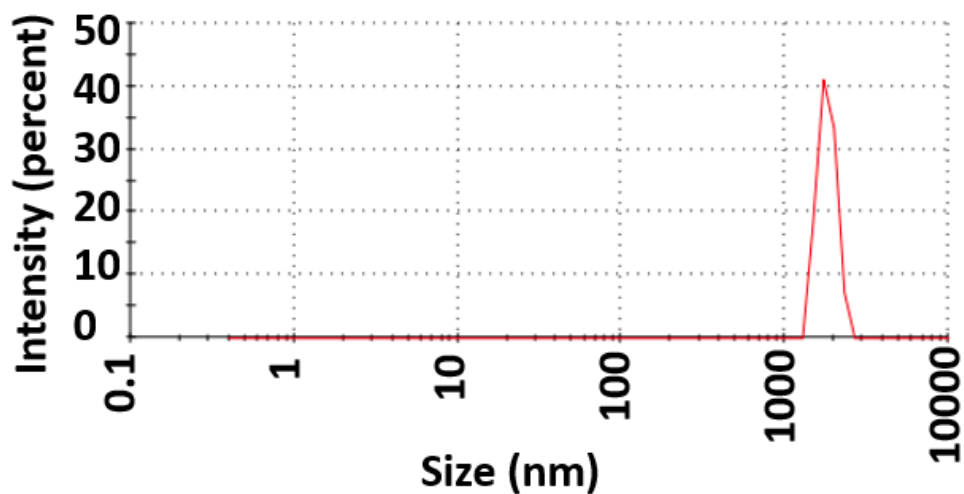


Figure S3-1. Particle size distribution of IO-CMS.

Table S3-1. Preliminary studies on arsenic adsorption capacities of raw, calcined, and iron oxide-modified calcined mussel shells (IO-CMS) for As(III) and As(V).

Adsorbent	Initial concentration (mg L ⁻¹)	Adsorbent dose (g L ⁻¹)	Contact time (h)	Adsorbent capacity (mg/g)	
				As(III)	As(V)
Raw Mussel Shell	60	5	24	2.67	2.10
Calcined Mussel Shell (air)	60	5	24	9.43	9.81
Calcined Mussel Shell (Nitrogen)	60	5	24	11.48	12.92
IO-Modified Mussel	60	5	24	13.95	14.31

APPENDIX 2

Supplementary Information for Chapter 4

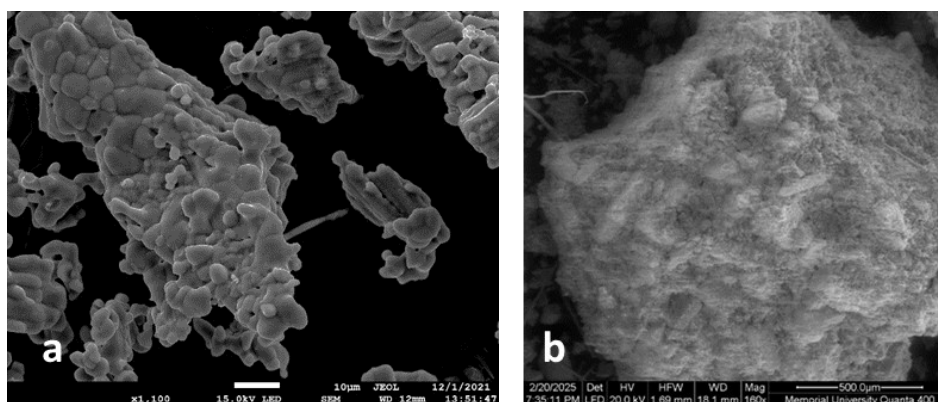


Figure S4-1. SEM images of the (a) virgin adsorbent, and (b) regenerated adsorbent.

APPENDIX 3

Supplementary Information for Chapter 5

Surface Modification of activated carbon with titanium dioxide nanoparticles

Materials and Quantities:

- Activated Carbon: 1 g (prepared separately from date seeds and orange peels)
- Titanium Dioxide (TiO₂) Nanoparticles: 0.1 g
- Distilled Water: 50 mL

Procedure:

1. Nanoparticle Dispersion: Initially, 0.1 g of TiO₂ nanoparticles was dispersed in 50 mL of distilled water. This dispersion was achieved by ultrasonication of the nanoparticles in water for 30 min to ensure a uniform suspension.
2. Impregnation: After achieving a well-dispersed TiO₂ suspension, 1 g of activated carbon (from either date seeds or orange peels) was added to the flask containing the dispersion. The resulting mixture was then ultrasonicated thoroughly for an additional 30 min at room temperature. This step facilitated intimate contact between the activated carbon and the TiO₂ nanoparticles, promoting effective deposition onto the carbon surface.
3. Filtration and Drying: The final suspension was filtered to separate the modified activated carbon from the liquid. The filtered material was rinsed with distilled water to remove any loosely bound nanoparticles or impurities. The washed material was then oven-dried overnight at 65 °C.